General Disclaimer

One or more of the Following Statements may affect this Document

- This document has been reproduced from the best copy furnished by the organizational source. It is being released in the interest of making available as much information as possible.

- This document may contain data, which exceeds the sheet parameters. It was furnished in this condition by the organizational source and is the best copy available.

- This document may contain tone-on-tone or color graphs, charts and/or pictures, which have been reproduced in black and white.

- This document is paginated as submitted by the original source.

- Portions of this document are not fully legible due to the historical nature of some of the material. However, it is the best reproduction available from the original submission.

Produced by the NASA Center for Aerospace Information (CASI)

UNIVERSITY OF HAWAII

(NASA-CR-175763) SPECTRAL REFLECTANCE OF CARBONATE MINERALS AND ROCKS IN THE VISIBLE AND NEAR INFRARED (0.35 - 2.55 MICRONS) AND ITS APPLICATIONS IN CARBONATE PETROLOGY (Hawaii Univ., Honolulu.) 256 p G3/46

N85-25973

Unclas 21212

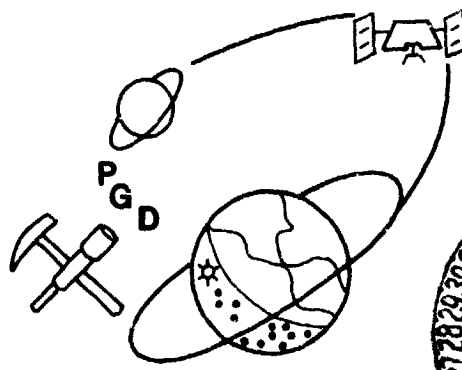

MAY 1985
RECEIVED
NASA STI FACILITY
ACCESS DEPT.

Planetary Geosciences Division

HAWAII INSTITUTE OF GEOPHYSICS

2525 CORREA ROAD • HONOLULU, HAWAII 96822

808-948-6488

SPECTRAL REFLECTANCE OF CARBONATE MINERALS AND ROCKS IN THE VISIBLE AND NEAR INFRARED (0.35 to 2.55μm) AND ITS APPLICATIONS IN CARBONATE PETROLOGY

SPECTRAL REFLECTANCE OF CARBONATE MINERALS AND ROCKS IN THE VISIBLE AND NEAR INFRARED (0.35 to 2.55μm) AND ITS APPLICATIONS IN CARBONATE PETROLOGY

A DISSERTATION SUBMITTED TO THE GRADUATE DIVISION OF THE
UNIVERSITY OF HAWAII IN PARTIAL FULFILLMENT
OF THE REQUIREMENTS FOR THE DEGREE OF

DOCTOR OF PHILOSOPHY

IN GEOLOGY AND GEOPHYSICS

AUGUST 1984

By

Susan Jenks Gaffey

Dissertation Committee

Bernard Ray Hawke, Chairman
Thomas B. McCord
Pow-Foong Fan
Kost Pankiwskyj
Fred T. Mackenzie
George Andermann, Outside Member

We certify that we have read this dissertation and that in our opinion it is satisfactory in scope and quality as a dissertation for the degree of Doctor of Philosophy in Geology and Geophysics.

DISSERTATION COMMITTEE

Chairman

ACKNOWLEGEMENTS

Funding for this work was provided by Jet Propulsion Laboratory Grant JPL #956370, by NASA Grant NSG #7312, and by Caylord, Leonard, and Edna Cobeen.

Mineral samples were kindly provided by the Smithsonian, by John Fuller of the British Museum, by George McCormick at the Geology Department, University of Iowa, and by Milton Manhoff, president of the Rock and Mineral Society of Hawaii. Fritz Theyer, of the Hawaii Institute of Geophysics, University of Hawaii at Manoa, provided samples of coccolith and foram oozes. Samples of calcareous ooze, chalk, and limestone were provided by the Deep Sea Drilling Project.

I would like to thank Edith Jenks, Michael Gaffey, Debbie Craven, and Mark Rognstad for their assistance in the field.

X-ray fluorescence analyses were provided by John Sinton. Kevin Reed performed the chemical analyses by spark spectrometery and atomic absorption spectrophotometry, and assisted with the X-ray diffraction analyses. Virginia Greenberg provided valuable advice on these analytical techniques. Karen Margolis assisted with the SEM photography and EDAX analyses.

I would like to thank John Adams at the Unversity of Washington and Robert Huguenin at the Center for Remote Sensing at the University of Massachusetts at Amherst for allowing me to use their reflection spectrophotometers and computer facilities.

Ted Roush wrote the program which translates data from the University of Washington instrument to our format. Pam Blake devised the method by which laboratory spectra were convolved to TM and SMIRR band passes. I would like to thank Bob Singer and Pam Blake for helpful discussions of the realities of remote sensing.

No one completes work for a degree without the assistance of teachers, fellow students, staff, family, and friends. I've been particularly fortunate in this regard and would like to express my gratitude to the many nice folks who've helped me along the way.

Special thanks to Bob Huguenin who first suggested this project and provided many of the samples used. His continuing interest and encouragement, and his helpful discussions of the work are greatly appreciated.

Thanks also to Tom McCord who encouraged me to return to graduate school, served as my advisor during my first years back, had the courage to let me do my own thing, and even found research funds with which to do it.

I also want to thank Ray Hawke who took over as my advisor when he joined the graduate faculty. He is most truly a gentleman and a scholar, and his guidance and help are greatly appreciated.

Many thanks also to my other committee members, Seymour Schlanger, Pow-Foong Fan, Kost Pankiwskyj, George Andermann, and Fred Mackenzie, for their help and encouragement.

I'd like to thank the many people at PGD who helped an old-style soft-rocker learn to cope with computers and state-of-the-art equipment: Lucy McFadden, Bob Singer, Roger Clark, Mark Rognstad, Jeff Bosel, and Rodney Kam. Special thanks to Pam Owensby who initiated me into the mysteries of GFIT.

Thanks to all the PGD grads who've helped make this a pleasant and fruitful place to work: Lucy, Jeff B., Paul, Bob B., Ted, Ed, Aaron, Marci, Steve, with special aloha for Pam L., Chuck, and Lisa, fellow-residents of the terrestrial ghetto.

Mahalo to our engineers, Mark Rognstad, Karl Hinck, Jeff Bosel and Wendy Harrison who make things run, keep them running, and then get them running again. Your services above and beyond the call of duty during crashes, equipment failures, and the recent air-conditioning crisis are greatly appreciated by all.

I'd also like to thank our user-friendly, scientist-compatable live-ware - Jeff Hoover, Graham Bromley, Rodney Kam, Duncan Chesley, and Tim Jackowski.

Thanks also to Sam, Zeny, Thomas, Phil, and all the other staff and admin people who make this place run.

I'd like to express special thanks to Kevin Reed. His persistence in the face of all the administrative hassles and bureaucratic red tape the University is able to generate, and his success in coping with the "kitchenette" deserve special mention.

I particularly want to express my gratitude to my mother. She's been in this with me since my Girl Scout rock badge - mother, source of funds, chaffeur, able field assistant, and very special friend. This is her degree, too.

Last, I want to thank my husband Mike, for sharing his knowledge of spectroscopy with me, and for sharing his life with me. I couldn't have done this without his encouragement, his support and his love. He made the impossible possible.

ABSTRACT

Reflection spectroscopy in the visible and near infrared (0.35 to 2.55μm) offers a rapid, inexpensive, nondestructive tool for determining the mineralogy and investigating the minor element chemistry of the hard-to-discriminate carbonate minerals, and can, in one step, provide information previously obtainable only by the combined application of two or more analytical techniques. When light interacts with a mineral certain wavelengths are preferentially absorbed. The number, positions, widths and relative intensities of these absorptions are diagnostic of the mineralogy and chemical composition of the sample. At least seven bands due to vibrations of the carbonate radical occur between 1.60 and 2.55μm. Positions of these bands vary from one carbonate mineral to another and can be used for mineral ide tification. Cation mass is the primary factor controlling band position; cation radius plays a secondary role.

Electronic processes in the d-shells of transition metal cations can also cause absorptions. Absorbing species in carbonate minerals include Fe^{2+}, Mn^{2+}, Ni^{2+}, Co^{2+}, and Cu^{2+}. Fe^{2+} bands are centered near 1.1μm. They vary in width, position, and shape from one calcite group mineral to another, reflecting differences in the size and symmetry of the octahedral sites in these minerals, and can aid in mineral identification. Relative intensities of transition metal absorptions increase with increasing cation abundance, and can be used to determine cation concentrations. Detection limits for Mn^{2+} are about 0.10 weight per cent Mn, for Fe^{2+} about 0.01 weight per cent Fe, and for Cu^{+} about 0.005 weight per cent Cu. Positions of carbonate bands may also vary with variations in chemical composition.

Absorption features due to water may also occur in spectra of carbonate samples. Liquid water has two strong absorptions near 1.4μm and 1.9μm. Absorptions due to water bound in clays are narrower and occur at shorter wavelengths than those due to liquid water. OH^- produces absorptions near 1.4μm and 2.2μm, but the 1.9μm feature is lacking. Absorptions due to water bound in hydrated carbonate minerals phases are broader and occur at longer wavelengths than those due to liquid water. Spectra indicate that hydrozincite and hydrocerussite, believed to contain only OH^-, actually contain bound H_2O as well.

Spectra indicate that aqueous fluid inclusions are nearly ubiquitous in carbonate rocks and minerals, and are particularly abundant in skeletal material. The quantity of inclusions varies from one type of organism to another, with coccoliths and planktonic forams containing the least water, corals and coralline algae containin the most. Inclusions are lost from skeletal material during diagenesis, and the amount of water lost may be related to the diagenetic environment.

Spectra taken both from powdered samples of different grain sizes and from whole samples indicate that band positions, shapes, and relative intensities don't change with changes in grain size and porosity of a sample, and spectra contain the same mineralogical and chemical information regardless of the form of the sample.

Three quite different types of spectrophotometers were used to measure sample spectra, and all give equivalent results.

Spectral reflectance also has potential as a remote sensing tool. Spectral features diagnostic of mineralogy and chemical composition occur in the atmospheric windows, and can be measured with high resolution instruments.

TABLE OF CONTENTS

ACKNOWLEDGEMENTS iii

ABSTRACT vi

LIST OF TABLES viii

LIST OF FIGURES ix

CHAPTER 1. INTRODUCTION 1

CHAPTER 2. METHODS 4

CHAPTER 3. SPECTRAL PROPERTIES OF CALCITE, ARAGONITE, AND DOLOMITE

Introduction 12
Carbonate Minerals 14
Results 19
Discussion 48
Mineralogical Applications 59

CHAPTER 4. DIFFERENCES IN SPECTRAL PROPERTIES RELATED TO DIFFERENCES IN MINERALOGY

Introduction 63
Carbonate Bands 70
Iron Bands 80
Weathering 85
Mineralogical Applications 88

CHAPTER 5. VARIATIONS IN SPECTRAL PROPERTIES WITH VARIATIONS IN CHEMICAL COMPOSITION

Introduction 91
Magnesium 96
Copper 98
Iron 107
Manganese 127
Other Cations 134
Future Work 137

CHAPTER 6. ABSORPTION FEATURES DUE TO WATER

Introduction 139
Water Bands 140
Water Bands in Rock Spectra 150

CHAPTER 7. HYDROUS CARBONATE MINERALS 160

CHAPTER 8. AQEOUS FLUID INCLUSIOND IN SKELETAL MATERIAL

Introduction 164
Fluid Inclusions in Modern Skeletal Material 165
Loss of Fluid Inclusions During Diagenesis 174

CHAPTER 9. REMOTE SENSING APPLICATIONS

Introduction 190
Spectral Properties of Carbonate Minerals . 192
Spectral Properties of Non-Carbonate Phases 193
Effects of Weathering 196
Applications of Spectral Information . . . 201
Spectral Information Obtainable from
Existing Data Sets 202
Future Work 209

CHAPTER 10. SUMMARY 212

REFERENCES CITED 219

LIST OF TABLES

Table 3.1 Numbers and localities of samples used 26

Table 3.2 Particle size fractions of sample #1531 in microns 30

Table 3.3 Carbonate band positions in microns 34

Table 3.4 Widths of carbonate bands in inverse microns . . . 41

Table 3.5 Band positions and assignments from the Literature for Calcite 56

Table 4.1 Numbers and localities of samples used 67

Table 4.2 Positions in microns of carbonate bands in spectra of common carbonate minerals. 68

Table 4.3 Differences between centers of adjacent carbonate bands in carbonate spectra 69

Table 4.4 Octahedral volumes, quadratic elongation, and M-O bond length for calcite group minerals 82

Table 5.1 Data from the literature on crystal field bands 95

Table 5.2 Positions of carbonate bands and major copper band in calcite spectra 102

Table 5.3 Positions of carbonate and iron bands in dolomite spectra 111

Table 5.4 Numbers and localities of samples used 117

Table 6.1 Positions and assignments of absorptions due to liquid water 142

LIST OF FIGURES

3.1 Rhombohedral and Hexagonal Unit Cells for Calcite . . 15

3.2 Rhombohedral and Hexagonal Unit Cells for Dolomite . 16

3.3 Unit Cell for Aragonite 17

3.4 Spectra of Calcite, Aragonite, and Dolomite 20

3.5 Gaussian Fit to Carbonate Bands 22

3.6a Data and Continua Used for Gaussian Analysis 23

3.6b Data and Continuum That Gave Best Fit 24

3.7 Band Centers for Fits Obtained with All Continua . . 25

3.8 Spectra of Different Particle Size Fractions of Iceland Spar 28

3.9 Ln-Ln Plot of Different Size Fractions of Iceland Spar 29

3.10 Spectra of Powdered and Whole Dolomite Sample 32

3.11 Ln-Ln Plot of Powdered and Whole Dolomite Spectra . . 33

3.12 Ratio Spectrum of Two Dolomites with Different Iron Contents 37

3.13 Centers of Band 2 Plotted vs. Centers of Band 1 . . . 38

3.14 Centers of Band 2 Plotted vs. Centers of Band 4 . . . 39

3.15 Centers of Band 4 Plotted vs. Centers of Band 3 . . . 40

3.16 Centers of Band 2 Plotted vs. Widths of Band 2. . . . 42

3.17 Spectra of Dolomites with Different Iron Contents . . 46

3.18 Spectra of Ferroan Dolomite and Ferroan Calcite . . . 47

3.19 Spectra of Limestone and Dolostone 60

4.1 Spectra of Common Calcite Group Minerals. 65

4.2 Spectra of Common Aragonite Group Minerals 66

4.3 Average M-O Bond Length Plotted vs. Position of Band 2 for Carbonate Minerals 75

4.4 Cation Radius Plotted vs. Position of Band 2 76

4.5 Cation Mass Plotted vs. Position of Band 2 77

4.6 Electronegativity of Cation Plotted vs. Position of Band 2 78

4.7 Iron Bands in Spectra of Calcite Group Minerals . . . 83

4.8 Spectra of Weathered and Unweathered Ferroan Dolomites 86

4.9 Spectra of Siderites Showing Different Degrees of Weathering 87

5.1 Spectra of High and Low Mg Calcites 97

5.2 Spectra of Cuprian Calcites 101

5.3 Relative Intensities of Copper Bands Plotted vs. Copper Content 102

5.4 Relative Intensities of Copper Band Plotted vs. Position of Copper Band 104

5.5 Spectra of Cuprian Smithsonite 105

5.6 Gaussian Fit to Ferroan Dolomite Spectrum 110

5.7 Residual Errors From Gaussian Fit Using Two and Three Fe Bands 112

5.8a Relative Intensities of Fe Bands Plotted vs. Fe Content, Unweathered Dolomite Samples 113

5.8b Relative Intensities of Fe Bands Plotted vs. Fe Content, All Dolomite Samples 114

5.9a Relative Intensities of Fe Bands Plotted vs. Fe Content, Unweathered Dolomite 115

5.9b Relative Intensities of Fe Bands Plotted vs. Fe Content, All Dolomite Samples 116

5.10 Carbonate Bands in Spectra of Four Dolomites with Different Fe Contents 122

5.11 Residual Errors for Fits to Four Dolomite Spectra . . 123

5.12 Position of Band 1 Plotted vs. Position of Band 2, All Calcites, Aragonites, and Dolomites 124

5.13 Position of Band 4 Plotted vs. Position of Band 2, All Calcites, Aragonites, and Dolomites 125

5.14 Position of Band 3 Plotted vs. Position of Band 4, All Calcites, Aragonites, and Dolomites 126

5.15a Spectrum of Siderite Plotted in Energy Space 129

5.15b Spectrum of Rhodochrosite Plotted in Energy Space . . 130

5.16 Spectrum of Manganoan Calcite 131

5.17 Spectra of Three Dolomites with Different Mn and Fe Content 132

5.18 Spectra of Calcite and Smithsonite Containing Co, and of a Magnesite Containing Ni 136

6.1 Spectra of Water-Containing Phases 143

6.2 Spectra of Calcite, Milky Quartz, Wet Calcite, and Average of Calcite and Milky Quartz 146

6.3 Spectra of Calcite, Montmorillonite, and Mixtures of the Two 147

6.4 Mixtures of Clays with Coarse Fraction of Calcite . . 148

6.5 Spectra of Limestones and Dolostones Containing Aqueous Fluid Inclusions 151

6.6a Photomicrograph of Aragonitic Cave Deposit 153

6.6b Closeup or Preceding Showing Aqueous Fluid Inclusions 154

6.7 Spectra of Argillaceous Limestones 155

6.8 Photomicrograph of Bellows Field Eolianite 156

7.1 Spectra of Hydrous Carbonate Minerals and Portlandite 161

8.1 Spectra of Aragonitic Skeletal Material 166

8.2 Spectra of Skeletal Material Composed of Low Mg Calcite 167

8.3 Spectra of Skeletal Material Composed of High Mg Calcite 168

8.4 Spectra of Two Different Layers Within Oyster Shell 169

8.5 Ln-Ln Plot of Powdered and Whole Coral Skeleton . . . 172

8.6 Spectra of Fossil Coral and Coralline Algae 176

8.7 Spectra of Modern and Fossil Coralline Algae . . . 177

8.8 Photomicrograph of Etched Surface of Fossil Coral . . 178

8.9 Spectra of Powdered Coral Skeleton Before and After Heating 179

8.10 Spectra of Calcareous Ooze, Chalk, and Limestone . . 180

8.11 Spectra of Fossil Oyster and Ammonite Retaining Original Skeletal Mineralogy 181

8.12 Spectra of Three Coral Samples with Different Diagenetic Histories 184

8.13a Photomicrograph of Pleistocene Coral Which Has Undergone Dissolution 185

8.13b Photomicrograph of Coral Altered in Vadose Environment 186

8.13c Photomicrograh of Coral Altered in Phreatic Environment 187

9.1 Spectra Showing Absorption Features Due to Non-Carbonate Components 195

9.2 Laminar Calcrete on Dune Rock 198

9.3 Spectra of Laminar Calcrete and Dune Rock on Which it Formed 199

9.4a Spectra of Carbonate Minerals and Rocks Convolved to TM Bands 203

9.4b TM Bands Alone 204

9.5a Spectra of Carbonate Minerals and Rocks Convolved to SMIRR Bands 205

9.5b SMIRR Bands Alone 206

CHAPTER 1

Introduction

Limestones and dolomites form one fifth to one fourth of the stratigraphic record. Carbonate rocks comprise 70% of all the stone quarried in the United States, and 50% of the world's oil is contained in carbonate reservoirs. Carbonate minerals also occur commonly in hydrothermal veins and in association with ore deposits. Thus carbonate rocks are of economic as well as academic interest.

Carbonate minerals are difficult, if not impossible to distinguish in thin section by the usual petrographic methods, and a number of other techniques, including staining, X-ray diffraction, cathodoluminescence, and electron microbe are used to study the mineralogy and chemical composition of carbonate samples. However, none of these techniques is entirely satisfactory, and usually some combination of two or more techniques is required to adequately characterize carbonate minerals.

Spectral reflectance in the visible and near infrared (0.35 to 2.55μm) offers a rapid, inexpensive, nondestructive tool for determining the mineralogy and investigating the minor element chemistry of these hard-to-discriminate minerals, and can, in one step, provide information previously obtainable only by the combined application of two or more analytical techniques. In addition, the technique is very sensitive to

the presence of water, and can be used to determine whether it is present as hydroxyl ion (OH^-) or as water molecules, and if present as water molecules, whether as liquid in the form of fluid inclusions, or as bound water in clays or hydrated carbonate minerals.

This technique has been used by igneous and metamorphic petrologists for over a decade to study pyroxenes and olivines, and to a lesser extent feldspars and other mineral groups (Adams, 1975; Burns, 1970; Hunt, 1977; Hunt and Salisbury, 1970, and others). Earlier work has shown that reflectance spectra of carbonate rocks and minerals in the visible and near infrared show a variety of features which are potentially useful for mineralogical and petrographic work (Adams, 1975; Hexter, 1958; Hunt, 1977; Hunt and Salisbury, 1971, 1976). However, no systematic effort has previously been made to relate these spectral features to the mineralogical and chemical composition of carbonates.

This technique has potential not only as a laboratory tool, but as a tool for remote sensing. The use of reflectance spectroscopy as a tool for mapping in the field, from aircraft, and from spacecraft is being explored (Goetz _et al._, 1983). A detailed knowledge of the spectral properties of carbonate rocks and minerals is essential in extracting information from existing data sets such as those collected by the Thematic Mapper and the Shuttle Mapping Infrared Radiometer, as well in designing new instruments so that they will be more effective in discriminating sedimentary rock units.

The study of carbonate spectra in this wavelength region entails special problems. Carbonate spectra contain features due to electronic processes in unfilled d-shells of transition metal cations, usually the province of spectral studies in the visible and near infrared. In addition they contain features due to vibrational processes which are

usually the concern of workers in the mid infrared (5-15μm). Vibrations of the carbonate radical produce absorption features in this region. Vibrations of water molecules do also, and since, as was found in the course of this study, aqueous fluid inclusions are nearly ubiquitous in carbonate rocks, the spectral properties of water, liquid, bound, and OH^-, had to be included in the study as well.

This study examines the spectral properties of carbonate minerals, with special attention being given to calcite, aragonite, and dolomite which comprise the bulk of modern and ancient carbonate sediments. The spectral properties of the more common solid solution series (e.g. the dolomite-ankerite series) are examined. The spectral properties of the carbonate-noncarbonate mixtures which commonly occur in carbonate rocks are investigated, with special attention given to carbonate-water mixtures.

In this study reflectance spectroscopy is viewed as a tool rather than a field. The purpose of the study was to define spectral parameters useful in discrimination of carbonate minerals and rocks, and to investigate the possible applications of this tool to petrologic problems. Although some discussion of solid state physics is included to give some understanding of the causes of spectral characteristics of carbonates, such investigations were not a primary purpose of the present study.

CHAPTER 2.

Methods

Samples for this study were obtained from a variety of sources, including museums, university collections, commercial establishments, chemical companies, and the field. Lists of samples and their sources are given in tables and in the text where their spectral properties are discussed.

Mineralogy of all samples was verified by X-ray diffraction on powdered samples.

Chemical data on samples was obtained using four different techniques. Samples for which sufficient material was available were analyzed for Ca, Mg, Fe, and Mn by X-ray fluorescence on fused glass discs following the procedures of Norrish and Hutton (1969). CO_2 content was calculated assuming stoichiometry and absence of water. Grains from powders of some of the calcite samples for which limited material was available were analyzed using a Cambridge Stereoscan S-4 SEM equipped with EDAX to determine the presence of minor chemical components in the samples. Spark spectrometry with a Vreeland Direct Reading Spectroscope, model 7, was also used to identify minor elements in some magnesites, siderites, and smithsonites for which sufficient material was available. Atomic absorption was done using a Perkin-Elmer

603 Atomic Absorption Spectrophotometer. All samples were washed three times in distilled, deionized water. Two tenths of a gram of sample was dissolved using concentrated HCl diluted to 10%, and distilled, deionized water was added to give 100ml of solution. A like amount of ultrapure $CaCO_3$ was added to standards. Each analysis was performed at least twice. Reproducibility for Fe analyses in dolomites are 2.5% or better, for Mn and Mg in dolomites 5% or better, for Cu in calcites 2.5% or better.

Water content of some samples was determined by heating samples and measuring the amount of water evolved. Powdered samples were weighed into platinum boats, oven dried at 110°C overnight, and reweighed to determine amount of adsorbed water. Samples were then placed in a dry air stream in a furnace at 1070°C for 30 minutes. Water was trapped in a glass collecting tube containing P_2O_5.

Mineral samples were ground or crushed by hand with a ceramic mortar and pestle. Since coarser particle sizes increase the optical path length and therefor the intensity of absorption features (see Chapter 3), samples were made as coarse-grained as was feasable. Because most scattering of light occurs at crystal-air boundaries light travels farther in coarse samples or non-porous rocks than in fine powders before it is scattered back to the detector. While this results in stronger absorption features in sample spectra which are dense or coarse-grained, light may pass through large, well-formed crystals or thin samples and be reflected off the sample holder as well as the sample. If sufficient material was available (a few grams) samples were crushed and wet-seived to give a fraction with particles ranging from 90 to 355μm. When smaller amounts of material were available, finer particle sizes were included in the sample to increase scattering and ensure

that all light reaching the detector had interacted only with the sample, and not with the sample holder.

Modern skeletal material was cleaned in H_2O_2 or sodium hypochlorite. Most samples were ground and bleached a second time, and spectra were taken of the powdered samples. Skeletal material was examined carefully to ensure that no material which had been altered (bored, micritized, or cemented) or coated by encrusting organisms was included in the samples.

Spectra of rock samples and of some mineral and skeletal samples were taken from whole samples on broken, sawed, or polished surfaces. Mention is made when whole samples were used, or when spectra were obtained from sands. Unless otherwise stated, spectra shown were obtained from powders.

Three different spectrophotometers were used to measure sample spectra. In general all reflection spectrophotometers consist of a light source, a mechanism such as a diffraction grating, prism, or circular variable filter to separate the light into different wavelengths either before or after it has interacted with the sample, and a detector which measures the intensity of the reflected light at different wavelengths.

The instrument on which the majority of the spectra were measured was built at the University of Hawaii and is described by Clark (1981), McCord _et al_. (1981), and Singer (1981). Much of the following discussion is taken from these sources. The instrument is designed to measure bidirectional reflectance (Hapke, 1981). It has a collimated light source, and light source and viewing mirrors are mounted on rocker arms to permit variations in viewing geometry. The light source is a 250-W quartz halogen bulb in an integrating sphere lined lined with Halon, and

is collimated by an f/8 off-axis parabolic mirror. A constant voltage power supply is used. The resulting beam is 5cm in diameter, and Clark (1981a) found the intensity of the light beam to be uniform to better than 2% over a 30mm diameter area. The moveable arms on which the light source and mirrors are mounted can be adjusted independently to $\pm 85^{\circ}$ of the vertical.

The instrument has a horizontally oriented sample holder assembly. A turntable with four positions, three for samples and one for the Halon standard, which can be rotated into the light beam was used to measure spectra of powders and small rock samples. Powdered samples were placed in holders made of the black plastic Delrin which has a flat spectrum with reflectance of about 20%. To measure spectra of large rocks the turntable was removed. An environment chamber described by Clark (1981a) can be used to take spectra of samples at liquid or solid nitrogen temperatures. One spectrum of Iceland spar was obtained in this way. The area of sample viewed by the spectrometer ranged from 2 to 5mm in diameter, depending on the aperture used.

The sample is imaged at the focal plane of the instrument using a 10.8cm diameter Cassegrain telescope operating in the inverted mode, and a series of flat mmirrors arranged in pairs to reflect in perpendicular planes to cancel mirror-induced polarization.

The visible and near-infrared portions of the spectrum are measured by continuously spinning circular variable filters (CVFs). The visible CVF covers the spectral interval from 0.35 to 1.0μm, the near infrared CVF from 0.6 to 2.55μm, giving an area of overlap. The infrared CVF consists of two 180° segments covering the regions 0.65 to 1.35μm and 1.32 to 2.60μm. These were obtained from Optical Coating Laboratory, Inc. Spectral resolution is about 1.5% throughout the spectral range.

Filters and detectors (a quatrz photodiode for the visible, an indium antimonide detector for the near infrared) were cooled to liquid nitrogen temperatures. For each revolution of the CVF, the incoming signal is compared to the signal from a black reference 240 times. Detector signal is converted to a pulse train by a V/F converter for digital processing. The difference in signal is counted, computed, and stored in the data system memory. The sum of two complete chop cycles makes one spectral channel, giving 120 data channels. An optical encoder monitors the position of the CVF and the black beam chopper is phase-locked to the CVF rotation to ensure that each channel corresponds to the same wavelength for each revolution. Wavelength calibration is checked at the beginning of each day with a narrow band pass filter. Data is stored on digital magnetic tapes along with sidereal and local times, object names, and any other information the operator wishes to record.

The other two instruments are commercially available ones - a Beckman DK-2A Ratio-Recording Spectroreflectometer and a Perkin-Elmer Model 330. The Beckman DK-2A, which is part of John Adams' laboratory at the Geology Department at the University of Washington in Seattle, uses a photomultiplier tube for the 0.35 to 0.6μm range, and a PbS detector for the 0.6 to 2.5μm range. Detectors were not cooled. The Perkin-Elmer 330, part of the facilities at the Remote Sensing Center at University of Massachusetts at Amherst headed by Robert Huguenin, has a photomultiplier tube for the 185 - 930nm range, and a PbS detector for the 850 - 2600nm range. The PbS detector is cooled to -30°C by a thermoelectric cooling device packaged in the detector case. The instrument uses a monochrometic light source with a double monochrometer holographic grating. Both commercial instruments have integrating spheres which allow light scattered from the sample in all directions to be measured

(directional-hemispherical reflectance, Hapke, 1981). The use of an integrating sphere somewhat reduces the flexibility of the instrument as samples must be in some form (e. g., a powder covered with a glass slide, or a small, flat rock slab) which can be held against a small hole in the side of the integrating sphere. Viewing geometries cannot be varied.

Halon, a fluorocarbon manufactured by Allied Chemical Corporation, which is close to a perfect diffuse reflector in this wavelength region (Venable et al., 1976; Weidner and Hsia, 1981), was used as a standard with all three instruments. Reflectance of Halon is 99% or higher in the 0.35 to 1.8μm region. The powder doesn't absorb or adsorb water, and its spectrum is nearly flat in the 0.2 to 2.5μm range, with the exception of a weak absorption feature near 2.15μm (Weidner and Hsia, 1981).

When spectra were taken with the University of Hawaii instrument, samples were viewed at a phase angle of 10°, with either the light source or the mirrors at the vertical. This viewing geometry was chosen to maximise the intensities of absorption bands while avoiding back-scatter effects. Each spectrum is an average of several separate observations of each sample. The near infrared spectra are averages of five runs, each run consisting of two complete revolutions of the CVF. The visible spectra are averages of three runs each with ten revolutions per run. Since carbonate samples are generally quite bright, long integrating times are not needed. Errors, plus or minus one standard deviation of the mean, are generally less than 0.2%.

The spectrum of the Halon standard was measured before and after each sample spectrum. Data were reduced using spectrum processing routines described by Clark (1980). Sample spectra were ratioed to the

Halon spectrum, and a correction was made for the fact that halon has a small absorption feature near 2.15μm, giving a result felt to be within a few per cent of absolute bidirectional reflectance (Singer, 1981). Vertical axes of spectra are thus labelled "absolute reflectance". Where spectra have been offset vertically, e.g. by continuum removal or to create stacked plots, vertical axes are labelled "relative reflectance".

Precise band positions, intensities, and widths were determined using our GFIT (Gaussian Fitting Program) routine which was adapted from the work of Kaper et al. (1966) and is described by Farr et al. (1980), and Clark (1981b). This routine fits gaussian functions to all absorption bands simultaneously, quantitatively specifying their positions, widths, and depths.

Spectra from the Beckman DK-2A are single runs. No errors are given. A program written by Ted Roush was used to translate data from this instrument to our format. Data taken with this instrument consistently gives band positions which are 0.025μm shortward of those determined by the University of Hawaii instrument (Roger Clark, Michael Gaffey, personal communication). Correction was made by adding 0.025μm to the wavelength files for these data so that data from the two instruments could be compared. Data from the Perkin-Elmer 330 appears to be directly comparable to that taken with the University of Hawaii instrument, although this has not been investigated in detail.

Spectra taken with the Perkin-Elmer 330 are averages of three runs each in the visible and near-infrared, but errors are not included.

Spectra of nearly all samples were measured on the University of Hawaii instrument. These spectra were used for detailed mineralogical studies. Spectra of some samples were measured on the other two

instruments, which have greater resolution and extend to slightly shorter wavelengths that the University of Hawaii instrument. When spectra from either of the commercial instruments are used in the ensuing discussion, specific mention will be made. Unless otherwise stated, the spectra shown were obtained with the University of Hawaii instrument.

CHAPTER 3

Spectral Properties of Calcite, Aragonite, and Dolomite

INTRODUCTION

Spectral reflectance in the visible and near infrared (0.35 to 2.55μm) offers a rapid, inexpensive, nondestructive technique for determining the mineralogy and something of the minor element chemistry of the hard-to-discriminate carbonate minerals, and can, in one step, provide information previously obtainable only by the combined application of two or more analytical techniques. The technique has been used by mineralogists and igneous and metamorphic petrologists for more than a decade to study pyroxenes and olivines, and to a lesser extent feldspars and other mineral groups (e. g., Adams, 1975; Burns, 1970; Runciman et al., 1973). Previous work has shown that reflectance spectra of carbonate minerals in the visible (VIS) and near infrared (NIR) show a variety of features which are caused by overtones and combination tones of the fundamental internal and lattice vibrational modes of the carbonate radical, and by electronic processes within the unfilled d-shells of transition metal cations if present (Adams, 1975; Hexter, 1958; Hunt and Salisbury, 1971). However, as yet no systematic attempt has been made to relate these spectral features to the mineralogical and chemical composition of carbonate rocks and minerals.

Considerable work has been done with transmission and reflection spectra of carbonates in the mid-infrared (5 to 15μm) region (MIR) where absorption features caused by the fundamental vibrational modes occur. Spectra in this region have been used to study the structure of carbonate minerals (Adler and Kerr, 1962, 1963a,b; Gatehouse et al., 1958; Hexter and Dows, 1956; Scheetz and White, 1977; Schroeder et al., 1962; Weir and Lippincott, 1961; and many others), and some efforts have been made to use spectra in this region for mineralogical and petrographic studies of carbonates (Adler and Kerr, 1962; Chester and Elderfield, 1966, 1967; Farmer and Warne, 1978; Hovis, 1966; Huang and Kerr, 1960; Hunt et al., 1950; Keller et al., 1952; White, 1974). However, spectra in this region do not contain features directly attributable to transition metal ions such as Fe^{2+} and Mn^{2+} which are of considerable importance in studies of the deposition and diagenesis of carbonates. In addition, reflectance spectra in the VIS and NIR are more easily obtained than those in the MIR. Transmission spectra in the MIR are most readily obtained from material which has been ground to a powder and pressed into alkali halide pellets or discs. Particle size effects in both transmission and reflection spectra in the MIR can cause significant variations in spectra which are unrelated to mineralogy or chemical composition of the samples (Estep-Barnes, 1977; Farmer and Russell, 1966; Russell, 1974; Tuddenham and Lyon, 1960). Spectra in the VIS and NIR, on the other hand, may be obtained from samples in any form: powders, sands, and broken, sawed or polished rock surfaces. Thus, while transmission studies in the MIR, where the fundamental modes occur, are preferable for structural studies, reflectance spectra in the VIS and NIR are more suitable for petrographic work.

This chapter will deal with spectra of the three most common carbonate minerals, calcite, aragonite, and dolomite, and will describe the changes in spectral properties which reflect changes in crystal structure (calcite to aragonite) and chemical composition (calcite to dolomite). Changes in spectral properties with mineralogy will be dealt with more extensively in Chapter 4, and changes with chemical composition of common calcite group minerals will be dealt with quantitatively in Chapter 5.

CARBONATE MINERALS

Carbonate minerals consist of the carbonate (CO_3^{2-}) ion and a cation with a charge of +2. Anhydrous carbonate minerals are of two basic structral types - The rhombohedral or calcite group minerals and the orthorhombic or aragonite group minerals.

The rhombohedral carbonates may be thought of as consisting of layers of cations and layers of carbonate ions alternating along the c-axis (Lippmann, 1973; Reeder, 1983). Figure 3.1 shows the rhombonedral unit cell for calcite. X-ray diffraction studies show that C - O bond lengths in all carbonate group minerals are very similar (≈1.284 Angstroms, according to Effenberger _et al._, 1982) and that the carbonate group forms a rigid unit in the form of an equilateral triangle with the carbon in the center and the oxygens at the corners. (Lippmann, 1973; Reeder, 1983). Cations are in six-fold coordination, the six oxygens forming an octahedron which is slightly elongated along the c-axis, so that the O - O lengths parallel to the basal plane are less than those inclined to the base (Lippmann, 1973).

The structure of dolomite, and some other double carbonates, is similar to that of calcite. The unit cell for dolomite is shown in Figure 3.2, where it can be seen that every other cation layer is composed

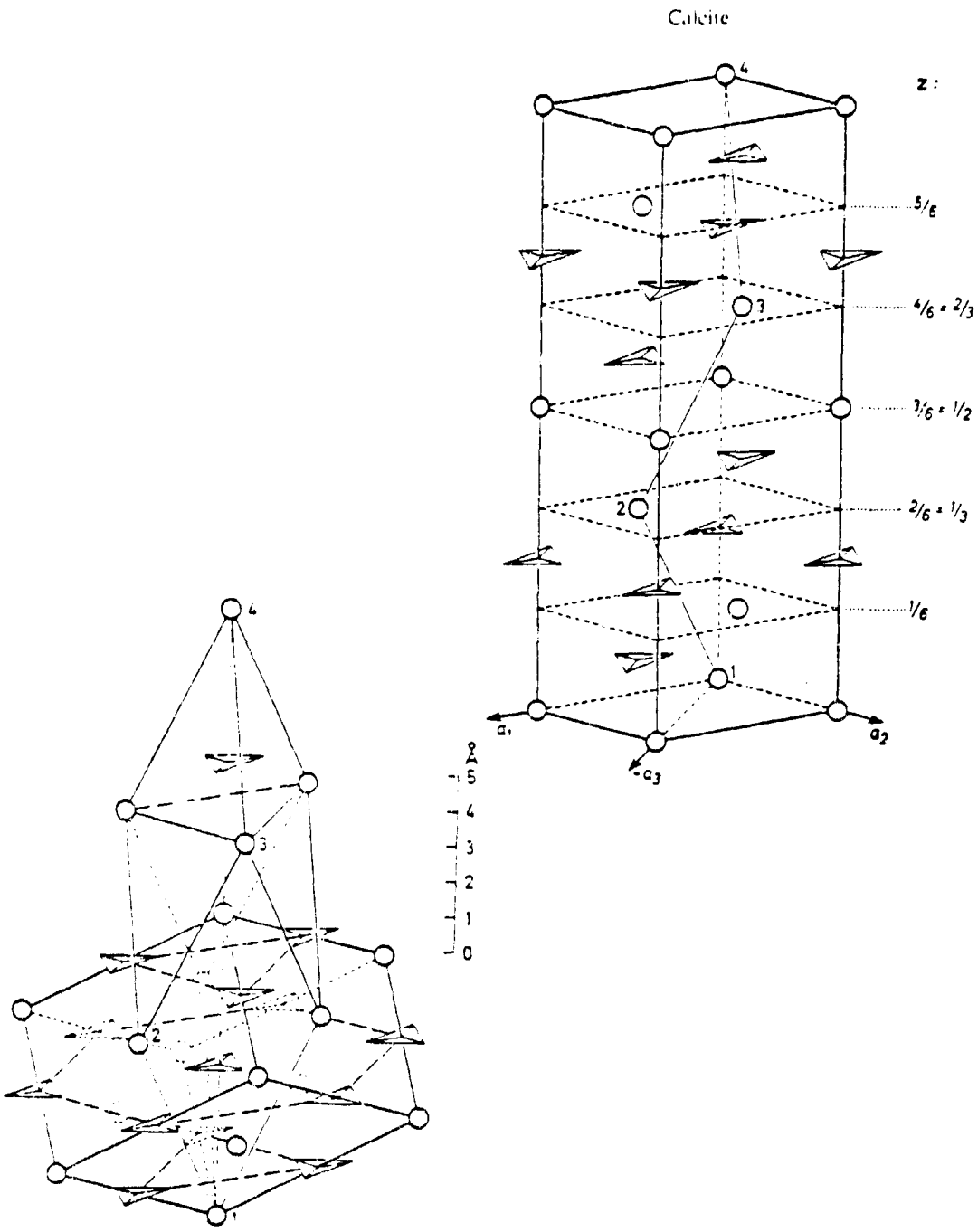

Figure 3.1 Rhombohedral and hexagonal unit cells for calcite. From Lippmann (1973, p.10-11). Ca atoms - open circles, Triangles - CO_3 groups.

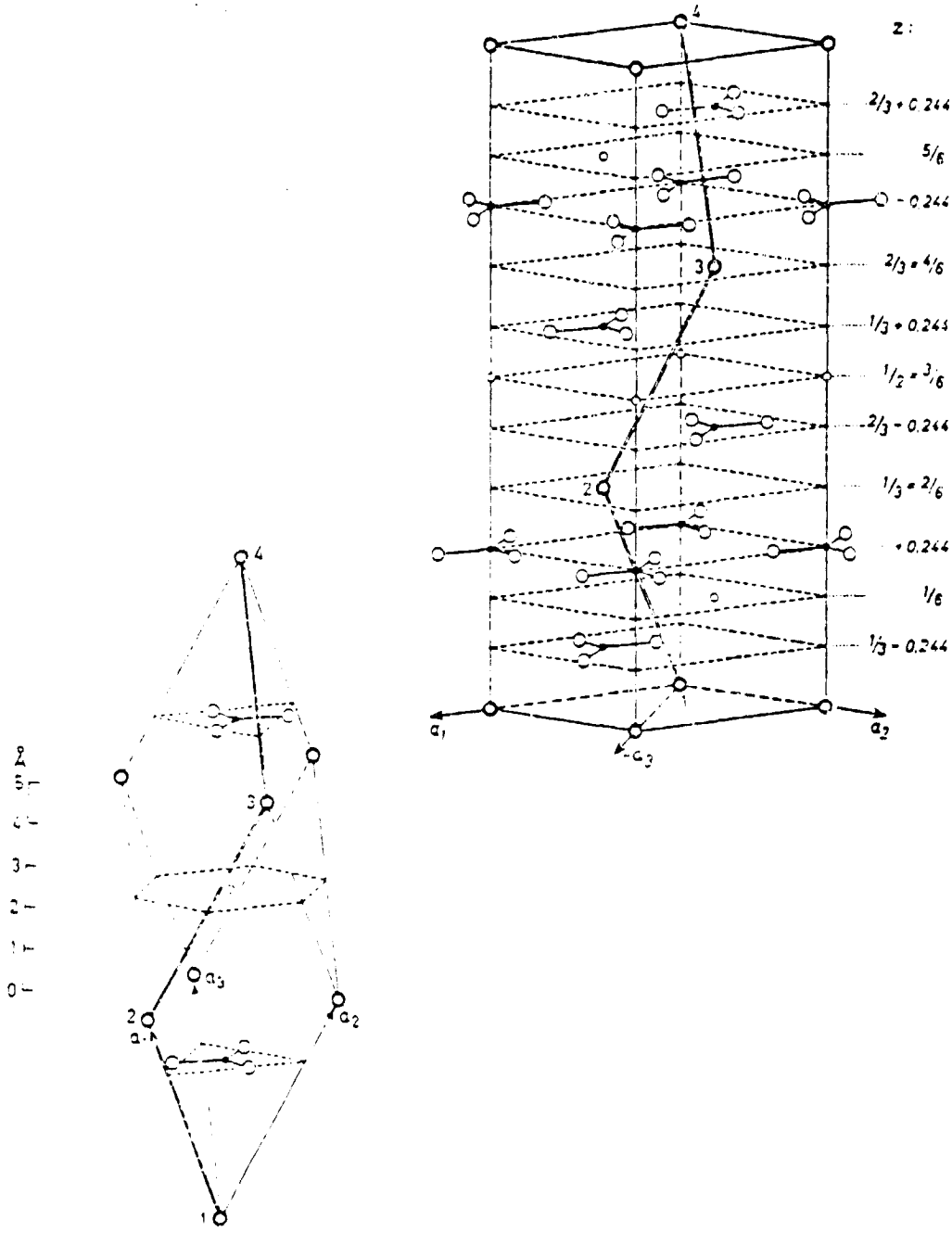

Figure 3.2 Rhombohedral and hexagonal unit cells for dolomite. From Lippmann (1973, p.22-23). Open circles - Ca, O, and Mg in order of decreasing size. Small closed circles - C. The Ca atoms marked 1, 2, 3, 4 show positions of rhombohedral unit cell with respect to the hexagonal cell.

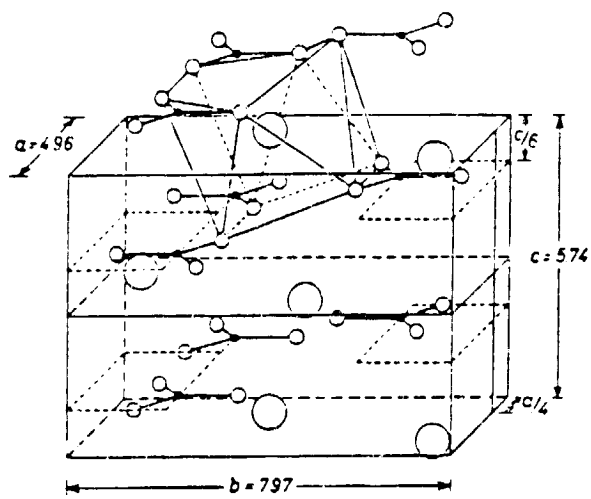

Figure 3.3 Unit cell for aragonite, showing coordination polyhedron for calcium. From Lippmann (1973, p.57). Large circles - Ca, Small circles - O, Dots - C.

of magnesium ions rather than calcium ions (Lippmann, 1973). The cations in dolomites also reside in octahedral sites, but there are now two sites, the A-site, occupied by calcium, and the B-site, occupied by magnesium (Reeder, 1983). For more detail on the structure of carbonate group minerals, the reader is referred to Lippmann (1973) and Reeder (1983).

Aragonite group minerals are orthorhombic. The difference in structure between calcite and aragonite group minerals is generally attributed to the difference in cation size, calcium being of intermediate size and therefore able to fit into either structure (Huribut and Klein, 1977).

Like calcite, aragonite is made up of alternating layers of calcium ions and carbonate groups. However, unlike calcite, the layers in aragonite, as described by Speer (1983), are not planar. In the cation layers, alternating atoms are displaced by about 0.05 Angstroms out of the plane. Carbonate groups form two distinct types of "corrugated" layers with differing displacements of carbonate groups parallel to the c-axis. Figure 3.3 shows the unit cell of aragonite, and the coordination polyhedron around the cation which is composed of nine oxygens. The carbonate group in aragonite has very nearly the same shape and dimensions as the carbonate group in calcite, although the carbon atom is displaced slightly out of the plane of the oxygens toward the nearest calcium atom (Speer, 1983). Speer (1983) reviews what is currently known about the crystal structure and chemical composition of the aragonite group minerals.

RESULTS

Carbonate Bands

Figure 3.4 shows spectra of the three most commonly occurring carbonate minerals: calcite, aragonite, and dolomite. Spectra of powders of carbonate minerals containing no transition metal cations are nearly straight lines near unity reflectance at wavelengths shorter than 1.6μm. At wavelengths greater than 1.6μm there is a series of absorption features which increase in intensity with increasing wavelength. These bands are due to vibrational processes of the carbonate radical (Hexter, 1958; Hunt and Salisbury, 1971; Matossi, 1928; Schroeder *et al.*, 1962).

Although the three spectra shown in Figure 3.4 are grossly similar, inspection reveals differences. At the shortest wavelengths, the aragonite spectrum has a marked drop-off toward the ultraviolet. The drop-off in the dolomite spectrum is less pronounced, and is nearly absent in the calcite spectrum. Inspection of the spectra shows that the deepest band in the dolomite spectrum appears to occur at slightly shorter wavelengths than the same band in the calcite spectrum. Note that in Figure 3.4 this band (centered at ≈2.5μm) in the dolomite spectrum has its lowest point at the third channel from the end of the spectrum, but the same band in calcite has its lowest point at the second channel from the end. The calcite and dolomite spectra have a shelf-like feature at ≈2.0μm (indicated by an arrow in the dolomite spectrum), while the aragonite spectrum shows a smoother drop-off in this region.

These and other differences in the carbonate bands in spectra were studied quantitatively using the GFIT program. Because these and other spectra were approximately straight lines at short wavelengths, a straight line continuum was selected and removed from the spectrum by

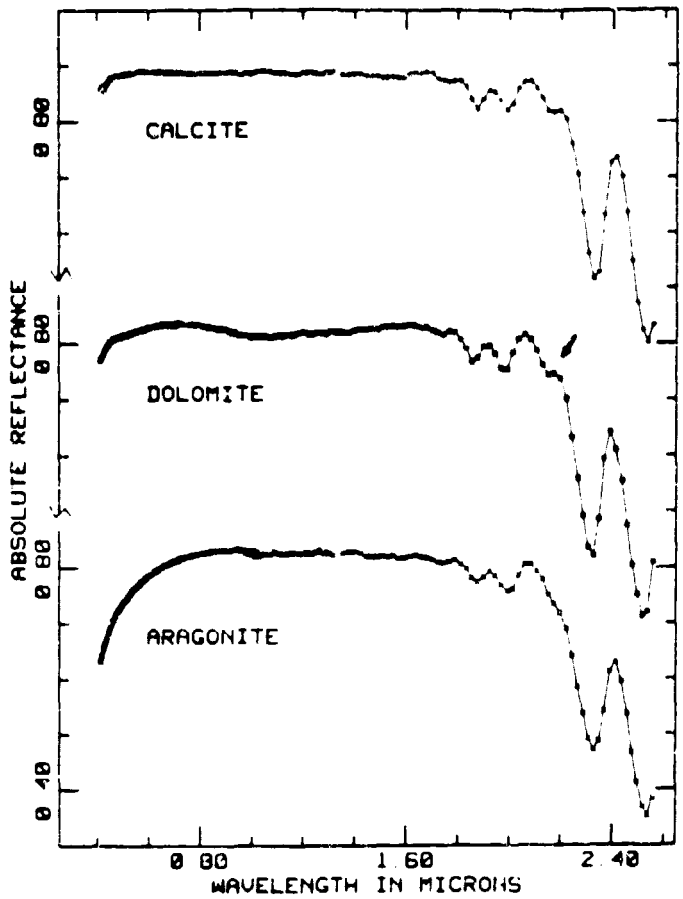

Figure 3.4 Spectra of the three most commonly occurring carbonate minerals: calcite, aragonite, and dolomite.

division, leaving only the absorption bands. Gaussian curves were then fit in energy space with band intensities on a log scale. Several (four or more) continua with slightly different slopes were divided into each spectrum, and the result fitted. One of these fits is shown in Figure 3.5. The best fit was selected on the basis of the errors (residual errors for each data point, errors in band position for each band, and errors in the integrated intensities of the gaussians, i.e., the width times the height) and examination of plots of the data and fits. Figures 3.6a and b show an example with the original data, the different continua tried, and the data with the continuum which gave the best fit. As can be seen the continuum which gave the best fit coincides quite closely with the straight-line portion of the spectrum shortward of 1.6μm. This was generally true, and would seem to indicate that the straight line continua have some physical as well as mathematical meaning. Slopes of continua varied somewhat from one mineral sample to another, and showed no correlation with mineral type. All were close to the horizontal.

As mentioned above, several continua were used with each spectrum and band positions were determined for each. For a single mineral spectrum, continua with different slopes for which a fit could be achieved in GFIT gave slightly different band positions. However, as Figure 3.7 shows, differences in band position due to variations in continuum slope are generally much smaller than differences in band position between different samples of the same mineralogy, and are significantly smaller than differences in band positions due to differences in mineralogy (compare Fig. 3.7 to Fig. 3.13). Figure 3.7 shows positions of centers of band 1 plotted vs. the positions of centers of band 2 for all fits achieved for nine different spectra - three aragonites, three dolomites,

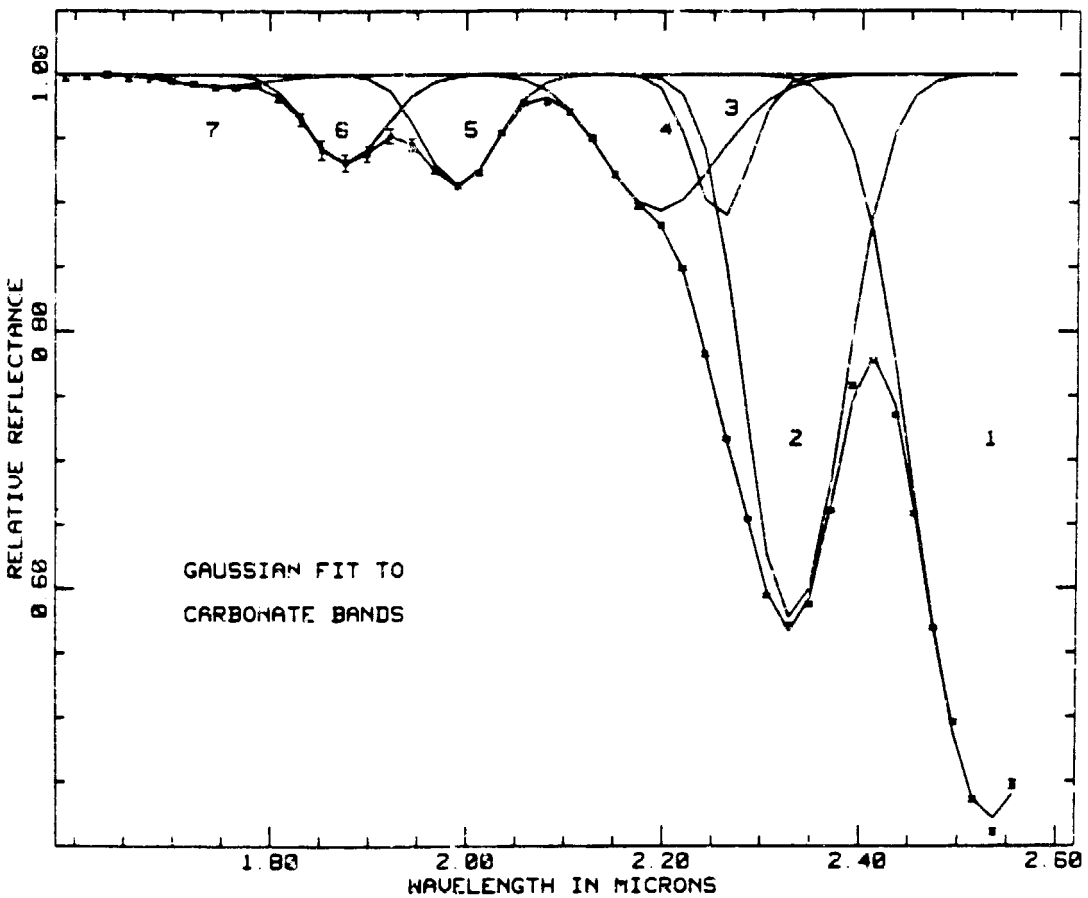

Figure 3.5 Gaussian fit to carbonate bands in aragonite spectrum.

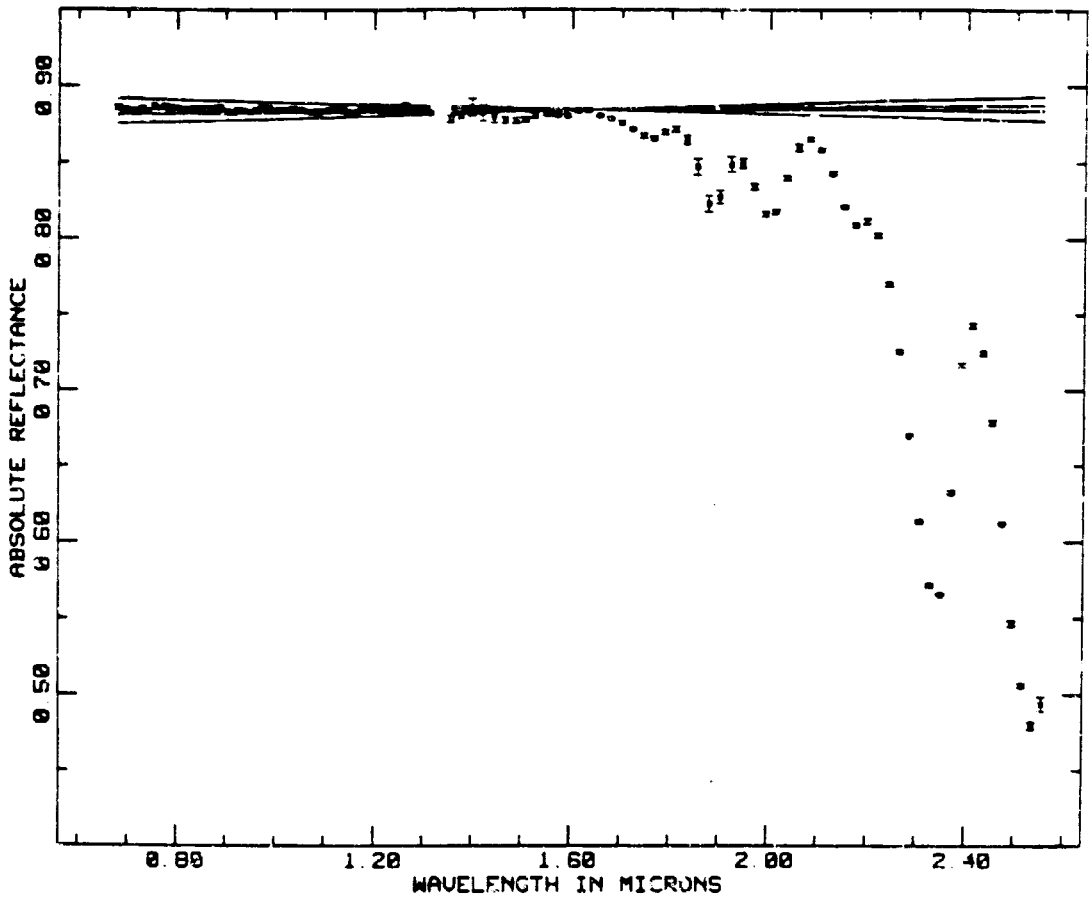

Figure 3.6a Plot of original data (dots) and the different continua divided out of the data for gaussian fitting (lines).

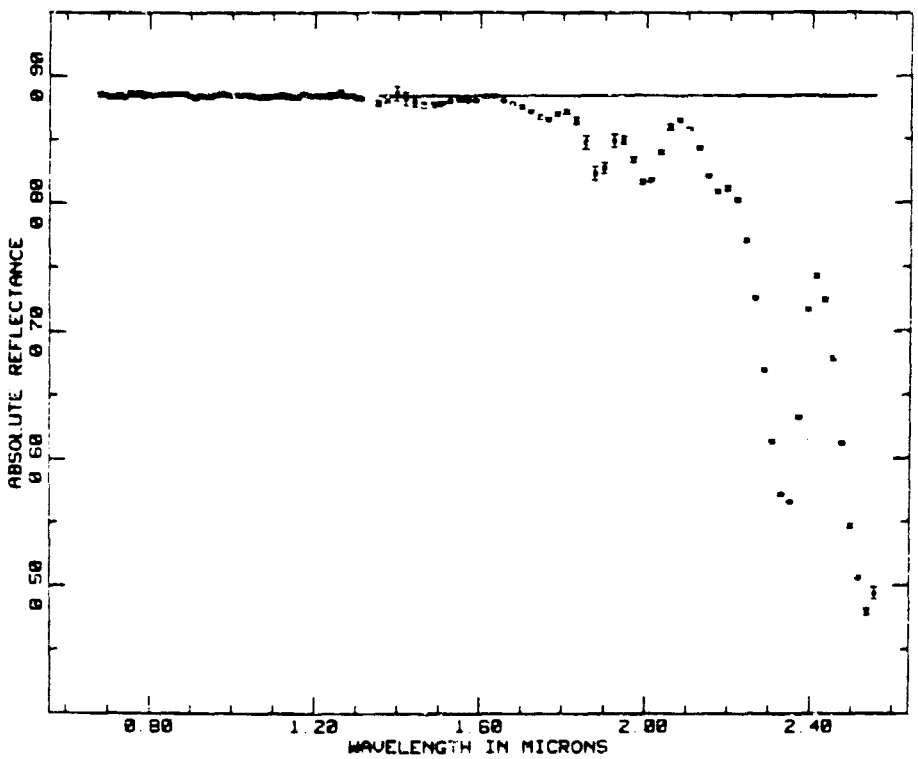

Figure 3.6b Plot of original data (dots) and continuum which gave the best fit (line).

OF POOR QUALITY

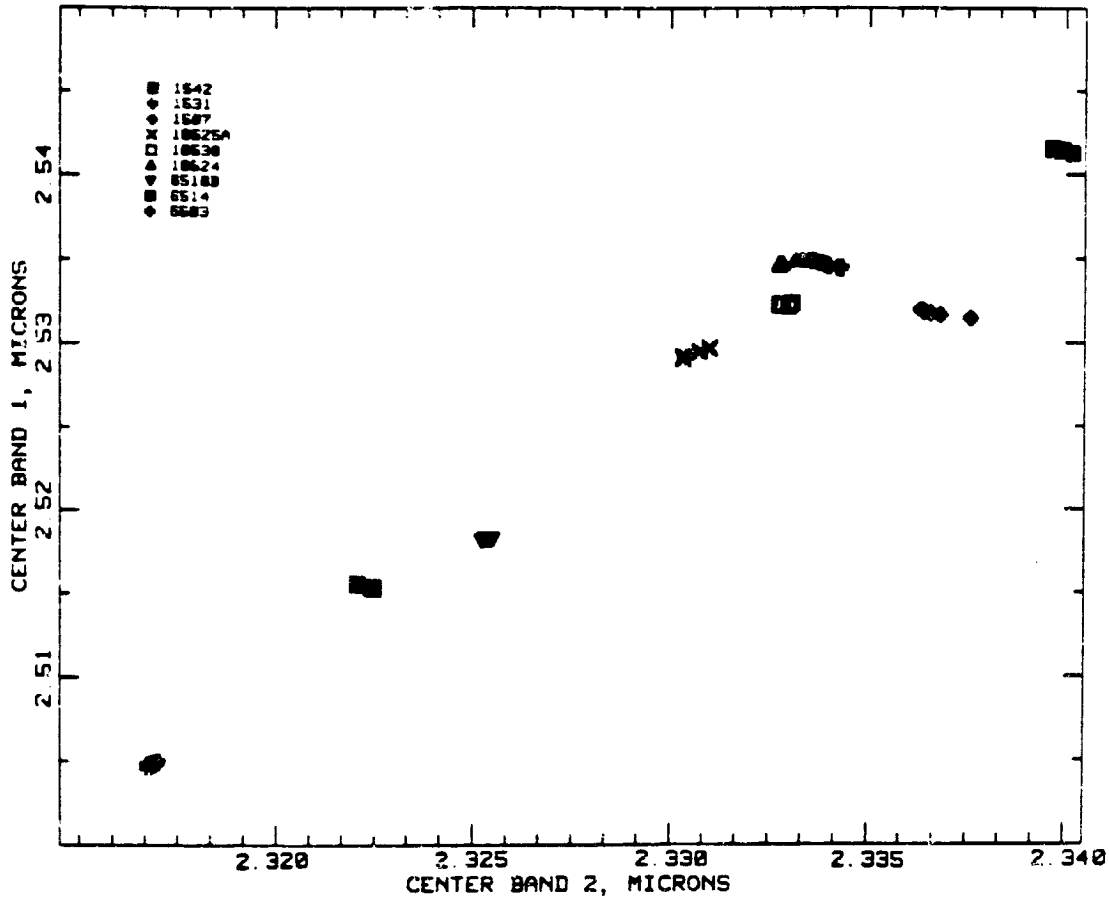

Figure 3.7 Centers of band 1 plotted vs. centers of band 2 for all fits achieved for nine different spectra. Each dot represents a band center determined for one continuum. Although overlap of symbols makes some of them difficult to distinguish, between four and nine points are plotted for each sample, depending on the number of continua tried.

Calcites

1507 Pine Pt., Canada[1]

1530 Ultrapure $CaCO_3$ powder, Alfa Division, Ventron[2]

1531 Iceland spar, Chihuahua Mexico[3]

1542 Egremont, England[4]

6506 Prairie du Chien Fm., Allamakee Co., Iowa

10519 Mexico[5]

Aragonites

10530 Bilin, Bohemia[4]

10525A Molina de Aragon, Spain

10524 Spain

Dolomites

2501 Styria, Austria[6]

5501 Gilman, Colorado[7]

6503 Bahia, Brazil[8]

6509 Deep Springs, Inyo County, Calif.[9]

6510b Bamle, Telemark, Norway[9]

6514 Binnenthal, Valais, Switzerland[10]

1. Smithsonian Inst. #122283; 2. Alfa Div., Ventron, 152 Andover St., Danvers, Ma.; 3. Wards Natural Science Establishment; 4. Geology Dept., Univ. of Iowa, Iowa City, Iowa; 5. Rainbow Collection, Honolulu, HI.; 6. Smithsonian Inst. #B9764; 7. Smithsonian Inst. #R15143; 8. Smithsonian Inst. #103165 9. Minerals Unlimited, Ridgecrest, Calif.; 10. British Museum #1912,133.

Table 3.1 Numbers and localities of samples used in this study.

and three calcites. Each dot represents a band center determined for one continuum. There are between four and nine points plotted for each samle, depending on the number of continua tried. Samples 1542, 1531, and 1507 are calcites, 10525a, 10530, and 10524 are aragonites, and 6510b, 6514, and 6503 (the last two represented by squares and crosses in the lower left-hand portion of the graph) are dolomites. Table 3.1 lists the samples discussed in this chapter, and the localities from which they were obtained.

The effects of grain size on spectral properties can be seen in Figure 3.8, which shows the spectra of some of the size fractions of calcite sample 1531 listed in Table 3.2. These spectra show that the only spectral parameters which vary with grain size are overall brightness of the sample and absolute band intensity. Number of bands, band positions and widths, and relative band intensities do not change. This was verified by GFITting these spectra.

Fitting of curves in GFIT was done with a vertical scale of the logarithm of the intensity. This is in accordance with Lambert's Law, which states that if I_o is the original light intensity, I the intensity of the light after passing through a thickness x of a mineral whose absorption coefficient is k, then

$$I = I_o e^{-kx}$$

Figure 3.9 is a plot of the natural log of spectra of the 53-63μm fraction plotted against the natural log of the 355-500μm fraction of sample #1531, two of the different particle size fractions shown in Figure 3.8.

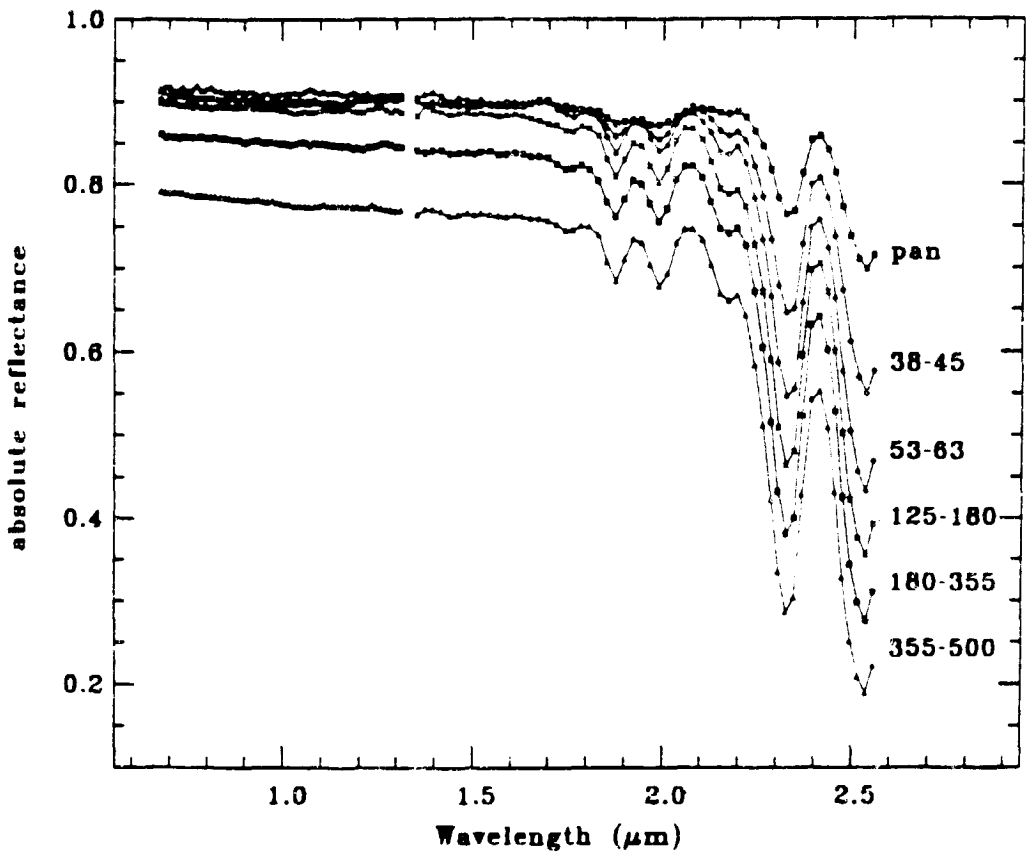

Figure 3.8 Spectra of different grain size fractions obtained by grinding and wet seiving an Iceland spar sample (#1531).

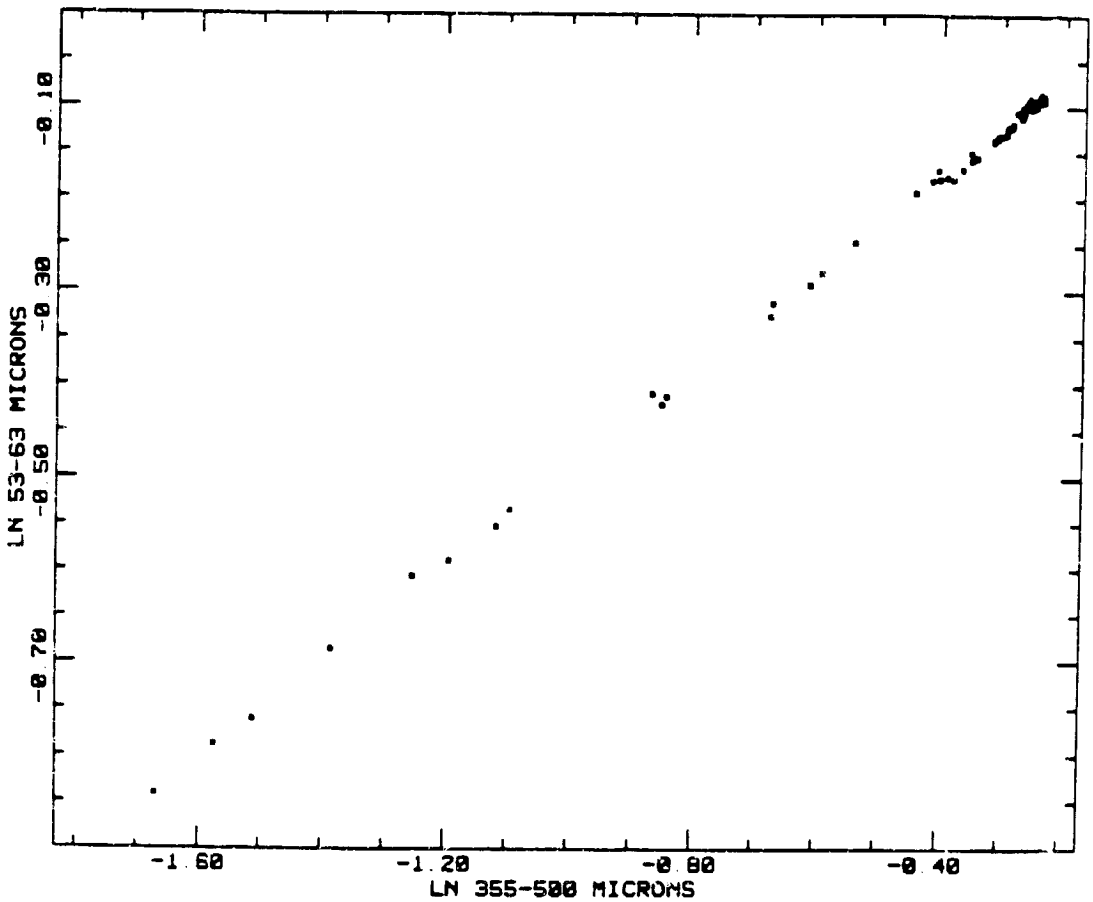

Figure 3.9 Natural log of the spectrum of the 53 - 63μm fraction plotted as a function of the natural log of the 355 - 500μm fraction of sample #1531.

500 - 1000
355 - 500
180 - 355
125 - 180
90 - 125
63 - 90
53 - 63
45 - 53
38 - 45
pan

Table 3.2 Particle size fractions of sample #1531 in microns.

The ln-ln plots of these two particle size fractions as well as all other combinations tried, fall along a straight line, to a very good first approximation. This shows that absorption of light by carbonate minerals approximates that predicted by Lambert's Law, and lends support to the use of this particular model in studying absorption features in carbonates. The more commonly employed Kubelka-Munk model is strictly applicable only to weakly absorbing materials; strong absorbers show marked deviation from the theory (Wendlandt and Hecht, 1966). Clark and Roush (1984) found that this marked deviation from the predicted linear trend of the remission function of Kubelka - Munk theory occurs below values of relfectance of ≈64%.

Clark and Roush (1984) summarize other problems which result from attempts to apply Kubelka - Munk theory to these laboratory data. One problem mentioned by these authors is that for K - M theory to be strictly valid, bihemispherical reflectance must be measured. The University of Hawaii spectrophotometer with which these data were taken measures bidirectional reflectance. Bidirectional reflectance is also measured when remotely sensed data are taken. Clark and Roush (1984) also note that K - M theory assumes isotropic scattering, and ignores mutual shadowing of particles, assumptions which limit the applicability of this theory to geologic problems.

Clark and Roush (1984) also present discussions of other theoretical models describing absorption and scattering of light by particulate media, and the advantages and difficulties inherent in each.

Another factor affecting both the absolute intensities of spectral features, and the overall brightness, or albedo, of the samples, is porosity or packing of the sample. Figure 3.10 shows two spectra of the same sample, in powdered and whole form. The sample is a coarse

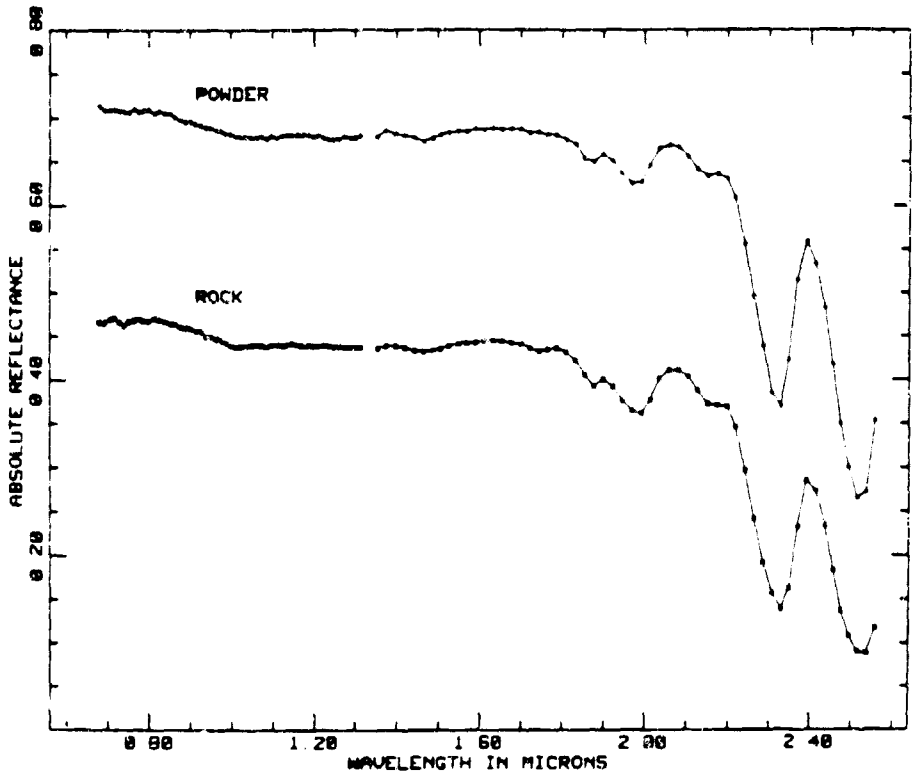

Figure 3.10 Two spectra obtained from the same dolomite sample (#6509) in powdered and whole form.

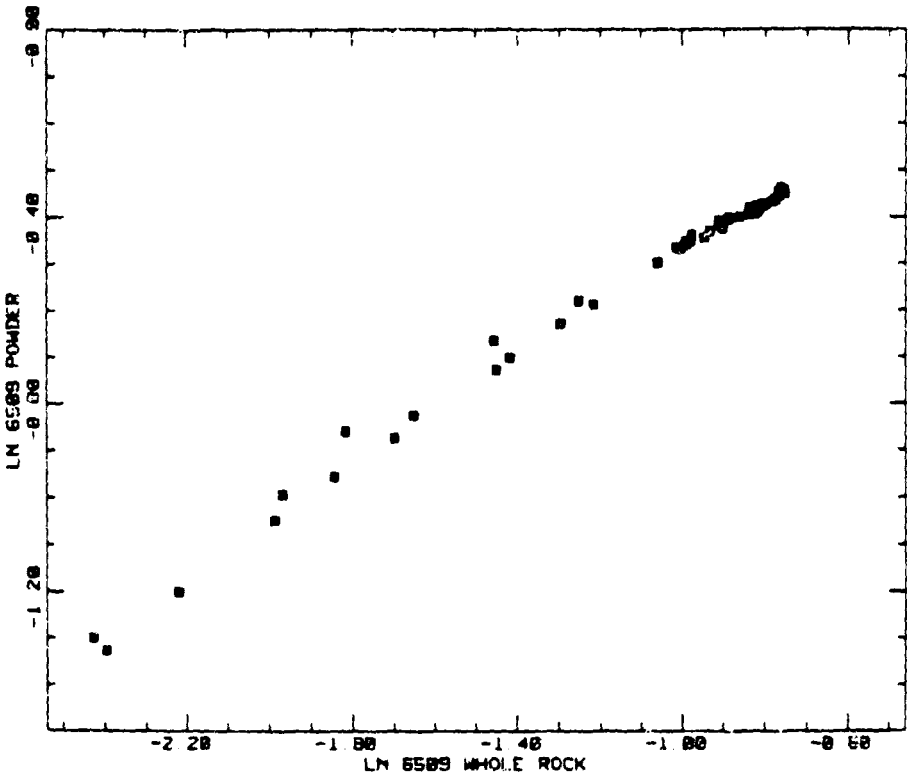

Figure 3.11 Ln - Ln plot of the two dolomite spectra shown in preceding figure.

Sample #	Band Number 1	2	3	4	5	6	7
Calcites							
1507	2.532	2.337	2.265	2.171	1.995	1.882	1.756
1530	2.530	2.334	2.254	2.169	1.995	1.881	1.762
1531	2.535	2.333	2.261	2.167	1.991	1.876	1.763
1542	2.541	2.340	2.272	2.179	1.998	1.885	1.758
6506	2.535	2.334	2.263	2.174	1.974	1.871	1.753
10519	2.533	2.334	2.259	2.169	1.979	1.875	1.770
Dolomites							
2501	2.508	2.313	2.234	2.155	1.971	1.872	
5501	2.513	2.323	2.244	2.150	1.975	1.882	
6503	2.505	2.312	2.235	2.157	1.971	1.853	1.735
6509	2.516	2.320	2.248	2.165	1.974	1.869	
6510b	2.518	2.322	2.247	2.170	1.977	1.867	
6514	2.516	2.319	2.244	2.165	1.979	1.862	1.740
Aragonites							
10524	2.535	2.331	2.257	2.195	1.992	1.877	1.748
10525A	2.529	2.328	2.254	2.186	1.990	1.873	1.744
10530	2.532	2.332	2.258	2.201	1.993	1.874	1.737

Table 3.3 Band positions determined from GFIT routine in microns.

grained, dense dolomite (sample #6509). Only intensity of bands and overall brightness of the spectra are affected. The number of features, their form, positions, and relative intensities (intensity of a band in a spectrum relative to the intensity of other bands in the same spectrum) are not. A ln-ln plot of these two spectra is shown in Figure 3.11. Here the points also fall along a straight line. Thus Lambert's Law appears to describe absorption features in carbonates, regardless of the form of the sample (i.e., powder, rock, etc.)

Carbonates show seven vibrational bands in the NIR region of the spectrum (see Fig. 3.5). Table 3.3 lists the band positions determined in this study. Bands are labelled in order of decreasing intensity, the strong 2.5μm band being band 1. The broad, weak band 7 appears in some spectra to actually be composed of two bands. However, the resolution in this portion of the spectrum on our instrument made discrimination of these two bands possible in only a few of the spectra, so the two bands were fit as one. In spectra of some other samples, most notably the ferroan dolomites, band 7 was either absent or too weak for its position to be determined using GFIT, and no band positions are reported for band 7 for these samples.

In general, all of the bands in dolomite spectra are centered at shorter wavelengths than the equivalent bands in calcite spectra (see Table 3), although there is some overlap in the case of band 4. Band 5 in two of the calcite spectra (samples 10519 and 6506) occur at the shorter wavelengths typical of the spectra of dolomites. The positions obtained for band 5 in these two spectra by GFITting is ≈0.02μm shortward of that in the other calcite spectra. Reflectance spectra are extremely sensitive to the presence of water, which has a strong absorption feature at 1.9μm (Hunt and Salisbury, 1971). In the course of the

present study it was found that water, most probably in the form of fluid inclusions, is nearly ubiquitous in carbonate minerals and rocks. Absorptions due to water are discussed in detail in Chapters 6 through 8. The spectra of both these samples indicate minor amounts of water are present (a few hundredths of a per cent by weight as determined by heating the sample to 1000°C for one half hour and measuring the amount of water evolved). The strong, asymmetric absorption feature due to liquid water which occurs in the 1.9μm region probably causes the apparent shift of the measured band positions in these two samples to shorter wavelengths. In spectra of all of the dolomites studied except sample #5501 band 6 occurs at shorter wavelengths than the same band in calcite spectra. Band 7 is difficult to find in some dolomite spectra because this very weak feature occurs on the flanks of the iron bands which are two to three orders of magnitude wider than the carbonate bands. However, the limited data available indicate that band 7, like the other bands, occurs at shorter wavelengths than its calcite counterpart.

In addition, there is a shift in position of carbonate bands in dolomite with varying iron content. Figure 3.12 is a ratio spectrum of two dolomites, one containing 0.04 weight per cent Fe, the other 2.7 weight per cent Fe, showing the shift in the positions of bands 1 and 2 to longer wavelengths with increasing iron content. The spectrum of one dolomite was divided by that of another of similar grain size. If the band positions in the two spectra were the same, the result would be a smooth curve. The presence of peaks reflects the difference in position of the carbonate bands in the two spectra. This and other chemical variations are probably responsible for the scatter in band positions seen in Figures 3.13, 3.14, and 3.15. These trends will be dealt with in more detail in Chapter 5.

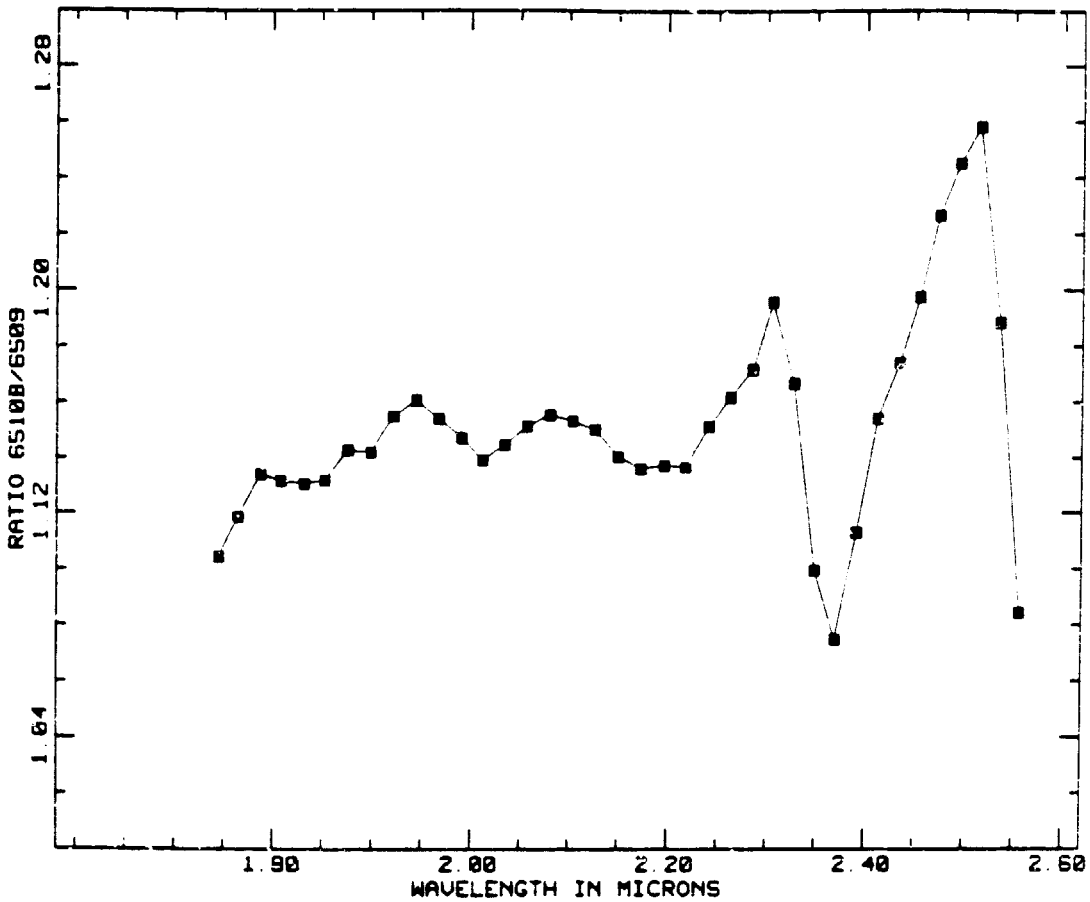

Figure 3.12 Ratio spectrum of two dolomites of different iron content reflecting shift in band position.

ORIGINAL PAGE IS
OF POOR QUALITY

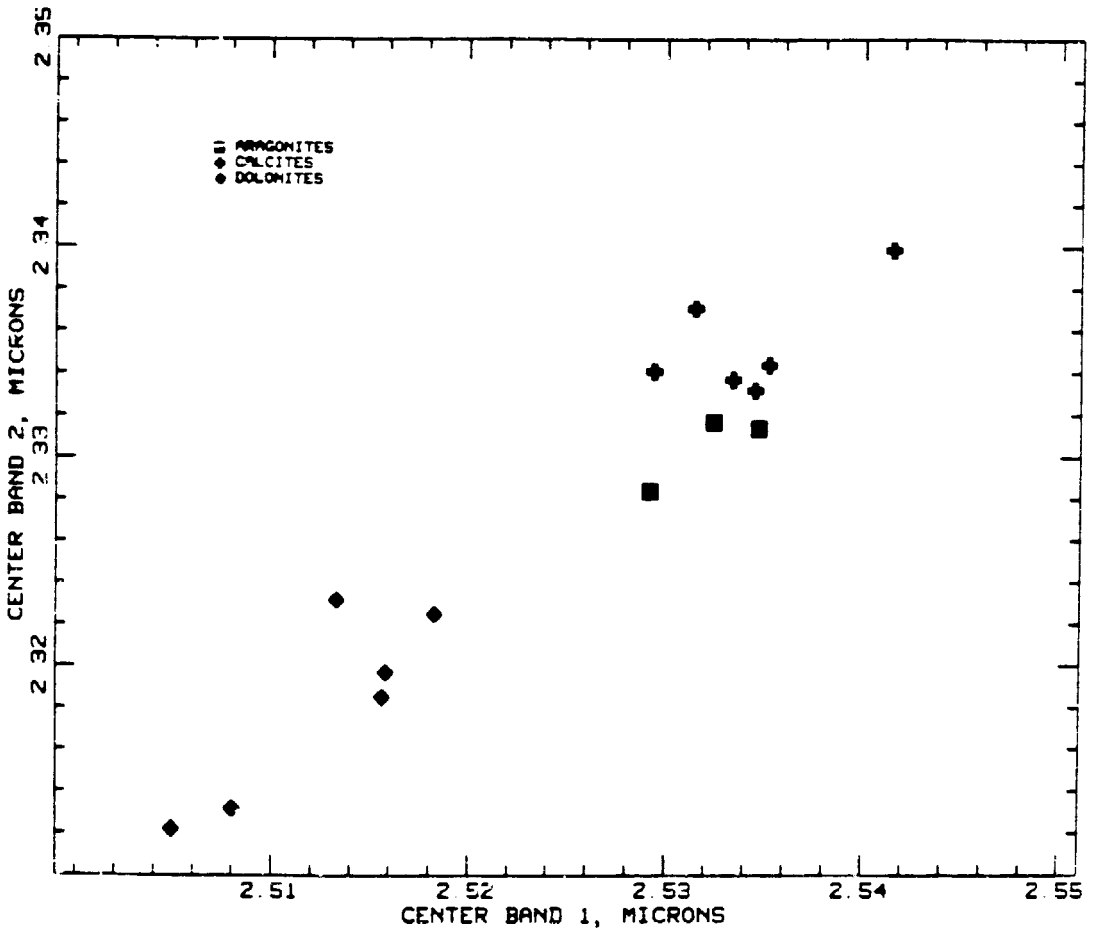

Figure 3.13 Position of center of band 2 plotted against the position of the center of band 1 in microns for each sample. Aragonites - squares, Calcites - crosses, Dolomites - diamonds.

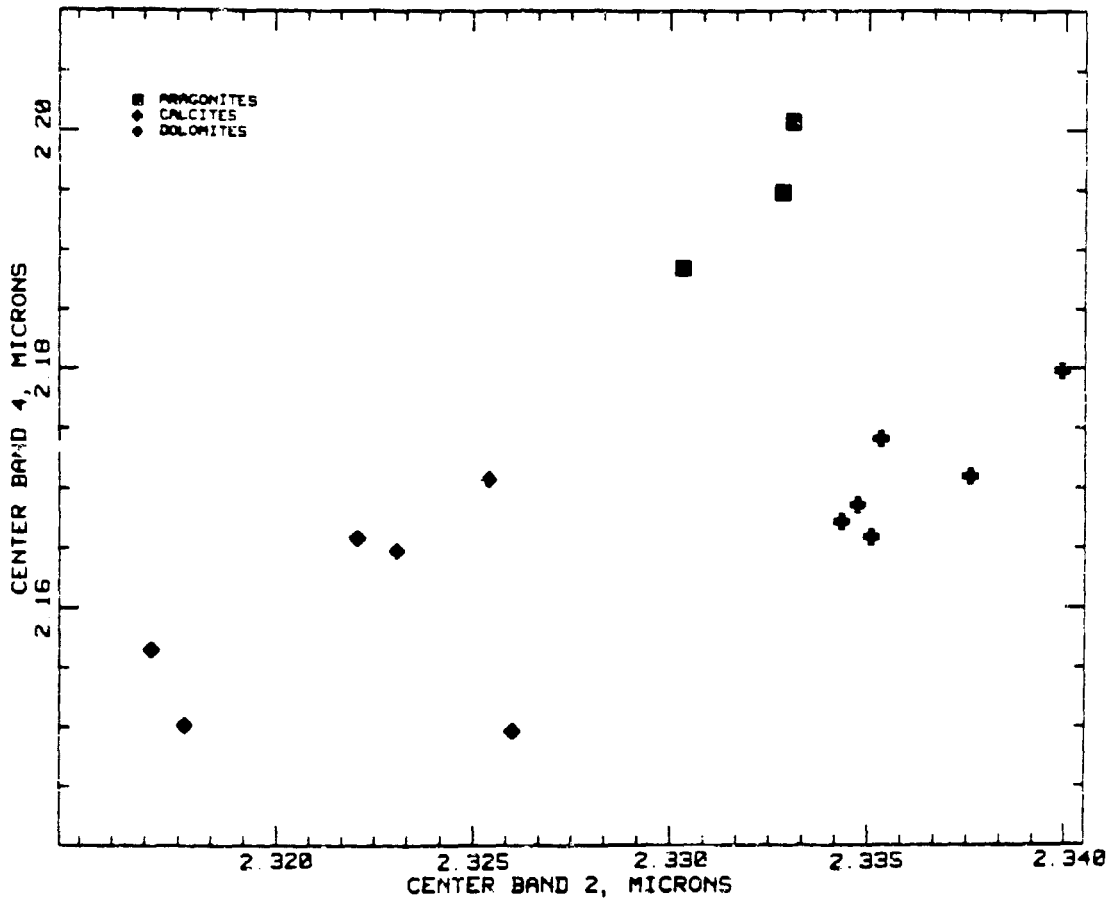

Figure 3.14 Position of center of band 2 plotted against that for band 4 for each sample. Aragonites - squares, Calcites - crosses, Dolomites - diamonds.

ORIGINAL PAGE IS
OF POOR QUALITY

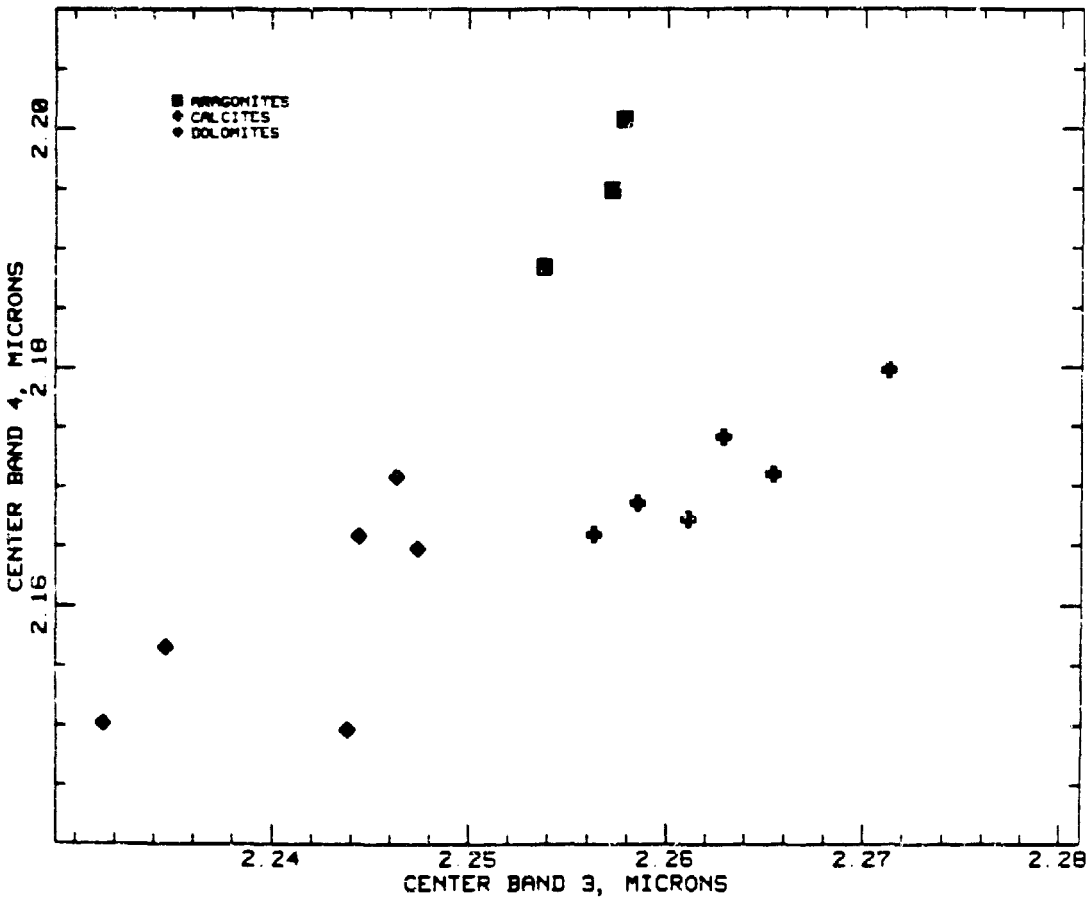

Figure 3.15 Position of center of band 4 plotted against that for band 3 for each sample. Aragonites - squares, Calcites - crosses, Dolomites - diamonds.

Sample #	Band Number 1	2	3	4	5	6	7
Calcites							
1507	0.0223	0.0154	0.0149	0.0170	0.0183	0.0190	0.0256
1530	0.0228	0.0168	0.0121	0.0288	0.0278	0.0229	0.0255
1531	0.0233	0.0157	0.0139	0.0210	0.0195	0.0206	0.0271
1542	0.0255	0.0161	0.0142	0.0252	0.0223	0.0193	0.0430
5506	0.0237	0.0164	0.0136	0.0268	0.0330	0.0246	0.0305
10519	0.0232	0.0163	0.0144	0.0235	0.0305	0.0241	0.0425
Dolomites							
2501	0.0218	0.0191	0.0138	0.0266	0.0322	0.0188	0.0178
5501	0.0223	0.0178	0.0109	0.0188	0.0233	0.0241	
6503	0.0221	0.0201	0.0099	0.0306	0.0341	0.0261	0.0330
6509	0.0208	0.0173	0.0104	0.0265	0.0218	0.0222	
6510B	0.0226	0.0187	0.0113	0.0310	0.0236	0.0226	
6514	0.0228	0.0186	0.0110	0.0281	0.0206	0.0234	0.0395
Aragonites							
10524	0.0243	0.0192	0.0130	0.0278	0.0218	0.0258	0.0351
10525A	0.0234	0.0197	0.0126	0.0256	0.0275	0.0240	0.0280
10530	0.0247	0.0196	0.0128	0.0296	0.0211	0.0252	0.0357

Table 3.4 Widths of carbonate bands in μm^{-1}.

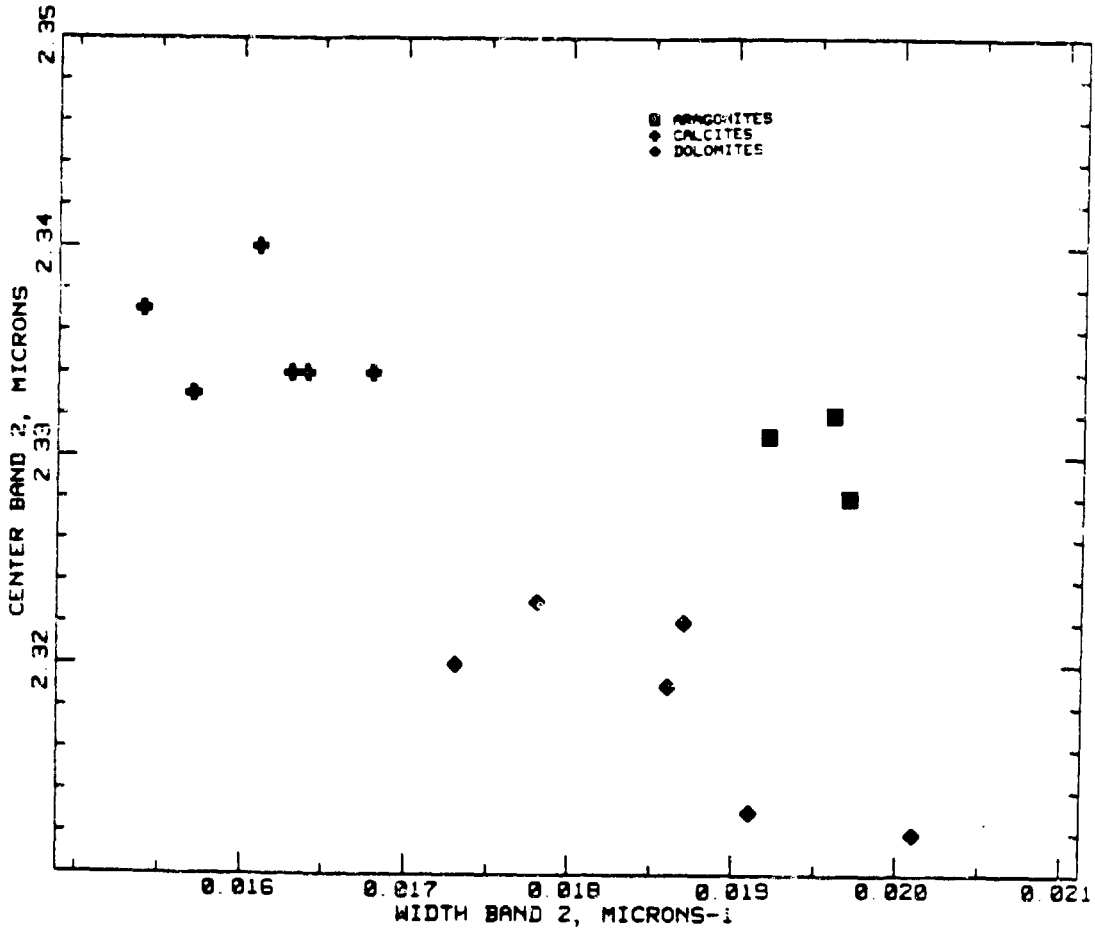

Figure 3.16 Position of centersof band 2 in microns plotted against width of band 2 in μm^{-1}.

Positions of carbonate bands in aragonite spectra do not show the same trends relative to equivalent bands in calcite spectra that bands in dolomite spectra do (see Table 3.3 and Figs. 3.13 to 3.15). Bands in spectra of aragonites may occur at the same, shorter, or longer wavelengths than the equivalent bands in calcite spectra. The position of band 1 is approximately the same for both aragonite and calcite spectra, and bands 5 and 6 in aragonite spectra occur at the same or slightly shorter wavelengths than the same bands in calcite spectra. Bands 2, 3 and 7 occur at shorter wavelengths in aragonite spectra than in calcite spectra, while band four occurs at longer wavelengths.

Band widths also vary with mineralogy. Table 3.4 shows band widths determined by GFIT for the spectra of the three common mineral types. These widths are given in inverse microns (μm^{-1}) rather than microns because the absorptions are believed to represent a gaussian distribution of energies around a central value (Farr et al., 1982). Energy is inversely porportional to wavelength, so bands won't be symmetric in wavelength space. Band 1 appears to be narrower in dolomite than in aragonite spectra. Band 1 tends to be narrower in dolomite spectra than calcite spectra as well, although there is some overlap in values. In general band 2 appears to be wider in aragonite than in dolomite or calcite spectra (see Fig. 3.16). Band 3 appears to be narrowest in dolomite spectra, wider in aragonites, and widest in calcites. There are no clear trends in widths of band 4. It is difficult to generalize about trends in widths of bands 5 and 6 because presence of minor amounts of water in the sample can make bands 5 and 6 appear wider than data from dry samples would indicate they are (for example, compare widths of band 5 for 10519 and 6506 to those for 1507, 1531, and 1542 in Table 3.4).

Dolomite spectra show much greater variation in band widths than aragonite and calcite spectra. This might be related to stoichiometry or lack thereof in dolomite composition, to differences in Fe^{2+} and Mn^{2+} content, or to the occurrence of zones of different chemical composition within dolomite crystals. This will be dealt with in more detail in Chapter 5.

Figures 3.13, 3.14, and 3.15 are plots of some of the data in Table 3.3. They show how positions of the first four carbonate bands vary with mineralogy, and how samples cluster into groups in these plots according to mineralogy. Here only one fit to the spectrum for each mineral was used, that selected as best according to the criteria discussed above, and each point represents one sample.

Figure 3.13 shows positions of the centers of band 2 plotted as a function of positions of centers of band 1 for each sample. Here it can be seen that although band 2 occurs at slightly shorter wavelengths in aragonite spectra than in those of calcites, calcites and aragonites fall together in one group, while the dolomites form a second. Figure 3.14 shows positions for band 2 plotted vs. positions for band 4 for each sample. This shows the trends in band position discussed above for the different minerals, and shows that the three minerals fall into three distinct groups. Figure 3.15 plots positions of centers of bands 3 and 4. Again the three mineral types cluster into separate groups.

Band widths may also be used to distinguish carbonate minerals from each other. Figure 3.16 is a plot of the center of band 2 vs. the width of band 2. The samples again fall into three groups of different mineralogy.

Iron Bands

Although variations in spectral properties with variations in chemical composition will be dealt with in detail in Chapter 5, a brief

discussion of absorption features due to the presence of ferrous iron in calcite and dolomite is presented here, as these features can be used in mineral identification. A broad band centered around 1.0 μm occurs in some calcite spectra and all dolomite spectra in this study, but is absent in aragonite spectra. We can infer that this broad feature is caused by the presence of Fe^{2+} because:

1. Broad features in the 1.0μm region in spectra of other minerals, most notably pyroxenes and olivines, are attributed to the presence of iron (Adams, 1974; Burns, 1970; Runciman _et al._, 1973; and others).
2. The common occurrence of Fe^{2+} substituting for Ca^{2+} and Mg^{2+} in calcites and dolomites (Deer, Howie, and Zussman, 1962; Lippmann, 1973; and others) makes it the most likely transition metal ion to result in such a commonly occurring absorption band.
3. Chemical analyses done by Hunt and Salisbury (1971) and in this study indicate the presence of iron in minerals whose spectra show these features.
4. Increase in intensity of this broad band is positively correlated with increasing iron content in dolomites. (see Fig. 3.17).
5. This feature is absent from all aragonite spectra measured in the course of this study (over 30 samples). The aragonite crystal structure will not accommodate Fe^{2+} because of the small size of the cation, and bivalent iron is not present in aragonite samples (Lippman, 1973).

Absorption bands due to the presence of Fe^{2+} differ in position and shape in calcite and dolomite spectra. Figure 3.18 shows spectra of a

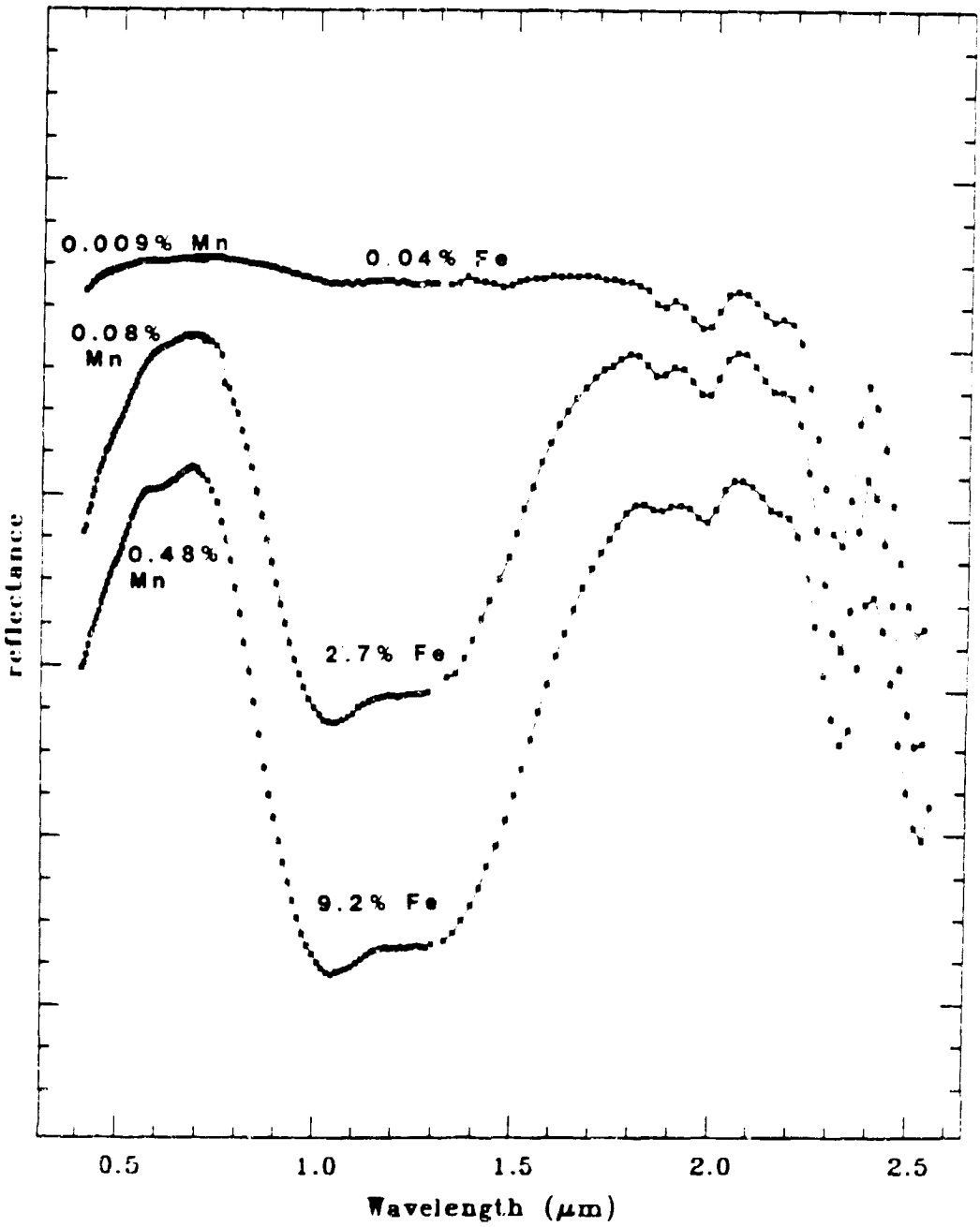

Figure 3.17 Spectra of dolomites containing different amounts of iron, given in weight per cent FeO, as determined by XRF.

ORIGINAL PAGE IS
OF POOR QUALITY

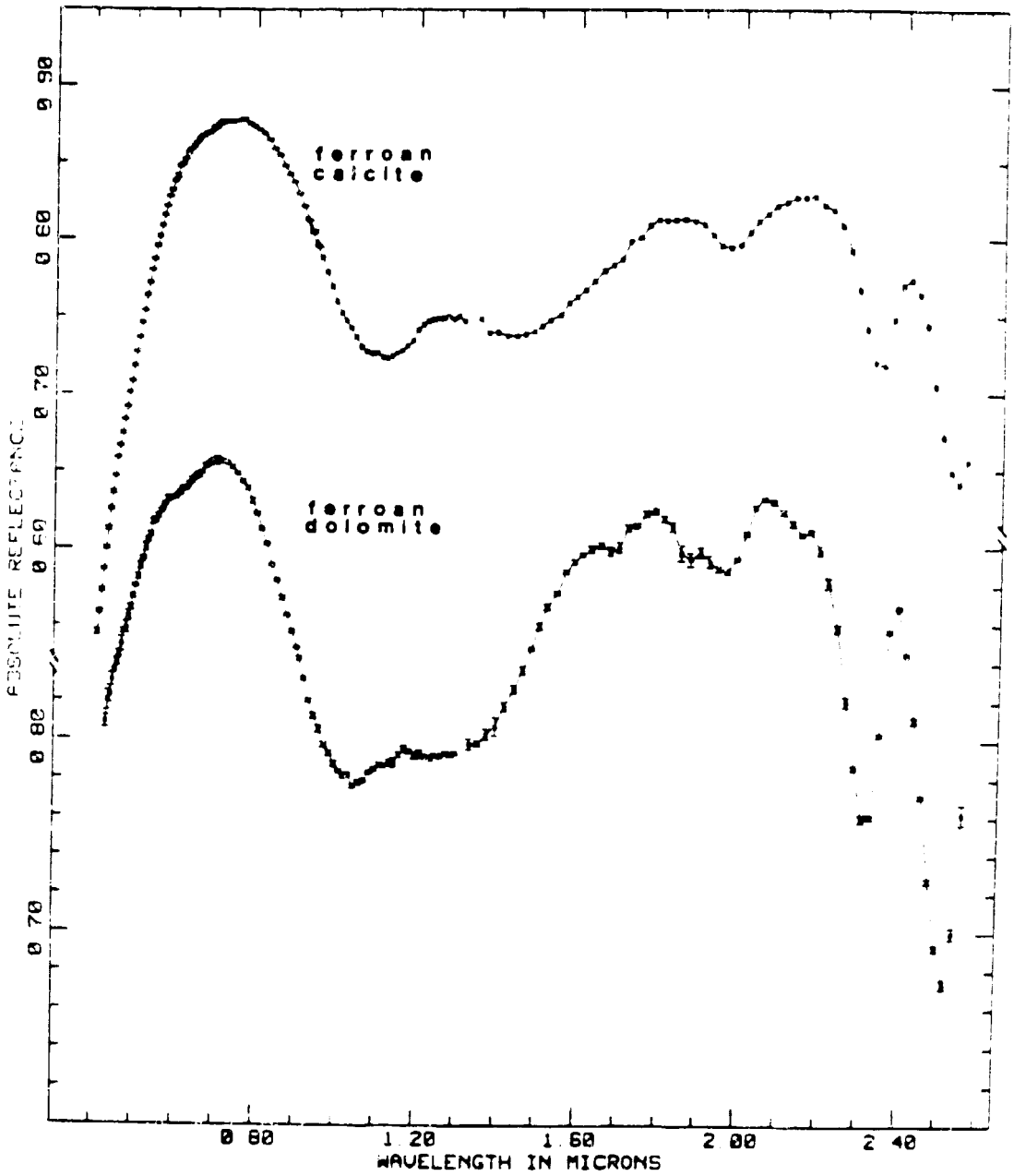

Figure 3.18 Spectra of ferroan dolomite and ferroan calcite.

ferroan calcite and a ferroan dolomite. Note that this feature in calcite is a broad double band centered at 1.3μm while that in dolomite is centered at ≈1.2μm. Although the dolomite feature is composed of at least two large bands, the splitting between the bands is not as marked as in the calcite spectrum.

While particle size and packing determines the intensity of features due to vibrational processes of the carbonate radical, intensities of bands caused by transition metal cations are influenced by concentration of the particular cation in the crystal as well. Figure 3.17 shows spectra of three dolomites containing different concentrations of iron. Note that the carbonate bands in all three samples are of about the same intensity, indicating that the particle size distribution of the powdered samples are comparable. The iron bands, however, are of different intensities, intensity increasing with Fe^{2+} concentration.

DISCUSSION

Carbonate Band Positions

Band positions for carbonates in this spectral region reported by previous workers are given in Table 5. Although the positions reported by Hunt and Salisbury (1971) for bands which correspond to bands 4, 5, and 6 of this study are similar to those reported here, their reported positions for bands 1 and 2 in both calcites and dolomites are at longer wavelengths than those reported in this study. This may be due to some difference in internal calibration of the instrument, or may result from the different methods used to determine band position. Or, since Hunt and Salisbury (1971) did not verify the mineralogy of their samples, it may be due to presence of mineral phases other than those assumed to be present.

Hunt and Salisbury (1971) report only five bands in this spectral region, while seven are reported here. Hexter (1958), Hunt and Salisbury (1971), and Schroeder et al. (1962) all noted that the two strong bands near 2.3 and/or 2.5μm are asymmetric with a shoulder on the short-wavelength side. In this study the shoulder on the band in the 2.3μm region has been resolved as band 3. It was not possible to fit the 2.5μm feature as two bands using the GFIT program, so that feature was fit as one band. The absence of this extra band in the fits results in the differences between the fit curve and the data seen in the 2.5μm region (see Fig. 3.5). Thus there are at least eight carbonate bands in the NIR region. Plots such as Figure 3b indicate there may be additional weak absorption features at wavelengths shorter than 1.6μm, but no attempt was made to fit these. Since they are so weak, very coarse samples will have to be used in order to study them. As mentioned above, band 7 may actually be composed of two bands. Thus, the seven bands reported give a minimum number for carbonate bands in this region of the spectrum.

Exact positions of bands due to internal vibrations of the carbonate radical may be a function of the coordination number of the cation, the interatomic distances between anion and cation, the reduced mass of the cation, the radius of the cation, the electronic structure or periodicity of the cation, and the coefficient of relative bond strength, which varies according to the degree of covalency of the bond (Adler and Kerr, 1963a,b; Povarennykh, 1978, and others). The differences in carbonate band positions and widths in VIS and NIR spectra of aragonites, calcites, and dolomites show patterns similar to those discussed by Adler and Kerr (1963b) and Chester and Elderfield (1967) for the fundamental frequencies in the MIR region in transmission spectra.

Bands in aragonites may occur at the same, longer, or shorter wavelengths than equivalent bands in calcites. This reflects the difference in crystal structure. In aragonites the lowered site symmetry leads to lifting of the degeneracies of the ν_3 and ν_4 fundamentals, and doubling of these bands in MIR spectra (e.g. Adler and Kerr, 1963b). This doubling of the fundamental bands may cause some of the bands in aragonite spectra in the NIR to be broader than their counterparts in calcite spectra.

In general, all the dolomite bands in the NIR occur at shorter wavelengths than their calcite equivalents. This reflects the difference in chemical composition. The same is true of the fundamental bands in the MIR (Adler and Kerr, 1963a; Chester and Elderfield, 1967; and others). These shifts in fundamental frequencies were found to correlate both with mass of the cation and ionic radius, Mg^{2+} having a smaller mass and radius than Ca^{2+} (Adler and Kerr, 1963b).

Band Assignments

Infrared absorption by a molecule takes place when a photon interacts with the molecule and raises in it from one energy level to another (Harris and Bertolucci, 1978). In order for a vibration to be infrared acitve , i.e., cause infrared light to be absorbed, the vibration must result in a change in dipole moment. Although it is known that the absorption features described here are due to vibrations of the carbonate radical, the exact nature of these vibrational processes is not agreed upon.

The literature on the infrared spectra of carbonate minerals, particularly of calcite, is voluminous. Hexter (1958, p. 280) states

> "In the early history of infrared spectroscopy, the mineral calcite played an

important part in the development of both technique and theory. The availability of excellent samples of the mineral and the ease of sampling begged its examination by early spectroscopists. The ease of manipulation of the classical equations of motion of its fundamental unit, the carbonate ion, made for reasonably close agreement between its calculated and observed vibrational spectrum. Moreover, its geometry, made precise with advances in structure determination by X-ray diffraction techniques, together with the early but thorough experimental spectroscopic history of the mineral, have make it a touchstone in the application of various modern theories of spectra of the solid state."

The vast majority of this literature deals with the mid- and far-infrared (i. e., wavelengths longer than about 5μm, where the fundamental vibrational modes of the carbonate ion and of the crystal lattice occur.)

The free carbonate ion has 12 degrees of freedom, with six internal or molecular modes resulting from distortion of the carbonate radical, and six external or lattice modes which reflect translational and rotational motions of the rigid ion. The ideal carbonate ion has point group summetry D_{3h}. The six internal fundamental vibrations are a symmetric stretch (ν_1), an out-of-plane bend (ν_2), a doubly degenerate

antisymmetric stretch (ν_3), and a doubly degenerate in-plane bend (ν_4). The ν_2, ν_3, and ν_4 are infrared active. The external modes of the free carbonate radical are 3 translations along the x, y, and z directions, and 3 rotations about each of these axes. The three translational modes of the ion would be infrared active, but the rotational modes would not (Adler and Kerr, 1963a; Schroeder *et al.*, 1962).

When a molecule or molecular ion is incorporated into a crystal lattice the number and frequencies of its fundamental modes may change, and the infrared spectrum observed will not be that predicted by the simple free ion approximation. Its vibrations may now be viewed as the "motions of one molecule moving in a potential field reflecting the symmetry of the surrounding crystal" (Halford, 1946, p. 10). The carbonate ion in calcite occupies a site of symmetry D_3. The site symmetry for the carbonate ion in dolomite is C_3. In aragonite the carbonate radical occupies a site of symmetry C_s (Adler and Kerr, 1963a; White, 1974). In calcite-group minerals each cation is surrounded by six oxygens, in aragonite-group minerals by nine. There is a change in coordination of cations around the oxygens from two-fold in calcite-group minerals to three-fold in the aragonite group (Adler and Kerr, 1963b; Lippmann, 1973).

In calcite, the site group approximation predicts that, as in the free ion, ν_2, ν_3, and ν_4 will be infrared active, and ν_1 will not. Both ν_3 and ν_4 will remain doubly degenerate. The approximate positions of these modes have been reported by a number of workers (Adler and Kerr, 1962, 1963a,b; Chester and Elderfield, 1967; Huang and Kerr, 1960; Weir and Lippincott, 1961; and others) and occur approximately at the following wavelengths: ν_2 ~ 11.40μm, ν_3 ~ 7.00μm, and ν_4 ~ 14.05μm. The ν_1 mode, although theoretically infrared inactive, does cause a weak

absorption band. Goldsmith and Ross (1966) found that it occurred at 9.23μm. Approximate positions for these same bands in dolomites are as follows: ν_2 - 11.36μm, ν_3 - 6.95μm, ν_4 - 13.74μm. ν_1 is Raman active and Griffith (1970) determined it's position to be 9.10μm. In aragonite the lower site symmetry predicts the stretching mode, ν_1, will become infrared active, and the degeneracies of the ν_3 and ν_4 modes (antisymmetric stretch and in-plane bend, respectively) will be lifted (Schroeder et al., 1962; Halford, 1946). Absorption bands corresponding to these fundamental modes have been observed by several authors as follows ν_1 - 9.23μm, ν_2 - 11.60μm, ν_3 - 6.80μm, and ν_4 - 14.05μm (Adler and Kerr, 1962, 1963a,b; Chester and Elderfield, 1967; Huang and Kerr, 1960; Weir and Lippincott, 1961; and others). The predicted splitting of ν_3 and ν_4 have been observed by Schroeder _et al_. (1962), Weir and Lippincott (1961), and others.

In a carbonate crystal, the carbonate ion does not rotate freely. One model of lattice motions, perhaps the most frequently invoked in studies of carbonate minerals, suggests that rigid molecules or molecular ions undergo translational vibrations of their centers of mass, and rotational vibrations about their centers of mass, these latter also being called torsional oscillations or librations. (Singh and Chaplot, 1982; Trevino _et al_, 1974; Yamamoto _et al_., 1975a,b). The bonding between the carbon and three oxygens in the carbonate radical is strong, the bonding between the carbonate ions and the rest of the crystal lattice relatively weak (Yamamoto et al, 1975a). Califano (1980) states that it can be assumed that the carbonate radicals behave as rigid bodies because the internal and external frequencies are well separated. If molecules possess very low frequency internal vibrations they may overlap in frequency with the lattice modes, in which case the rigid ion model would not apply (Califano, 1980, p.223).

The site group approximation for the carbonate ion in calcite predicts four lattice modes, all of which are infrared active. Two are translational, two rotational. In aragonite the site group approximation predicts six lattice modes, all of which are infrared active (Halford, 1946; Schroeder _et al._, 1962) The lattice modes in carbonates occur at very long wavelengths (longer than 25 μm) while the internal fundamentals occur between 6 and 15μm. Thus the lowest internal vibrational mode has about twice the frequency of the highest-frequency lattice mode (Plihal and Schaack, 1970).

In actual infrared spectra of calcite and aragonite, a great many more bands, including those which are the subject of this study, are observed than are predicted by the above models. Another model used to explain the many features found in infrared spectra of carbonates is the factor group approximation, in which the symmetry elements of the entire unit cell, rather than just those of the site in which the carbonate ion resides, are considered (Hornig, 1948; Winston and Halford, 1949). In the factor group approximation, a band or line expected in the site group approximation (ν_1, ν_2, etc. above) may become duplicated several times, not to exceed the number of sites in the unit cell, as a result of coupling between the carbonate groups in the primitive cell (Winston and Halford, 1949).

Calcite has a space group symmetry of D_{3d}^6, with two molecules per unit cell. The space symmetry of dolomite is lowered to C_{3v}^6. (Adler and Kerr, 1963a; White, 1974). Coupling between the two carbonate groups in calcite-group minerals gives two sets of internal vibrations, one in which the two groups vibrate in phase, and a second in which they vibrate out of phase. White (1974) presents diagrams of these modes. Group theory gives the following irreproducible representations for the

intramolecular vibrational modes in calcite and dolomite:

$$\Gamma_{int} = A_{1g}+A_{1u}+A_{2g}+A_{2u}+2E_g+2E_u$$

and for the extramolecular or lattice vibrations:

$$\Gamma_{ext} = 2A_{2g}+A_{1u}+2A_{2u}+2E_g+3E_u$$

(Denisov et al., 1982; Yamamoto et al., 1975a,b) The A_{2u} and $2E_u$ intramolecular modes and the $3E_u$ and $2A_{2u}$ lattice modes are infrared active (Rutt and Nicola, 1974).

Aragonite has symmetry D_{2h}^{16}, with four molecules per primitive unit cell (Adler and Kerr, 1963a; Frech et al., 1980; White, 1974). Coupling between the four carbonate groups results in each of the six fundametnal modes of the free ion appearing four times, giving 24 internal modes. The internal optical modes predicted by the factor group approximation have the irreproducible representations

$$\Gamma_{interanl}=4A_g+2B_{1g}+4B_{2g}+2B_{3g}+2A_u+4B_{1u}+2B_{2u}+4B_{3u}.$$

All of the g (gerade) modes are Raman active, and all of the u (ungerade) modes except A_u are infrared active. The external optic modes are

$$\Gamma_{ext}=5A_g+5B_{2g}+4B_{1g}+4B_{3g}+4B_{1u}+3B_{2u}+4B_{3u}.$$

Again the g modes are Raman active, the u modes are infrared active (Frech et al., 1980).

In the factor group approximation there are effectively no selection rules governing combination and difference bands. Essentially any combination of the above bands is possible (Schroeder et al., 1962; Winston and Halford, 1949).

White (1974) gives an extensive review of work on spectra of carbonate minerals in the MIR and FIR up to that time.

	Band Position	Band Assignment
Hunt and Salisbury (1971)		
	2.55μm	$\nu_1+2\nu_3$
	2.35μm	$3\nu_3$
	2.16μm	$\nu_1+2\nu_3+\nu_4$ or $3\nu_1+2\nu_4$
	2.00μm	$2\nu_1+2\nu_3$
	1.90μm	$\nu_1+3\nu_3$
Hexter (1958)	2.55μm	$2\nu_3+270+2x416$
	2.37μm	$2\nu_3+270+3x416$
Schroeder et al. (1962)		
	2.54μm	
Matossi (1928)	2.533μm	$2\nu_3+\nu_1$
	2.500μm	"
	2.330μm	$3\nu_3$
	2.300μm	"

Table 3.5 Band positions and assignments of previous workers for calcite.

Work done in the NIR (0.7 to 2.6μm) is much less extensive than that in the MIR and FIR. There is no concensus in the literature on the assignments for bands in this region, and no attempt is made at specific band asssignments here. However, workers in this region of the spectrum have used some of the same models to describe the absorption features in this region that are used in the longer-wavelength studies. In this region there are no fundamental frequencies, and all bands are sums of two or more fundamentals. These bands are much weaker than the fundamentals. Hadni (1974, p.46) states that "... three-phonon processes in general give an absorption coefficient ten times weaker than that for two-phonon processes which are still ten times weaker than the classical one-phonon processes." A phonon is a quantum of vibrational energy.

Hunt and Salisbury (1971) measured spectra of a number of carbonate minerals, and made band assignments assuming all bands were overtones and combination tones of internal fundamental vibrations of the carbonate ion, using the fundamental band assignments given by the site group approximation. Their band assignments are listed in Table 3.5. Schroeder _et al_. (1962) used the factor group approximation. They made no specific band assignments in this region, but concluded that bands observed at about 3.0μm could be explained by the same model they proposed for bands at longer wavelengths, i. e., they are summation bands of fundamental frequencies (perhaps in this specific case the overtone $2\nu_3$) with successive levels of a low frequency (about $30cm^{-1}$) librating oscillator. Fexter (1958) concluded these bands were summation bands of $2\nu_3$ plus two fundamental libration frequencies which he calculated to be $270cm^{-1}$ and $416cm^{-1}$. His band assigments are given in Table 3.5 as well.

A number of problems arise when trying to calculate band assigments in this spectral region by calculating sums and multiples of internal and external modes reported in the literature for the MIR and FIR. The principal problem is the lack of an adequate data set from which calculations can be made. A range of values for the fundamental modes, both internal and external, have been reported in the literature. Chester and Elderfield (1967) list many of the values that have been reported for the internal fundamental modes. Some differences are relatively small. Values reported for ν_4, for example, range from 710 to 715cm^{-1}. On the other hand, values reported for ν_3 range from 1418 to 1471cm^{-1}. Farmer (1974) notes differences between published values for measurements made on powders and single crystals. Calibration problems such as that found to exist between the University of Hawaii and University of Washington instruments undoubtedly also occur between instruments working at longer wavelengths. Many workers do not verify the mineralogy of the material on which measurements are made, and studies of variations of band positions with chemical composition are rare. When spectra are taken at low (e.g. liquid nitrogen) temperatures, bands narrow and sharpen, and more bands become evident than are seen in room temperature spectra (Hellwege _et al._, 1970; Schroeder _et al._, 1962)

Although there is good agreement on assignments, if not the precise positions, of the fundamental modes for calcite, there is still debate about the assignments for the weaker bands which occur with the fundamental modes in the MIR region. Nor is there agreement on the mode or degree of interaction between the internal and external lattice vibrations. White (1974, p.236) states "Hellwege _et al._ (1970) and Schroeder _et al._ (1962) presented measurements on high quality single crystals but the agreement between them is surprisingly poor. Hellwege

et al. (1970) used oriented crystals with polarized IR measurements and determined more detail .... Hellwege et al. do not observe the regular progression of satellite lines that form the main evidence for a set of harmonics of a librational mode and instead assign the bands to binary combinations of internal and lattice modes with additional structure arising from the zone boundary phonons."

When reported values are used to calculate energies of absorptions due to sums of three or four fundamentals such as those dealt with in this study, the uncertainties are compounded. The models listed in Table 3.5 all agree resonably well with band positions for calcite in this region. Other workers have tried to apply a more complicated model in the MIR and FIR than those cited here (see for example Cowley and Pant, 1973; Davydov, 1962; Denisov et al., 1982; Hellwege et al., 1970; and others). However, these workers haven't made any assignments in the NIR using this model.

MINERALOGICAL APPLICATIONS

Positions of the carbonate bands are diagnostic of mineralogy. The presence of iron bands, and their shape and position can also be used to identify carbonate minerals of the calcite group.

Band-band plots shown in Figures 3.13, 3.14, and 3.15 are a convenient way to display the data listed in Table 3.3 and discussed above. Figure 3.13 shows the position of the center of band 2 for each sample plotted as a function of the position of the center of band 1. This shows that the aragonites and calcites fall together in one group, while the dolomites cluster in a second group. Figure 3.14 shows band 2 plotted versus band 4. Here the three minerals can be separated into three distinct groups based on band position. Figure 3.15 is a plot of centers of bands 3 and 4, and shows that again the three minerals

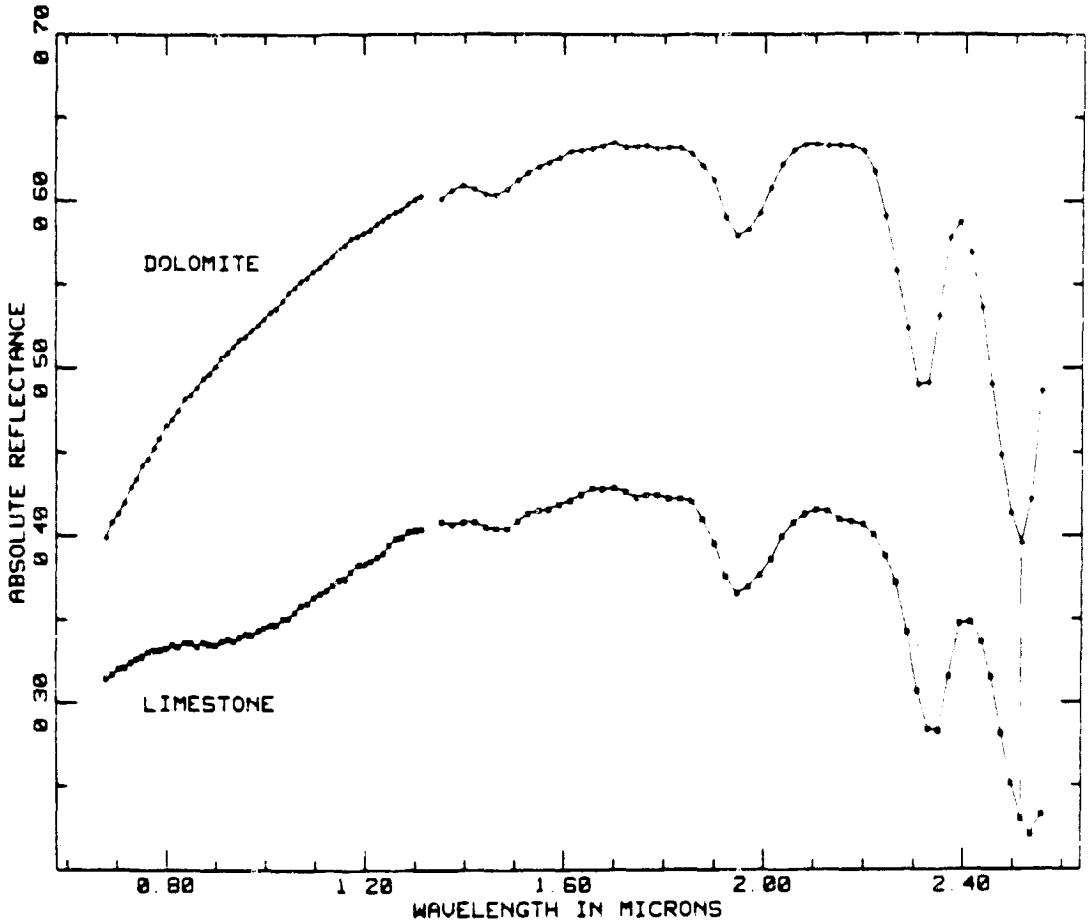

Figure 3.19 Spectra of an oolitic limestone and a dolomite from the Mississippian Lodgepole Formation, central Montana.

cluster into separate groups. Thus while dolomites may be separated from calcite and aragonite on the basis of the positions of bands 1 and 2 alone, bands 2, 3, and 4 are more useful in distinguishing aragonite from calcite.

Band width may also be a useful parameter in mineral identification. Figure 3.16 shows the position of band 2 plotted against the width of band 2 for each sample spectrum. Again the three minerals separate into three distinct groups.

As described above, positions of bands 5 through 7 also vary with mineral type. However, even small amounts of water present as fluid inclusions can cause apparent shifts in the positions of these bands. Or if the water bands are strong enough they may dominate the spectrum in the 1.9μm region and mask the carbonate bands entirely, so that only a single feature at 1.9μm can be seen in the spectrum, rather than bands 5 and 6 near 1.88 and 1.99μm respectively. (see Fig. 3.19). The four bands in the 2.0 to 2.5μm region, however, are relatively unaffected by amounts of fluid inclusions which this study indicates are common, and are sufficient for mineral identification. An example of this is shown in Figure 3.19. This figure shows spectra of a dolomite and a limestone from the Mississippian Lodgepole Formation in central Montana. Although water bands mask the carbonate bands in the 1.9μm region, the stronger bands at longer wavelengths can be used to distinguish the two samples, even without the aid of the GFIT program. Additional features in the spectra include a weak band near 1.4μm which is also due to the presence of water (Hunt and Salisbury, 1971). The limestone spectrum contains a weak iron band near 1.3μm. The absorption bands near 0.9μm are probably due to Fe^{3+} in iron oxides (Singer, 1982) formed by weathering of pyrite (Jenks, 1972). The dolomite spectrum shows no iron bands but does have

a smooth drop-off at shorter wavelengths, the origin of which isn't understood at present.

The simple presence of an Fe^{2+} absorption band near 1.1μm is indicative of a calcite group mineral. However, the absence of an iron band does not necessarily indicate the sample belongs to the aragonite group, as non-ferroan calcites and dolomites are common. A broad double feature centered near 1.3μm is characteristic of Fe^{2+} in calcite, while a broad double band centered around 1.2μm is characteristic of dolomites. Thus these features, in addition to indicating the presence of ferrous iron, can aid in mineralogical identification as well.

CHAPTER 4

Differences in Spectral Properties Related to Differences in Mineralogy

INTRODUCTION

In the preceding chapter the spectral properties of the three most common carbonate minerals were examined, and their spectral characteristics were related to differences in crystal structure and chemical composition. In this chapter the spectral properties of other common carbonate minerals will be examined. There are five common calcite group minerals:

Calcite	$CaCO_3$
Siderite	$FeCO_3$
Smithsonite	$ZnCO_3$
Rhodochrosite	$MnCO_3$
Magnesite	$MgCO_3$

Dolomite ($CaMg[CO_3]_2$) will be included in this discussion as well.

Common aragonite group minerals include:

Aragonite	$CaCO_3$
Strontianite	$SrCO_3$
Witherite	$BaCO_3$
Cerussite	$PbCO_3$

This chapter will deal only with the spectral properties of end-member carbonates. The effects of changes in chemical composition on spectral characteristics will be dealt with in Chapter 5.

Spectra of these common calcite and aragonite group minerals are shown in Figures 4.1 and 4.2 respectively. Samples used in this portion of the study, and the localities from which they were obtained are listed in Table 4.1. Positions of carbonate bands determined from these spectra are given in Table 4.2.

Two spectra each of calcites, aragonites, and non-ferroan dolomites are included for comparison. Band positions for all minerals except smithsonite, magnesite, and siderite were determined using the GFIT routine. Band positions given for these three minerals are estimates only, made using a horizontal continuum. All smithsonite and magnesite samples obtained thus far appear to contain enough water to introduce absorption features in the 1.4 and 1.9μm regions of their spectra. As was seen in Chapter 3, very minor amounts of water (a few hundredths of a per cent water by weight) will change the apparent positions of carbonate bands in the 1.9μm region. Larger amounts of water introduce stronger features in this region. As a result of these stronger features, the GFIT program fails to converge, and a precise fit can't be obtained. The fits to the siderite spectra are estimates only, because

ORIGINAL PAGE IS
OF POOR QUALITY

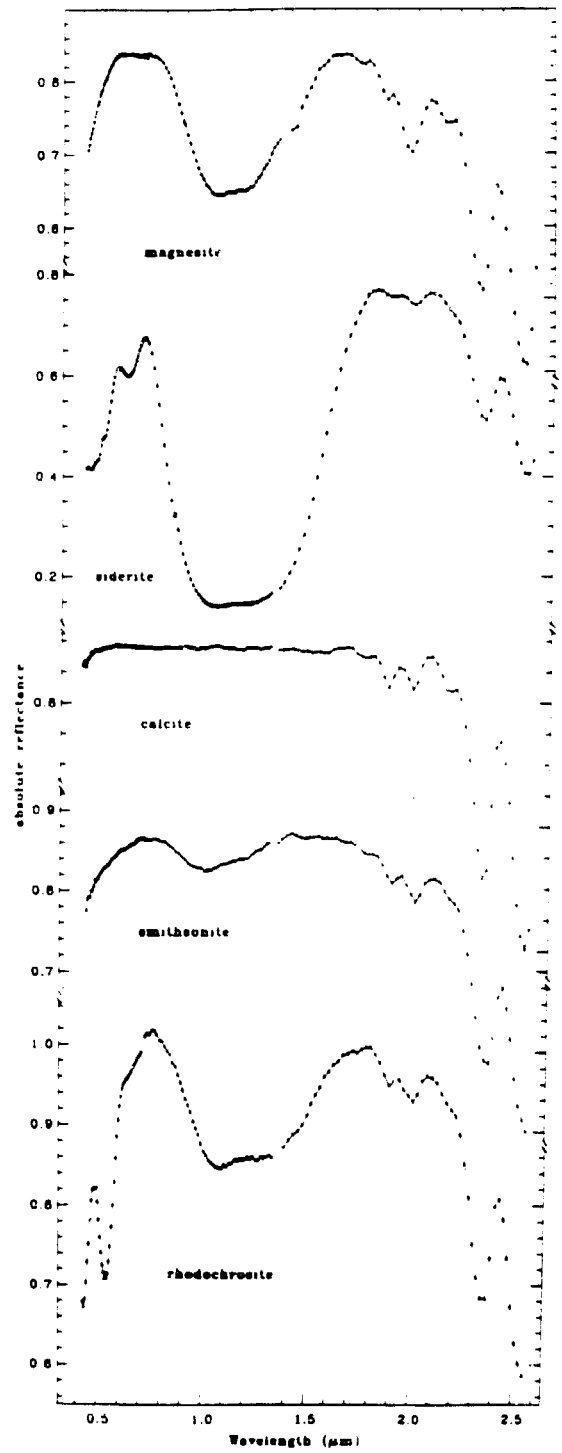

Figure 4.1 Spectra of common carbonate group minerals.

ORIGINAL PAGE IS
OF POOR QUALITY

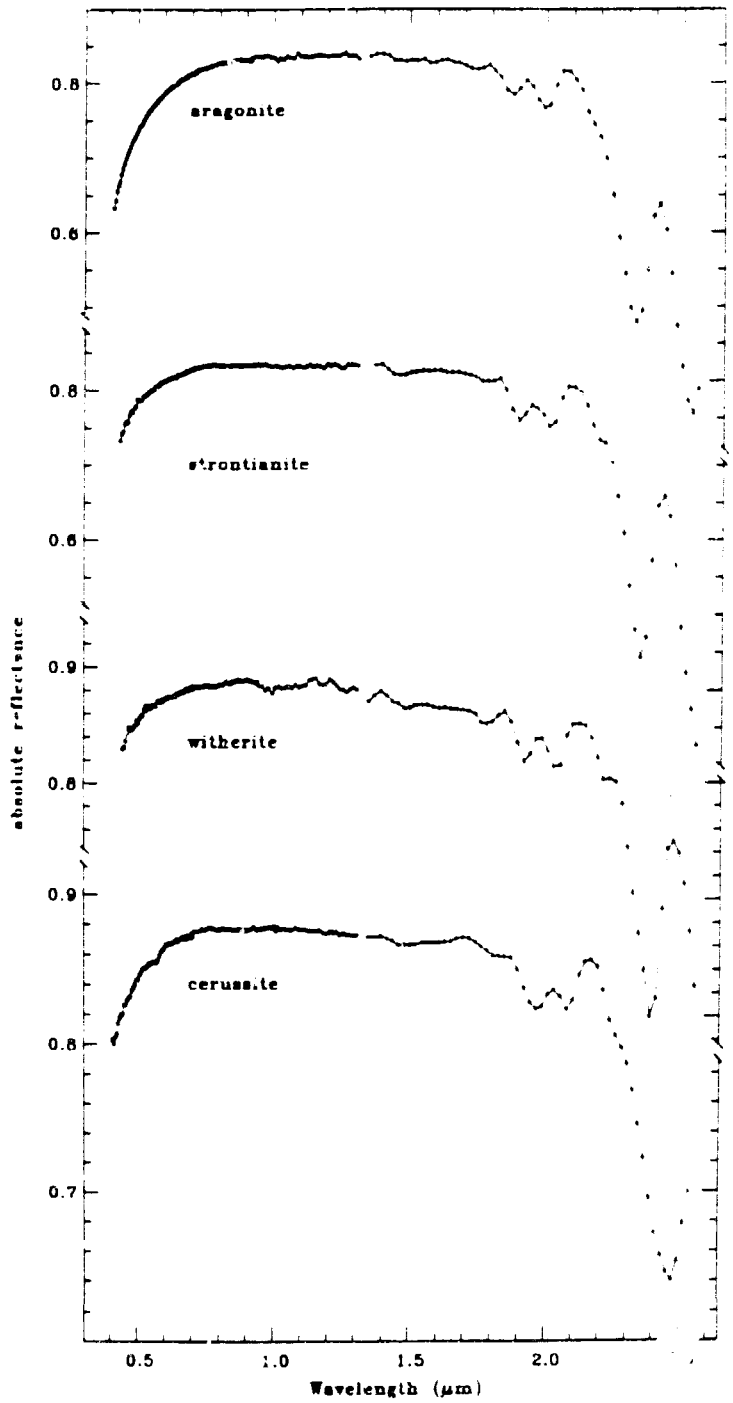

Figure 4.2 Spectra of common aragonite group minerals.

Magnesite	2502	Modum, Norway[1]
	2506	Snarum, Norway[2]
Dolomite	6509	Deep Springs, Inyo County, California[2]
	6514	Binnenthal, Telemark, Norway[3]
Siderite	6515b	Morro Velho, Brazil[4]
	9504	Ouro Preto, Minas Gerais, Brazil[5]
Calcite	1531	Chihuahua, Mexico[6]
	1542	Egremont, England[7]
Smithsonite	4505	Tsumeb, South West Africa[5]
Rhodochrosite	3505	unknown[8]
	3507	Champion Miner, Lake County, Colorado[2]
Aragonite	10524	Spain
	10530	Bilin, Bohemia[7]
Strontianite	11502	Hamm, Westphalia[6]
	11503	Strontian, Scotland[9]
Witherite	13504	Hardin County, Illinois[10]
	13506	Minerva Mine, Hardin County, Illinois
Cerussite	12502	Tsumeb, South West Africa[5]
	12504	Mibladen, Morocco[10]
	12505	Kellogg, Idaho[2]

1. Smithsonian Inst. #114955; 2. Minerals Unlimited, Ridgecrest, Calif.; 3. British Museum #1912,133; 4. Horn Minerals, Smithtown, Long Island, New York; 5. Nature's Treasures, Hawthorne, California; 6. Wards Natural Science Establishment; 7. Geology Dept., University of Iowa, Iowa City, Iowa; 8. Scotch Rocks, Edinburgh, Scotland; 9. Excalibur Mineral Co., Dover, New Jersey; 10. Walstrom Enterprises, Carson City, Nevada;

Table 4.1 Mineral samples discussed in this chapter, and the localities from which they were obtained.

Mineral	1	2	3	4	5	6	7
magnesites							
2502	2.503	2.305	2.235	2.130	1.964	1.846	1.745
2506	2.500	2.305	2.238	2.137	1.965	1.843	1.739
dolomites							
6509	2.516	2.320	2.248	2.165	1.974	1.869	
6514	2.516	2.319	2.244	2.165	1.979	1.862	1.740
siderites							
6515b	2.528	2.329	2.252	2.183	1.990	1.887	
9504	2.526	2.326	2.252	2.183	1.988	1.879	
calcites							
1531	2.535	2.333	2.261	2.167	1.991	1.876	1.763
1542	2.541	2.340	2.272	2.179	1.998	1.885	1.758
smithsonite							
4505		2.362	2.273	2.183	2.012	1.896	1.787
rhodochrosites							
3505		2.367	2.300	2.219	2.007	1.900	1.748
3507		2.372	2.323	2.217	2.029	1.938	
aragonites							
10524	2.535	2.331	2.257	2.195	1.992	1.877	1.748
10530	2.532	2.332	2.258	2.201	1.993	1.873	1.737
strontianites							
11502	2.596	2.350	2.273	2.206	2.014	1.904	1.774
11503	2.580	2.350	2.273	2.214	2.013	1.908	1.765
witherites							
13504		2.398	2.323	2.242	2.042	1.929	1.783
13506		2.397	2.323	2.241	2.041	1.929	1.785
cerussites							
12502		2.469	2.362	2.272	2.091	1.969	1.820
12504		2.464	2.335	2.257	2.087	1.970	1.827
12505		2.473	2.357	2.273	2.094	1.964	1.832

Table 4.2 Positions in microns of carbonate bands in spectra of common carbonate minerals.

Mineral	Band - Band Differences, cm^{-1}				
	1 - 2	2 - 3	3 - 4	4 - 5	5 - 6
magnesite					
2502	343	137	220	397	326
2506	338	130	212	410	335
dolomite					
6509	336	138	171	445	286
6514	338	143	162	435	318
siderite					
6515b	337	147	140	444	276
9504	341	140	140	450	292
calcite					
1531	340	137	191	410	306
1507	338	129	188	414	301
smithsonite					
4505		166	180	390	305
rhodochrosite					
3505		123	159	475	280
aragonite					
10524	344	141	126	465	308
10530	340	140	115	473	318
strontianite					
11502		144	134	431	287
11503		144	118	450	275
witherite					
13504		136	154	437	288
13506		134	156	439	285
cerussite					
12502		183	168	381	295
12504		225	147	361	284
12505		199	157	375	316

Table 4.3 Differences between centers of adjacent carbonate bands in carbonate minerals spectra. Differences in inverse centimeters.

it has not been possible to fit the iron bands. The iron bands in the siderites are extremely strong, and it may be that they have begun to saturate and are no longer gaussian shaped. This could be checked by taking spectra of a very fine particle size fraction of a sample, or of a sample mixed with halon, to weaken the absorption beature, and then making ln-ln plots like those shown in Figures 3.9 and 3.11. As can be seen from Figures 4.1 and 4.2, in many of the mineral spectra, carbonate band 1 occurs at wavelengths longer than 2.5μm, and its center is not covered by the data. For these spectra, only positions of bands 2 through 6 are given.

CARBONATE BANDS

Examination of Table 4.2 reveals a number of trends in these carbonate spectra. Samples are listed in the table in order of increasing wavelength for positions of bands 1 and 2. Differences in band positions between successive calcite group minerals are on the order of 0.01μm. Differences between succesive aragonite group minerals are much larger, ranging from ≈0.02μm up to 0.07μm.

Table 4.3 shows differences between successive band positions, differences between band 1 and band 2, band 2 and band 3 and so on for each mineral spectrum. These are given in cm^{-1}, which is proportional to energy.

Within the aragonite group minerals these differences in energy are quite similar for the first three minerals - aragonite, strontianite, and witherite, with the exception that the difference between band 3 and band 4 increases down the list. Cerussite is anomalous, and does not follow the pattern characteristic of the others.

Few orderly trends can be discerned in energy differences between absorption bands for the calcite group minerals. In general, the

differences between bands 1 and 2, and between bands 4 and 5 are larger than the others. Differences between bands 2 and 3 are generally the smallest. Differences in energy between other bands show a range of values. There are several possible reasons for this. The apparent lack of clear trends among some of the bands may be due to the different degrees of distortion of the lattice in different minerals (see below). Or it may be due to variations in chemical composition, and the fact that many of these mineral samples are not pure end members. The possible presence of water bands in some spectra certainly complicates the pattern, as this can cause shifts in the apparent positions of bands in the 1.9μm region.

On the other hand, the apparent lack of order may be due at least in part to uncertainties in the positions of some bands in spectra which could not be fit using GFIT.

Differences in spectral properties among the different carbonate minerals may be attributed to a number of causes. Adler and Kerr (1963) and Weir and Lippincott (1961) believed that C-O distance in the carbonate radical would prove to be the primary factor in determining positions of the fundamental modes. However, Effenberger _et al_. (1981) found by single crystal X-ray studies of calcite group minerals that "the variation of the C-O bond length in this group of minerals is very slight, if at all real" (p.235). They found these distances to be (in Angstroms, p.238):

magnesite - 1.2852
calcite - 1.2815
rhodochrosite - 1.2867
siderite - 1.2869
smithsonite - 1.2859
dolomite - 1.2853

When a correction for riding motion is made these differences are (p.238):

magnesite - 1.2873

calcite - 1.2902

rhodochrosite - 1.2898

siderite - 1.2895

smithosonite - 1.2881

dolomite - 1.2895

Greater bond lengths should result in bands shifting to longer wavelengths. Neither of these sets of values correlates precisely with bands positions reported by Adler and Kerr (1963) for the MIR, nor with band positions for the NIR reported here.

Since the size and symmetry of the carbonate radical is essentially the same in all carbonate minerals (Reeder, 1983; Speer, 1983), some other factor must be invoked to explain these differences in spectral characteristics. A possible explanation would be the differences in crystal structure between calcite group and aragonite group minerals. The carbonate radical in these two mineral groups resides in sites and unit cells of different sizes and symmetries. This may explain some of the differences observed. However, if crystal structure and site symmetry were the only factors influencing spectral properties of these minerals, they would cluster into just two groups. The calcite group minerals would all have the same spectral properties, and the aragonite group would form another uniform set.

Since all differences in characteristics of the vibrational absorption features in different mineral spectra can't be explained by differences in the carbonate radical, differences in spectral characterisitcs must be related to differences in the major cations in these minerals.

Povarennykh (1978) states that the main factors which affect the positions of absorption bands in the infrared spectra of minerals are those factors which determine the relative strength of the chemical bonds between adjacent atoms. These factors are: the valences of the cations and anions, the coordination number of the cation, the reduced mass of the cation (the sum of atomic weights of a given cation and of all the anions that coordinate it), and the degree of covalency of the bond (Povarennykh, 1978).

The valence of the cations and anions are the same in all these carbonate minerals. The coordination number of the cation is six in the calcite group minerals, and nine in the aragonite group minerals. Povarennykh (1978) states that in general vibrations shift to higher frequencies (shorter wavelengths) with decreasing coordination number. Although this is true in a general way for the carbonate minerals, there are many areas of overlap between band positions in mineral spectra of the two groups, and other factors must be involved.

Many properties of carbonate minerals are considered to be a function of the size of the major cation, which would largely control the cation - anion (M-O) bond length. Adler and Kerr (1963) in a study of this same group of minerals in the MIR (5 to 15μm) found that three of the four internal fundamentals (ν_2 being the exception) shifted to shorter wavelengths with decrease in cation radius. They concluded that while frequency changes might be correlated with variation in the ionic radius of the cation, this relationship was dependent on the electronic periodicity of the elements involved. Adler and Kerr (1963) stated that these minerals fell into three subgroups, calcite, strontianite, and witherite in the aragonite group, and magnesite, dolomite and calcite, and siderite, rhodochrosite, and smithsonite in the calcite group.

Trends in the relationships between band position and cation radius could be defined within these groups, but not between them.

Figures 4.3 and 4.4 show average M-O bond length and cation radius plotted against the position of band 2 for the common carbonate minerals. Values for M-O bond length and cation radius were taken from the review articles of Reeder (1983) and Speer (1983). Band positions used are averages of the values given in Table 4.2. Band 2 was used because it was felt that its position could be determined with the greatest degree of confidence. As can be seen from Figures 4.1 and 4.2, band 1 is centered outside the wavelength range of this study for many of the mineral spectra, and so cannot be used. Band 2, on the other hand, could be determined for all spectra. Band 2 is an order of magnitude stronger than bands 3 through 7 in these spectra. Bands 3 and 4 overlap, and therefore their positions as determined by GFIT are more sensitive to changes in continuum slope than positions of bands 1, 2, 5, and 6. For several minerals, bands 5 and 6 in their spectra occur in the 1.9μm region affected by water bands. Since some of these mineral spectra may contain water features, positions determined for bands 5 and 6 may be shifted from their true values.

Plots for M-O bond length (Fig. 4.3) and cation radius (Fig. 4.4) are very similar, as would be expected. If smithsonite, rhodochrosite, and cerussite are removed from the picture, there is a rough correlation between band position and M-O bond length and cation radius.

Povarennykh (1978) states that increase of atomic mass in minerals causes absorption features to shift to lower frequencies (longer wavelengths). Figure 4.5 shows cation mass plotted against the position of band 2. The correlation here is quite good. Magnesite (Mg),

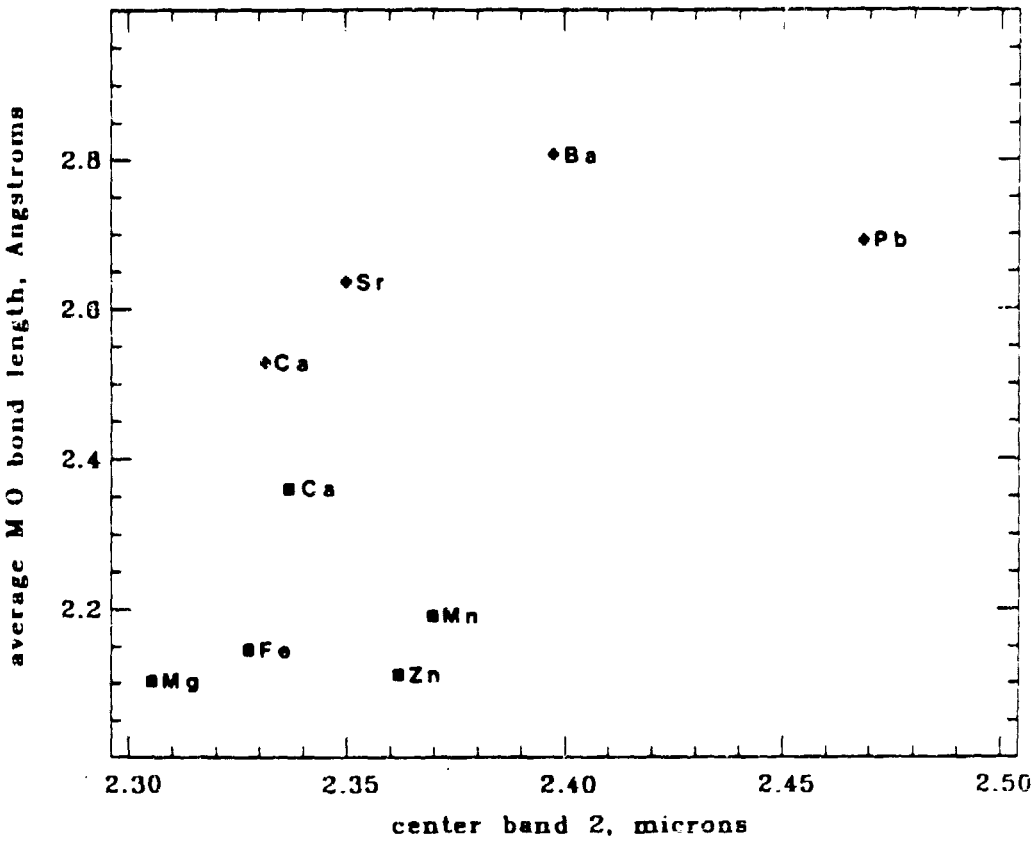

Figure 4.3 Average M–O bond length plotted against the average position of band 2 for each mineral. Calcite group - squares, Aragonite group - crosses.

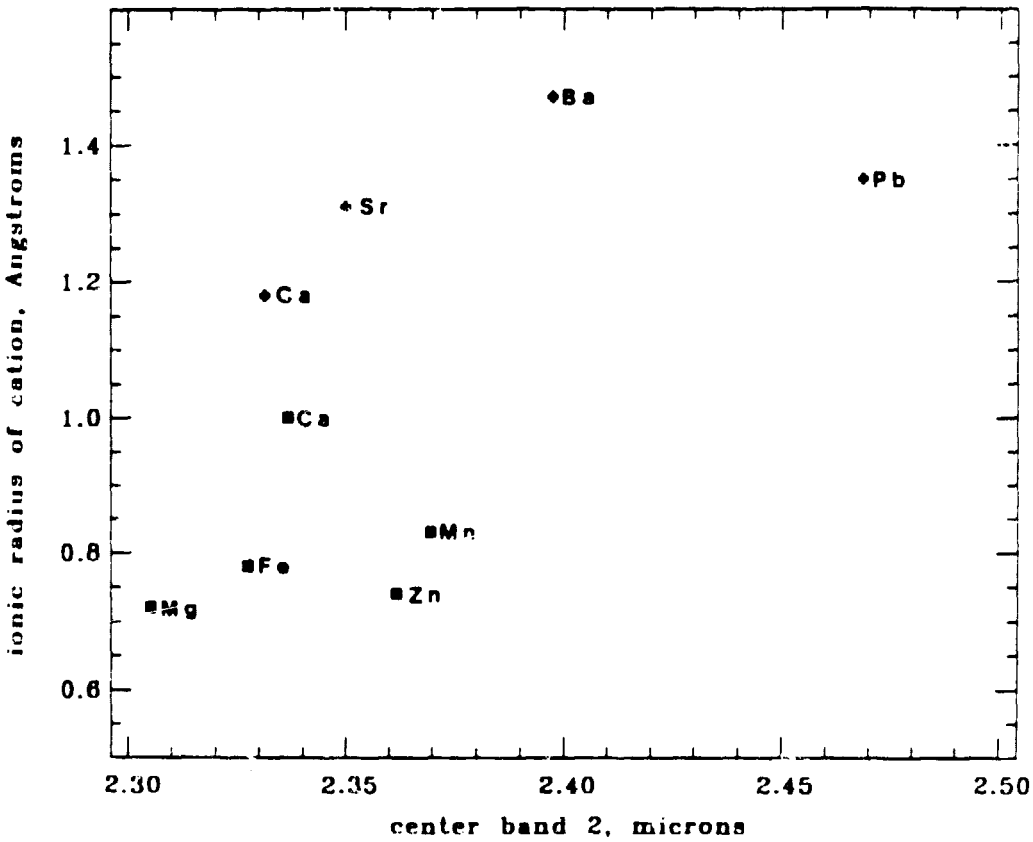

Figure 4.4 Cation radius plotted against average position of band 2 for each mineral. Calcite group - squares, Aragonite group - crosses.

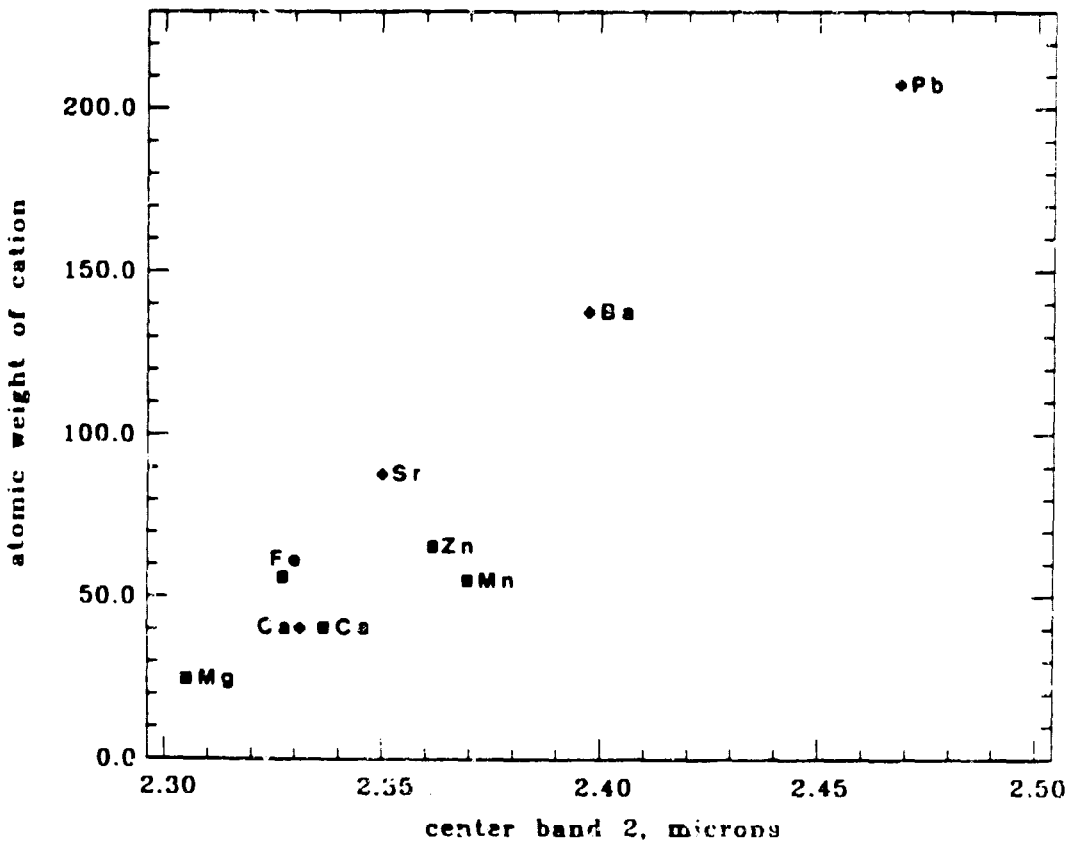

Figure 4.5 Cation mass plotted against average position of band 2 for each mineral. Calcite group - squares, Aragonite group - crosses.

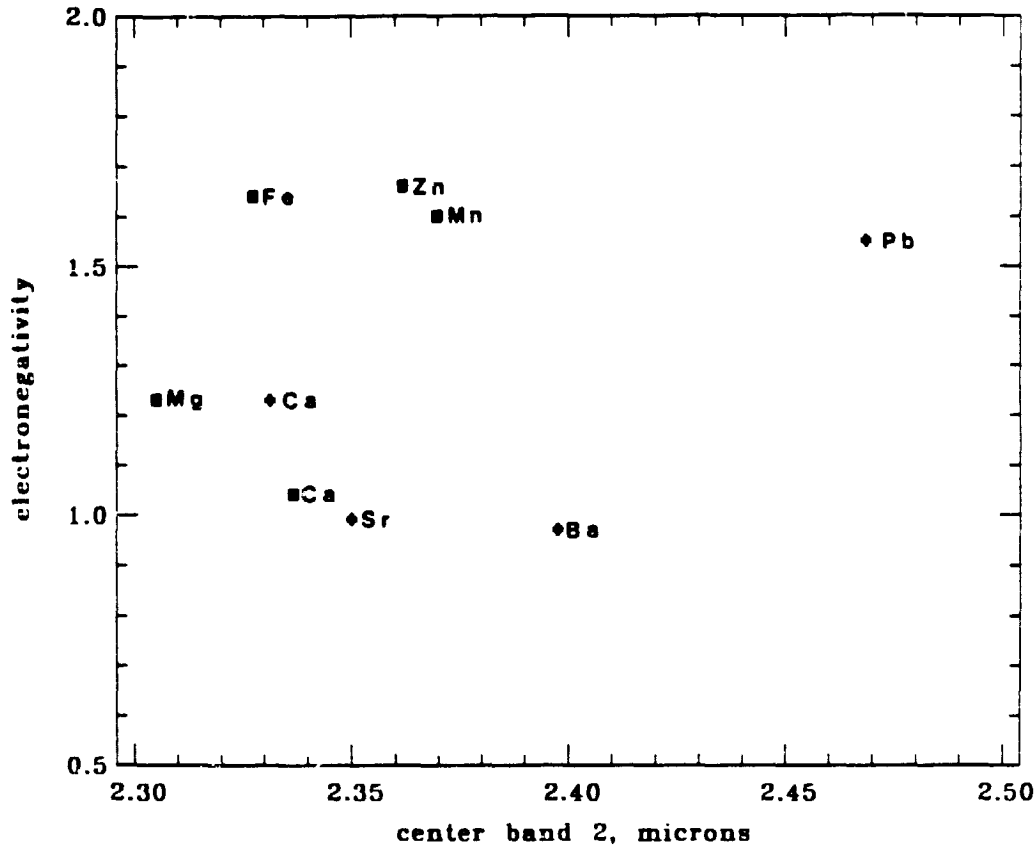

Figure 4.6 Electronegativity of cation plotted against average position of band 2 for each mineral. Calcite group - squares, Aragonite group - crosses.

siderite (Fe), strontianite (Sr), witherite (Ba), and cerussite (Pb) all fall approximately along a straight line. This trend spans the two mineral groups, and seems to transcend differences in crystal structure. Although calcite and aragonite do not fall directly on this line, it is worth noting that while M-O bond lengths and cation radii of the two are quite different, the cation masses are, of course, the same. Their carbonate band positions are very similar, again suggesting that mass, rather than cation size, is the dominating factor.

Smithsonite (Zn) and rhodochrosite (Mn) fall below the line along which the other minerals lie. This may be attributable to the small radii of these ions, which offset them from the general trend followed by the others in the cation radius and M-O bond length plots.

The slightly anomalous behavior of calcite and aragonite is puzzling. Perhaps it is related to the fact that the radius of Ca^{2+} lies at the upper and lower boundaries which can be accommodated by the calcite and aragonite structures, respectively, which results in greater distortion of the crystal lattice.

Adler and Kerr (1963) suggested that electronic structure of the cation might be another factor in determining band positions. Electronegativity, the power of an atom to attract electrons, was included in the discussion here as one expression of these differences. Values for electronegativity are as quoted in Berry et al., (1980). Figure 4.6 shows electronegativity plotted against the position of band 2 for each mineral.

From Figures 4.3 through 4.6 it would appear that the major factor controling positions of absorptions due to vibrations of the carbonate radical in this wavelength region is the mass of the major cation. However, the correlation with cation mass is not perfect and other factors

are involved. The most important of these secondary factors appears to be M-O bond length.

IRON BANDS

Ferrous iron is the major cation in the mineral siderite, and can substitute for the major cation in any of the other calcite group minerals (Deer, et al. 1962). Thus spectra of any of the calcite group minerals may contain absorptions due to Fe^{2+}, and spectra containing absorption features attributable to ferrous iron were found for each of the common calcite group minerals examined in this study.

Bonds between metal cations and the carbonate groups in these minerals are ionic (Hurlbut, 1965; Mason and Berry, 1968). Thus crystal field theory should be adequate to explain many of the spectral characteristics of iron absorptions in spectra of the rhombohedral carbonates. In an isolated transition metal ion all of the five 3d orbitals have the same energy (are degenerate), and electrons in an isolated transition metal ion have an equal probability of being located in any of the d orbitals. When the transition metal ion is incorporated into a crystal structure, the five degenerate d orbitals are split by the non-spherical electrostatic field of the surrounding ligands (Burns, 1970). In an undistorted octahedral site, Fe^{2+}, which has a $3d^6$ configuration, will have one absorption band due to a Laporte-forbidden transition $^5T_{2g} \rightarrow {}^5T_g$ near 1.0μm (Burns, 1970; Ballhausen, 1962). If the octahedral site is not symmetric, degeneracies of the t_{2g} and e_g orbital groups will be lifted, and more bands will be observed. For Fe^{2+} in aqueous solution, the Jahn-Teller effect causes splitting and the formation of a double band (Ballhausen, 1962).

The number, positions, and intensities of absorption bands due to a given transition metal ion depend on the type, position, and symmetry of

the surrounding ligands (Burns, 1970). In the calcite group minerals, all cations occur in octahedral sites, coordinated by six oxygens. Thus the principal variable affecting absorptions due to Fe^{2+} in spectra of those minerals will be the size and symmetry of the octahedral site. Table 4.4 lists the values for octahedral volume, average M-O bond length, and quadratic elongation of the coordination octahedron for each calcite group mineral, as given in Reeder's (1983) review paper. Robinson _et al_. (1971) found quadratic elongation to be the most useful quantitative measure of polyhedral distortion. Quadratic elongation for octahedra was defined as

$$\lambda_{oct} = \sum_{i=1}^{6} (l_i/l_o)^2/6$$

where l_o is the center-to-vertex distance for an octahedron with O_h symmetry whose volume is equal to that of the distorted octahedron with center-to-vertex distance l_i (Robinson _et al_., 1971).

Figure 4.7 shows iron bands from spectra of each of the commonly occurring end member calcite group minerals, and dolomite. Two possible candidates for iron bands were found in calcite and smithsonite spectra. The best choice for Fe^{2+} absorptions in these minerals are shown in Figure 4.7. The reasons for this selection are discussed in Chapter 5, where variations in spectral properties with variations in chemical composition are discussed. These Fe^{2+} bands differ in shape and width from one mineral spectrum to another.

Smithsonite, the mineral with the smallest quadratic elongation (QE), .i .e, the least distorted octahedral sites, has the narrowest Fe band, which is close to being the single band predicted by theory. Magnesite and rhodochrosite, with slightly larger QE, also have narrow Fe

	Octahedral Volume (Angstroms)	QE	M-O Bond Length (Angstroms)
Magnesite	12.40	1.001	2.102
Siderite	13.12	1.0013	2.145
Calcite	17.46	1.002	2.360
Smithsonite	12.52	1.0008	2.111
Rhodochrosite	13.99	1.0009	2.190
Dolomite			
A-site	17.92	1.0016	2.38
B-site	12.04	1.0008	2.08

Table 4.3. Octahedral volumes and quadratic elongation for common calcite group minerals (from Reeder, 1983).

ORIGINAL PAGE IS
OF POOR QUALITY

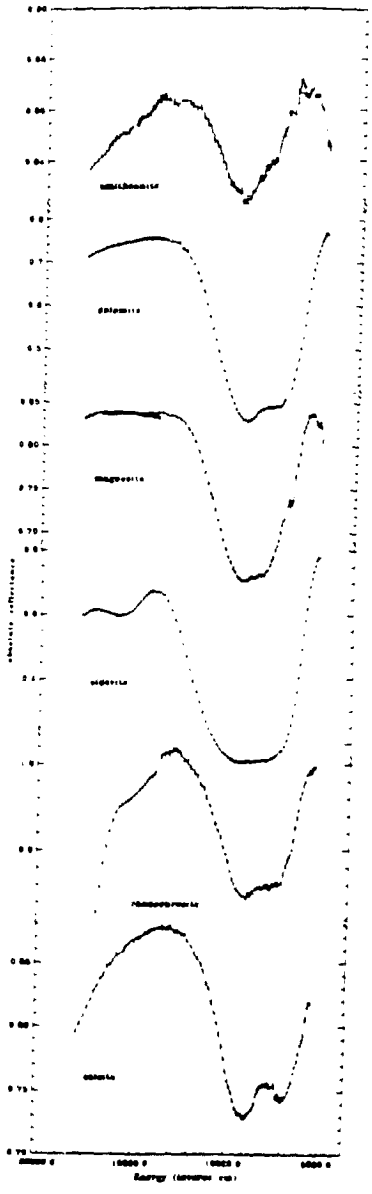

Figure 4.7 Iron bands in calcite group minerals. Horizontal axis in inverse centimeters.

bands, although there is stronger evidence of splitting and the existence of two separate features. Calcite and siderite, with the largest QE, have the broadest bands. The Fe band in the calcite spectrum shows a marked splitting into two features.

The position of an absorption band reflects the energy difference between the t_{2g} and e_g orbitals, or crystal field splitting. One factor which determines the amount of splitting is the distance between metal and ligand, with small differences in the interatomic distances leading to large increases in the splitting (Burns, 1970). M-O bond lengths and octahedral volumes for each mineral are given in Table 4.4.

Iron bands for smithsonite and magnesite, which have the smallest M-O distances and octahedral volumes occur at the shortest wavelengths (highest energies). Calcite, with the largest M-O distance, has its Fe band situated at the longest wavelengths. The other Fe bands occur at intermediate wavelengths, in essentially the order that this model predicts.

The Fe band in dolomite is somewhat harder to explain. It is generally assumed that Fe^{2+} substitutes for Mg^{2+} in the dolomite structure (Reeder, 1983). This is the B-site, which, as can be seen in Table 4.4, has the smallest octahedral volume and QE of any of the sites in these minerals. However, the Fe band in dolomites shows definite doubling, and is centered at longer wavelengths than the Fe^{2+} bands in smithsonite and magnesite. Introduction of Fe^{2+} into the dolomite structure causes distortion of the cation octahedra (Rosenberg and Foit, 1979), which may result in the observed splitting of the Fe band. It is also possible that Fe^{2+} may occupy more than one site in dolomites. Reeder (1983) notes that while majority opinion favors the B-site as the most probable site for the location of Fe^{2+}, no systematic studies of site

distributions in ferroan dolomites have been done. Structural data on M-O bond lengths and some bulk chemical analyses indicate some Fe^{2+} may substitute for Ca^{2+} in the A-site (Reeder, 1983). Although the amount of Fe^{2+} substituting into the A-site may be small, carbonates are so transparent in this region that very minor amounts of Fe in the A-site could contribute features to the dolomite spectrum. Thus, the anomalous appearance of the Fe band in dolomites may be due to contribution of features from Fe^{2+} in two sites rather than one.

WEATHERING

The way in which minerals alter can aid in their identification. Ferroan dolomites are unstable under earth surface conditions (Rosenberg and Foit, 1979) and will alter to form iron oxides which give dolostones the buff color that characterizes them in outcrop (Pettijohn, 1975). Figure 4.8 shows spectra of weathered and unweathered ferroan dolomite (sample #5501 and 6515a, respectively). The presence of iron oxides in 5501 masks the Mn^{2+} bands and the 0.63μm band which can seen in the spectrum of 6515a. Iron oxides greatly intensify the drop-off into the UV, lower the entire short-wavelength end of the curve, and add an absorption band near 0.5μm.

Siderites are very unstable under earth surface conditions and readily alter to form iron oxides. When seen in thin section, siderite is commonly stained yellow-brown by oxides along crystal borders and cleavage traces (Pettijohn, 1975). Figure 4.9 shows spectra of a series of siderites which have been altered to varying degrees. Even the freshest of these shows absorption features due to Fe^{3+}. These occur in the same region of the spectrum as Mn^{2+} bands. These features are discussed in greater detail in Chapter 5. Spark spectrometry indicates that all these samples contain Mn^{2+}, and the first spectrum shows

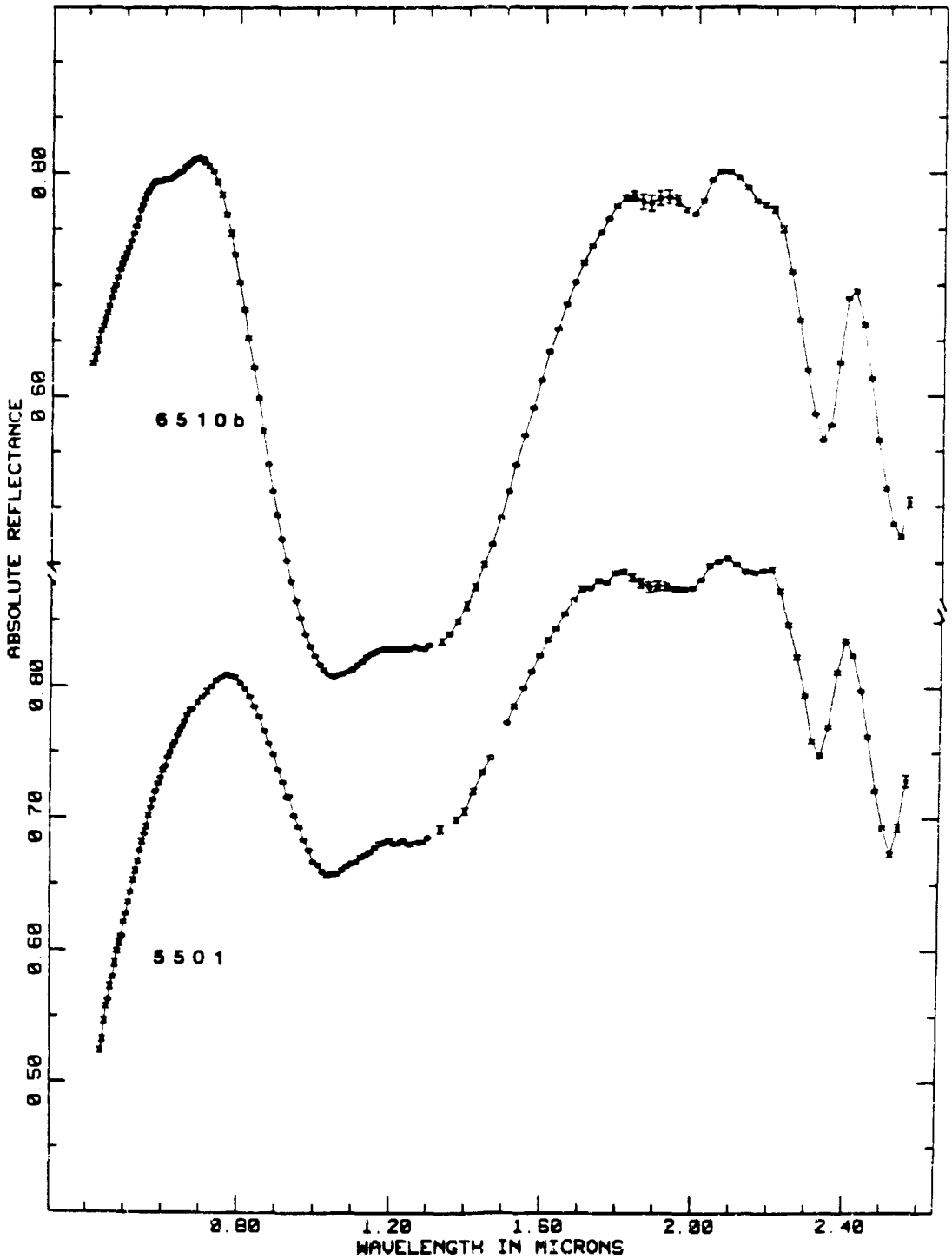

Figure 4.8 Spectra of weathered (#5501) and unweathered (#6515a) ferroan dolomites.

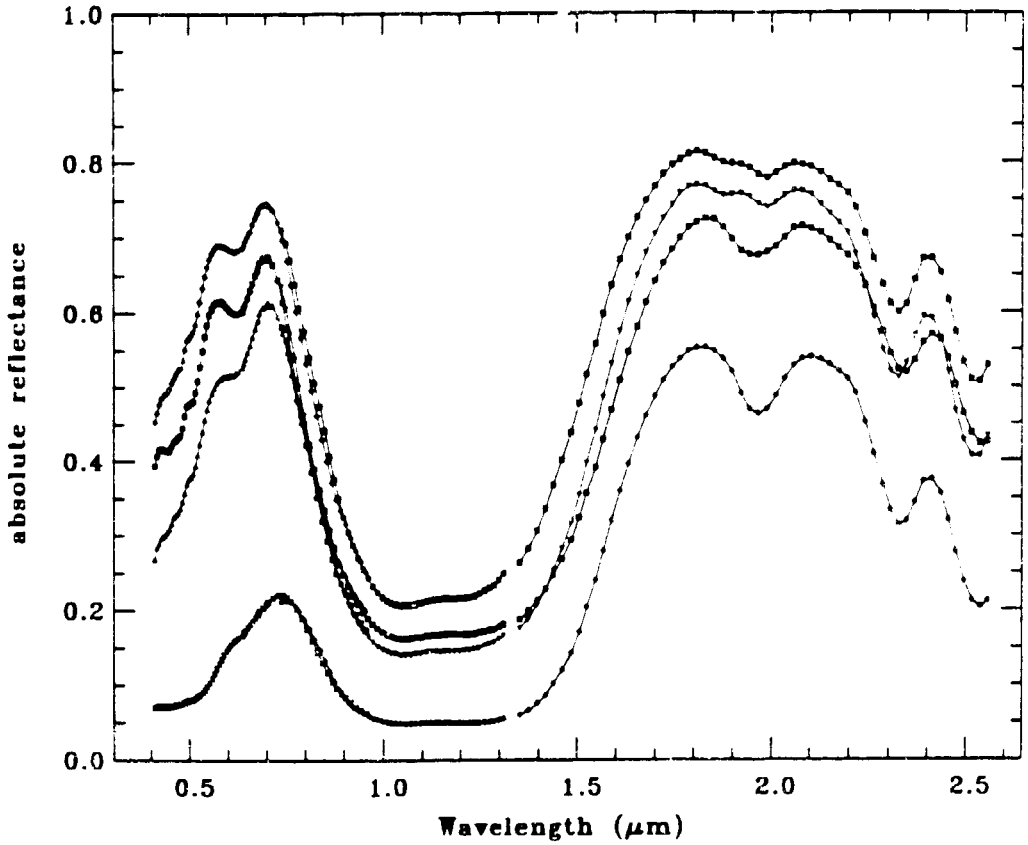

Figure 4.9 Spectra of siderites showing different degrees of alteration.

absorption features due to both Mn^{2+} (bands near 0.48 and 0.45μm) Fe^{3+} (bands near 0.6 and 0.5). This spectrum also shows the 0.63μm band which may be due to Fe^{2+} (see Chapter 5 for discussion). Spectra of more intensely weathered spectra contain greater proportions of iron oxides, which dominate the short wavelength portion of the spectrum. Iron oxides absorb strongly in the VIS portion of the spectrum, but are quite bright in the NIR (Singer, 1982). Thus, although the Fe^{3+} bands are very strong in spectra of the intensely altered samples, the carbonate bands which occur at longer wavelengths can still be seen.

In addition the iron oxides contain some water. This is reflected in the change in shape of the curve in the 1.9μm region. In the first spectrum the two carbonate bands can be clearly distinguished. However, as the intensity of the alteration increases, the carbonate bands are masked by the water band and there is a single asymmetric feature in this region.

MINERALOGICAL APPLICATIONS

As discussed in Chapter 3, calcite, aragonite, and dolomite can be identified by their spectral propterties in the VIS and NIR. Can other carbonate minerals be distinguished in this way?

It was found that positions and shapes of carbonate bands can be used to distinguish calcite, aragonite, and dolomite. Carbonate band positions should be sufficient for distinguishing some of the other carbonate minerals as well. Absorption bands in magnesite and dolomite spectra occur at shorter wavelengths than carbonate bands in any of the other carbonate minerals. Studies thus far indicate that all carbonate bands in magnesite spectra occur at wavelengths 0.01 to 0.02μm shorter than equivalent bands in dolomite spectra, and should be sufficient for identification.

Carbonate bands in spectra of witherites and cerussites occur at longer wavelengths than those in spectra of any other common carbonate minerals, and also should prove sufficient for identification. Differences in band positions between witherite and cerussite spectra are marked, as can be seen in Figure 4.2. Those differences range from 0.04 to 0.07μm.

As was seen in Chapter 3, absorptions due to transition metal cations can also aid in mineral identification. Since substitution of these cations for the major cations in aragonite group minerals is very limited (Deer _et al._, 1962; Speer, 1983) the presence of these absorption features in a mineral spectrum indicate the mineral belongs to the calcite group. The precise position and shape of these bands can help distinguish the calcite group. The precise position and shape of these bands can help distinguish one mineral from another. The differences in shapes and positions of iron bands in different calcite group minerals discussed above are an example.

Carbonate bands in siderite spectra also occur at wavelengths which show little overlap with positions of carbonate bands of other common carbonates. In addition, siderites have the extremely strong iron band which is diagnostic.

In rhodochrosite spectra studied thus far, the carbonate band positions vary considerably, and are similar to those in smithsonite and strontianite spectra. However, these bands do identify the mineral as a carbonate, and the strong Mn^{2} bands are diagnostic.

Band positions for calcite and aragonite are similar, but as was seen in Chapter 3, detailed analysis of band positions allows the two to be distinguished. A similar situation probably exists between strontianite and smithsonite. Carbonate band positions are not strikingly

different, and their major cations do not have any absorption features which make their spectra distinctive. However, careful examination of the spectra of these two minerals shows that differences in band positions do exist. For example, band two in the strontianite spectra occurs at shorter wavelengths and is narrower than the same band in the smithsonite spectrum. In addition, substitution of transition metal cations for the major cation in smithsonites is a common phenomenon, while such substitutions in strontianites should be relatively rare (Deer et al., 1962; Speer, 1983). Presence of absorption features due to Fe^{2+} and other transition metal cations will aid in identification of smithsonite.

At this time the lack of good spectra limits what can be said about carbonate bands in smithsonite spectra. More spectra, preferrably of water-free samples, will be needed to characterize the spectral properties of smithsonites, and determine what spectral characteristics are most useful for mineral identification.

CHAPTER 5

Variations in Spectral Properties with Variations in Chemical Composition

INTRODUCTION

In chapters 3 and 4. it was shown that reflectance spectroscopy in the VIS and NIR can be used to derive information about the mineralogy of carbonates. This chapter will deal in greater detail with the chemical information which can be obtained from reflectance spectra.

Information on the chemical composition of carbonates can be obtained from reflectance spectra. In Chapters 3 and 4 the absorptions due to Fe^{2+} were examined. The effect of variations in iron content, as well as the effects of variations in the concentrations of other cations on carbonate spectra in the VIS and NIR region of the spectrum will be examined.

Reflectance spectroscopy in the VIS and NIR can also be used to determine the valence of transition metal cations occurring in carbonate minerals. Charge balance requires that all major cations in carbonates have a charge of +2, and studies by electron paramagnetic resonance (Wildeman, 1969) and Mossbauer spectroscopy (Takashima and Ohashi, 1968) indicate that for Mn^{2+} and Fe^{2+} at least, this is the case. However, there is little other direct evidence for the divalent state of cations in carbonates.

There are eight naturally occuring rhombohedral anhydrous single carbonates (Reeder, 1983):

calcite	$CaCO_3$
magnesite	$MgCO_3$
siderite	$FeCO_3$
rhodochrosite	$MnCO_3$
otavite	$CdCO_3$
smithsonite	$ZnCO_3$
sphaerocobaltite	$CoCO_3$
gaspeite	$NiCO_3$

In addition there are several ordered double carbonates, of which dolomite $[CaMg(CO_3)_2]$ and ankerite $[Ca(MgFe)(CO_3)_2]$ are the most common. Others include kutnahorite $[CaMn(CO_3)_2]$ and minrecordite $[CaZn(CO_3)_2]$ (Reeder, 1983).

Calcite and dolomite are the most abundant carbonate minerals, accounting for more than 90% of naturally occurring carbonates. Solid solution between aragonite group minerals is limited, and involves only Ca, Sr, Ba, and Pb (Speer, 1983). For these reasons, this chapter will deal only with carbonate group minerals, and the bulk of the discussion will deal with calcite and dolomite. Although gaspeite and sphaerocobaltite are rare and samples of them could not be obtained for this study, their major cations have absorption features in the VIS and NIR regions of the spectrum, and occur in solid solution in other calcite group minerals.

Formation of isomorphous solid solutions is common in calcite-group minerals, the degree of miscibility between end-member carbonates being largely a function of cation sizes (Reeder, 1983). Small differences in cation radii, e.g. Fe^{2+} and Mg^{2+}, Fe^{2+} and Mn^{2+}, and Mg^{2+} and Mn^{2+}, lead to complete miscibility, while larger differences in cation radii, i. e., between Ca^{2+} and Mg^{2+}, Ni^{2+} and Mg^{2+}, Ca^{2+} and Fe^{2+}, Ca^{2+} and

Mn^{2+} and Ca^{2+} and Ni^{2+}, lead to limited miscibility (Deer et al., 1962; Goldsmith, 1983; Reeder, 1983). Goldsmith (1983) gives a thorough review of phase relations of rhombohedral carbonates.

There are few published studies of spectral properties of carbonates in this wavelength region. However, information on spectra of transition metal cations may be obtained from measurements of spectra of aqueous solutions of these cations. The number, positions, and intensities of absorption bands due to a given transition metal ion depend on the type, position, and symmetry of the ligands (Burns, 1970). In calcite group minerals, all cations are surrounded by six oxygens forming slightly distorted octahedral sites (Reeder, 1983). Transition metal cations in aqueous solutions form hexaquo complexes, which also have approximately octahedral symmetry and in which the oxygen atom is the nearest neighbor of the cation (Berry et al., 1980).

Transition metal cations which can cause crystal field absorptions in this region of the spectrum in the divalent state are Ti^{2+}, V^{2+}, Cr^{2+}, Mn^{2+}, Fe^{2+}, Co^{2+}, Ni^{2+}, and Cu^{2+} (Burns, 1970). Of these cations, those which form stable end-member carbonate minerals and which occur in solid solution in common calcite-group minerals are Mn^{2+}, Fe^{2+}, Co^{2+} and Ni^{2+} (Reeder, 1983). It should be possible to eliminate Ti^{2+} and V^{2+} from the discussion here, as Ti^{2+} complexes are very unstable (Ballhausen, 1962) and V^{2+} is rare. Table 5.1 gives some of the data on absorption features in the VIS and NIR due to transition metal cations in carbonates, in solutions, and in hydrated compounds in which the cation is in octahedral coordination by water molecules.

Other cations of end-member calcite-group single and double carbonates (Ca^{2+}, Mg^{2+}, Cd^{2+}, and Zn^{2+}) do not absorb in this region (Burns, 1970), but may affect spectral properties of carbonate minerals

Cation		Form	Band Position	Source
V^{2+}	d^3	$V(H_2O)_6^{2+}$	11,800 17,500	1
Cr^{2+}	d^4	$Cr(H_2O)_6^{2+}$	14,000 14,000	1 2
Mn^{2+}	d^5	$MnCO_3$	18,180 22,220 24,390 27,030 29,410	3
		$Mn(H_2O)_6^{2+}$	18,900 23,000 25,000 28,000 29,750 32,400	1
		$Mn(H_2O)_6^{2+}$	18,800 23,000 24,900 25,150 28,000 29,700	4
		$Mn(H_2O)_6^{2+}$	18,870 23,120 24,960 25,275 27,980 29,750 32,960 40,810	5
Fe^{2+}	d^5	$Fe(H_2O)_6^{2+}$	10,000	2
		$Fe(H_2O)_6^{2+}$	10,000	1
		$Fe(H_2O)_6^{2+}$	10,400	6
		$Fe(H_2O)_6^{2+}$	10,400 8300	7
		$Fe(H_2O)_6^{2+}$	10,400	4

Cation		Form	Band Position	Source
Co^{2+}	d^7	$CoCO_3$	19,250 20,800 22,875	8
		$Co(H_2O)_6^{2+}$	8,100 19,400	6
		$CoSO_4.7H_2O$	8,350 19,800	1
		$Co(H_2O)_6^{2+}$	8,350 20,000	2
Ni^{2+}	d^8	$Ni(H_2O)_6^{2+}$	8,500 13,500 15,400 25,300	6
		$Ni(H_2O)_6^{2+}$	8,500 13,500 15,400 25,300	9
		$Ni(H_2O)_6^{2+}$	8,000 14,000 25,300	4
		$NiSO_4.7H_2O$	8,600 14,700 25,500	1
Cu^{2+}	d^9	$Cu(H_2O)_6^{2+}$	9,430 12,660	10
		$CuSO_4.5H_2O$	13,000	1

1. Holmes and McClure (1958); 2. Ballhausen (1962); 3. Hunt and Salisbury (1971); 4. Jorgensen (1954); 5. Heidt et al. (1959); 6. Jorgensen (1955); 7. Cotton and Meyers (1960); 8. Le Paillier-Malecot (1983); 9. Jorgensen (1956); 10. Bjerrum et al. (1954)

Table 5.1 Data from the literature on number and positions of absorptions due to transition metal cations. Band positions in inverse centimeters.

in other ways. The effect of both transition and non-transition metal cations on the spectral properties of carbonates will be discussed below.

MAGNESIUM, Mg^{2+}

High magnesian calcites are important constituents of modern marine sediments (Milliman, 1974). Therefor it would be highly desirable to determine the effect of solid substitution of Mg for Ca in calcites on their spectral properties. Unfortunately, Mg^{2+} itself has no characteristic absorptions in this region, and information on Mg^{2+} can only be derived from the carbonate bands. All the high Mg calcites studied thus far contain water (see Chapter 6), and the strong absorptions due to water have made it difficult thus far to do any detailed studies of the changes of spectral properties of calcite with variations in Mg^{2+} content.

Figure 5.1 shows spectra of a low Mg calcite (Crassostrea) and a high Mg calcite (Echinometra). Despite the strong water bands, it can be seen that the strongest carbonate band, band 1, occurs at shorter wavelengths in the high Mg calcite than the same band in the low Mg calcite spectrum. This is typical of spectra of biogenic high Mg calcites.

The shift of the carbonate band to shorter wavelengths with increased Mg^{2+} content is in accord with the fact that carbonate bands in dolomite [$CaMg(CO_3)_2$] and magnesite ($MgCO_3$) spectra occur at shorter wavelengths than those in calcite spectra (see Chapter 4).

Before more detailed studies can be done, some means of isolating the spectral component due to water in these spectra must be developed. Blake (1983) used the LOWTRAN model to remove effects of absorptions due to atmospheric water from remotely obtained spectra. Similar corrections for absorptions due to liquid water in laboratory spectra should also be possible.

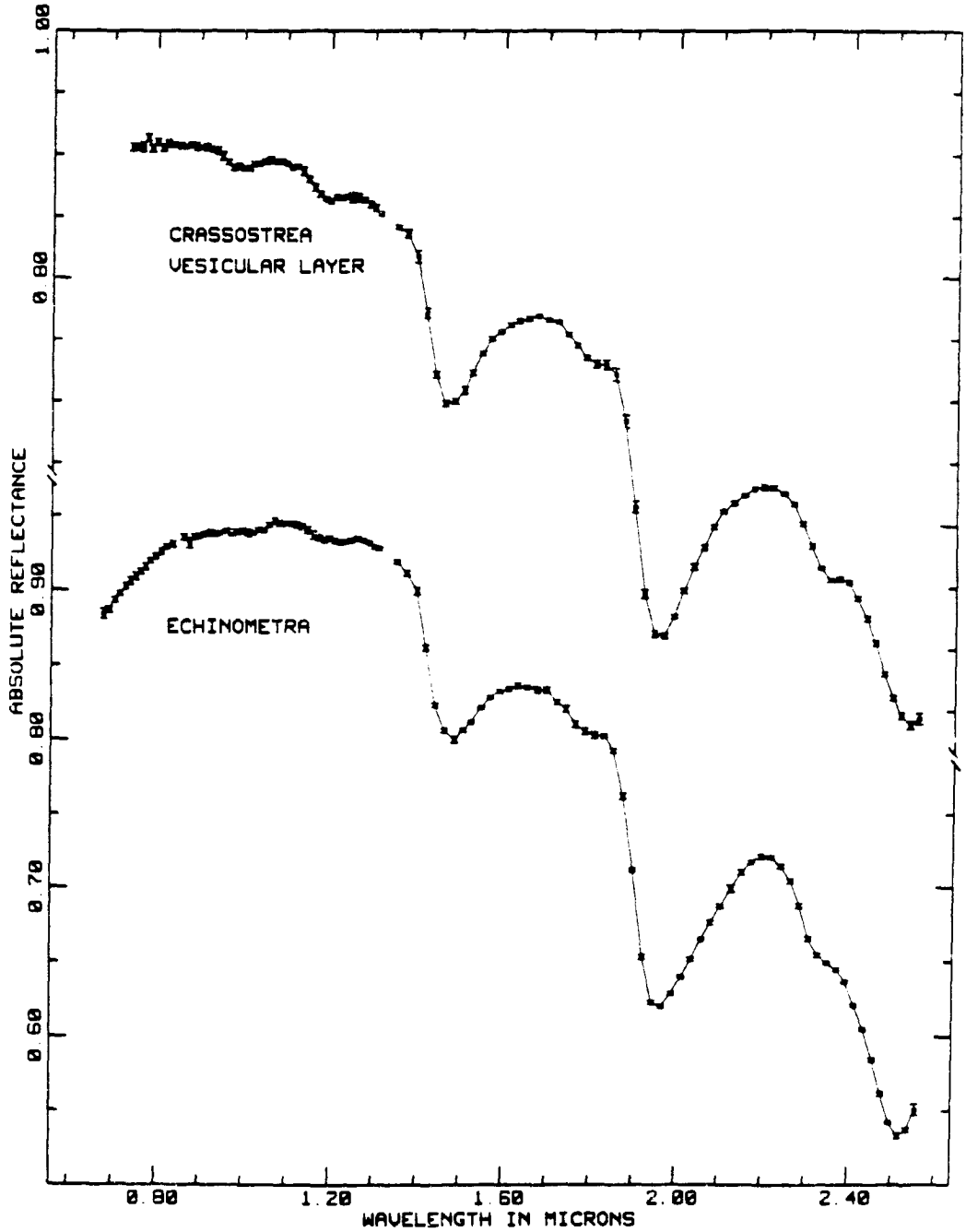

Figure 5.1 Spectra of biogenic high Mg (Echinometra) and low Mg (Crassostrea) calcites, showing difference in position of carbonate band 1.

COPPER, Cu^{2+}

As mentioned in Chapter 4, two absorption features observed in calcite spectra in this study were possible choices for Fe bands. Both occurred near 1.0μm, where Fe bands commonly occur. However, Cu^{2+} in aqueous solutions also gives absorptions between 0.7 and 1.0μm (Bjerrum et al., 1954; Holmes and McClure, 1957). Positions of absorption bands due to transition metal cations can vary widely, depending on the size and symmetry of the site in which the ion occurs. For example, although bands due to Fe^{2+} generally occur in the 1.0μm region, pyroxene spectra have an absorption feature due to Fe^{2+} near 2.0μm (Adams, 1975). Thus band position alone can't be used to assign a new absorption feature to a given cation.

Cu^{2+} has a $3d^9$ electronic configuration, and in an undistorted octahedral site has a ^2E_g $(t_{2g})^6$ $(e_g)^3$ ground state. The only excited state is $^2T_{2g}$ $(t_{2g})^5$ $(e_g)^4$ (Ballhausen, 1962). The ^2E_g state is susceptible to a strong Jahn-Teller distortion, and no regular octahedrally coordinated Cu^{2+} complex should exist (Ballhausen, 1962). This mechanism is invoked to explain the fact that there are no naturally occurring anhydrous copper carbonate minerals (Reeder, 1983). There are two hydroxyl-bearing copper carbonate minerals: malachite and azurite. Data on their crystal structure is summarized by Andersen (1978). The copper ions in malachite ($Cu_2CO_3[OH]_2$) occur in two axially elongated octahedral sites, one coordinated by four CO_3^{2-} and two OH^- ions, the other by two CO_3^- and four OH^- ions The spectrum of malachite has absorptions due to Cu^{2+} near 1.08μm, 0.77μm and 0.45μm. Copper ions in azurite ($Cu_3[CO_3]_2[OH]_2$) also occur in two different sites, which are so distorted that one is essentially square planar, the other a square based pyramid. Azurite has two absorptions due to Cu^{2+} near 0.77μm and

0.62μm (Andersen, 1978). Hunt and Salisbury (1971) found malachite and azurite spectra to have a band centered near 0.8μm, and a fall-off into the UV beyond 0.52μm in malachite spectra, and beyond 0.45μm in azurite spectra.

Unfortunately the existence of two distinct sites for copper in these minerals, and the large degree of distortion of the sites in which the Cu^{2+} resides make close comparisons between absorption features due to Cu^{2+} in malachite and azurite spectra and in calcite spectra of limited value. It would be anticipated that Cu^{2+} in aqueous solution would be a much better analogue. Bjerrum et al. (1954) found that an absorption spectrum of aqueous Cu^{2+} has a broad feature which can be resolved into two gaussian curves centered at 0.79 and 1.06μm.

The calcite spectra shown in Figure 5.2 have absorption bands near 0.9μm which are due to copper. Localities for samples discussed in this chapter not included in preceding tables are given in Table 5.4. As mentioned above, an absorption feature in this region could also be due to Fe^{2+}, a cation which is reported to occur much more commonly in solid solution in calcites than is Cu^{2+}. In fact substitution of Cu^{2+} for Ca^{2+} in calcites is not even discussed in review articles and summaries on carbonate chemistry by Deer et al. (1962), Goldsmith (1983), Lippman (1973) or Reeder (1983). This particular absorption feature was found in the spectra of five of the calcite samples used in this study, and it would be logical to attribute such a common feature to a common ion, such as Fe^{2+}. However, all five of the samples which show this feature are from Arizona, and four are from Bisbee, the site of large copper mines. Palache et al. (1951) note that crystals and stalactites from this area are sometimes colored green by malachite inclusions. Anthony et al. (1977) also note that calcites from the Bisbee area contain

copper salts. Atomic absorption analyses of four of these samples (1511, 1513, 10527, and 1504) indicate that they contain copper.

Negative evidence also supports the assignment of this feature to Cu^{2+}. X-ray flourescence and atomic absorption analyses of some of the samples containing this feature indicate the Fe^{2+} content of these samples is very low. Atomic absorption analysis of the same three samples analysed for copper indicate they contain less than 0.005% Fe by weight. This concentration of Fe is below the detection limits determined for Fe^{2+} in dolomite and calcite spectra (see below), and other calcites containing similar amounts of Fe have no absorption features in this region. In addition, this feature does not fit the trends for shapes and positions of Fe^{2+} bands in rhombohedral carbonate mineral spectra outlined in Chapter 4. If this feature were indeed due to Fe^{2+}, it would mean that the iron band which occurs at the highest energies, and most nearly approximates the ideal single band predicted for iron bands in octahedral sites would occur in the mineral with the largest M-O bond lengths and the most distorted coordination octahedra.

A similar feature occurs in a smithsonite spectrum (Fig. 5.5). Beaden (1925) published an analysis of smithsonite from Kelly, New Mexico, the site from which sample 4504 was obtained, which showed the sample contained 3.48% CuO, and only trace amounts of FeO. Spark spectrometry also indicates this sample contains Cu.

These absorption features in both the calcite and smithsonite spectra are centered at shorter wavelengths than iron bands in the same minerals, and do not show the marked doubling that the iron bands do.

Cu^{2+} in calcite produces a broad band centered near 0.9μm. When the spectrum is plotted in inverse wavelength space, it can be seen that

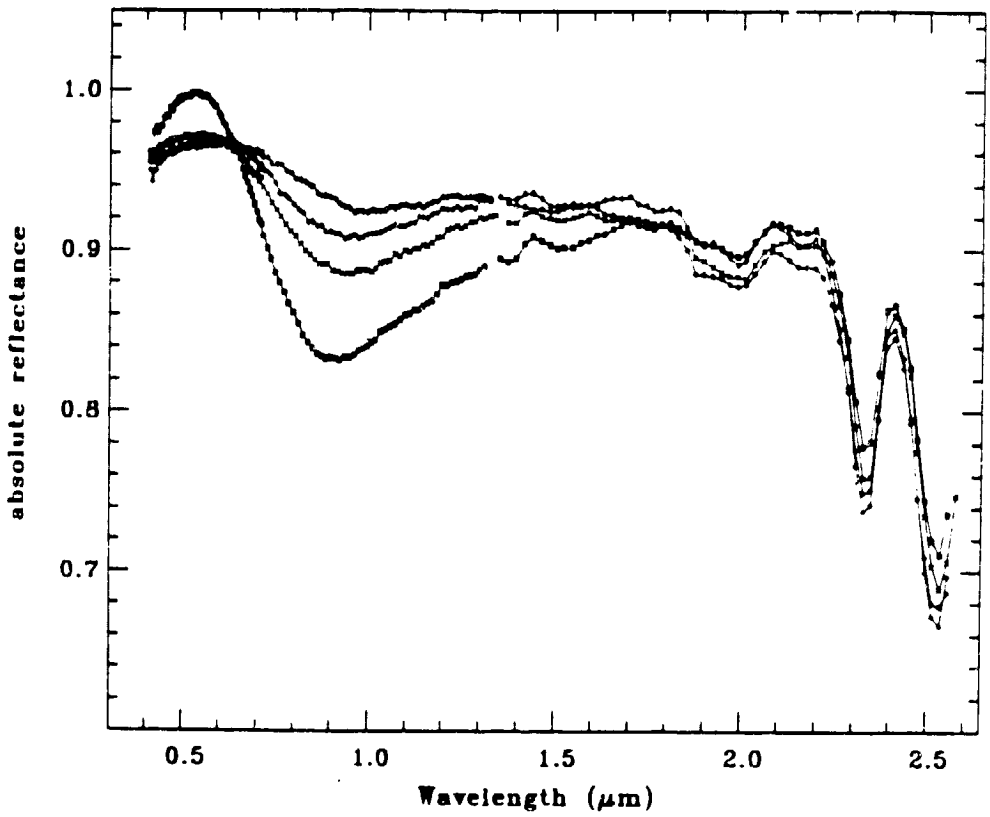

Figure 5.2 Spectra of cuprian calcites.

	Carbonate Bands							Cu
Sample	1	2	3	4	5	6	7	Band
1510	2.533	2.388	2.269	2.165	1.992	1.884	1.788	0.979
10527	2.547	2.343	2.268	2.170	1.993	1.884	1.764	0.956
1511	2.527	2.333	2.254	2.158	1.989	1.883	1.774	0.948
1513	2.535	2.336	2.258	2.170	1.989	1.889	1.808	0.931
1504	2.529	2.334	2.258	2.160	1.991	1.890	1.763	0.903

Table 5.2 Positions of carbonate bands and major copper band in calcite spectra as determined with the Gaussian fitting routine.

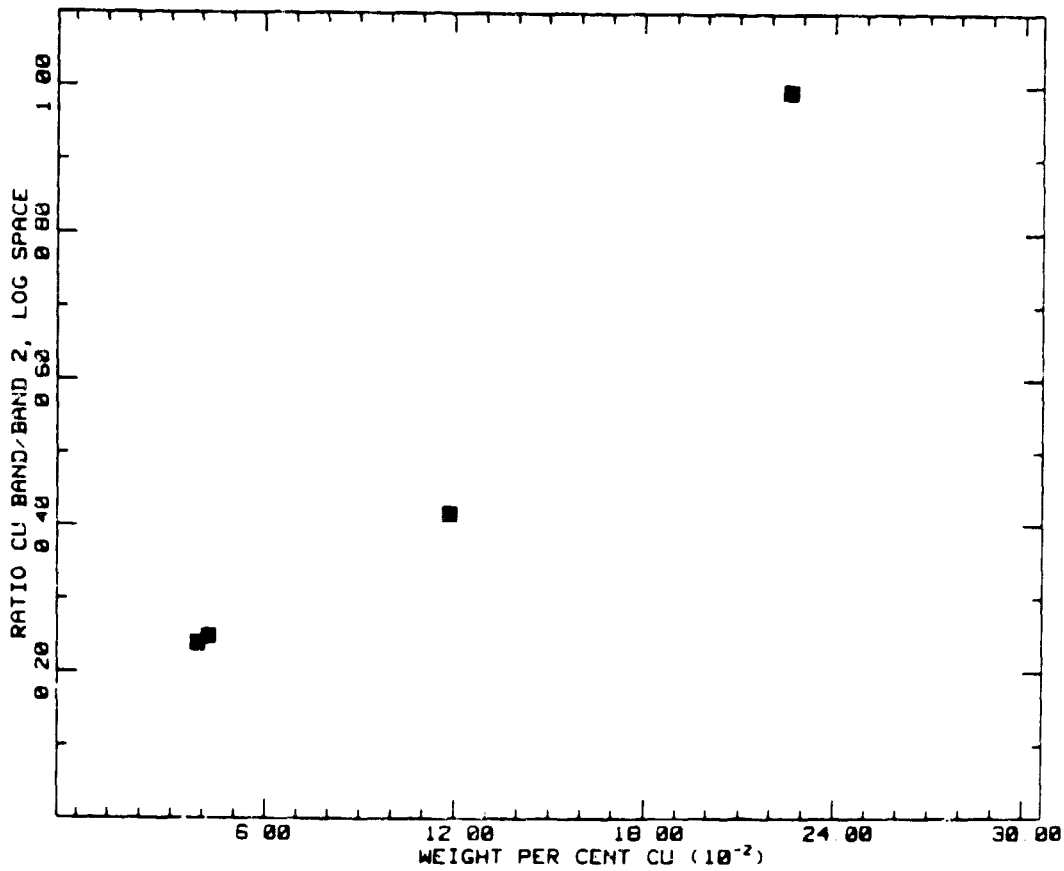

Figure 5.3 Relative intensities of copper bands plotted as a function of copper content.

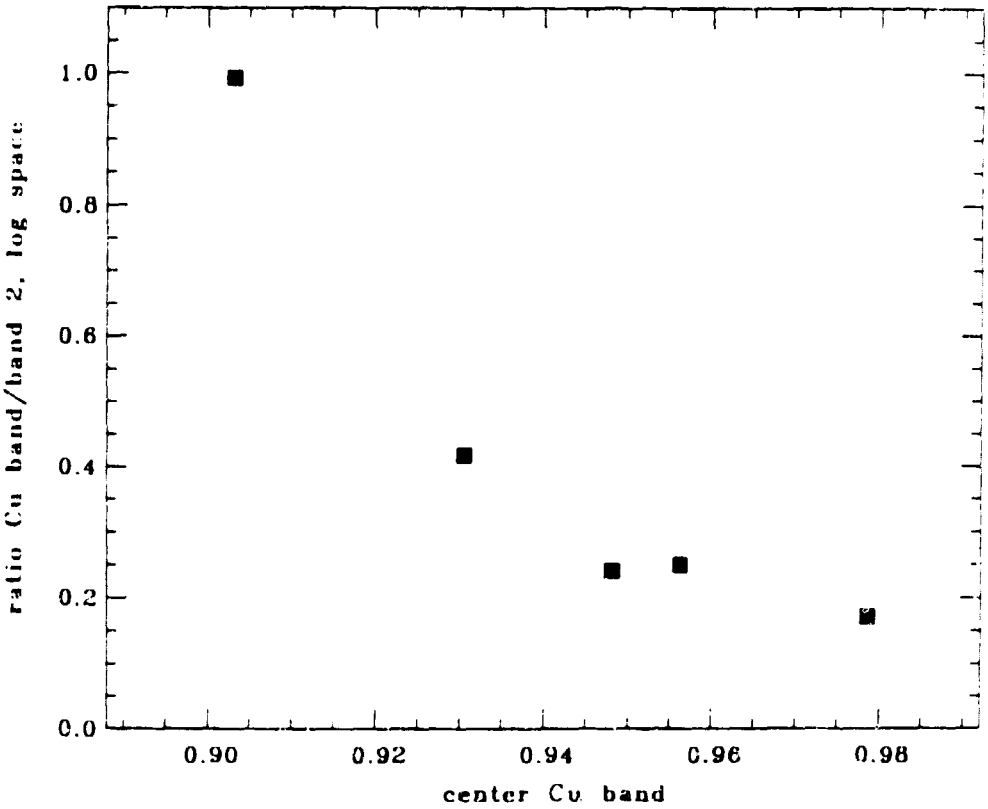

Figure 5.4 Relative intensities of copper bands plotted vs. position of strongest copper band.

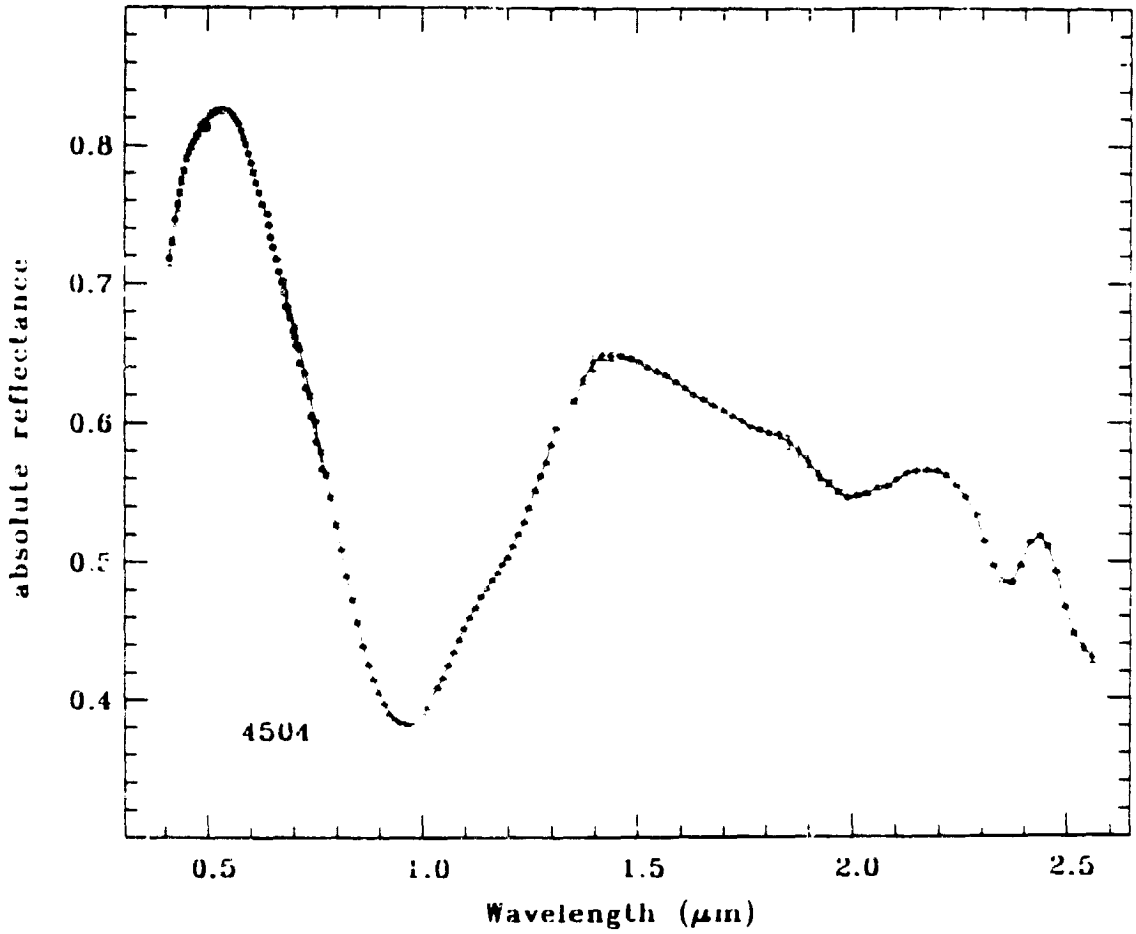

Figure 3.5 Spectrum of a cuprian smithsonite.

this feature actually consists of at least two bands. The stronger of the two is centered near 0.9μm, the weaker is centered in the 1.5μm region, and may actually be composed of two bands. Although the presence of minor amounts of water in some samples, and the possible presence of other absorbing cations in some samples precluded precise determination of the intensities and positions of this weaker band, it appears that when measured on a log scale, as is done when GFITting spectra, the intensity of the stronger band is three to four times that of the weaker band.

Chemical analyses show that as with Fe^{2+} and Mn^{2+}, relative intensities of bands increase with increase in concentration of the absorbing cation. Figure 5.2 shows spectra of four cuprian calcites (adjectival form used by Palache _et al._, 1951). Intensities of all the carbonate bands are similar, indicating the particle sizes of the samples were approximately the same. The differences in intensities of coppper bands, then, are due to differences in copper content. Figure 5.3 shows the intensity of the copper band ratioed to the intensity of carbonate band 2 (to correct for particle size effects, see discussion of iron bands below) plotted against the Cu content of the four samples for which analyses were available. These data bear out the conclusion that band intensity increases with copper content.

With increasing Cu^{2+} content, the stronger Cu^{2+} band moves to shorter wavelengths. In addition, the drop-off into the ultraviolet becomes steeper as copper content increases. Figure 5.4 shows a plot of relative intensity of the copper band plotted against the position of the center of the copper band for five sample spectra containing this absorption feature. This illustrates the shift in band position with increasing Cu content. The limited scatter in the data may be due to

the fact that other absorbing species, either transition metal cations or water, add features to the spectrum.

Detection limits for copper appear to be lower than for iron. Similar quantities of iron in dolomites give barely perceptible absorption features. Holmes and McClure (1957) found that molar extinction coefficients for Cu^{2+} were about three times that for Fe^{2+}.

The centers of carbonate bands in spectra of cuprian calcites occur at the same or slightly shorter wavelengths than equivalent bands in non-cuprian calcites. Table 5.2 gives positions of bands for five cuprian calcites as determined by GFITting.

Copper features in a smithsonite spectrum are shown in Figure 5.5. This spectrum was not analysed usinng GFIT, and the band positions given are estimates only. This band is narrower than the copper band in calcite spectra. The band is centered near 0.97μm, and as with the copper feature in calcite spectra, there is a second weaker feature which causes a shoulder on the main band. However the second band occurs at shorter wavelengths than its calcite counterpart, being centered at approximately 1.2μm. The fact that the splitting between the two copper features is much less in the smithsonite spectrum than in the calcite spectrum probably reflects the fact that, as discussed in Chapter 4, the octahedral sites in calcites are more distorted than those in smithsonites.

IRON, Fe^{2+}

Ferrous iron very commonly substitutes into calcites and dolomites, as well as other calcite group minerals (see Chapter 4). Crystal field theory predicts that a d^6 ion in and octahedral site will produce one absorption band due to a transition from $^5T_{2g}$ $(t_{2g})^4$ $(e_g)^2$ to ^5E_g $(t_{2g})^3$ $(e_g)^3$ (Burns, 1970; Cotton and Meyers, 1960). The data in Table 5.1

indicate that this ion forms a strong absorption near 1.0μm. If the octahedral site is distorted, the degeneracies of the d-orbitals will be lifted and two or more absorption bands may occur (Burns, 1970).

As seen in Chapter 4, Fe^{2+} in calcite produces a broad double absorption band centered near 1.3μm. Only two ferroan calcite spectra have been obtained thus far, but based on this limited data set it appears that carbonate band positions in ferroan calcite spectra are essentially the same as those of non-ferroan calcites.

The number and positions of the bands indicate that the iron is actually Fe^{2+} rather than Fe^{3+}. Fe^{3+} in aqueous solution has three bands near 0.8, 0.55, and 0.41μm (Cotton and Meyers, 1960). In Chapter 9 the effect of ferric iron in the form of iron oxides on the spectral properties of carbonate rocks is discussed.

Detection limits for Fe are quite low. X-ray fluorescence analyses of two calcite samples (6506 and 10519) indicate they contain ≈0.01% Fe by weight. Atomic absorption analysis of 6506 confirms this. These spectra have very weak Fe^{2+} absorptions, indicating this is just at the detection limit for Fe.

Fe^{2+} also substitutes into dolomites. The majority of ferrous iron in dolomites substitutes for Mg^{2+}, and occurs in the same B-site as the Mg^{2+} (Reeder, 1983). Up to 70% of the Mg may be replaced by Fe, and these high iron dolomites are also called ankerites (Deer _et al._, 1962; Lippman, 1973).

As was seen in Chapter 4, Fe^{2+} in dolomites produces a broad double band in their spectra centered near 1.1μm. The intensity of this band increases with increasing iron content, as can be seen in Figure 3.17. In addition, the drop-off into the ultraviolet increases in intensity and extends to shorter wavelengths as iron content increases.

Spectra of eight dolomite samples were analyzed using the GFIT routine. Figure 5.6 shows a completed gaussian fit to one of the dolomites, and the results of this analysis are given in Table 5.3.

Bands numbered 1 through 7 are the carbonate bands discussed in Chapter 3, and bands 8 through 10 are iron bands. The iron bands were initially fit with two bands, corresponding to the two obvious bulges in the spectrum near 1.0 and 1.35μm. While this allowed a fit to be achieved at high accuracy (0.005) there still remained some areas of the curve which were not well matched. This can be seen in Figure 5.7a, which shows the residual errors for a two-iron-band fit. The wavelike features in the residual errors near 1.0μm indicate a feature is missing. A third band in the 1.25μm region was added to the first two and the fits were done again. The fit was done so that the first two bands used were large, and the third band added in the middle was kept as the smallest band. As can be seen in Figure 5.7b the three-band fit to the iron band gave an improved fit as shown by the residual errors. There remains a small wave-like feature in the errors near 1.0μm, which is evidenced by a slight miss-match between the data and fit curve in Figure 5.6. However the errors in this region for most spectra are less than 1%, and the three bands were taken as an adequate fit to the data.

Adding the extra band to the iron feature did not affect the fit to the carbonate bands. As can be seen in Figure 5.7, the residual errors in this region do not change. Carbonate band positions determined in both fits are the same.

The cause of band 11 is not certain. It occurs in spectra of ferroan dolomites, rhodochrosites, and siderites. It occurs at longer wavelengths than band positions reported for Mn^{2+}, and may be one of the weak spin-forbidden bands which occur in Fe^{2+} spectra (Burns, 1970).

ORIGINAL PAGE IS
OF POOR QUALITY

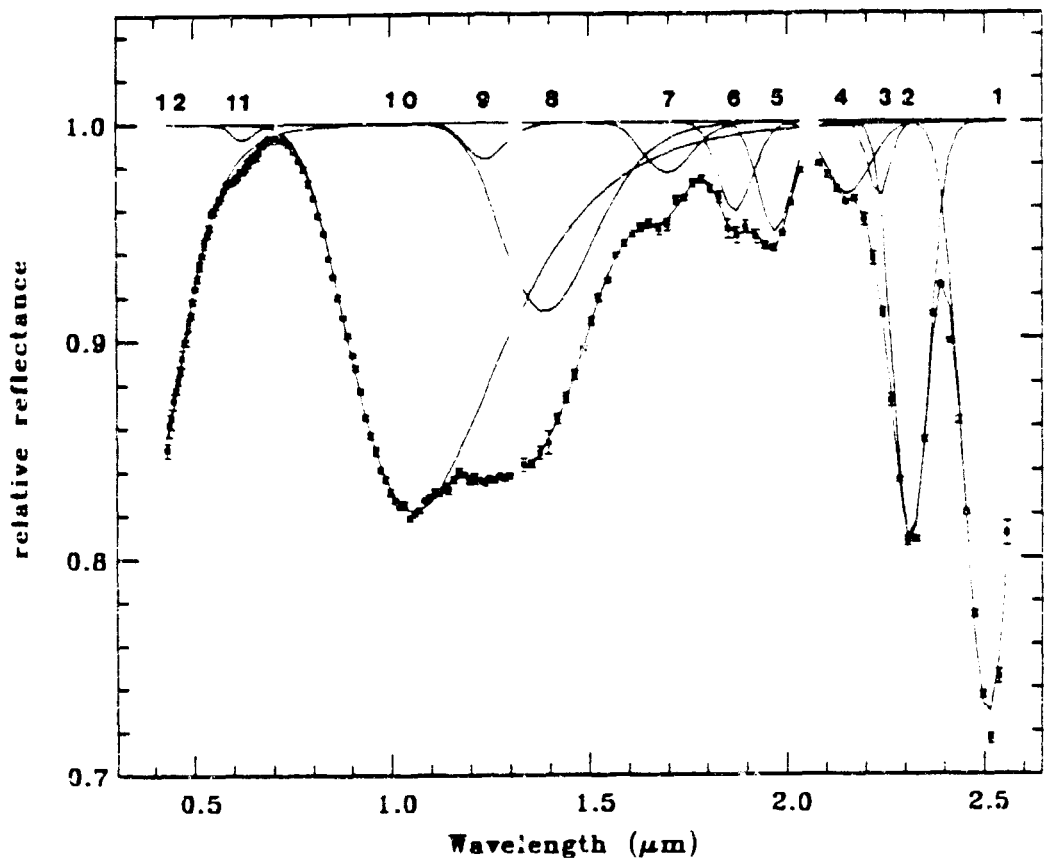

Figure 5.6 Gaussian fit to dolomite spectrum (#2501) showing all bands fit to dolomite spectra.

	Carbonate Bands					
Sample	1	2	3	4	5	6
6514	2.516	2.319	2.244	2.165	1.979	1.862
6509	2.516	2.320	2.248	2.165	1.974	1.869
6503	2.505	2.312	2.235	2.157	1.971	1.853
2501	2.508	2.313	2.234	2.155	1.971	1.872
6510b	2.518	2.322	2.247	2.170	1.977	1.867
5501	2.513	2.323	2.244	2.150	1.975	1.882
6515a	2.530	2.333	2.262	2.185	1.986	1.888
6502	2.532	2.330	2.251	2.191	1.976	1.912

	Iron Bands		
Sample	8	9	10
6514	1.343		1.040
6509	1.379		1.050
6503	1.435	1.268	1.044
2501	1.389	1.237	1.055
6510b	1.409	1.269	1.051
5501	1.419	1.276	1.056
6515a	1.420	1.277	1.060
6502	1.411	1.256	1.063

Table 5.3 Positions of carbonate and iron bands in dolomite spectra determined using the Gaussian Fitting routine. Samples are listed in order of increasing Fe content, as determined by atomic absorption.

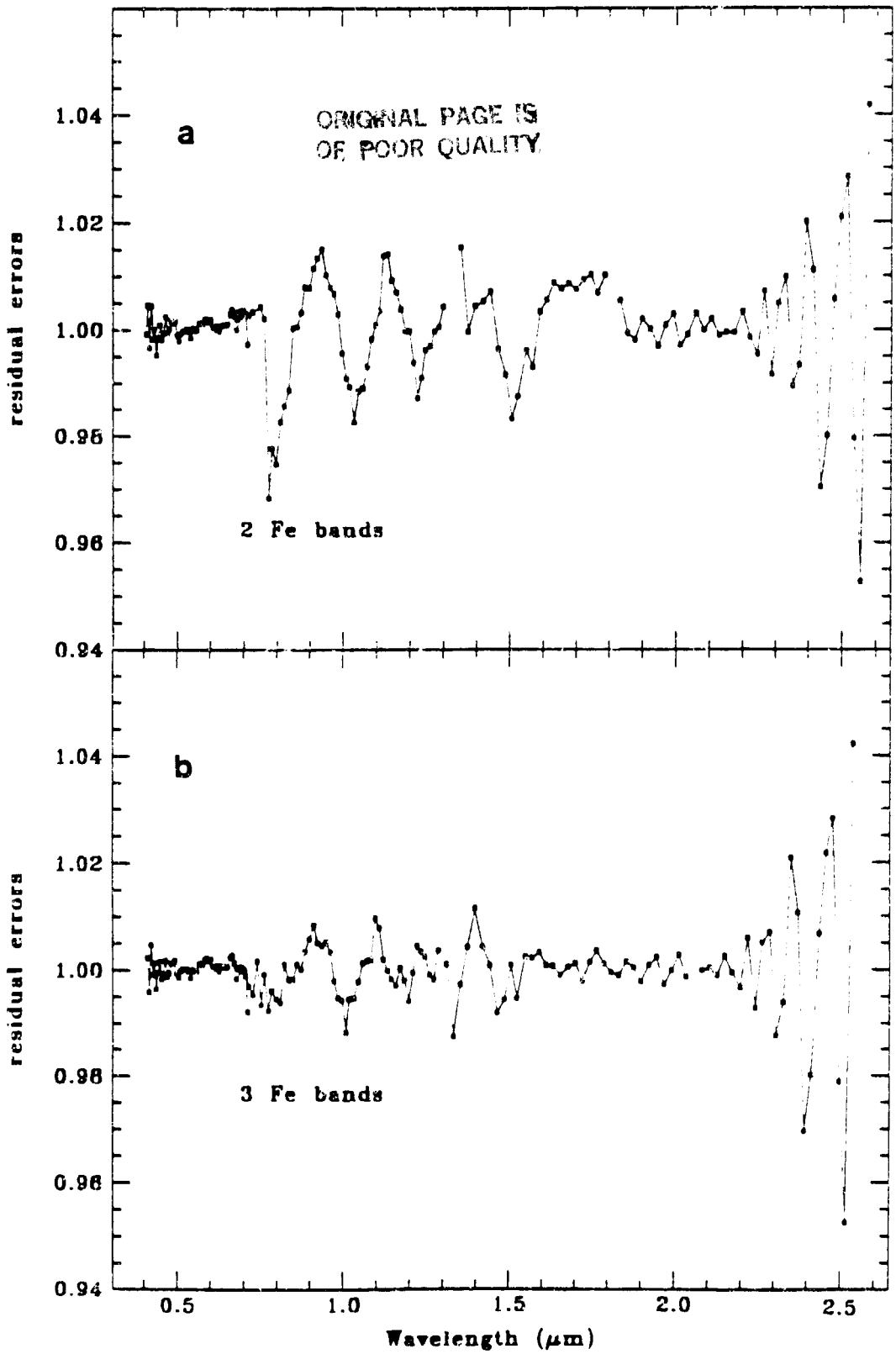

Figure 5.7 Residual errors from a gaussian fit to the spectrum of #6510b using two bands (a) and three bands (b) to fit the Fe feature.

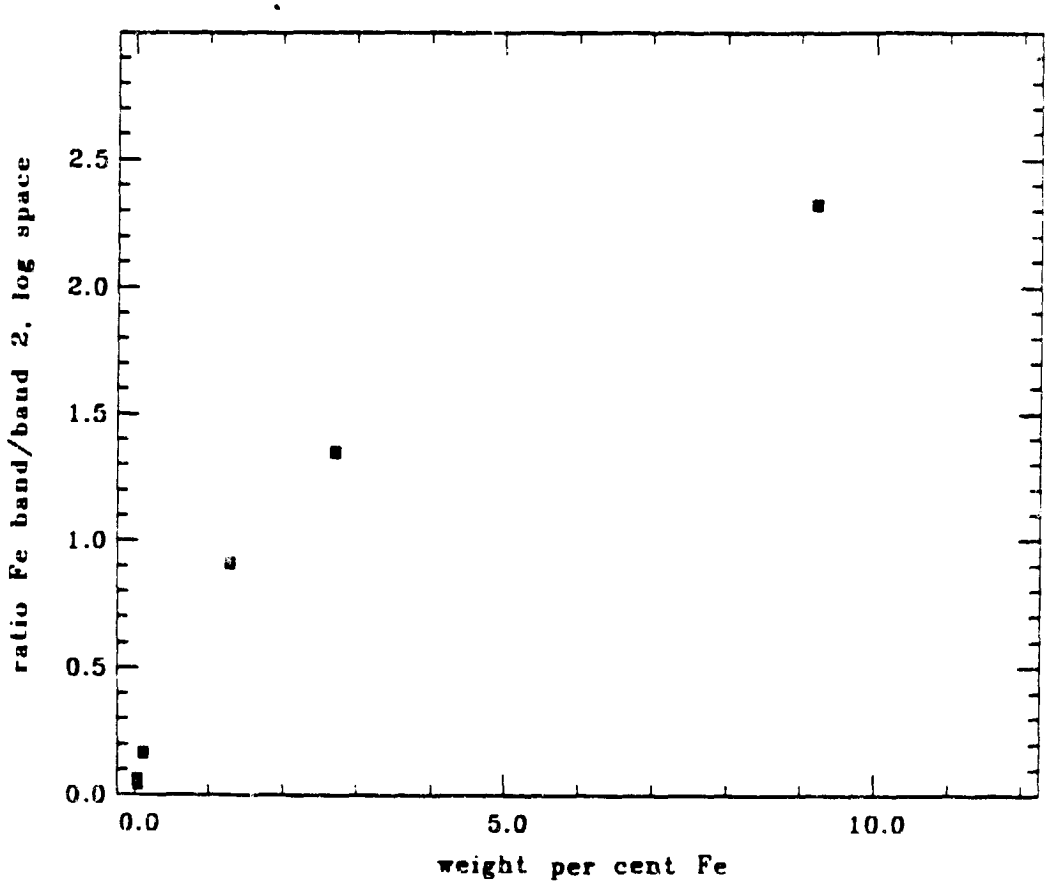

Figure 5.8a Relative intensities of Fe bands in spectra of dolomite samples, as determined using GFIT, plotted as a function of Fe content. Unweathered samples.

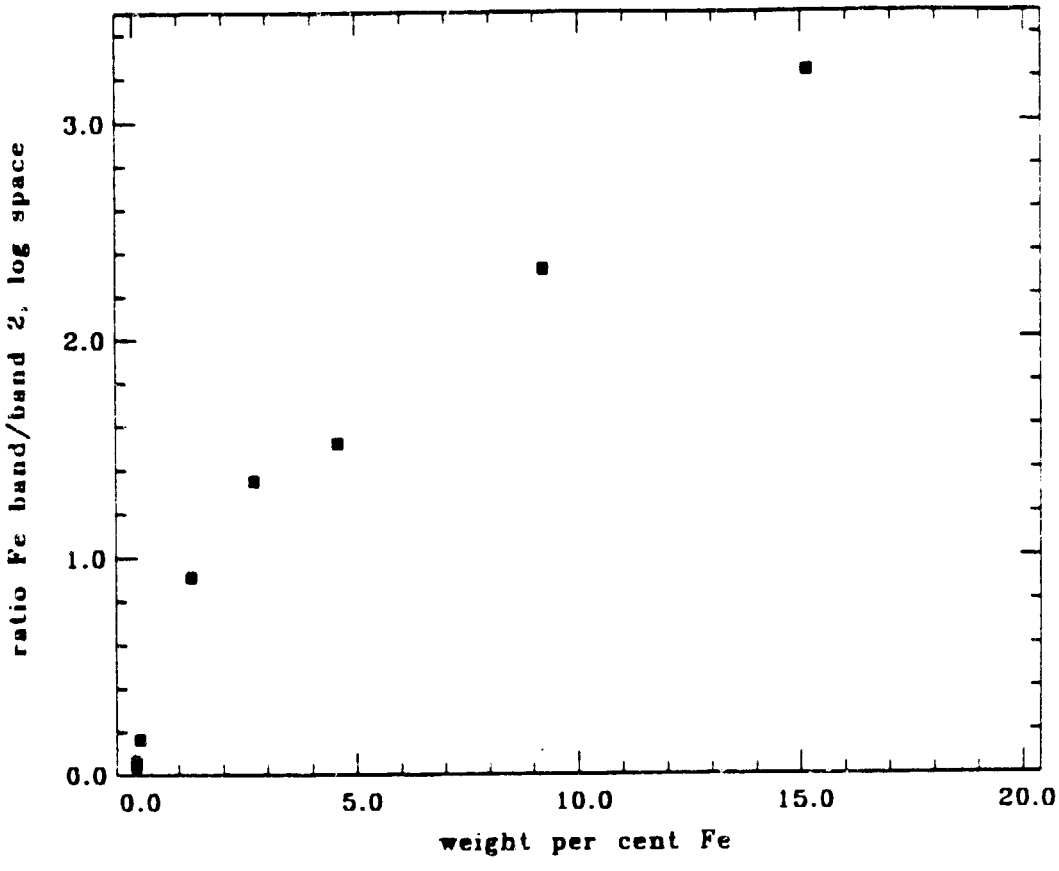

Figure 5.8b Relative intensities of Fe bands in spectra of dolomite samples, as determined using GFIT, plotted vs. Fe content. Weathered and unweathered samples.

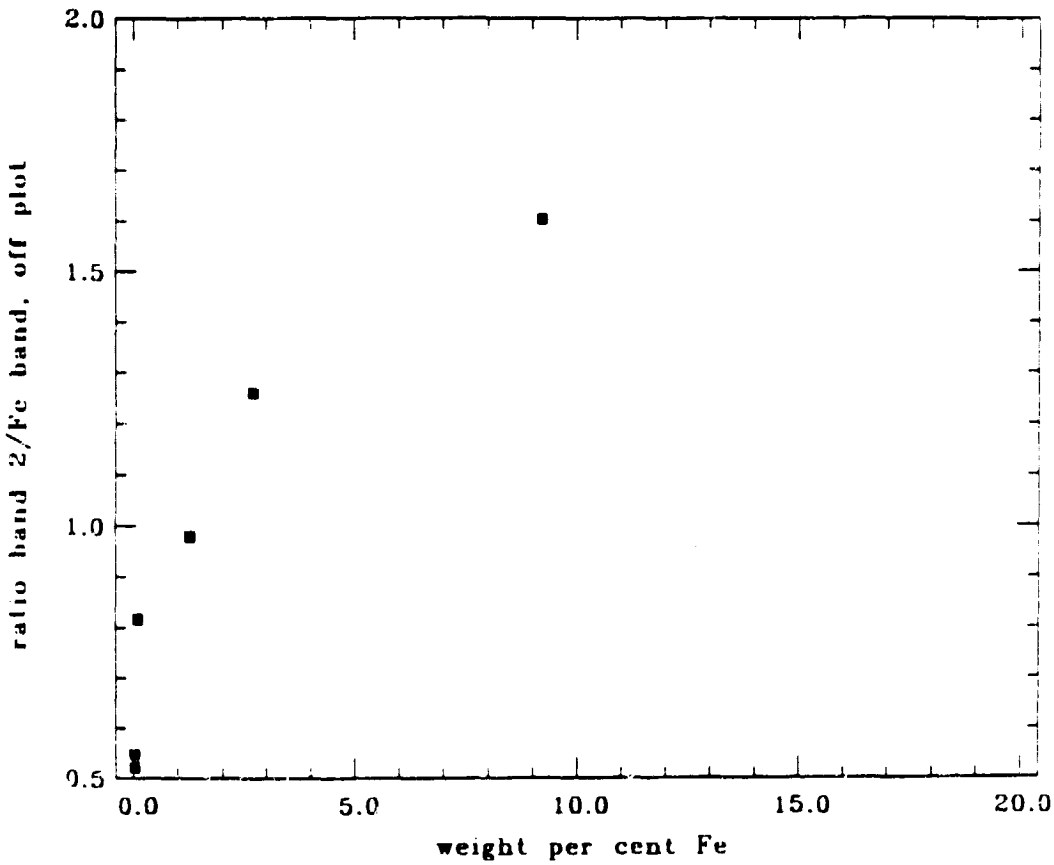

Figure 5.9a Relative intensities of Fe bands plottted vs. Fe content for unweathered samples. Intensities taken directly from data curve.

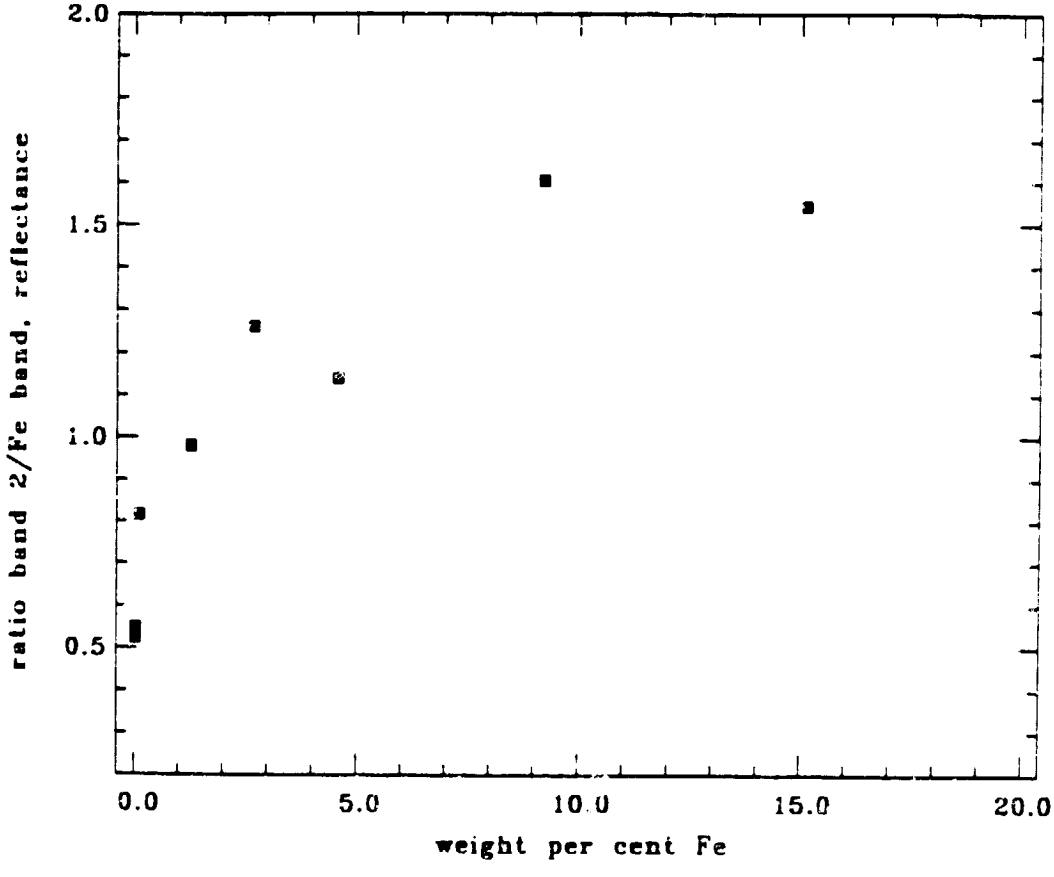

Figure 5.9b Relative intensities of Fe bands plotted vs. Fe contents. Intensities taken directly from data curve. Weathered and unweathered samples.

Calcite	1504	Santa Cruz Co., New Mexico[1]
	1505	Richelsdorf, Germany[2]
	1508	Franklin, New Jersey[3]
	1510	Bisbee, Arizona[4]
	1511	Bisbee, Arizona[5]
	1513	Bisbee, Arizona[6]
	1515	Moresnit, Germany[7]
Dolomite	6515a	Morro Velho, Brazil[8]
	6502	Cumberland, England[9]
Aragonite	10501	Horschenz, Czechoslovakia[10]
Smithsonite	4501	Laurium, Greece[11]
	4504	Kelly, New Mexico[12]
	4506	Chihuahua, Mexicon[8]
Siderite	6515b	Morro Velho, Brazil[8]
	9503	Copper Lake, Antigonish Co., Nova Scotia[12]
	9504	Ouro Preto, Minas Gerais, Brazil[13]
	9506a	Roxbury, Litchfield Co., Connecticut[14]
Magnesite	2507	Kurnalpi, Western Australia[15]

1. Smithsonian Inst. #125127; 2. Smithsonian Inst. #84055; 3. Smithsonian Inst. #C6336; 4. Smithsonian Inst. #82364; 5. Smithsonian Inst. #82362; 6. Smithsonian Inst. #B9624; 7. Smithsonian Inst. #104454; 8. Horn Minerals, Smithtown, Long Island; 9. Smithsonian Inst. #81674; 10. Smithsonian Inst. #R12050; 11. Smithsonian Inst. #R2518-9; 12. Wards Natural Science Establishment; 13. Nature's Treasures, Hawthorne Calif.; 14. Minerals Unlimited, Ridgecrest, Calif.; 15. Excalibur Minerals, Dover, N. J.

Table 5.4 Mineral samples discussed in this chapter, and localities from which they were obtained.

Band 12 outlines the absorption edge into the UV which is probably due to a charge transfer band centered at wavelengths too short to be measured by our instrument.

Unlike the Cu bands in calcites, there is no discernable trend in position of iron bands associated with the changes in iron content.

However, the intensity of iron bands increases with increased Fe content. These eight dolomites were analyzed for iron by atomic absorption spectrophotometry. Since, as seen in Chapter 3, absorption band intensities are affected by particle size and packing, absolute intensities of iron bands could not be used as a measure of iron content. As seen in Chapter 3, however, intensities of carbonate bands do not vary significantly with changes in chemical composition. Thus the intensities of the carbonate bands can be taken as a measure of grain size and packing, and intensities of Fe bands relative to the carbonate bands can be used as a measure of Fe content. The intensity of the strongest Fe band (band 10 in Figure 5.7) was ratioed to the intensity of band 2, the carbonate band for which, as discussed in Chapter 4, parameters could be most reliably determined, and these ratios were plotted as a function of Fe content.

Six of the eight samples were unweathered: 6509, 6514, 6503, 2501, 6510b and 6515a. Samples 5501 and 6502 were buff-colored from Fe oxides. Figure 5.8a shows a plot of the ratio of the intensity of the Fe band to the intensity of band 2 plotted as a function of Fe content. Intensities used were those determined in log space using the GFIT program. The points form a smooth curve, with the ratio increasing with increasing Fe content. Figure 5.8b includes the data for the two weathered samples. Although sample 5501 falls slightly off the curve, the correlation is still good. Ratios determined using intensities in

linear space rather than log space are very similar to these, and show the same relationships. Either values could be used.

Was all that GFITting useful? For comparison, ratios for values of intensities taken directly from the data curves were used. The value for the lowest data point in the iron band and the lowest data point in the 2.3μm carbonate band were ratioed and these values plotted against Fe content. Figure 5.9a shows the values for the six unweathered samples. The curve outlined by the points shown here, although not as smooth as that seen in Figure 5.8a, shows a relatively good correlation between this ratio and Fe content. However, when the data points for the weathered samples are added, as in Figure 5.9b, it can be seen that the correlation is rather poor. The gaussian analysis has removed some of the effects of weathering products on the spectrum, and allowed the spectral component due to Fe^{2+} to be isolated.

Dolomite is a complex mineral. Mn^{2+} as well as Fe^{2+} may substitute into the dolomite lattice, and may replace either Ca^{2+} or Mg^{2+}, although EPR spectra indicate the Mg-site is more populated than the Ca-site (Wildeman, 1969). Pierson (1981) analysed 86 dolomite samples and found that concentrations of iron and manganese are positively correlated, and fall around a straight line on a log-log plot. He also found the samples to contain traces of lead, chromium, nickel, cobalt and strontium.

In addition, the composition of many dolomites is not stoichiometric, i. e., their composition deviates from the ideal $Ca_{0.50}MgO_{0.50}CO_3$. Although deficiences of $CaCO_3$ of up to one mole per cent occur, more commonly there is an excess of calcium of up to seven mole per cent $CaCO_3$ (Goldsmith, 1983; Lumsden and Chimahusky, 1980; and others), and dolomites containing as much as 62 mole % $CaCO_3$ (12 mole % excess) (Katz, 1971) have been observed. Thus it is difficult to

isolate one cation and judge its effects on carbonate band parameters as other variations in chemical composition may also be involved. However, the large range in Fe^{2+} content of the dolomites studied here made it possible to outline some of the trends associated with this compositional variation.

Bands 1 through 7 shown in Figure 5.6 are carbonate bands. Although band 7 is visible to the eye in most dolomite spectra, it is too weak in most spectra to fit using the GFIT routine, and data was only obtained on bands 1 through 6.

Figure 5.10 shows the carbonate bands in spectra of four dolomites with different iron contents. As can be seen, the short wavelength side of the two strongest bands (bands 1 and 2) remain at approximately the same position, while the longer wavelength side moves to longer wavelengths. In addition the saddle between the two bands becomes progressively lower with increasing iron content. In the 1.9μm region, band 5 appears to remain approximately stationary, while band 6 moves to longer wavelengths until in the spectrum of 6502 the two bands overlap to form one feature.

These trends are reflected in parameters for carbonate bands as determined by GFIT (see Table 5.3). In general, bands 1, 2, 4, and 6 tend to move to longer wavelengths with increasing iron content. In addition, band 2 becomes wider.

The trend to longer wavelengths of bands 1 and 2 with increasing Fe content is not true for all sample spectra. For example, band 1 in spectra of samples 6509 and 6514 occur at shorter wavelengths than band 1 in the spectra of samples 2501 and 6503, even though 2501 and 6503 contain more iron. Obviously Fe content alone does not control the position of carbonate bands Non-stoichiometry may be a factor.

Carbonate bands in calcites occur at longer wavelengths than carbonate bands in non-ferroan dolomites, which in turn occur at longer wavelengths than carbonte bands in magnesites. Excess Ca in dolomites might shift carbonate bands to longer wavelengths. Or excess Mg, although less common, might shift bands to shorter wavelengths.

The same suite of carbonate and iron bands were used to fit all the dolomite spectra. The only exceptions were the cases where band 7 couldn't be fit, as mentioned above, and the omission of the weak third iron band (band 9, Figure 5.6) from fits to spectra of samples 6509 and 6514, in which the iron features were very weak. Despite the fact that all the dolomites were fit with the same set of bands, not all fits to the carbonate bands were equally good, as evidenced by the residual errors. The plots of residual errors shown in 5.11 for four different dolomites shows that the errors in the 2.3 to 2.5μm region for 6514, a dolomite which contains ≈0.03 weight per cent Fe, are large, as much as 5 to 6 per cent in this region. For 6502, however, which contains ≈15 weight per cent Fe, the fit in this region is very good, and the residual errors are less than 1%. It would appear that in this region an additional band is appearing, or that one already present is increasing in intensity. Or distortion of the crystal lattice by addition of Fe may change the band shapes.

The carbonate bands in spectra of ferroan dolomites or ankerites become almost aragonite-like in shape and position. This similarity also appears in band-band plots of carbonate band positions. Figure 5.12 is a plot of the position of band 1 plotted against the position of band 2 for calcites, aragonites, and dolomites. To the data plotted in Figure 3.13 were added the band positions for two high iron dolomites, 6515a and 6502, and an aragonite, 10501. Note the overlap in band

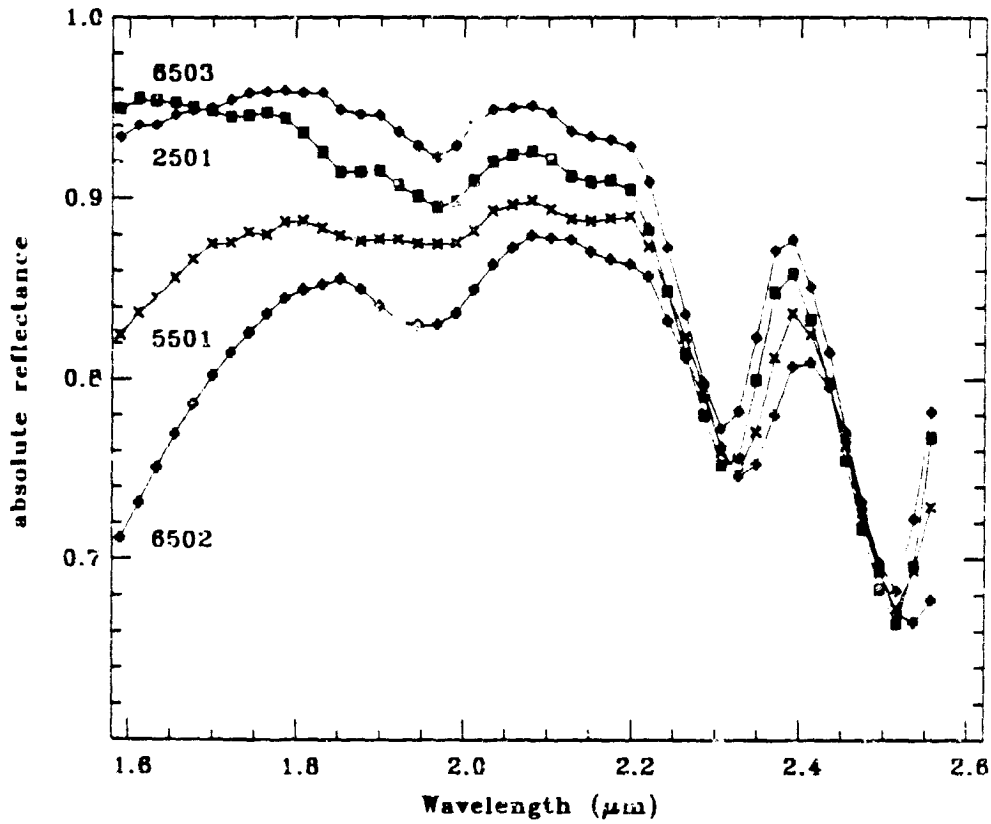

Figure 5.10 Carbonate bands in spectra of four dolomites with different Fe contents.

ORIGINAL PAGE IS
OF POOR QUALITY

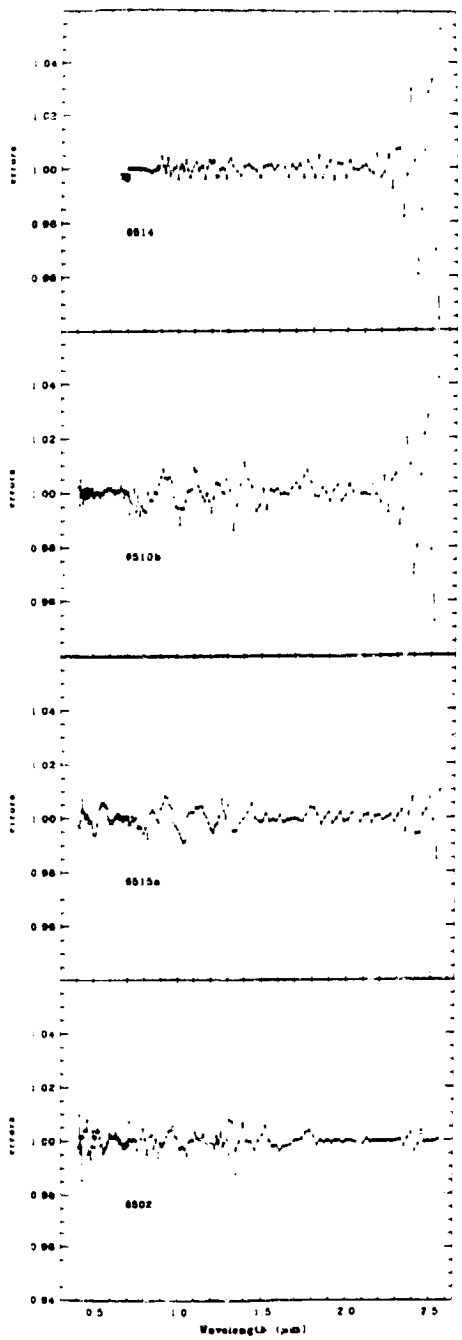

Figure 5.11 Residual errors for fits to four dolomite spectra in order of increasing Fe content.

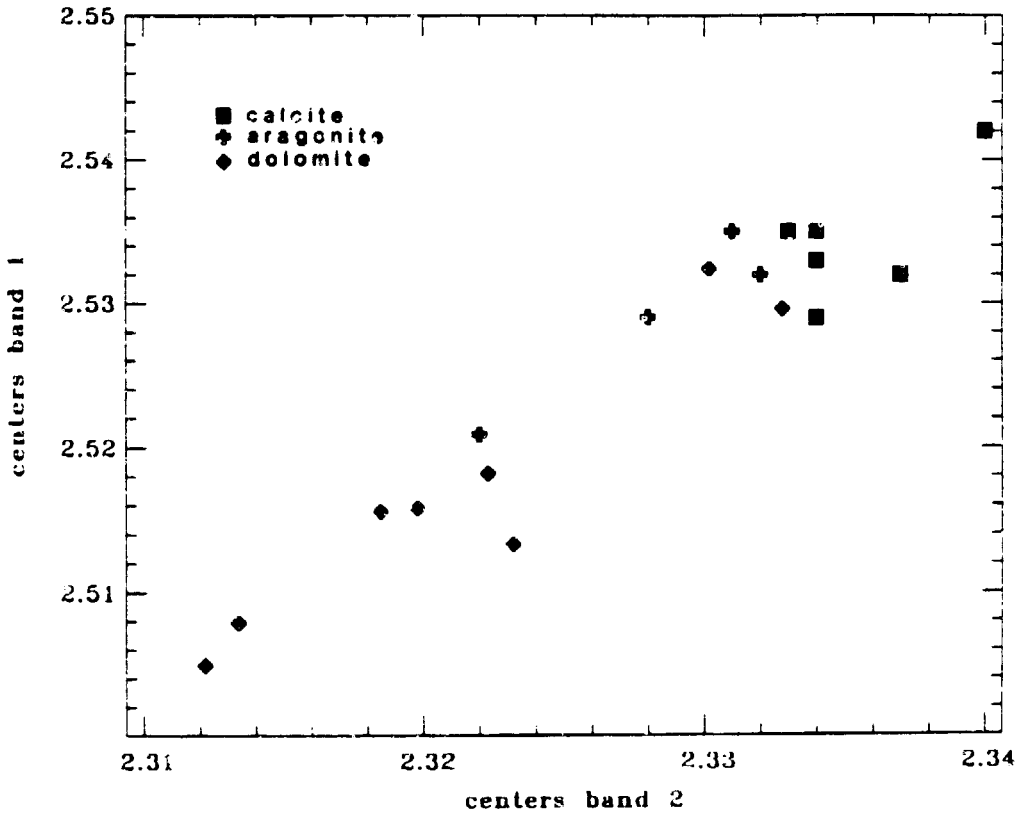

Figure 5.12 Position of band 1 plotted against position of band 2 for all dolomites, aragonites, and calcites.

ORIGINAL PAGE IS
OF POOR QUALITY

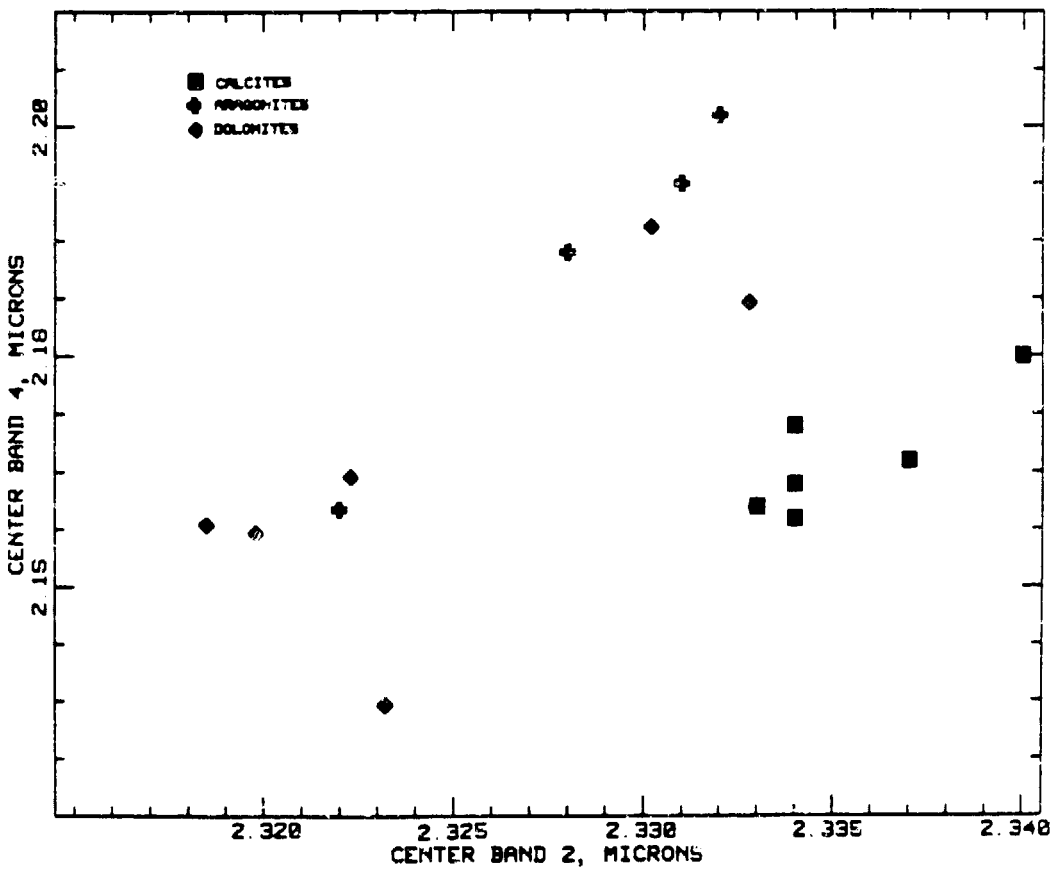

Figure 5.13 Position of band 4 plotted against position of band 2 for all dolomites, aragonites, and calcites.

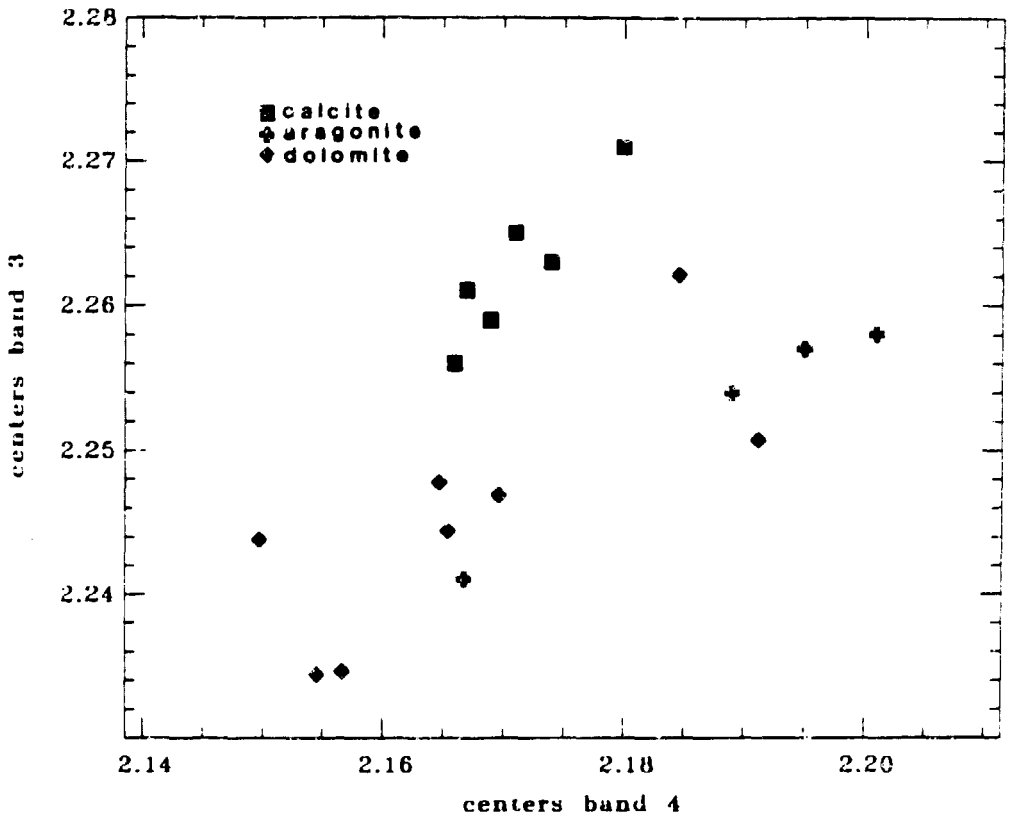

Figure 5.14 Position of band 3 plotted against position of band 4 for all dolomites, aragonites, and calcites.

positions for the aragonites and high iron dolomites. Note also that in this plot it can be seen more clearly that bands 1 and 2 in aragonite spectra occur at slightly shorter wavelengths than equivalent bands in calcites. Figure 5.13, a plot of the position of band 2 vs. the position of band 4, and Figure 5.14, a plot of band 3 plotted vs. band 4, show the same areas of overlap between the aragonites and ferroan dolomites. The fact that the dolomites overlap with the aragonites rather than with the calcites may be related to the distortion of the crystal lattice which Rosenberg and Foit (1979) found resulted from the substitution of Fe^{2+} into the dolomite structure.

This similarity in carbonate band shapes and positions in dolomite and aragonite spectra would not lead to confusion between the two minerals because the ferroan dolomite spectra have the very strong iron band, which aragonite spectra will lack.

Interestingly, but not surprisingly, carbonate bands in spectra of ferroan dolomites, samples 6515a and 6502, occur at longer wavelengths than equivalent bands in siderite spectra. Possible reasons for these differences in band positions are discussed in Chapter 4, where changes in band positions were related to differences in crystal structure and characteristics of the cation. Cation mass and cation radius appear to be the most important factors.

MANGANESE, Mn^{2+}

Manganese in carbonates gives rise to a number of absorption features at wavelengths shorter than 0.6μm (Hunt and Salisbury, 1971) as can be seen in the rhodochrosite spectrum shown in Figure 4.1. This spectrum was taken on the Beckman DK-2A. Mn^{2+} has a d^5 electronic configuration and in octahedral coordination gives rise to a $^6A_{1g}$ ground state (Ballhausen, 1962; Hunt and Salisbury, 1971). Hunt and Salisbury

(1971) give the following band positions and assignments for divalent manganese in rhodochrosite:

from $^6A_{1g}$ to:

$^4T_{1g}$ 0.34μm

^4E_g 0.37μm

$^4A_{1g}$, ^4E_g 0.41μm

$^4T_{2g}$ 0.45μm

$^4T_{1g}$ 0.55μm

Rhodochrosite spectra taken with the Perkin-Elmer 330 show that there are actually five bands in the 0.35 to 0.6μm region. The four strongest bands occur near 0.36, 0.40, 0.44, and 0.54μm. These bands correspond to those observed by Hunt and Salisbury (1971) in this same region. A weaker band occurs near 0.38μm. Heidt _et al._, (1958) assigned two features in a spectrum of $Mn(H_2O)_6^{2+}$ near 0.40 and 0.39μm to the ^4E_g and $^4A_{1g}$ transitions which energy level diagrams calculated by Heidt _et al._, (1959), and Orgel (1955) indicate should have essentially the same energy.

Ballhausen (1962) states that all these transitions are spin forbidden, and that this is reflected in their low extinction coefficients.

This is also reflected in the differences in relative intensities between Fe^{2+} and Mn^{2+} bands in their respective end-member carbonates. Spectra shown in Figure 5.15a and b, plotted in energy space, show that while the Fe^{2+} bands in siderite spectra bottom out at intensities of 0.2 or less, and attempts at gaussian fitting indicate the bands may have begun to saturate and are no longer gaussian shaped, the Mn^{2+} bands in rhodochrosite spectra do not saturate and indeed the centers of the bands generally only drop to intensities of 0.6 or more.

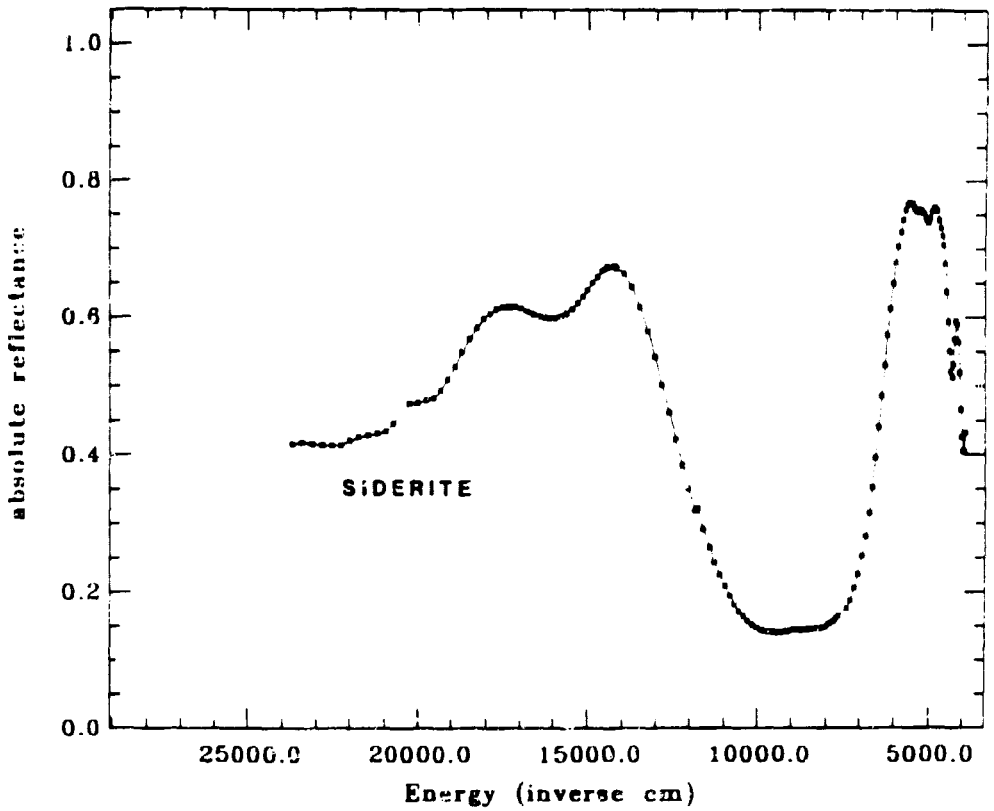

Figure 5.15a Spectrum of siderite plotted in energy space on a scale of 0 to 100. Note difference in widths of Fe band and carbonate bands.

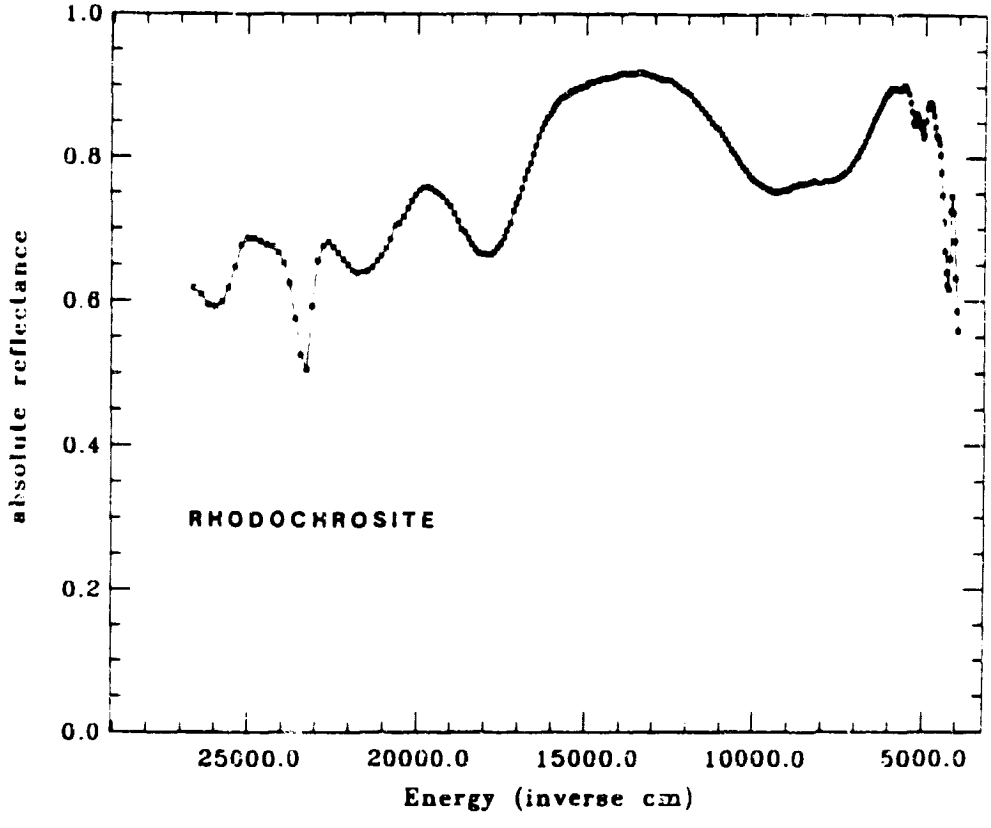

Figure 5.15b Spectrum of rhodochrosite plotted in energy space on a scale of 0 to 100. Note relative widths of Mn and Fe bands and of carbonate bands.

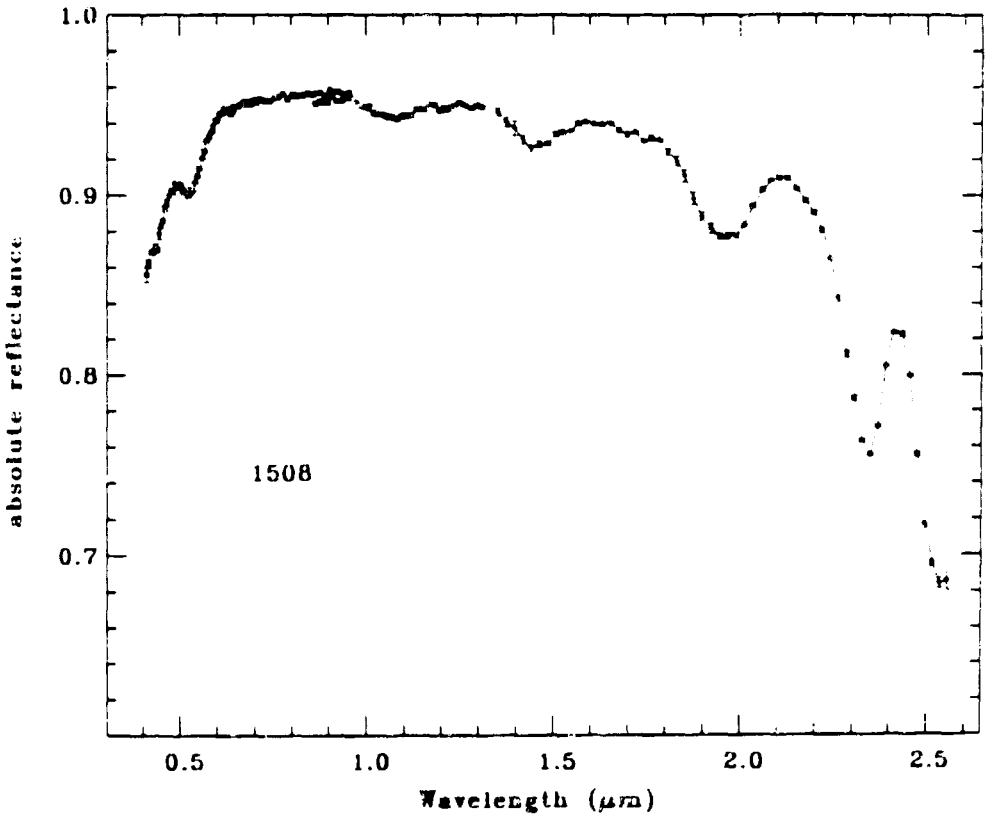

Figure 5.16 Spectrum of manganoan calcite (sample #i508).

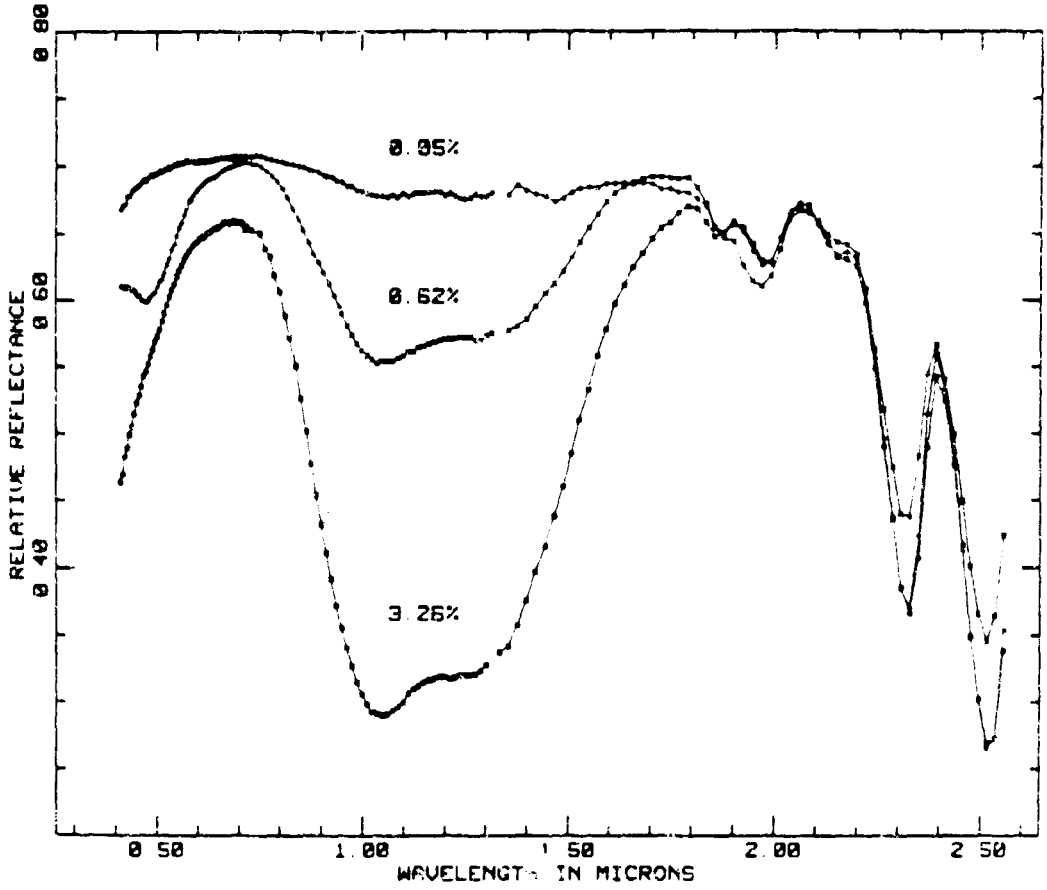

Figure 5.17 Spectra of three dolomites with different Mn and Fe contents.

Figure 5.16 shows the spectrum of a manganoan calcite, sample 1508 from Franklin, New Jersey. A chemical analysis of a calcite quoted by Palache et al., (1944) indicates calcites from this locality contain large amounts of manganese (in that case, 16.7% MnO). EDAX analysis of 1508 indicates it contains Mn, too. This spectrum has absorptions at ≈19,000 cm^{-1} (0.526μm) and 22,800 cm^{-1} (0.439μm). These bands occur at slightly shorter wavelengths than the equivalent bands in rhodochrosite spectra.

Carbonate bands in the spectrum of sample 1508 occur at slightly longer wavelengths than those in spectra of non-manganoan calcites. This would seem to agree with the fact that, as was seen in Chapter 4, carbonate bands in rhodochrosite spectra occur at longer wavelengths than carbonate bands in calcite spectra.

Manganese also substitutes for Mg^{2+} and Ca^{2+} in dolomites. Unlike Fe^{2+} it occurs in both the Ca and Mg sites, although the Mg site is preferred (Wildeman, 1969). Figure 5.17 shows spectra of three dolomites containing different amounts of Mn^{2+} as determined by atomic absorption spectroscopy. Intensities of absorptions due to Mn^{2+}, and the absorption edge into the UV increase in intensity with increasing Mn content. As mentioned above, Mn^{2+} is not as strong an absorber as Fe^{2+}, and data show the detection limits are correspondingly higher, ≈0.1 weight per cent Mn. It has proved difficult to fit gaussian curves to Mn^{2+} bands in dolomite spectra taken with the University of Hawaii spectrometer. Data from one of the spectrometers which extends to shorter wavelengths will be required to determine precise reltationships between band intensities and positions and Mn^{2+} content. Because carbonate bands in rhodochrosite spectra occur at longer wavelengths than the same bands in dolomite spectra, it would be expected that increasing Mn^{2+} content in

dolomites would cause carbonate bands to move to longer wavelengths. However, because Mn^{2+} concentration tends to be roughly correlated with Fe^{2+} concentration (Pierson, 1981), and because carbonate bands in siderites and calcites also occur at longer wavelengths than the same bands in dolomite spectra, it is difficult to isolate the effects of Mn^{2+} on the positions of carbonate bands from the effects of increased Fe^{2+} content or non-stoichiometry. A large number of well characterized samples will be needed to isolate these effects. A combination of Mn^{2+} band intensities, Fe^{2+} band intensities, and carbonate band positions should allow the composition of a dolomite to be determined relative to the four most abundant components.

These spectra show that the ion present is Mn^{2+} rather than Mn^{3+}. Mn^{3+} has a $3d^4$ electronic configuration, and Holmes and McClure (1957) found that the spectrum of $CsMn(SO_4)\cdot 12H_2O$ had a single broad absorption centered near 21,000cm^{-1}.

OTHER CATIONS

Table 5.1 gives some of the data on absorption features due to transition metal cations in the VIS and NIR. As can be seen, a number of other absorption features besides those due to Fe, Cu, and Mn occur in this wavelength region. Some of these have been found in spectra of calcites, magnesites, and smithsonites. Figure 5.18 shows some of these spectra. All of these spectra contain water bands and none have been analyzed with the gaussian fitting routine. Band positions are estimates only.

The first spectrum is that of a calcite (1505) which EDAX analysis indicates contains cobalt. Co^{2+} has a $3d^7$ configuration. In an octahedral site, the ground state is $^4T_{1g}$ $(t_{2g})^5$ $(e_g)^2$, and a number of transitions are possible (Le Paillier-Malecot, 1983). Hydrated Co^{2+}

complexes show an absorption near 8100cm^{-1} (1.23μm) assignable to the transition $^4T_{1g}$ -> $^4T_{2g}$ (Ballhausen, 1962), and a complex band near 20,000cm^{-1} (0.5μm) which reportedly is composed of two or more bands assignable to $^4T_{1g}$ -> $^4A_{2g}$ transitions, and $^4T_{1g}$ -> $^4T_{1g}$ transitions, among others (Holmes and McClure, 1957; Orgel, 1955). Le Paillier-Malecot (1983) found that a spectrum of $CoCO_3$ had overlapping absorption bands due to cobalt at 19,250, 20,800, and 22,875 cm^{-1} (0.52, 0.48, and 0.44μm respectively), which, he states (p. 234), "in the cubic field approximation, one may consider ... are connected with $^4A_2(^4F)$ and $^4T_1(^4P)$ excited levels".

The calcite spectrum has a very broad, weak absorption near 8000cm^{-1} (1.25μm) and a stronger band near 18,500cm^{-1} (0.54μm), with a shoulder near 19,500cm^{-1} (0.51μm). The 1.25μm absorption is so broad that the 1.4μm water band overlaps with it in this spectrum.

A spectrum of a smithsonite, sample 4506, also shows these same features. The bands occur at slightly higher energies (shorter wavelengths) in the smithsonite spectrum than in the calcite spectrum, being centered near ≈8300cm^{-1} (1.2μm) and 19,200cm^{-1} (0.52μm). The shoulder on the band in the smithsonite spectrum is more pronounced. The fact that the Co^{2+} bands occur at shorter wavelengths in the smithsonite spectrum than in the calcite spectrum is comparable to the changes in positions of iron bands outlined in Chapter 4. The smaller M-O bond length in smithsonite means the transitions in the Co^{2+} ions will occur at higher energies than for Co^{2+} ions in the calcite lattice.

Absorption bands due to Ni^{2+} occur in a magnesite spectrum shown in Figure 5.18. Ni^{2+} has a $3d^8$ configuration, and in octahedral coordination will always possess two unpaired spins (Ballhausen, 1962). Octahedral complexes of Ni^{2+} have three spin-allowed transitions from

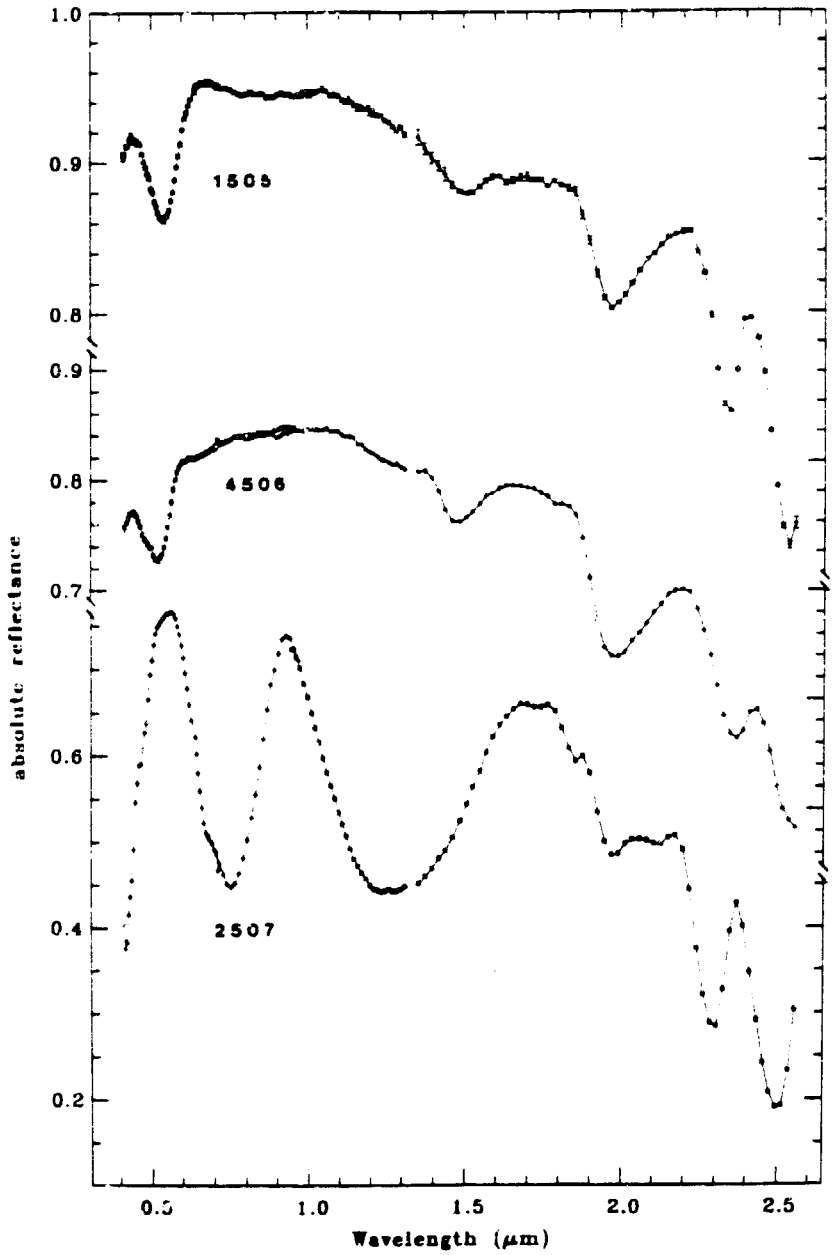

Figure 5.18 Spectra of a calcite (#1505) and a smithsonite (#4506) containing Co, and of a magnesite (#2507) containing Ni.

the $^3A_{2g}$ ground state to triplet excited states with symmetries of $^3T_{2g}$, $^3T_{1g}$ (I), and $^3T_{1g}$(II) (Ferguson et al., 1963; Solomon and Ballhausen, 1975). Ni^{2+} in aqueous solution shows a double band for the $^3T_{1g}$(I) transition centered near 6600cm^{-1} split by spin-orbit coupling (Solomon and Ballhausen, 1975).

The spectrum of the magnesite, sample 2507, illustrated in Figure 5.18 shows these same features. Spark spectrometry indicates that the sample contains nickel, but no detectable amounts of other transition metal cations. There are three strong absorptions centered near 8000, 14,000, and 24,000cm^{-1} (1.25, 0.70, and 0.42μm, respectively). The band near 14,000cm^{-1} (0.70μm) is double, with lobes centered near 13,200 and 14,600cm^{-1}.

FUTURE WORK

It is clear that the work presented here on changes in spectral properties of carbonates with changes in chemical compositions has only scratched the surface.

As mentioned above, the chemistry of dolomites varies considerably, and wide variations in Ca, Mg, Fe, and Mn content have been observed. These complexities are too great to be outlined by the eight samples studied here. Acquiring samples which contain no water and which are, preferably, unweathered is a slow process. Analyzing their spectra is even slower, and many years of work will be required to outline all the permutations in chemical composition and their attendant changes in spectral properties.

It has become clear in this study that reflectance spectroscopy is sensitive to the presence of of a number of cations, including Ni, Co, and Cu which have been given little attention in carbonate studies in recent years. Analyses of carbonate minerals and rocks tend to be

limited to Ca, Mg, Fe, and Mn, with recent increases in interest in Sr and Zn (e.g. Kinsman, 1968; Land, 1980; Pingitore, 1978). Other elements are largely ignored so there is little data available on them in the literature. Studies of solid solution behaviour of Ni, Co, and Cu in carbonate minerals are scarce (Goldsmith, 1983). It is clear that minor quantities of transition metal cations can produce absorption features in carbonate spectra. Future spectral studies of carbonate minerals will have to be accompanied by complete analyses for Ca, Mg, Fe, Mn, Cu, Ni, Co, Ca, Zn, Sr, Ba, and Pb. This involves another very long-term effort.

CHAPTER 6

Absorption Features Due to Water

INTRODUCTION

It became clear early in this study that water, in one form or another, is nearly ubiquitous in carbonate rocks and minerals. It proved difficult to find enough water-free samples to do the mineralogical and chemical work. Dry aragonites and magnesites proved especially difficult to acquire.

Since water is so widespread in carbonate samples, it was necessary to include it as an additional phase, along with the other mineral phases already discussed. And because carbonate minerals seemed to occur in association with water much more commonly than they did with other carbonate minerals, it seemed appropriate to give studies of carbonate-water mixtures higher priority than studies of carbonate-carbonate mixtures.

This chapter will illustrate absorption features due to OH^- and liquid and bound H_2O, will show how these features appear in clay-carbonate and water-carbonate mixtures prepared in the lab, and compare spectra of these laboratory mixtures to spectra of rock samples.

WATER BANDS

Absorption bands in the NIR and MIR caused by water are due to vibrational processes of the H_2O molecule. Water has three fundamental vibrational modes, all of which are infrared active:

ν_1 - ≈2.90μm, symmetric stretch

ν_2 - ≈6.00μm, bend

ν_3 - ≈3.11μm, antisymmetric stretch

Although these fundamentals are centered outside the spectral region covered in this study, the two stretching modes form very strong bands, wings of which may affect spectra in the NIR (Singer, 1981).

The hydroxyl ion, OH^-, has one fundamental stretching mode, which is infrarod active and occurs near 2.75μm (Hunt, 1977).

Liquid water has two strong absorption bands in the VIS and NIR, one near 1.4μm and one near 1.9μm (Bayly et al., 1963; Hunt and Salisbury, 1970; Curcio and Petty, 1951). Weaker bands occur at approximately 0.76, 0.97, 1.19, and 1.80μm (Bayly et al., 1963; Petty and Curcio, 1951). The positions of these bands, and a few of the assignments given for them in the literature are listed in Table 6.1.

Positions and shapes of water bands vary depending on the type of site on or in which the water molecule resides (Hunt, 1977; Hunt and Salisbury, 1970). In carbonates water may be present as liquid water in fluid inclusions, as adsorbed water on the surfaces of grains, as part of the crystal structure in hydrated carbonate minerals such as monohydrocalcite ($CaCO_3 \cdot H_2O$) or in clay minerals occurring with carbonate minerals in argillaceous limestones and dolostones.

Hydroxyl ions (OH^-) may also be present in clays such as kaolinite, or in carbonate minerals such as hydrozincite ($Zn_5[CO_3]_2[OH]_6$) and hydrocerussite ($Pb_3[CO_3]_2[OH]_2$) (Chemical formulas are as given in Fleischer, 1980).

Figure 6.1 shows spectra of several of these different water- and hydroxyl-containing phases, as well as the spectrum of a powdered sample of an Iceland spar (the pan fraction of sample 1531 whose spectrum is shown in Figure 3.8) mixed with enough water to give the sample the consistency of library paste.

The kaolinite spectrum (kaolinite purchased from Baker Chemical Company) shows features due to the hydroxyl ion. The strong, sharp band near 1.4μm is due to the first overtone of the OH stretching mode ($2\nu_{OH}$) (Hunt and Salisbury, 1970); the band near 2.2μm is due to combinations of lattice modes with the OH stretch (Hunt and Salisbury, 1970; Whitney et al., 1983). The strong band centered near 2.2 to 2.3μm is characteristic of hydroxyl-containing minerals, and is probably due to combinations of lattice modes with the OH stretch (Hunt, 1977). In addition to this strong feature, spectra of minerals containing hydroxyl ions may also show a number of weaker bands between 2.0 and 2.6μm (Mara and Sutherland, 1953; Hunt and Salisbury, 1970; Whitney et al., 1983). Hydroxyl ions will not produce the 1.9μm feature because it contains the HOH bending mode.

Spectra of other OH-containing phases including amphiboles (Hunt and Salisbury, 1970), chlorites (Hunt and Salisbury, 1970), muscovite (Adams, 1975; Hunt, 1977; Whitney et al., 1983) brucite (Mara and Sutherland, 1953), azurite (Andersen, 1978) and $Ca(OH)_2$ (see Chapter 7) all show these same features. The exact positions of these features depends on the cation the OH^- is directly attached to (e.g. whether H, Si, Al, or Mg) and on the site it occupies in the crystal structure (Hunt, 1977). OH^- groups may be located in several different sites within the same material, resulting in several bands appearing in the same spectrum, all due to overtones and combination tones of the OH stretching

Hunt and Salisbury (1970)	1.4μm	$2\nu_3$
	1.9	$\nu_2+\nu_3$
Curcio and Petty (1951)	0.76μm	
	0.845	
	0.97	
	1.19	
	1.45	
	1.94	
Bayly et al. (1963)	0.749μm	$3\nu_1+\nu_3$
	0.880	$2\nu_1+\nu_2+\nu_3$
		or $\nu_2+3\nu_3$
	0.981	$2\nu_1+\nu_3$
	1.210	$\nu_1+\nu_2+\nu_3$
	1.449	$2\nu_3$
		or $\nu_1+\nu_3$
		or $2\nu_2+\nu_3$
	1.787	$\nu_2+\nu_3+\nu_L$
	1.934	$\nu_2+\nu_3$
Ceccaldi et al. (1956)	0.763μm	$4\nu_3$
		or $\nu_1+3\nu_2$
	0.855	$\nu_2+3\nu_3$
	0.971	$3\nu_3$
		or $\nu_1+2\nu_2+\nu_3$
		or ν_1
	1.190	$\nu_1+\nu_2+\nu_3$
		or $\nu_2+2\nu_3$
	1.449	$2\nu_3$
		or $2\nu_2+\nu_3$
	1.789	$\nu_2+\nu_3+\nu_L$
	1.790	$\nu_1+\nu_3$
	1.923	$\nu_2+\nu_3$

Table 6.1 Positions of absorptions due to liquid water in the NIR, and some of the band assignments given for them in the literature.

ORIGINAL PAGE IS
OF POOR QUALITY

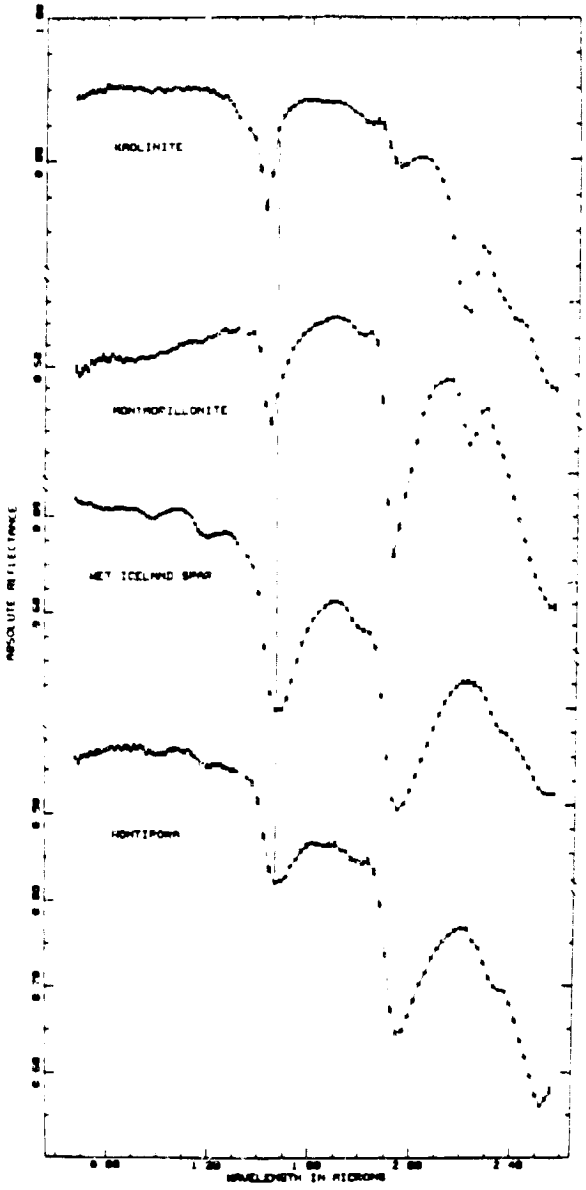

Figure 6.1 Spectra of samples containing liquid and bound water and hydroxyl ions.

mode (Hunt and Ashley, 1979). Hunt (1977) and Hunt and Ashley (1979) show spectra which illustrate the changes in numbers and positions of OH bands with differences in mineralogy.

The spectrum of the wet Iceland spar shows features due to liquid water and is shown with spectra of other water- and hydroxyl-containing species (Figure 6.1). Note that all spectra in this figure, including the kaolinite spectrum, show the weak 1.80μm feature, indicating that it is probably an overtone of the OH stretching mode, or a combination of OH stretch and lattice modes.

The spectrum of montmorillonite illustrates features typical of molecular water bound in interlayer clay sites (Hunt and Salisbury, 1970; Singer, 1981) - features near 1.4 and 1.9μm. Note that the 2.2μm feature due to OH is also present, and that the overtone of the OH stretch also contributes to the 1.4μm feature (Singer, 1981). This montmorillonite was purchased from Wards and seived to remove sticks and leaves.

Comparison of these three spectra shows that absorption features due to water bound in clays are sharper and narrower and occur at shorter wavelengths than equivalent bands in liquid water spectra. The OH band at 1.4μm is also sharper and narrower and occurs at shorter wavelengths than the 1.4μm band in liquid water spectra, and in spectra of minerals containing only OH^-, the 1.9μm is absent. On the other hand the strong OH^- band in the 2.2 to 2.3μm region is absent in the liquid water spectrum.

Spectra of skeletal carbonates contain strong water bands. A spectrum of a coral skeleton is included in Figure 6.1. This specimen belongs to the genus <u>Montipora</u> and was collected from a patch reef in Kaneohe Bay on the windward coast of Oahu. Comparison of the water

bands in this spectrum with the bands in the two clay spectra and in the wet Iceland spar spectrum indicate that they most closely resemble those of liquid water in shape and position. In addition X-ray diffraction analysis indicates this sample is composed entirely of aragonite. This would indicate the water is present in the form of fluid inclusions, rather than as bound water or OH^-.

Inflections in the curve near 2.3 and 2.5μm are the carbonate bands, partially masked by water bands. The drop-off in the curve at longer wavelengths is caused by the wings of the two strong fundamental bands centered near 2.9μm.

Although the wet Iceland spar sample was less than half water, the water bands dominate the spectrum. This is due to the fact that the water bands in this region are sums of two fundamental modes (see Table 6.1), while the carbonate bands are three and four (see Table 3.5). The intensities of vibrational absorption bands are proportional to the number of molecules existing in the excited state. Hadni (1974, p.46) states "... the three-phonon processes in general give an absorption coefficient ten times weaker than that for two-phonon processes which are still ten times weaker than the classical one-phonon processes." (A phonon is a quantum of vibrational energy.)

Figure 6.2 shows spectra of calcite, water (because quartz has no absorption features in this region of the spectrum, this is essentially a spectrum of fluid inclusions, Hunt and Salisbury, 1971), and two spectra of calcite plus water, one a physical mixture, the other a computer "mix" made by averaging the milky quartz and dry calcite spectra together. Both calcite+water spectra show the same features.

Figure 6.3 shows spectra of montmorillonite, the pan fraction of the Iceland spar discussed above, and mixtures of the two. In the

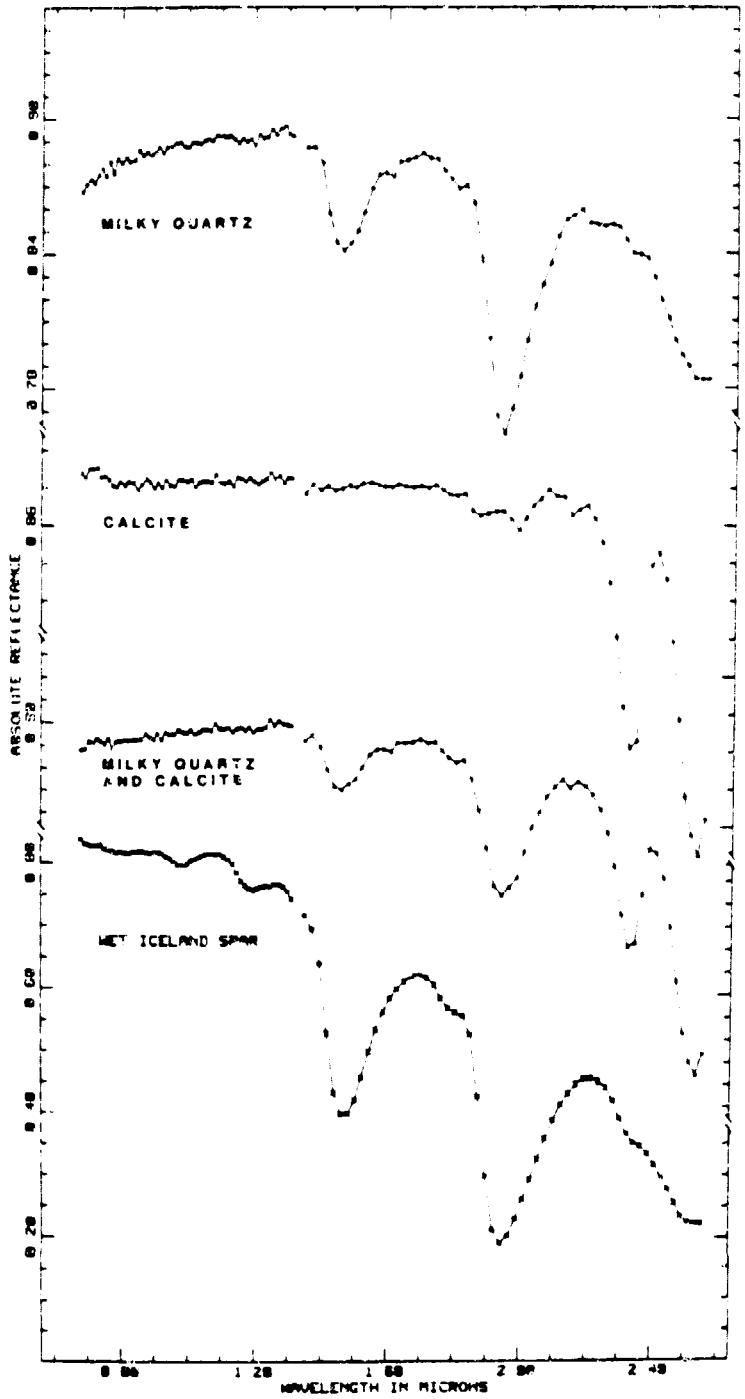

Figure 6.2 Spectra of calcite, milky quartz, wet calcite, and a computer average of the calcite and milky quartz spectra, showing that the physical mixture and computer mixture have essentially the same spectral features.

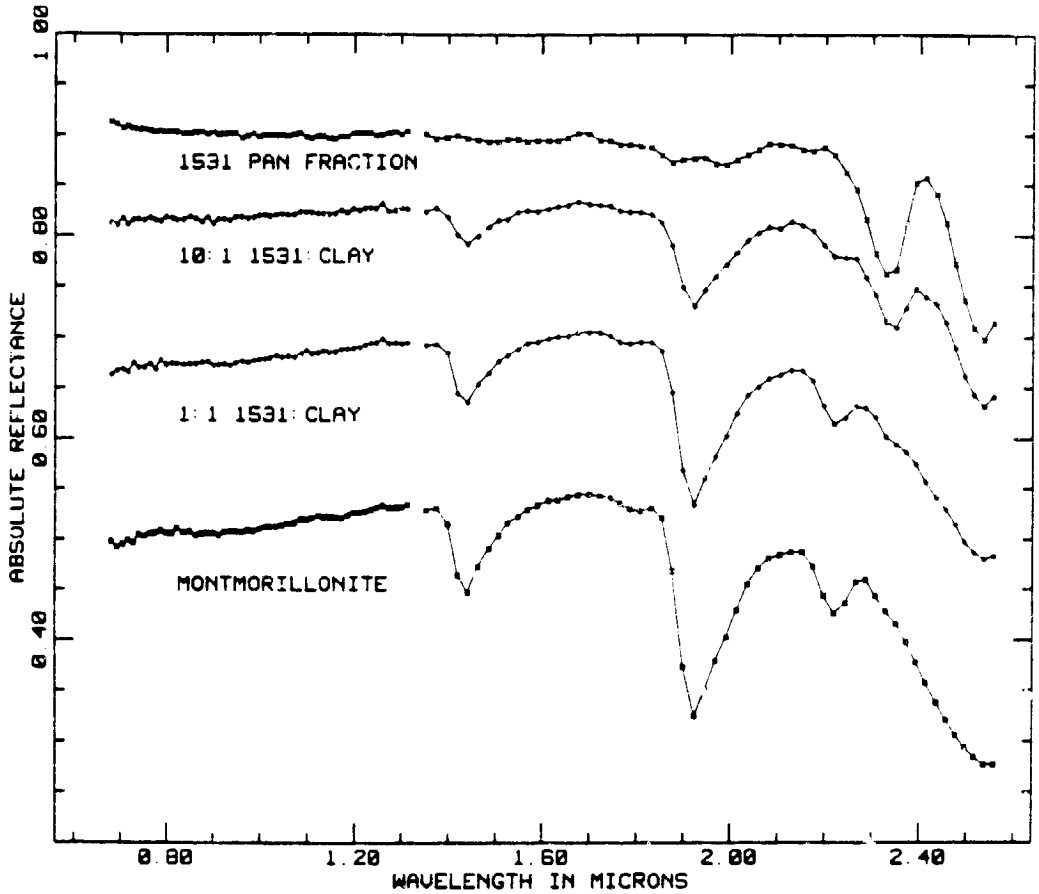

Figure 6.3 Spectra of calcite (pan fraction, sample #1531), montmorillonite, and mixtures of the two.

ORIGINAL PAGE IS
OF POOR QUALITY

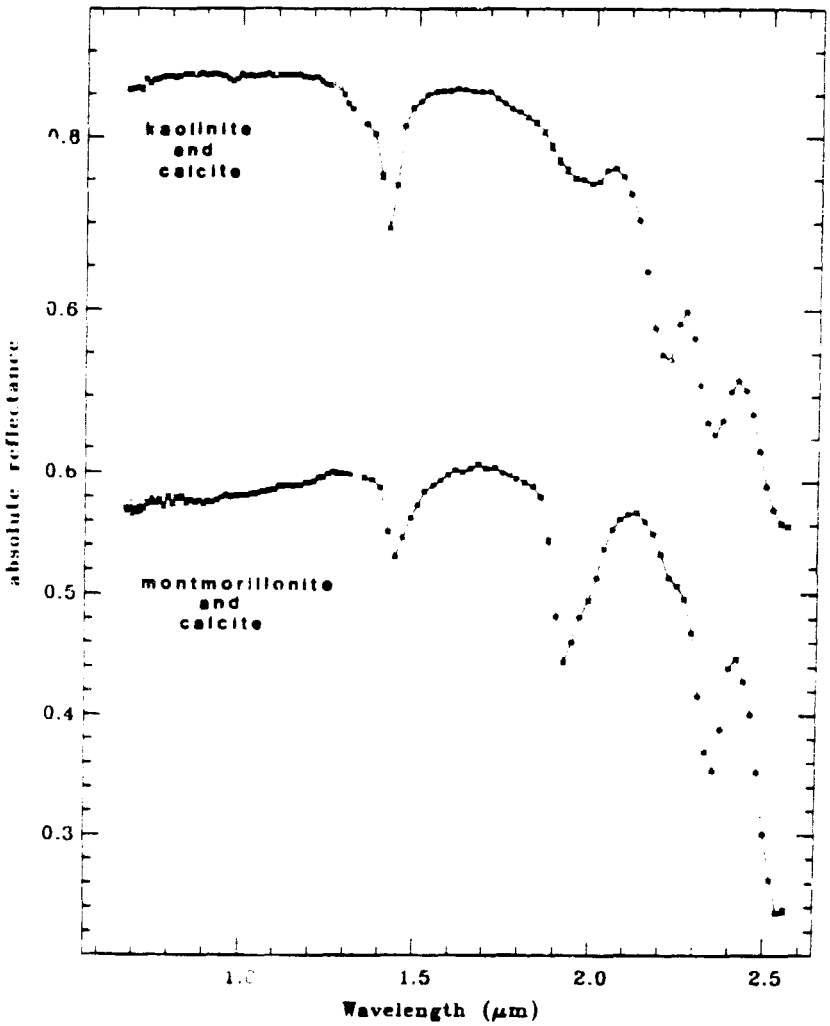

Figure 6.4 Spectra of two clay carbonate mixtures made with a coarse fraction of calcite (180 - 355μm fraction, sample #1531).

spectrum of a mixture of carbonate and clay in a ratio of ten to one by volume the two sharp clay bands at 1.4 and 1.9μm of the montmorillonite spectrum can be seen. The 1.9μm clay band masks the two carbonate bands at ≈1.88 and 1.99μm. However, the stronger carbonate bands at 2.3 and 2.5μm are visible. The 2.2μm clay band causes an inflection in the curve in this region.

In the spectrum of a mixture of equal volumes of calcite and clay, the composition of a marl, the spectrum is dominated by the clay features. The 2.3 and 2.5μm bands cause only a weak inflection in the curve.

Another factor governing the relative intensities of clay and carbonate bands are the relative grain sizes of the carbonate and clay fractions. Figure 6.4 shows the spectrum of a 50:50 mixture of montmorillonite and the 180-355μm fraction of the Iceland spar (sample #1531). Here the coarse particle size of the calcite increases the optical path length through the carbonate phase and results in much stronger carbonate bands relative to the clay bands than were seen in the spectrum of the 50:50 montmorillonite plus calcite mixture shown in Figure 6.3. The spectrum of a similar mix of kaolinite plus this coarse Iceland spar is also shown. Again, both the clay and carbonate bands give intense absorption features.

These spectra serve to illustrate the difficulties of using relative band intensities to determine precisely the amount of of different mineral phases present in a mixture. Clark and Lucey (1984) discuss this problem in terms of geometric optics, and offer possible mathematical solutions to the problem.

WATER BANDS IN ROCK SPECTRA

Figures 6.5 and 6.7 show examples of argillaceous and non-argilaceous limestones and dolostones.

Figure 6.5 shows spectra of rocks which X-ray diffraction analysis and examination in thin section indicate contain no clays. 10529a and b are spectra of an aragonite and calcite, respectively. These two samples, obtained from the Geology Department at the University of Iowa, formed two different layers in a cave deposit from Lead Caves, Dubuque, Iowa. These spectra have the strongest water bands of any non-biogenic carbonates studied thus far. The slight difference in band position for the 2.5μm band in these two spectra reflects the difference in mineralogy.

Figure 6.6a and b show photomicrographs of sample 10529a. In Figure 6.6b the fluid inclusions which occur within and between the fibrous aragonite crystals can be seen. Comparison of the spectrum of this sample with that of the coral Montipora shown in Figure 6.1 shows that the spectral properties of the biogenic and non-biogenic aragonites are very similar. This supports the conclusion that the water bands in the coral spectrum are due to aqueous fluid inclusions, although the individual inclusions themselves are too small to be seen with petrographic microscope or SEM.

The third spectrum was obtained from a micrite from the Devonian Cedar Valley Limestone, from Mitchell County, Iowa.

CL-52 is an oolite from the Mississippian Lodgepole Formation in central Montana. BC-11 is an encrinite obtained from the same unit.

CL-17 is a dolomite, also from the Lodgepole. This rock was originally a wackestone. The mud matrix was dolomitizied, and the remaining skeletal debris was removed leaving voids (Jenks, 1972).

ORIGINAL PAGE IS
OF POOR QUALITY

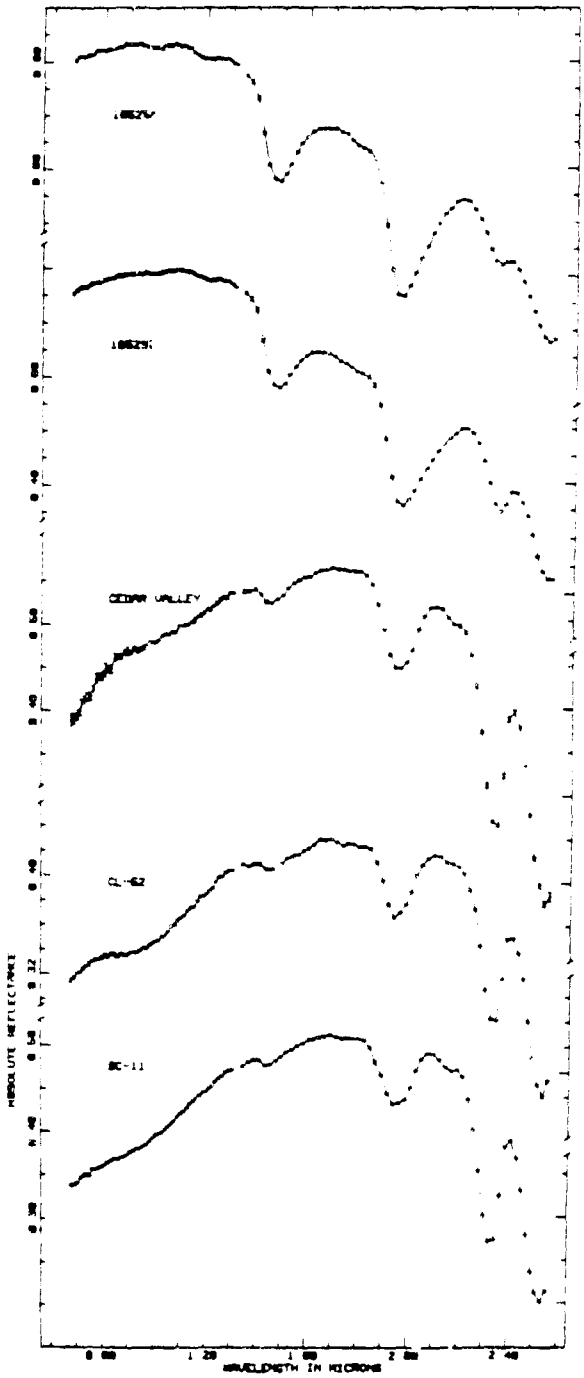

Figure 6.5 Spectra of limestones and dolostones containing aqueous fluid inclusions.

ORIGINAL PAGE IS
OF POOR QUALITY

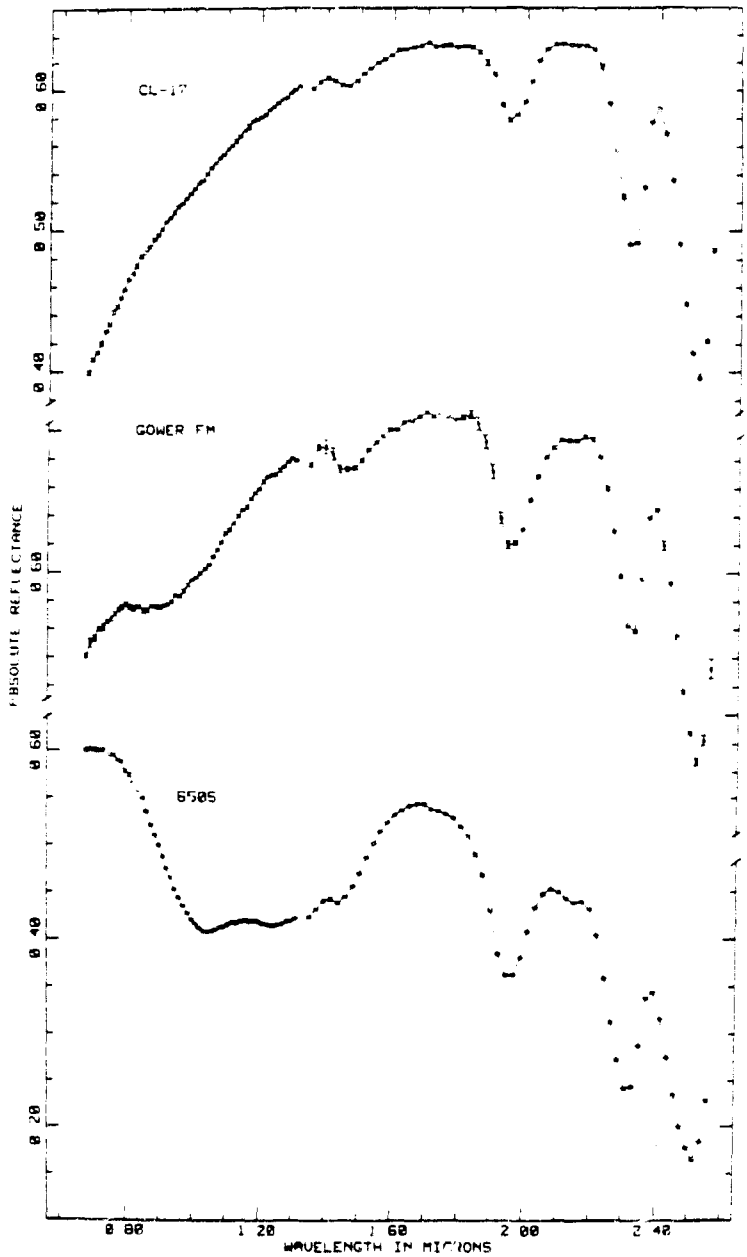

Figure 6.5 continued. Spectra of limestones and dolostones containing aqueous fluid inclusions.

ORIGINAL PAGE IS
OF POOR QUALITY

Figure 6.6a Photomicrograph of sample 10529a, an aragonitic cave deposit. Magnification 40X

ORIGINAL PAGE IS
OF POOR QUALITY

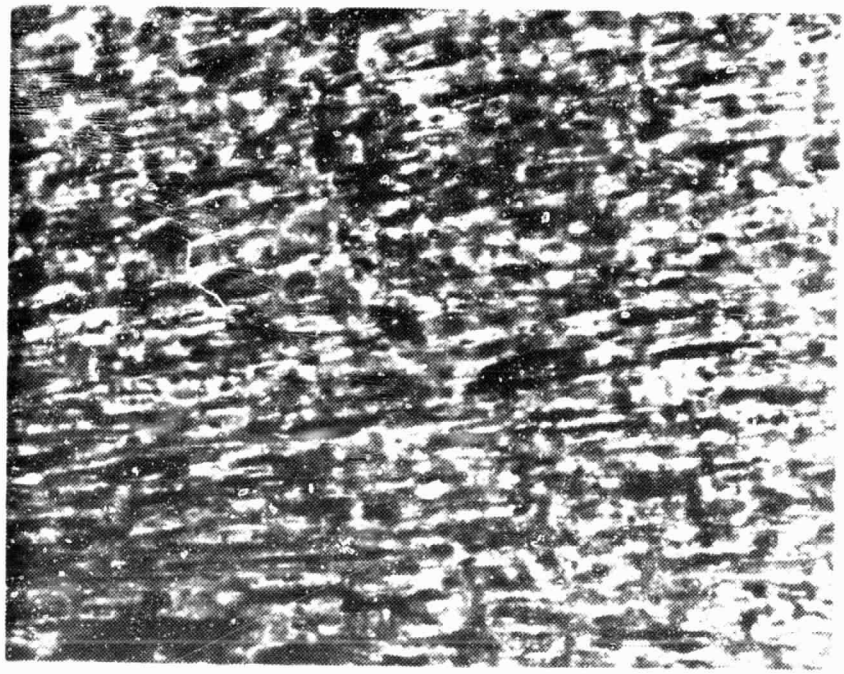

Figure 6.6b Photomicrograph of sample 10529a, an aragonitic cave deposit showing aqueous fluid inclusions. Enlarged view of bright layer in center of preceding photograph. Magnification 640X

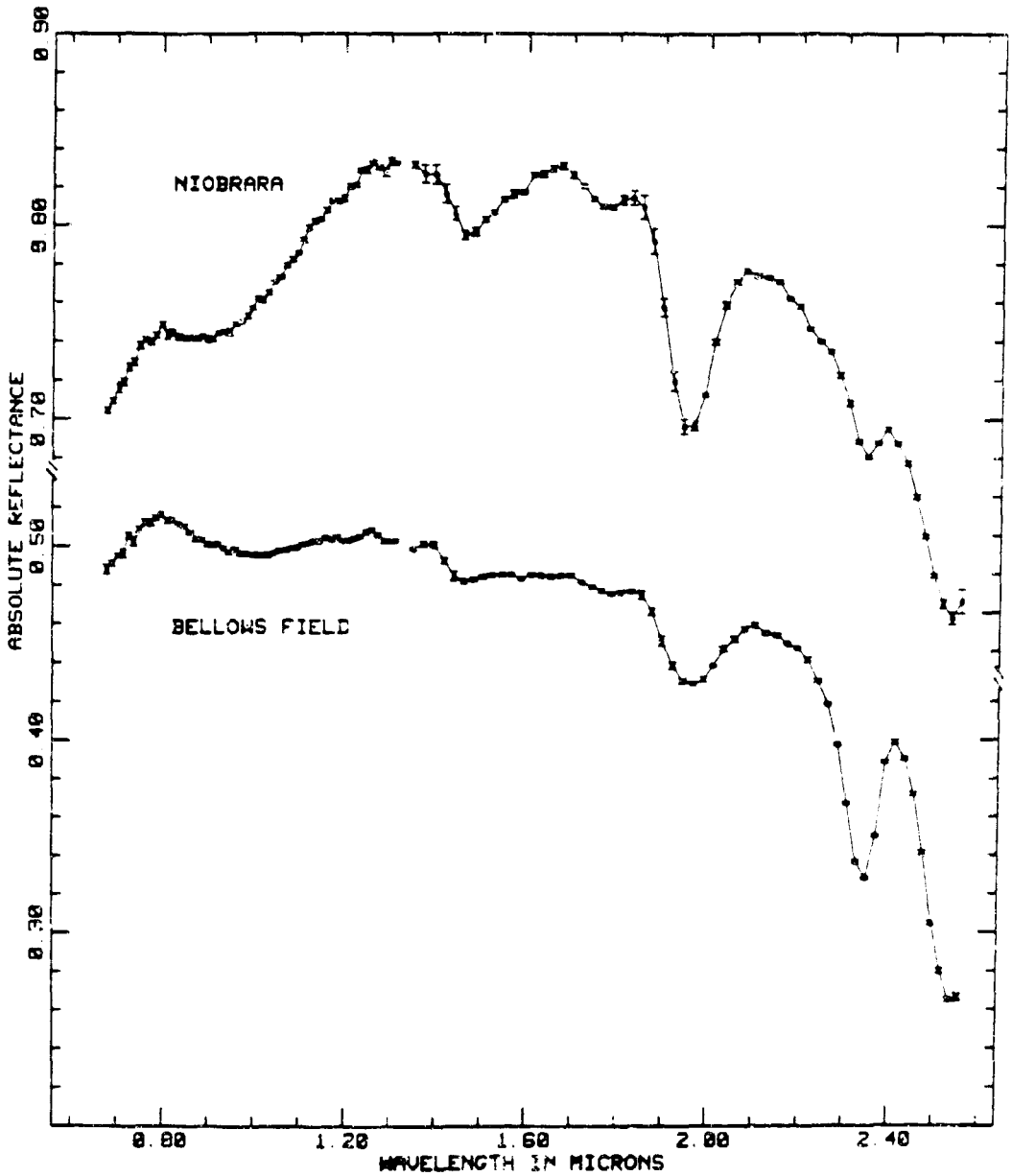

Figure 6.7 Spectra of argilleceous carbonates.

ORIGINAL PAGE IS
OF POOR QUALITY

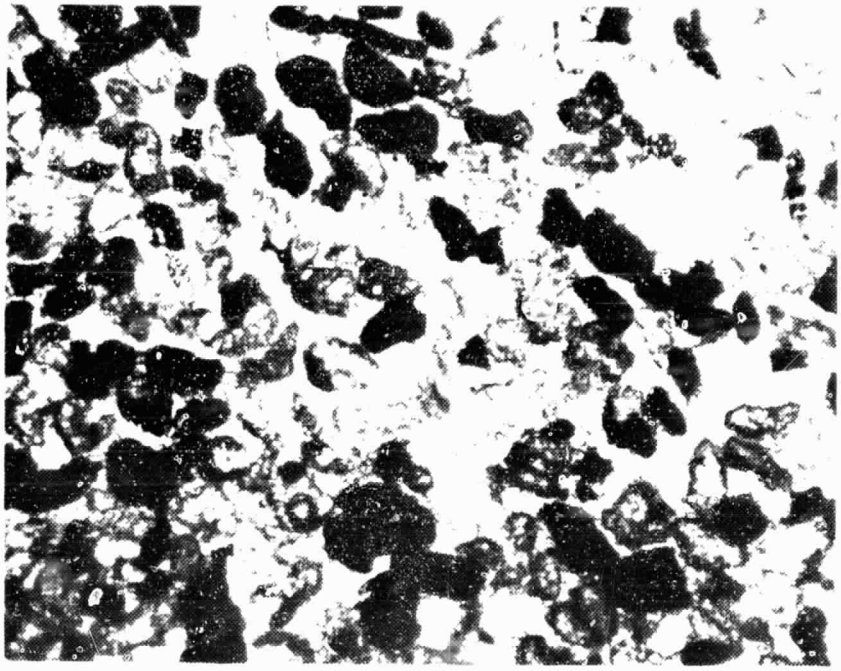

Figure 6.8 Photomicrograph of Bellows Field eolianite showing neomorphosed skeletal grains. Magnification 40X

The Gower Formation is a Silurian dolomite which outcrops in eastern Iowa. This sample was taken from the Anamosa Facies a tidal flat sequence from which much building stone is quarried (Philcox, 1972).

Spectrum 6505 is of a dolomitic marble fom New Jersey, purchased from Wards.

Although spectra of all these samples contain water bands, the bands generally are not strong, the cave deposits being the only exception. Although problems mentioned above may preclude precise determination of water content from spectra, these samples probably contain a few tenths of a per cent water by weight. Despite the presence of water in these samples, the two strong carbonate bands near 2.3 and 2.5μm can still be used to distinguish calcite from dolomite.

Figure 6.7 shows spectra of rocks containing some clay. The Niobrara Chalk is Cretaceous in age (Hattin, 1981). The sample from which the spectrum was obtained was collected in Scott County, Kansas. The sample is orange (10 YR 7/4) in color and examination with SEM shows it to be composed of coccoliths which have undergone some dissolution and reprecipitation, and clay. The rock is ≈10% by weight insoluble residues. The sharp bands at 1.4μm and 1.9μm are due to clay. There is undoubtedly some contribution to water bands by liquid water in the coccoliths, as spectra of coccolith oozes indicate that coccoliths do contain some fluid inclusions (see Chapter 8). The spectrum also shows absorption features which occur near 0.45, 0.62, and 0.97μm. Hunt and Ashley (1979) and Singer (1981) found that iron oxides have absorption bands in these regions, and the iron oxides which give the rock its orange color undoubtedly cause these absorption bands.

The second rock spectrum shown was obtained from a sample of dune rock collected from the Waimanalo Quarry on Oahu, dug in the Pleistocene Bellows Field Formation (Lum and Stearns, 1970). Note that although these rocks contain clay formed by weathering of volcaniclastic grains (the non-carbonate fraction comprises (≈5% of the rock by weight) and the carbonate fraction was originally composed of skeletal material, the water bands are relatively weak compared to the carbonate bands. There are probably two reasons for this, both related to diagenetic alteration of the rock. X-ray diffraction analysis shows the carbonate fraction is composed primarily of low Mg calcite. Skeletal debris originally forming the dune sand has been largely recrystallized with attendant loss of fluid inclusions (see Chapter 8). In addition, the solution and reprecipitation of the carbonate fraction has resulted in an increase in crystal size of the carbonate, and thus an increase in the optical path length through the carbonate fraction, increasing the intensity of the carbonate bands relative to the water bands. Figure 6.8 shows a photomicrograph of the Bellows Field eolianite sample from which this spectrm was obtained.

The spectra of carbonate rocks containing clay can be difficult to decipher because of the large number of features they contain. Studies done so far indicate that liquid water in fluid inclusions is to be found in nearly all carbonate rocks. Thus, if clay is present, absorption features due to clays are superimposed on those due to liquid water. In the 1.9μm region this is further complicated by the presence of two carbonate bands in the spectra. Variations in intensities of all these bands due to variations in abundance of these phases, or due to variations in crystal or inclusion size, will cause apparent shifts of absorption features in this region. Band shape will no doubt be an

important factor in determining the composition of a rock. It is hoped that at some future time it will become possible to deconvolve these spectra into their component parts of carbonate, water and clay. Work done by Pamela Blake (1983) in using the LOWTRAN model to make corrections for absorptions due to atmospheric water in remotely sensed data show that the potential exists for such a solution.

CHAPTER 7

Hydrous Carbonate Minerals

As discussed in the preceding chapter, Hunt and Salisbury (1970), Hunt (1977), and others have shown that the number, positions, and shapes of water bands in spectra can be used to discriminate between water and hydroxyl ions bound in clays. These relationships between spectral properties and the state of H_2O and OH^- in compounds will be used to examine some hydrated carbonate phases.

Figure 7.1 shows spectra of four water- and hydroxyl-containing compounds.

The first spectrum is of a reagent grade chemical which was labeled $Ca(OH)_2$. This spectrum was obtained with the Perkin-Elmer 330. X-ray diffraction indicates it is composed of Portlandite ($Ca(OH)_2$) and calcite. The ratio of the intensity of the major portlandite peak (2.63) to that of the the calcite major peak (3.035) is 10.6. All d-spacings are given in Angstroms. The relationship between intensities of reflection peaks due to different components in mineral mixtures and the concentration of these components in the mixture is not linear, but depends on such factors as grain size and shape, degree of crystal perfection,

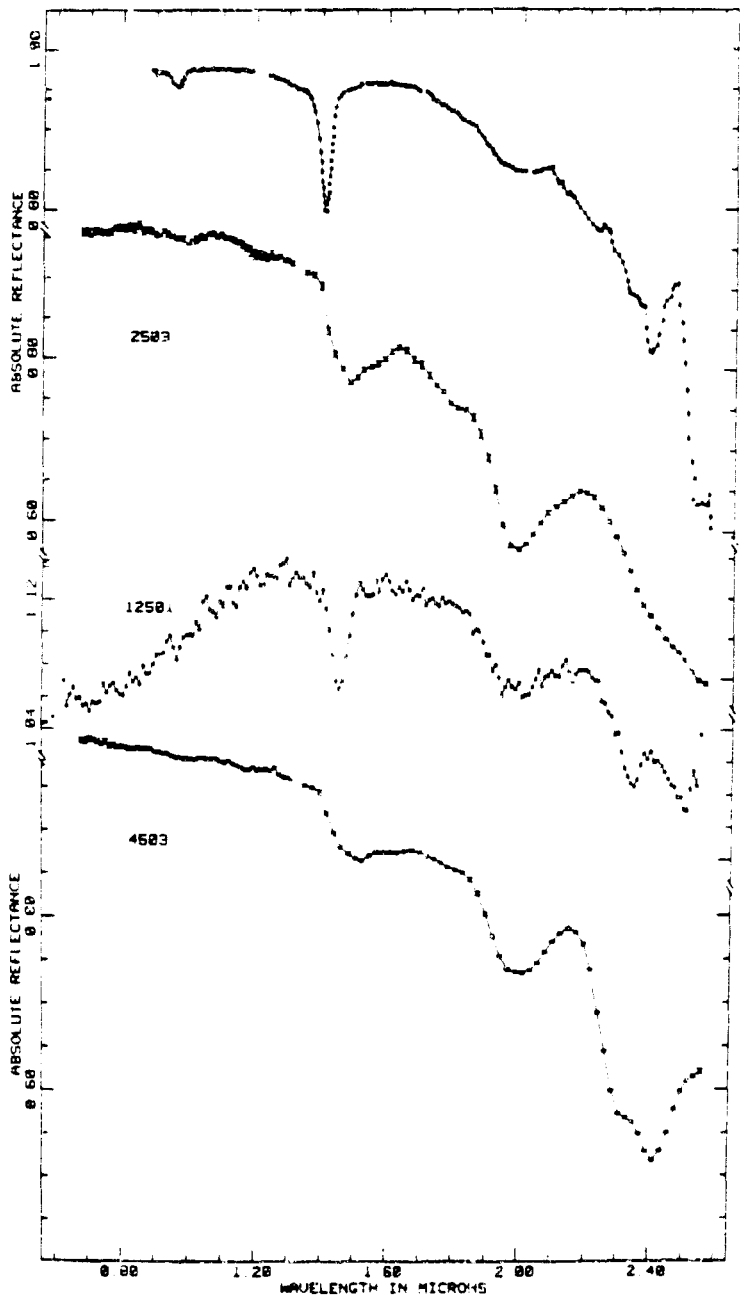

Figure 7.1 Spectra of hydrous carbonate minerals and portlandite.

and mass absorption coefficients (Nuffield, 1966). These ratios of peak intensities are only intended to give a qualitative picture of the degree of contamination.

This first spectrum shows the sharp 1.4μm band and the lack of a strong 1.9μm feature characteristic of OH^- bearing species.

The second spectrum (2503) is of a sample of a Baker Analyzed Reagent labeled $4MgCO_3.Mg(OH)_2.nH_2O$. X-ray diffraction analysis indicates that it is indeed hydromagnesite ($Mg_5[CO_3]_4[OH]_2.4H_2O$). The spectrum shows two broad absorptions near 1.4 and 1.9μm. The 1.4μm band has a sharp point due to the presence of a sharp OH band superimposed on the broader feature due to bound H_2O.

The third spectrum (12501) is of a Baker Anlyzed Reagent labelled lead carbonate, $PbCO_3$. X-ray diffraction analysis indicates the sample is composed of cerussite ($PbCO_3$) and hydrocerussite ($Pb_3[CO_3]_2[OH]_2$). The ratio of the intensities of the two major peaks, (hydrocerussite, 2.62, cerussite, 3.59) is ≈2.8. This spectrum was taken with the Beckman DK-2A and appears brighter than other spectra used in this study because MgO was used as a standard, rather than Halon. This spectrum shows the sharp 1.4μm band characteristic of hydroxyl bearing compounds. It also shows a broad feature near 1.9μm and two features of approximately equal intensity near ≈2.30 and 2.45μm. The spectrum of cerussite, shown in Chapter 4, has one strong absorption at 2.5μm (carbonate band 2), and weaker absorptions (bands 3 to 7) shortward of this. The 2.45μm feature here is probably this carbonate band 2. The 2.3μm feature is probably an OH stretch similar to that observed in clay spectra. Although the spectrum is quite noisy the 1.9μm band appears to be centered at longer wavelengths than the same band in spectra of liquid water, and so is not due to liquid water in fluid inclusions. In addition there appears to be a weak 1.4μm band which is partially masked by the OH band.

The last spectrum is of another Baker Analyzed Reagent labeled zinc carbonate. X-ray diffraction analysis indicates the sample is composed entirely of hydrozincite. The formula for hydrozincite is $Zn_5(CO_3)_2(OH)_6$ (Hurlbut and Klein, 1977). The spectrum of this sample has two broad features near 1.4 and 1.9μm. As in the hydromagnesite spectrum the 1.4μm band has a sharp OH band superimposed on a broad H_2O band. It also has a double band near 2.4μm.

These results have three major implications. First, both H_2O and OH occur in hydrozincite, rather than just OH, as previously supposed. The same is probably true of hydrocerussite, although it would appear to contain less water than hydrozincite.

Second, while absorption bands due to water in clays occur at longer wavelengths and are narrower than those in liquid water, H_2O bands in hydrated carbonate phases are broader and occur at longer wavelengths than equivalent bands in liquid water spectra.

Third, reagent grade chemicals are of dubious quality and and their composition should be checked. Reflectance spectroscopy in the VIS and NIR offers a rapid, easy method of doing this.

CHAPTER 8

Aqueous Fluid Inclusions in Skeletal Material

INTRODUCTION

As was seen in Chapter 6, water is a strong absorber in this spectral region and produces strong absorption features near 1.4 and 1.9μm, plus a number of weaker features. Hunt and Salisbury (1971, 1976) found water bands in some of their carbonate mineral and rock spectra which they attributed to the presence of microscopic fluid inclusions. It was found in this study that aqueous fluid inclusions are nearly ubiquitous in carbonate rocks and minerals, and are particularly abundant in skeletal material. The widespread occurrence of these inclusions was previously unsuspected, as previous studies were confined to those done with petrographic microscope (Roedder, 1979), and more recently with transmission electron microscopy (TEM).

Studies by Conger _et al_. (1977) and Green _et al_. (1980) of electron-transparent foils of coral skeletons, bivalve shells, and foraminifera tests show they contain "organic" inclusions within and between crystals making up the skeleton. In fusulinid tests, voids between crystals range from about 1000 to less than 50 Angstroms in size, while the intra-granular voids have diameters of 100 Angstroms or

less (Green et al., 1980). Bathurst (1971) notes that stromatoporoid and echinoderm skeletons have a dusty appearance due to the presence of inclusions. It is probable that these same inclusions produce the absorptions in the reflectance spectrum of a coral skeleton shown in Chapter 6.1, and in the spectra of other skeletal material shown in this chapter.

The widespread occurrence of these inclusions has important implications for the diagenesis of skeletal material. It is generally believed that all reactions within carbonate systems involve a liquid phase, even if it is only a microscopic film of water (Folk, 1965). The fluid inclusions in skeletal material can serve as a medium of reaction for these carbonates. It may also affect their relative stability, material with abundant inclusions being less stable than that which lacks them.

FLUID INCLUSIONS IN MODERN SKELETAL MATERIAL

Abundance of aqueous fluid inclusions in carbonate skeletal material varies from one type of organism to another. Figures 8.1, 8.2, and 8.3 show spectra of skeletal material from a variety of carbonate secreting organisms, grouped according to skeletal mineralogy. Figure 8.1 shows spectra of skeletons of organisms which secrete aragonite, Figure 8.2 low Mg calcite, and Figure 8.3 high Mg calcite. The coral Porites, the scaphopod Dentallium, the echinoid Echinometra, the gastropod Conus, and the coralline red algae are all indigenous to Hawaii (Fielding, 1979; Kay, 1979; Maragos, 1977).

As these spectra show, the amount of fluid inclusions varies from one type of organism to another. Relative intensities of water and carbonate bands can give a semiquantitative estimate of the amount of water present in a sample. Heating of skeletal material to 1000° for one half

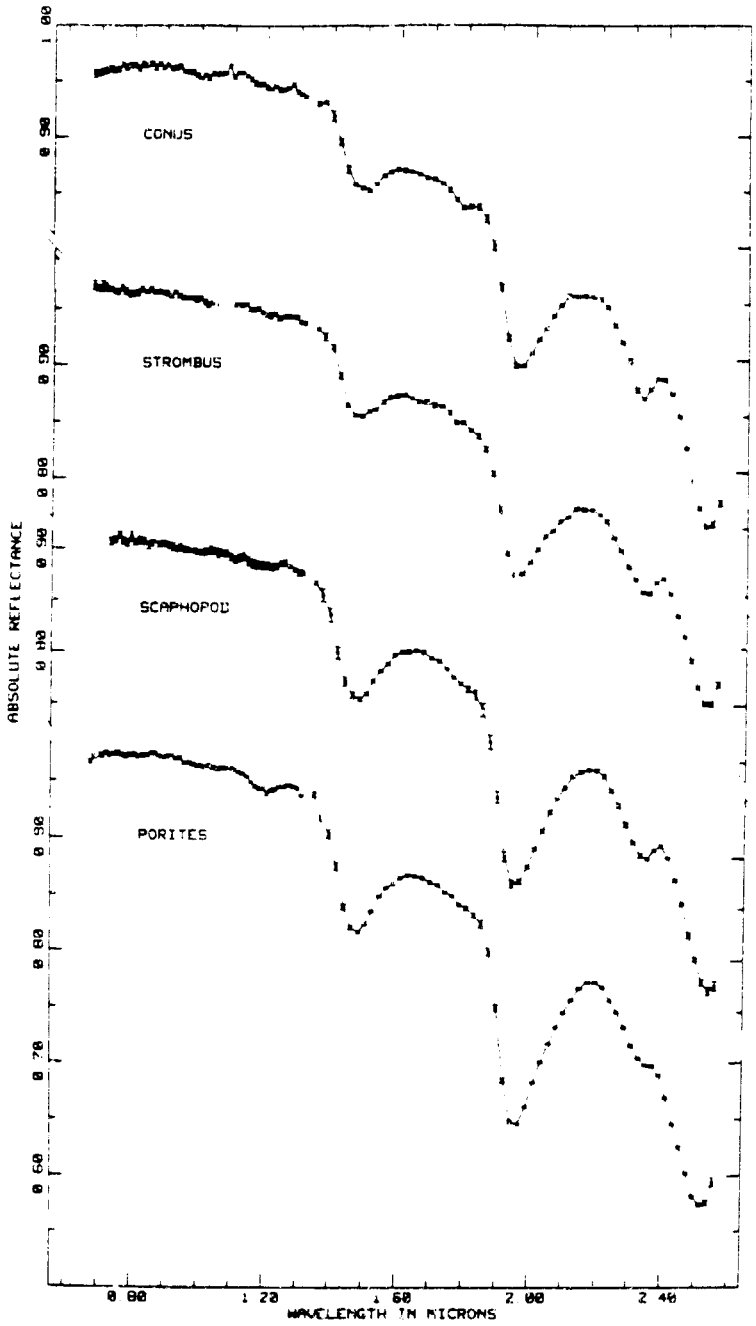

Figure 8.1 Spectra of aragonitic skeletal material.

ORIGINAL PAGE IS
OF POOR QUALITY

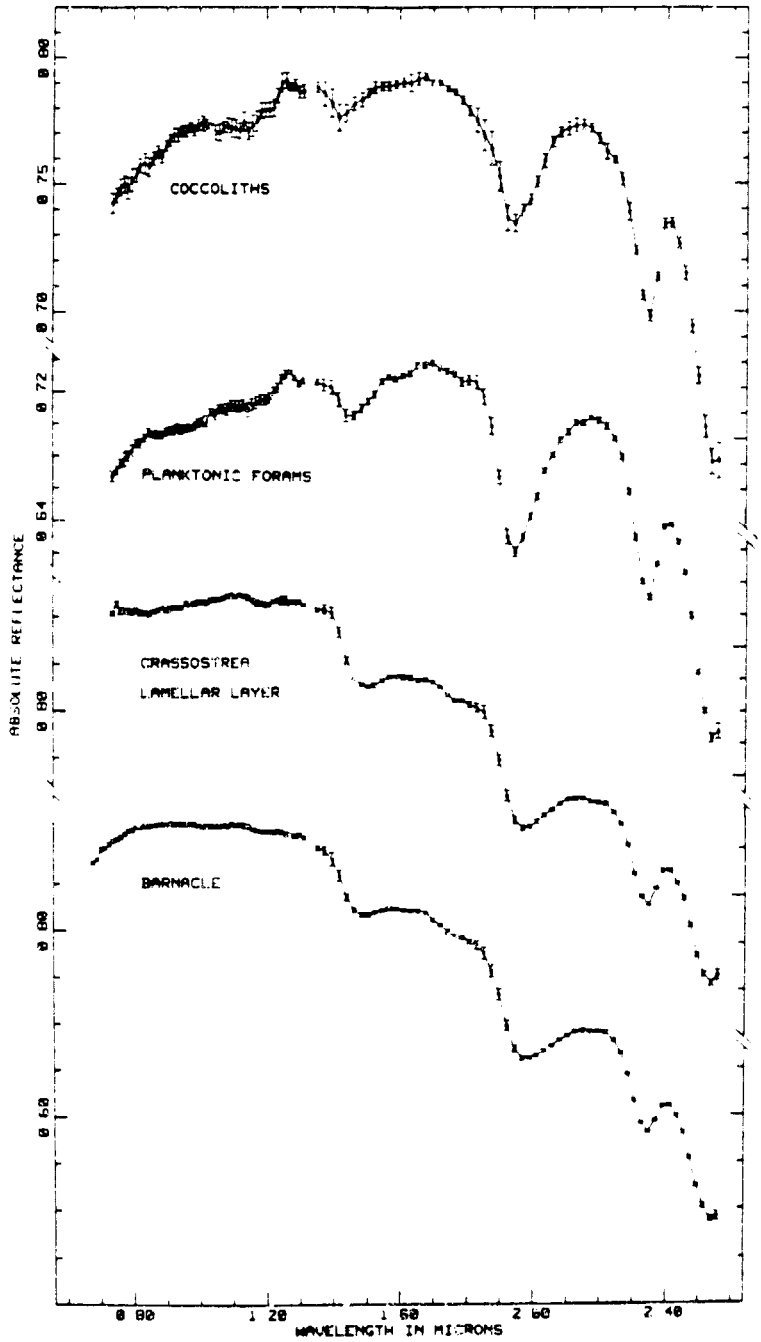

Figure 8.2 Spectra of skeletal material composed of low Mg calcite.

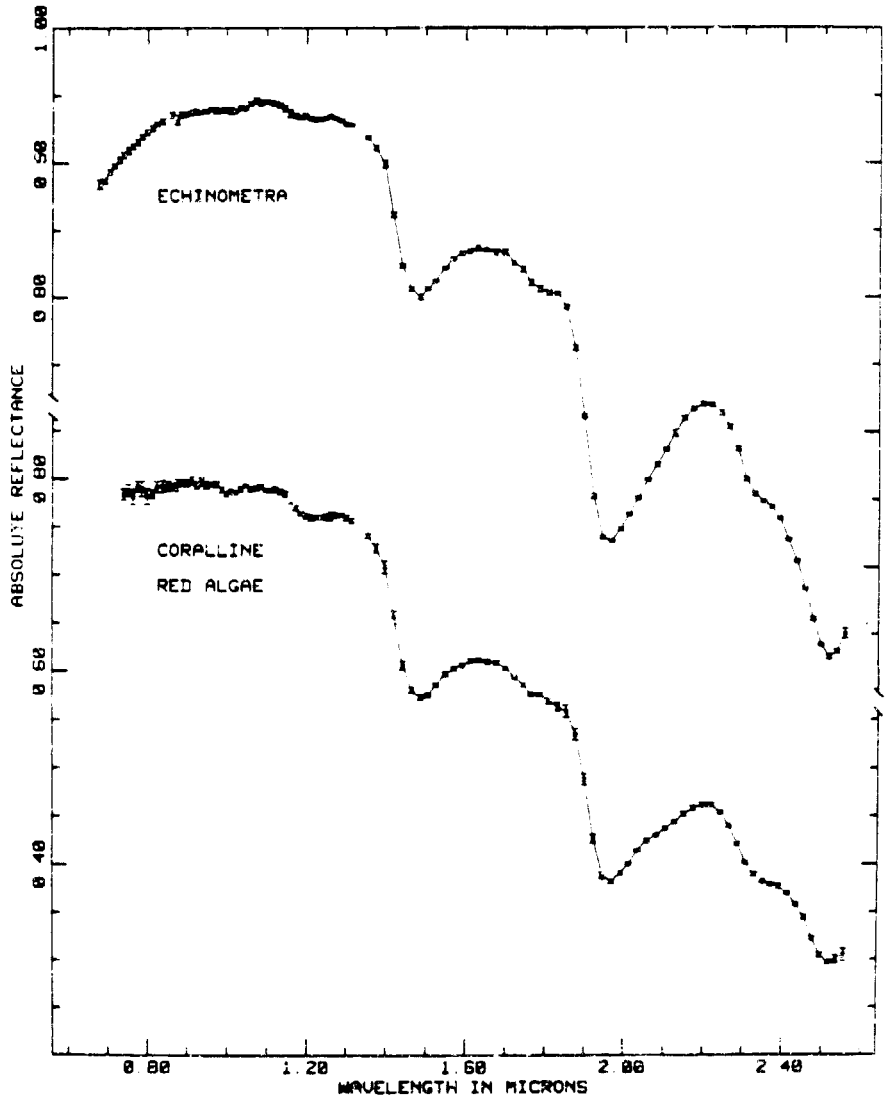

Figure 8.3 Spectra of skeletal material composed of high Mg calcite.

ORIGINAL PAGE IS
OF POOR QUALITY

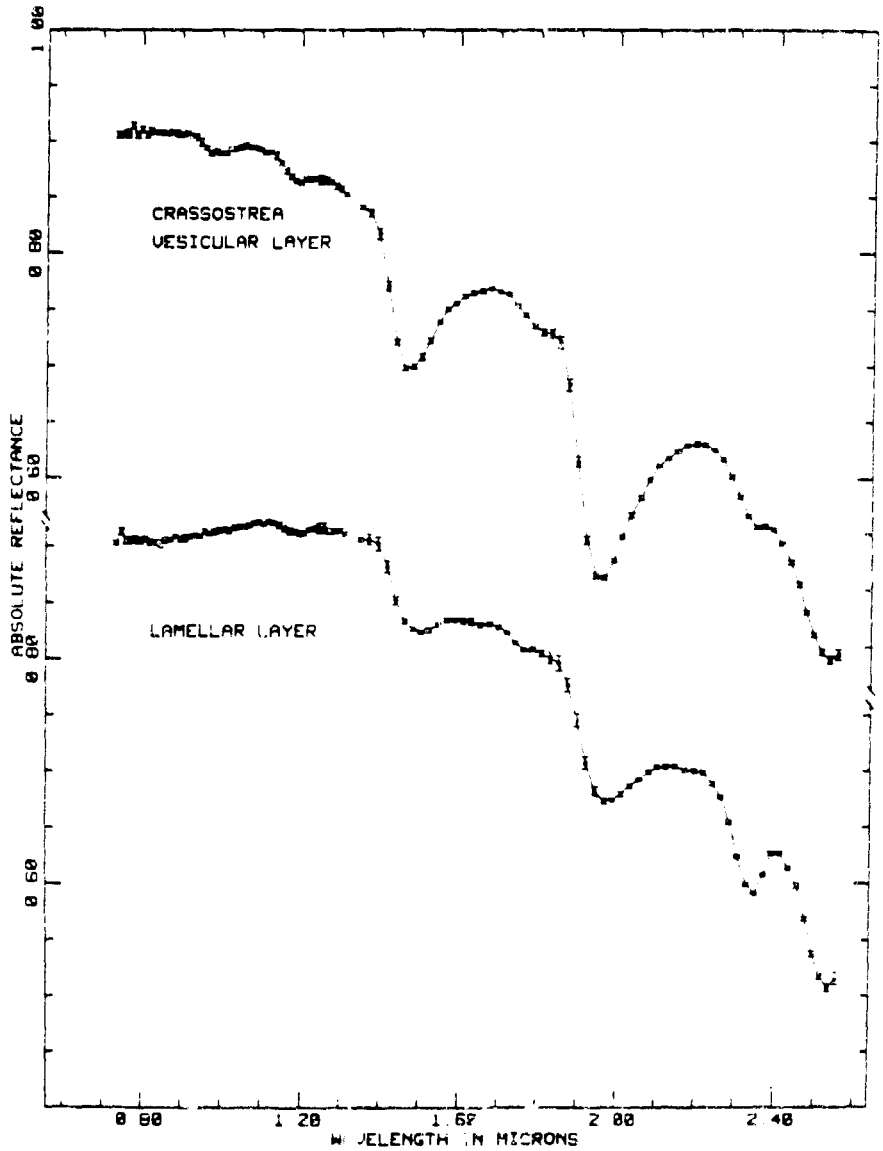

Figure 8.4 Spectra of two different layers within an oyster shell.

hour and measuring the amount of water evolved indicates corals and coralline red algae contain 2-3% water by weight. In general, skeletons of low Mg calcite seem to contain less water than those composed of aragonite or calcite. Shape and position of water bands in coccolith and planktonic foram spectra indicate some clay is present in these samples. Despite this, water bands in these spectra are weaker relative to the carbonate bands than in any other spectra of skeletal material studied here.

Limited data are available on variations in amounts of fluid inclusions in skeletons of individuals belonging to the same taxonomic group. In spectra of three different samples of Echinometra shapes, relative intensities, and positions of water bands are very similar. All spectra of skeletons of Scleractinian corals are also very similar. These include representatives of four different genera: Porites, Montipora, Pocillopora, and Fungia. The molluscs, on the other hand, show some variation. As Figure 8.4 shows, the lamellar and vesicular layers from a Crassostrea shell contain different amounts of fluid inclusions, as shown by the intensities of the water bands relative to the carbonate bands in their spectra.

When crystals grow in a fluid medium, any process that interferes with the growth of a perfect crystal can cause trapping of primary inclusions (Roedder, 1981). Roedder (1981) notes that rapid crystal growth can result in a porous, dendritic structure, whereas slower growth forms solid, impervious layers. Differences in fluid inclusion content among different organisms may reflect differences in rate of shell growth. Another possible cause of differences in inclusion content between different organisms may be differences in mechanisms by which skeletons and shells are built.

The exact form in which the water in skeletal material occurs is of interest. As was shown in Chapter 6, the water bands in the spectrum of the coral skeleton are similar in shape and position to those produced by liquid water. Thus the water in coral skeletons is probably in liquid form.

Results of spectral studies reflect the extremely small size of many of these inclusions. In the course of this study, spectra were taken of both whole and powdered skeletal material of a modern coral. Figure 8.5 shows a ln-ln plot of the spectra of a whole Montipora skeleton collected from a reef on the north shore or Oahu and bleached in H_2O_2, and a powdered sample of the same skeleton, ground and then bleached a second time. The plot forms essentially a straight line. As discussed in Chapter 3, this indicates that the relative intensities of absorption bands within the two spectra are the same, and that therefore the fluid inclusion content of the two samples is essentially the same. Grinding and bleaching the sample did not significantly alter its fluid inclusion content. This means that the inclusions are very small even in comparison with the grains of the powdered sample, and that after grinding, a substantial number remain.

It also means that, to a first order approximation, grinding and subjecting samples to a second bleaching treatment is unnecessary, as the spectral properties of the whole samples do not vary significantly from those of the powdered ones. Once the living tissue of the animal or plant has been removed, further treatment will not substantially alter the spectral properties of the sample. In fact, additional bleaching in H_2O_2 may be undesirable, as it is acid and might etch the sample, increasing its surface area and therefore the amount of water which is adsorbed on its surface. Detailed studies of etched and

ORIGINAL PAGE IS
OF POOR QUALITY

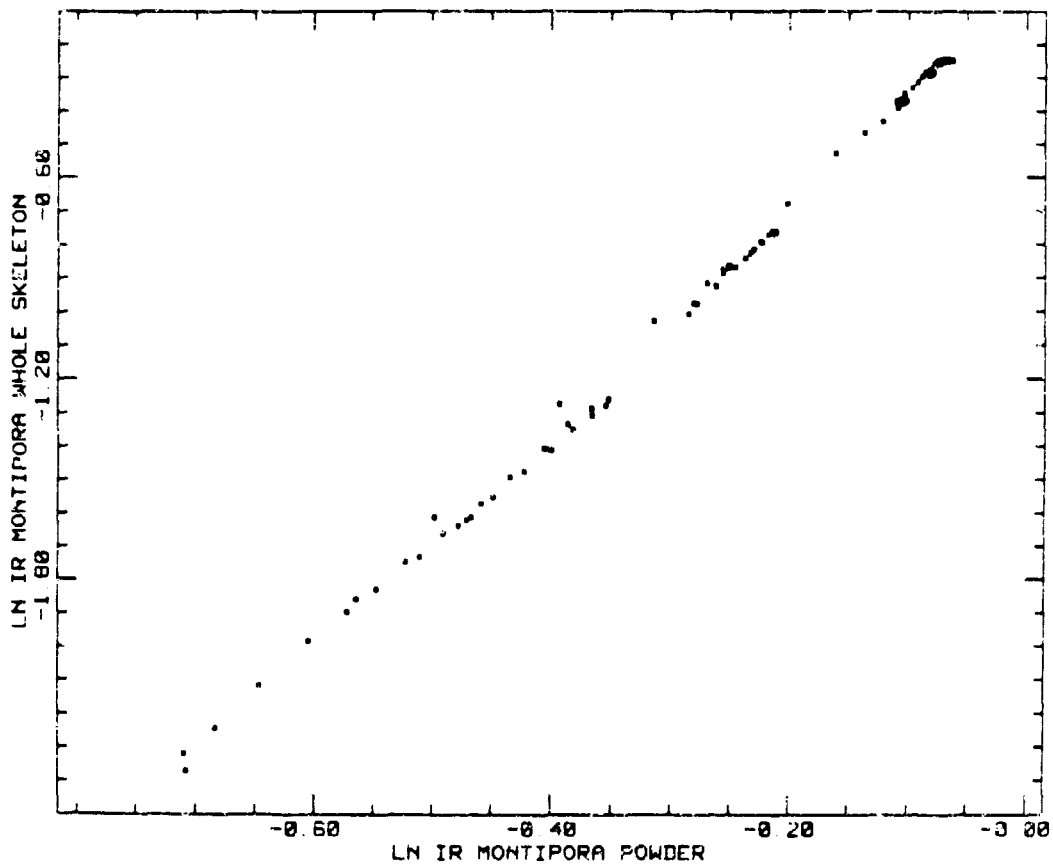

Figure 8.5 Ln-Ln plot of spectra of a whole and a powdered and bleached skeleton of the coral Montipora.

unetched samples will be needed to determine if carbonates can adsorb quantities of water large enough to add features to their spectra.

It may be that not all water in skeletal material is present as fluid inclusions. Close examination of the plots in Figures 8.1, 8.2, and 8.3 indicate that water bands in spectra of skeletal material vary in shape and position indicating water may occur in other forms.

Mackenzie et al. (1983) summarize the existing experimental evidence for the presence of hydroxyl groups or water in high Mg calcites, and presents transmission data in the MIR which indicate that OH or H_2O is present and is associated with the $MgCO_3$. However, they note that it is not possible to determine whether the phase present is OH or H_2O.

The fact that NIR spectra of high Mg calcites have a strong 1.9μm band indicates the phase present is H_2O rather than OH. Water bands in spectra of skeletons composed of high Mg calcite are broader and occur at slightly longer wavelengths than those in spectra of skeletal material composed of aragonite and low Mg calcite. As was seen in Chapter 7, water bands due to bound water in in hydrated carbonate minerals are broader and occur at longer wavelengths than those in liquid water. Thus, some of the water in skeletal material of echinoids and coralline red algae may be in the form of water of hydration.

X-ray diffraction work shows that some skeletal material of red algae contains Mg in the form of brucite ($Mg[OH]_2$) rather than as Mg calcite (Schmalz, 1965; Weber and Kaufman, 1965). There is no clear indication of features due to $Mg(OH)_2$ in the spectra shown here. However, spectra of all the high Mg calcites were taken on the University of Hawaii spectrometer. An instrument with greater spectral resolution than this one might allow detection of some of the features which Mara and Sutherland (1957) found are characteristic of brucite spectra in the 2.0 to 2.5μm region.

LOSS OF FLUID INCLUSIONS DURING DIAGENESIS

Spectral studies indicate diagenetic processes alter the fluid inclusion content of skeletal material. Figure 8.6 shows spectra of a fossil Porites skeleton collected at a depth of ≈15 meters from a core taken in a Pleistocene reef near Barbers Point on Oahu. X-ray diffraction analysis shows that the fossil skeleton has been altered to low Mg calcite. In thin section it can be seen that the coral has been altered to coarse, blocky calcite spar. Figure 8.6 also shows spectra of two Pleistocene encrusting coralline red algae. Again, X-ray diffraction indicates the fossil algae have been altered to low-Mg calcite. Spectra of these samples may be compared to those of the modern coral and modern coralline algae shown in Figures 8.1 and 8.2. Such comparison shows that in both cases, the coral and the coralline algae, the change in mineralogy has been accompanied by a loss of fluid inclusions, as indicated by a decrease in the intensity of the water bands relative to the carbonate bands in their spectra. Analysis for water as described above indicates the amount of water has dropped to a few tenths of a per cent by weight in the fossil material. The loss of water accompanying the change from high to low Mg calcite indicates that the water in these calcites is associated with the $MgCO_3$ component, as suggested by McKenzie. et al. (1983), and others.

Shapes of water bands may provide additional evidence for the association of H_2O with the $MgCO_3$ phase in high Mg calcites. Figure 8.7 shows spectra of the modern and fossil coralline red algae plotted together so that they may be more easily compared. Note that not only the relative intensities, but also the shapes of the water bands have changed in the spectrum of the fossil alga. The bulges on the long wavelength sides of the 1.4 and 1.9μm bands are gone in the fossil

spectrum and the water bands are shaped much like those in the wet Iceland spar spectrum shown in Figure 6.1.

When neomorphic calcite spar replaces original aragonitic skeletal material, relict skeletal aragonite crystals remain as solid inclusions constituting a few per cent, by volume, of the rock (Sandberg, 1975; Sandberg et al., 1973; Sandberg and Hudson, 1983). Scanning electron photomicrographs of a broken surface of the Pleistocene coral etched with dilute acetic acid show such relict crystals embedded in the coarse calcite spar (Fig. 8.8). Although the replacement spar undoubtedly contains some inclusions it may be that these relict aragonite crystals now contain the bulk of the liquid water which causes the absorption bands observed.

Limited laboratory data also illustrates the loss of fluid inclusions with change in skeletal mineralogy. Figure 8.9 shows spectra of powdered samples of a coral skeleton before heating and after the sample had been heated at 200°C for 26 hours, and at 230°C for 72 hours. As can be seen by weakening of the 1.4 and 1.9μm water bands relative to the carbonate bands, and by the disappearance of the 0.92 and 1.20μm water bands, the amount of water in the sample has decreased. X-ray diffraction analysis of the heated samples indicate they have been partially altered to calcite. At one atmosphere of pressure dry aragonite spontaneously alters to calcite at temperatures of 400°C or higher (Deer et al., 1962). Undoubtedly the change in mineralogy has been facilitated by the fact that the skeletal material is not dry.

Figure 8.10 shows that recrystallization of skeletal material even without change in mineralogy is accompanied by loss of fluid inclusions. These three spectra are of core samples from DSDP site 289 on the Ontong Java Plateau. The samples are 0.7, 28, and 57.7 million years old,

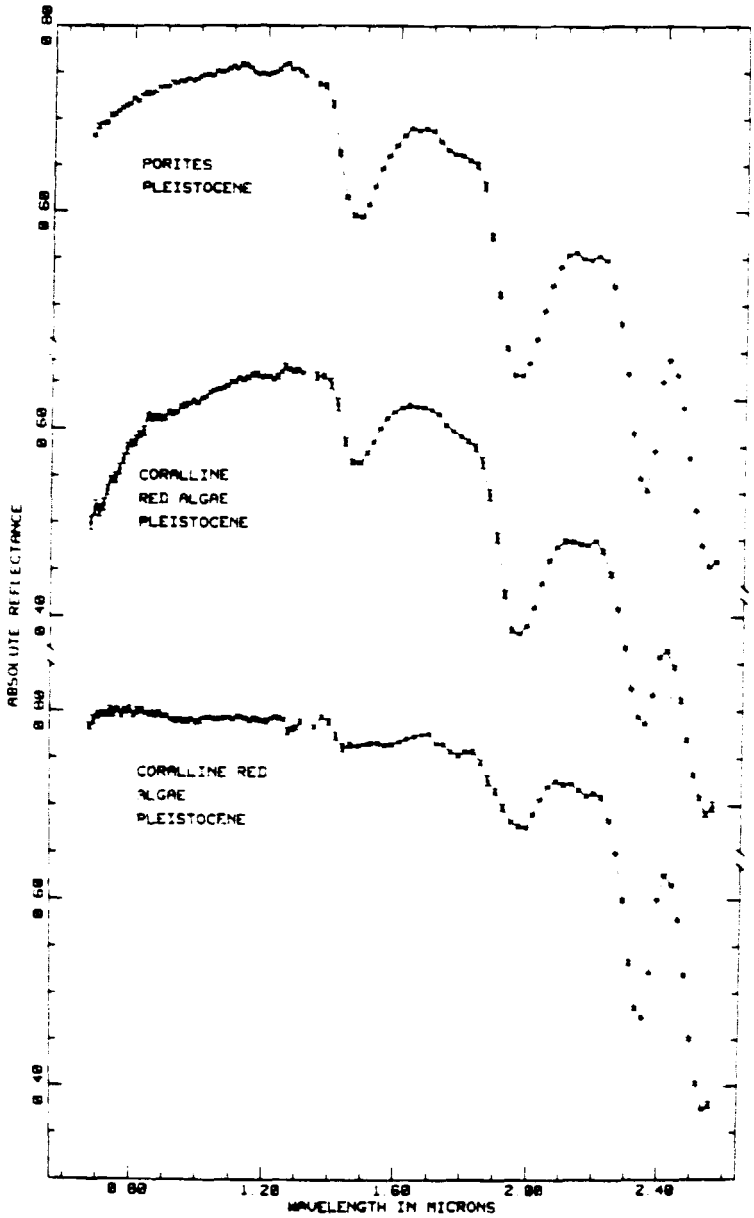

Figure 8.6 Spectra of fossil coral and coralline algae which have been altered to low Mg calcite.

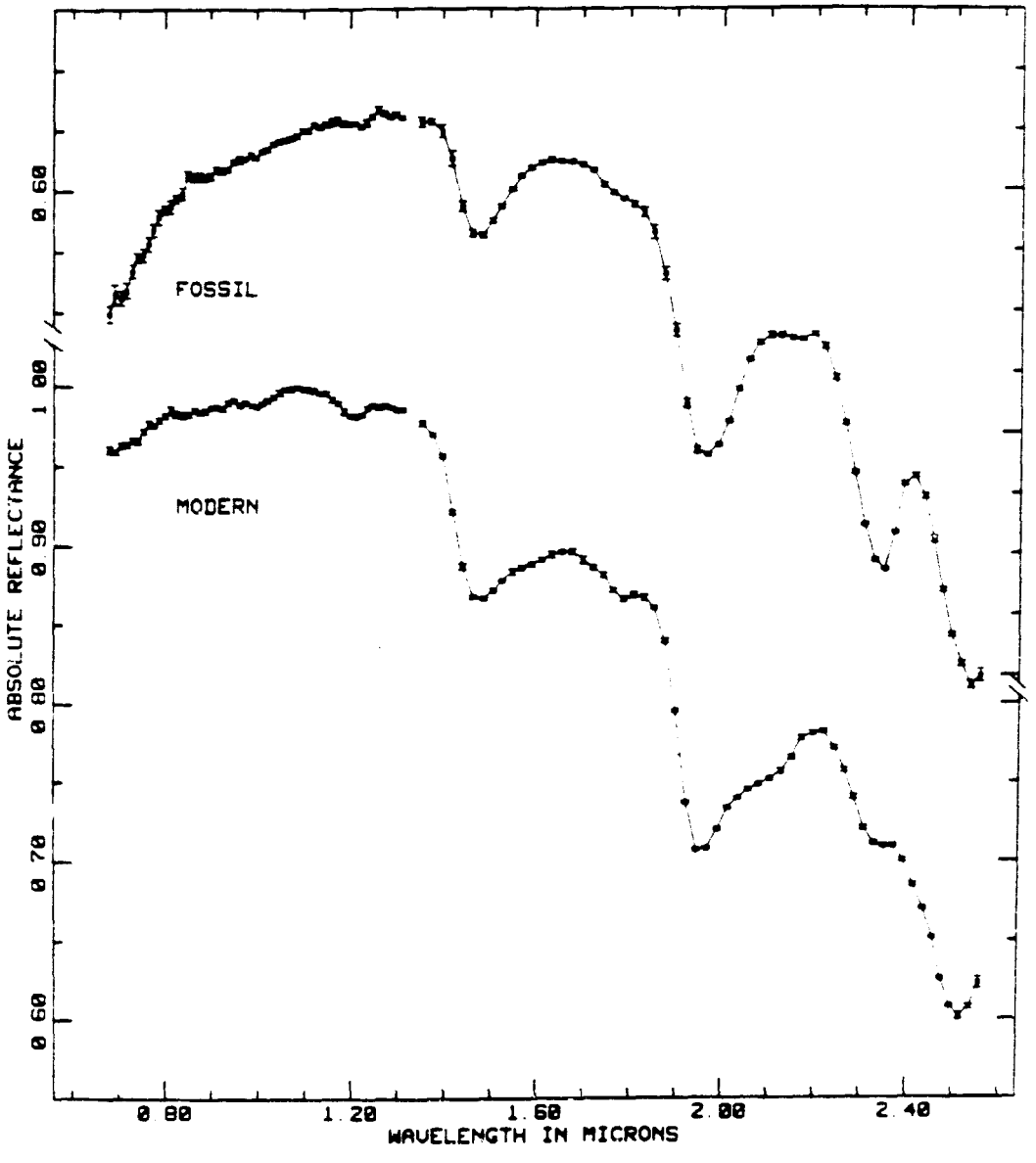

Figure 8.7 Spectra of modern and fossil coralline red algae showing change in shape and intensity of water bands accompanying change in mineralogy.

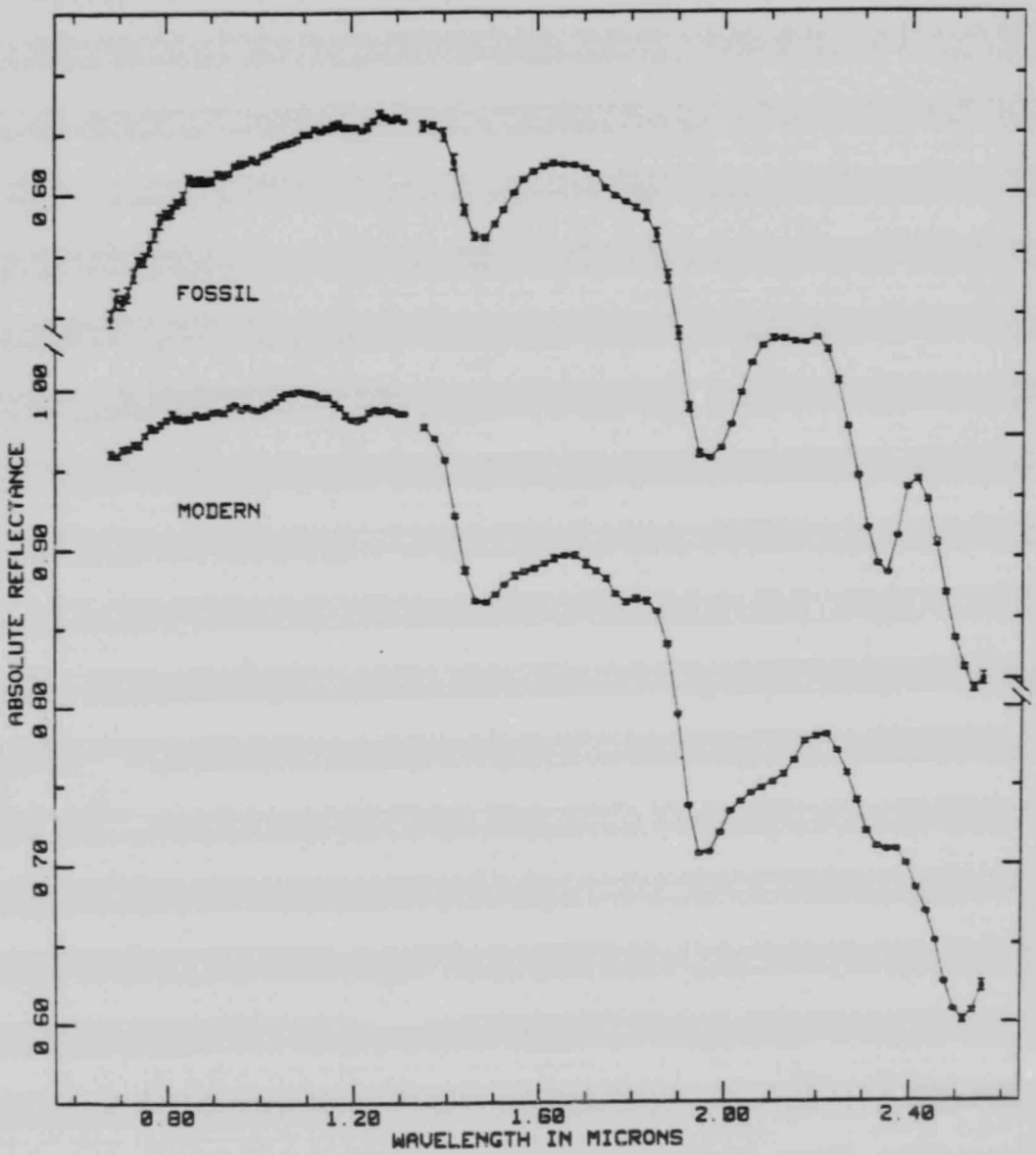

Figure 8.7 Spectra of modern and fossil coralline red algae showing change in shape and intensity of water bands accompanying change in mineralogy.

ORIGINAL PAGE IS
OF POOR QUALITY

Figure 8.8 SEM photo of etched surface of fossil coral showing relict aragonite crystals. Magnification 3000X.

ORIGINAL PAGE IS
OF POOR QUALITY

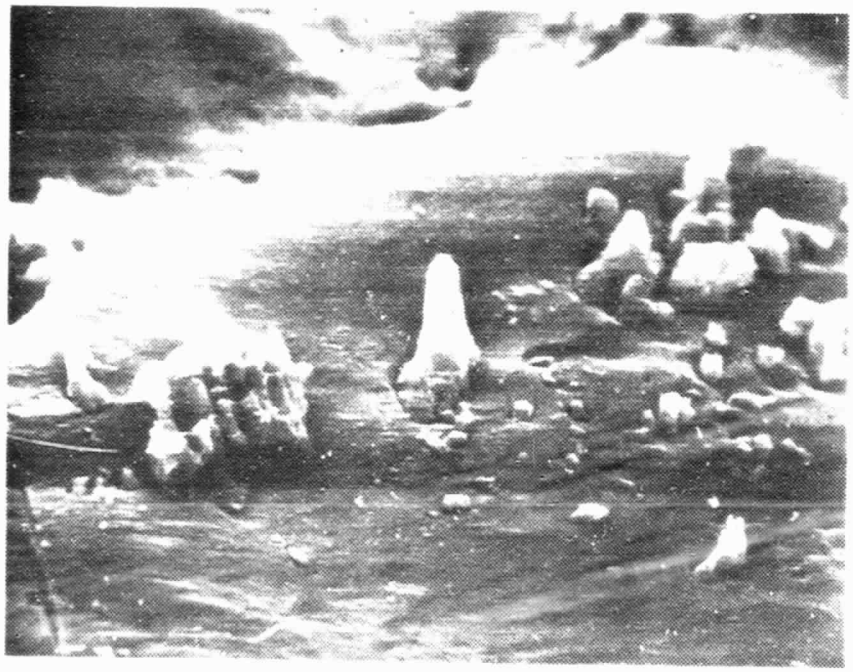

Figure 8.8 SEM photo of etched surface of fossil coral showing relict aragonite crystals. Magnification 3000X.

ORIGINAL PAGE IS
OF POOR QUALITY

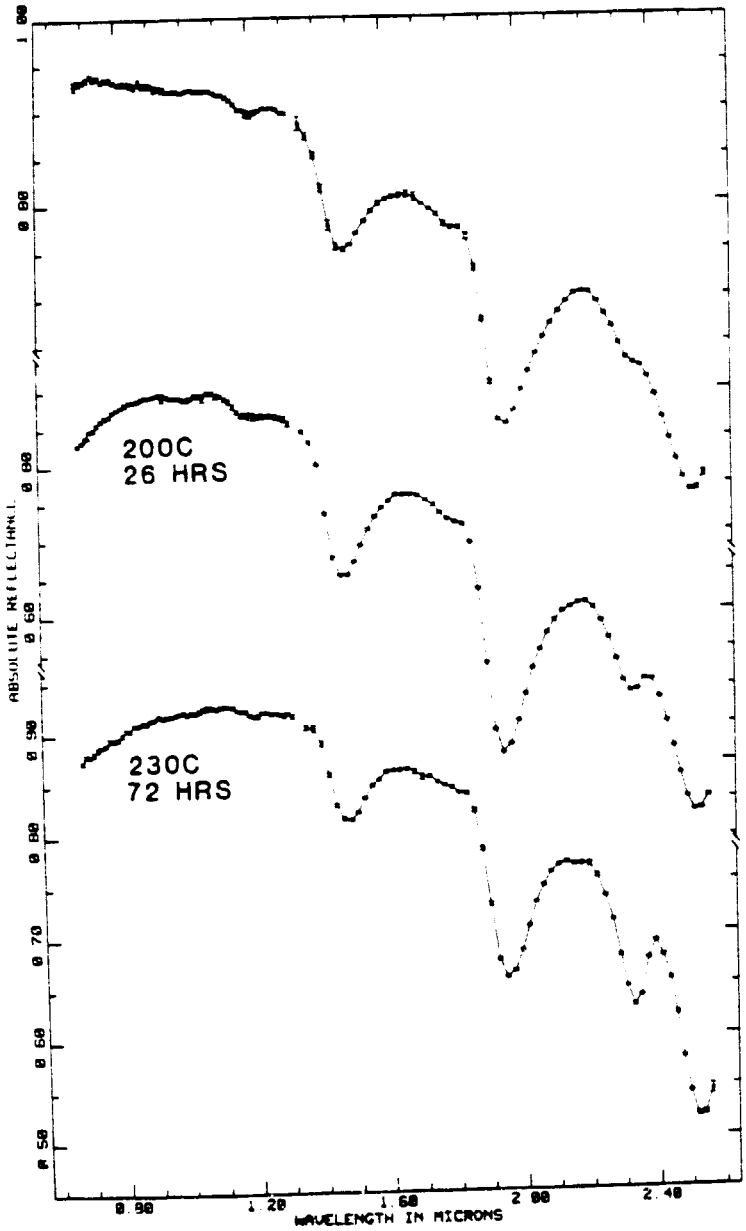

Figure 8.9 Spectra of powdered coral skeleton before and after heating.

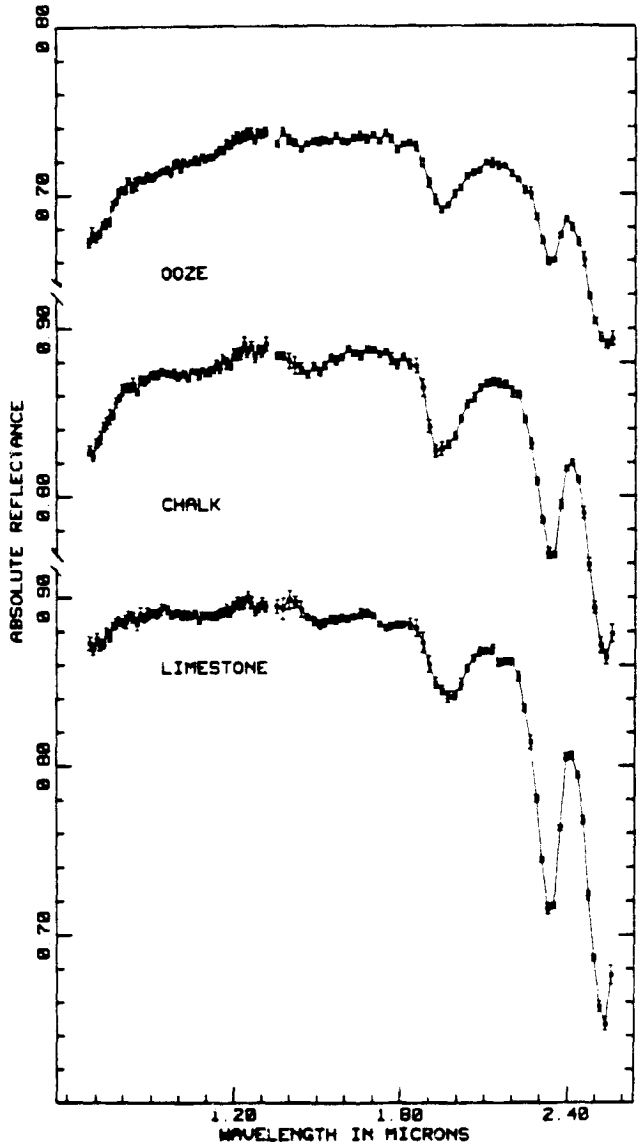

Figure 8.10 Spectra showing loss of fluid inclsuions during the ooze-chalk-limestone transition in deep sea carbonates.

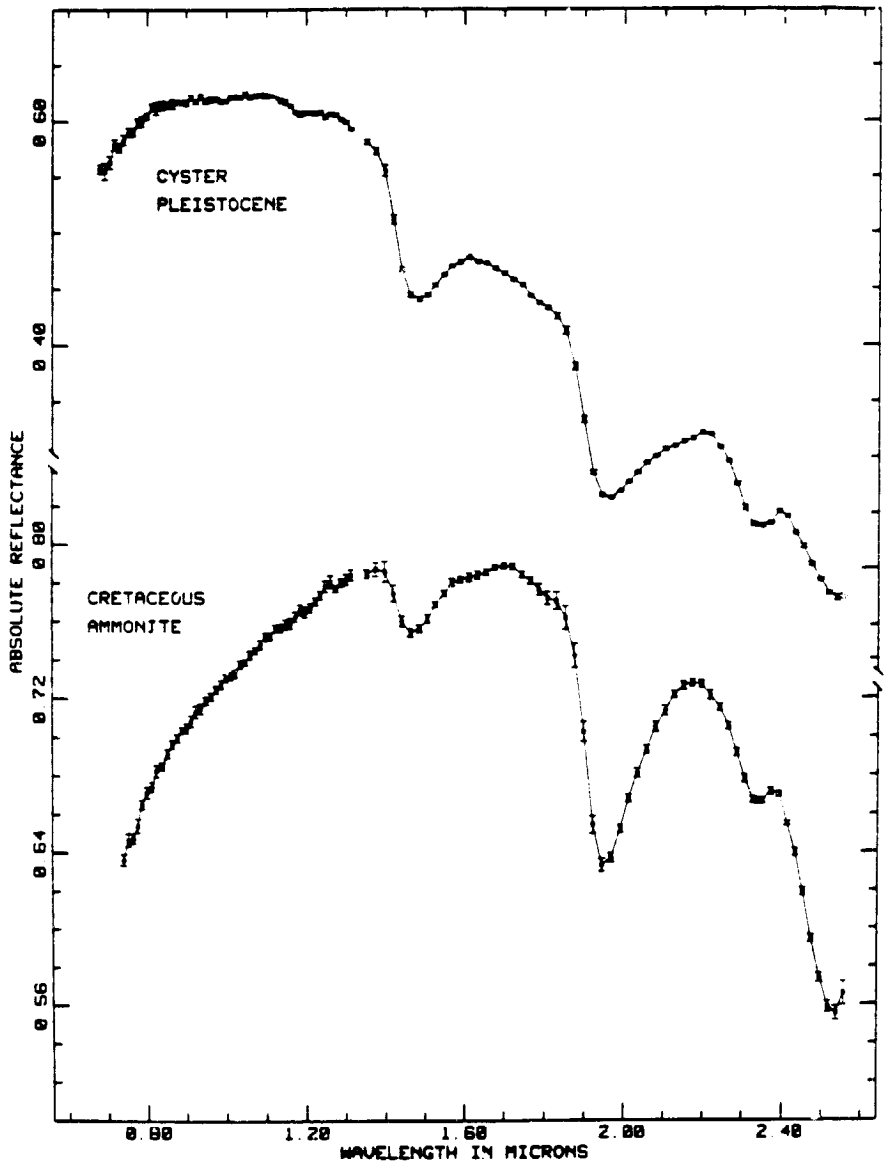

Figure 8.11 Spectra of unaltered fossil material which retains original skeletal mineralogy and fluid inclusion content.

respectively (Andrews *et al.*, 1975) and show the loss of fluid inclusions during the solution and reprecipitation of calcite accompanying the ooze-chalk-limestone transition. These samples are all composed of similar proportions of coccoliths and forams (Andrews *et al.*, 1975), so the differences in relative band intensities can't be attributed to taxonomic differences. The change in fluid inclusion content is reflected in the change in relative intensities of the water and carbonate bands. Calcareous oozes are composed almost entirely of coccoliths and test of planktonic foraminifera, both of which are composed of low Mg calcite (Milliman, 1974). During diagenesis accompanying burial, calcite is dissolved from the more soluble portions of foram tests and coccoliths, and is redeposited as cement and overgrowths on other calcite grains (Schlanger and Douglas, 1974). Manghnani *et al.* (1980) found that this process was accompanied by a loss of strontium. It would appear that it is also accompanied by a loss of fluid inclusions.

Increase in the absolute intensities of carbonate bands also accompanies this change. This reflects the coarsening of crystals within the rock as a result of solution and reprecipitation. This increase in intensity can be seen in these spectra in spite of the fact they had been disaggregated (oozes) and ground (chalk, limestone) for chemical analysis. Studies of spectral properties of a suite of unground DSDP samples from the same drilling site will give a more detailed picture of this type of alteration.

Spectra in Figure 8.11 show that where skeletal material has not been altered, the fluid inclusion content remains unchanged. The Cretaceous ammonite whose spectrum is shown is still composed of aragonite. The Pleistocene oyster *Chama* (Kay, 1979) was collected from a raised Pleistocene reef at Ulupau Head on the windward coast of Oahu, and is

composed of low Mg calcite, as are many modern oysters. In thin section the oysters show no evidence of recrystallization. The spectra of the ammonite and the oyster are very similar to spectra of shells of modern aragonitic and calcitic molluscs shown in Figures 8.1 and 8.2. This indicates fluid inclusion contents are very similar in the modern and fossil material. Thus, fluid inclusion content is potentially a useful tool for determining whether skeletal material is primary, or has undergone alteration.

Relative intensities of water and carbonate bands in the two Pleistocene coralline red algae spectra shown in Figure 8.6 indicate that while both samples are depleted in fliud inclusions relative to the modern skeleton, they have not been depleted to the same degree. The first spectrum is from an alga from the same raised Pleistocene reef as the oysters discussed above. This reef grew during the last interglacial during a time when sea level was higher than at present (Stearns, 1974, 1978), and since that time has been exposed in the vadose environment. The second spectrum was taken from a sample collected from a depth of 15m from the same core as the fossil Porites. Petrographic evidence indicates these samples have undergone diagenesis in the fresh water phreatic environment. Thus the two samples, altered in different environments, have different aqueous fluid inclusion contents.

Three coral samples whose spectra are shown in Figure 8.12 and which are pictured in Figures 8.13a, b, and c illustrate another example of variations in fluid inclusion content correlated with variations in diagenetic environment.

The first spectrum is of a coral sample taken from a depth of ≈8.3m in a core drilled by the Hawaii Department of Land and Natural Resources

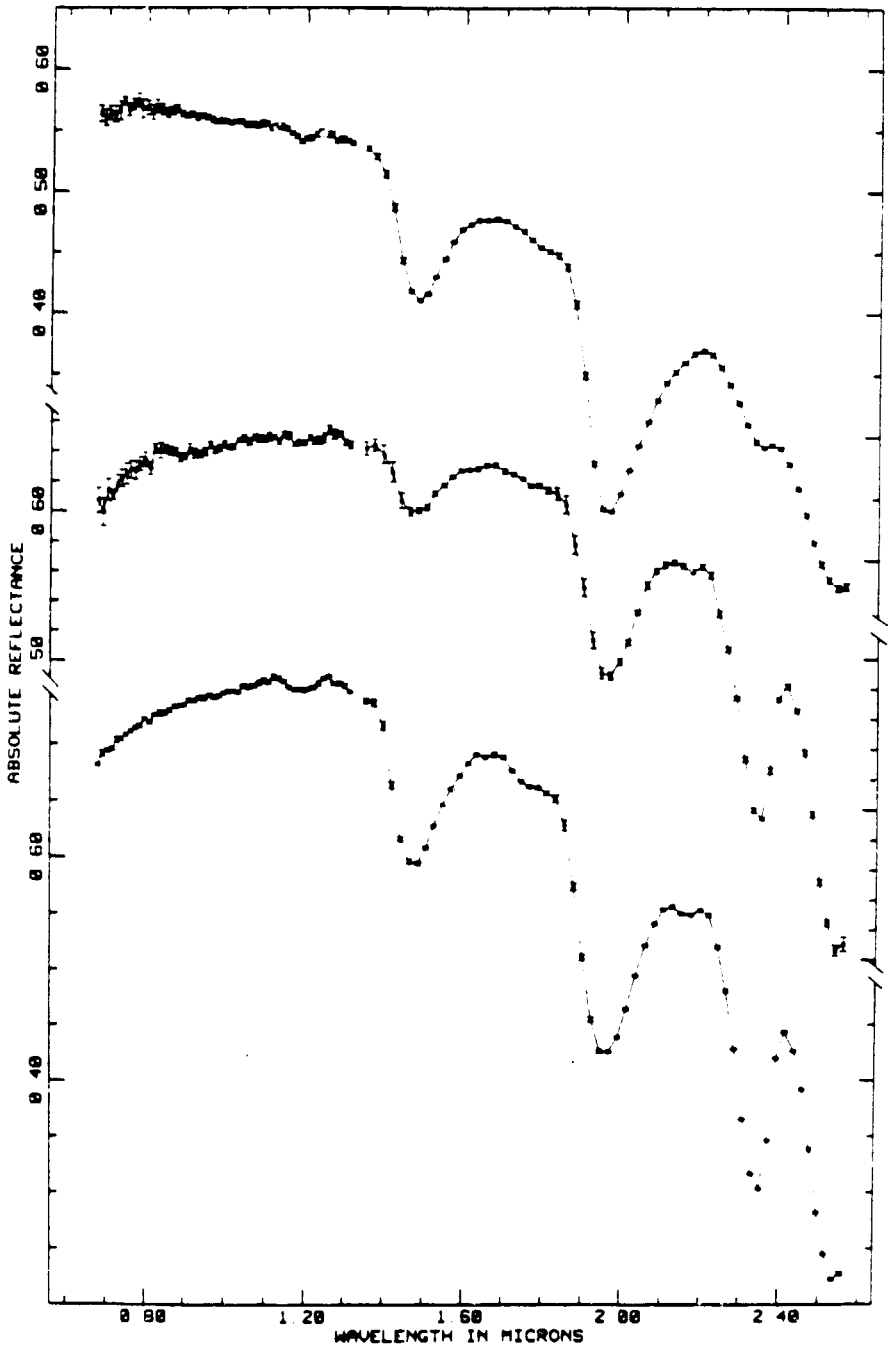

Figure 8.12 Spectra of three coral samples with different diagenetic histories.

ORIGINAL PAGE IS
OF POOR QUALITY

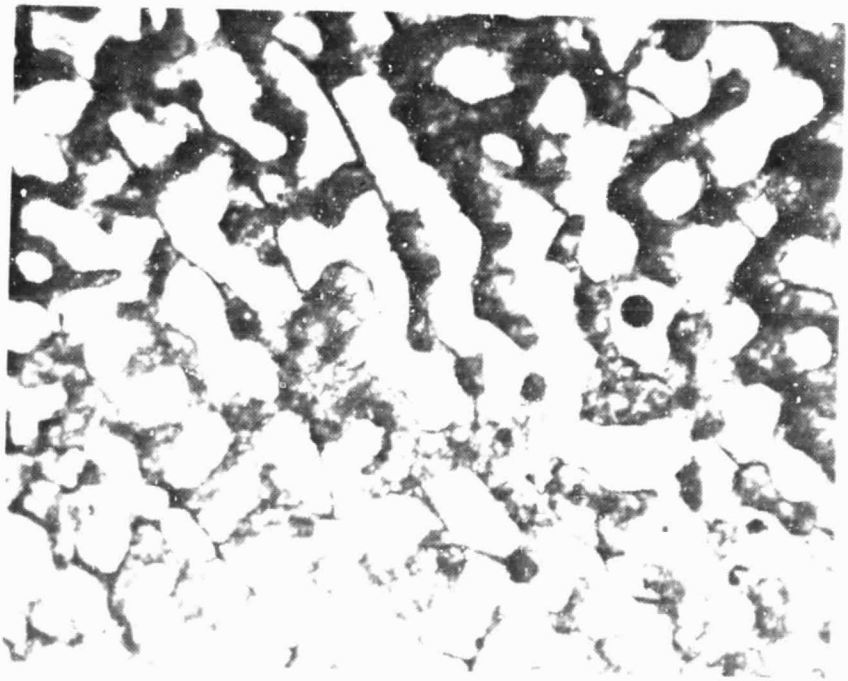

Figure 8.13a Photomicrograph of Pleistocene coral which has undergone dissolution. Magnification 40X

PRECEDING PAGE BLANK NOT FILMED

ORIGINAL PAGE IS
OF POOR QUALITY

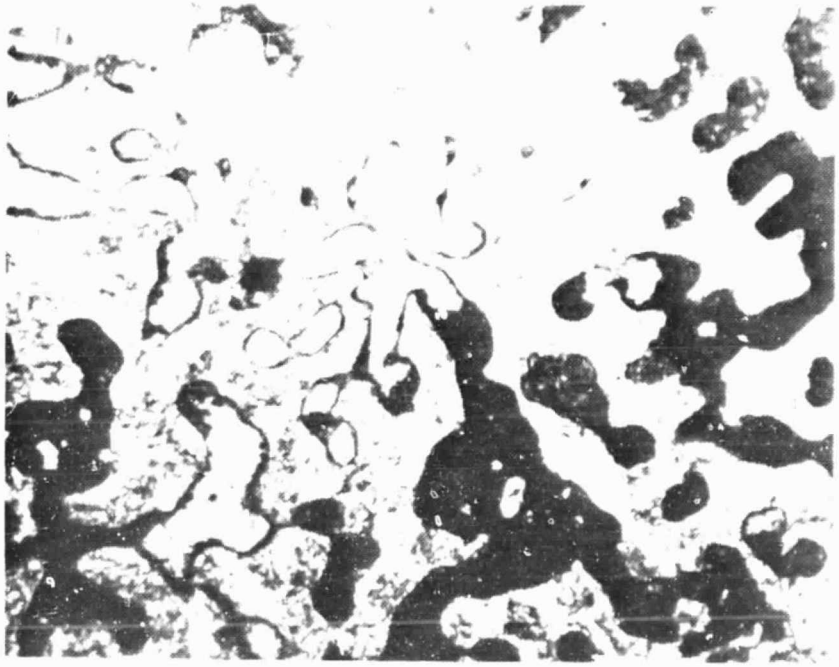

Figure 8.13b Photomicrograph of Pleistocene coral which has shows fabric selective mosaic characteristic of alteration in the vadose environment. Magnification 40X

ORIGINAL PAGE IS
OF POOR QUALITY

Figure 8.13c Photomicrograph of Pleistocene coral which shows coarse calcite mosaic characteristic of diagenesis in the phreatic environment. Magnification 40X

on the Waimanalo coastal plain. The sample is from the Waimanalo Formation which consists of reef and associated limestone, deposited during the last Pleistocene high stand of the sea (Lum and Stearns, 1970). Lum and Stearns (1970) report that this limestone is highly porous and has undergone only moderate leaching and recrystallization. A photomicrograph of the sample, shown in Figure 8.13a, shows that the sample has undergone some dissolution, but that no neomorphic replacement has occurred. The spectrum of this sample, the first in Figure 8.12, reflects this, as it looks much like those of fresh coral samples.

The second spectrum in Figure 8.12 is that of a coral sample taken from a depth of 33.8m in the same core. This sample came from the top of the Kaena Formation, another Pleistocene reef limestone (Lum and Stearns, 1970). The photomicrograph of this sample shown in Figure 8.13b shows the fabric selective calcite mosaic which Pingitore (1976) found to be characteristic of coral skeletons altered in the vadose environment.

The third spectrum in Figure 8.12 is the same as that shown in Figure 8.6. Figure 8.13c is a photomicrograph of this sample which shows that the coral has been altered to coarse spar which displays the cross-cutting calcite mosaic characteristic of alteration in the phreatic environment (Pingitore, 1976).

Both the second and third spectra show a marked drop in fluid inclusion content as a result of their neomorphic replacement by calcite. However, as with the red algae, the two specimens have not been depleted in fluid inclusions to the same degree, again indicating fluid inclusion content may be related to environment of diagenesis.

Although these results are in no way conclusive, they do suggest that fluid inclusion content may reflect diagenetic history of skeletal material.

While these results are in no way conclusive, they do suggest some interesting possibilities. Optical methods of studying fluid inclusions require that inclusions be 1 - 2μm in diameter, and the best material for such studies comes from large, well-formed crystals (Roedder, 1979) Roedder (1979) concluded that most environments of sedimentary diagenesis recorded by these fluid inclusions involve the presence of hot, saline brines. Reflectance spectroscopy can't provide the detailed information on the chemistry and phase relationships of aqueous inclusions which can be determined by optical and other techniques. However, it provides a technique for acquiring some information on formation and loss of aqueous fluid inclusions in materials which are too fine-grained to be analyzed by these other techniques, and will allow information to be obtained on near-surface diagenetic processes which do not form large, well-formed crystals.

Thus the presence and relative abundances of fluid inclusions are potentially useful diagenetic indicators, and may aid in determining whether skeletal material has undergone alteration. It may also be that fluid inclusions provide a medium in which diagenetic alteration can take place and so may be a factor affecting the relative stability of different types of skeletal material with the same mineralogy.

CHAPTER 9

Remote Sensing Applications

INTRODUCTION

Reflectance spectroscopy in the VIS and NIR (0.35 to 2.5μm) has potential applications not only as a laboratory tool, but also as a tool for remote sensing (Adams, 1975; Goetz et al., 1982, 1983; Hunt, 1977; Hunt and Salisbury, 1970; and others). This chapter will examine the types of data on carbonates which it should be possible to obtain remotely, and will discuss some of the problems involved in obtaining them, and how some of these problems may be overcome.

When collecting spectral data on rocks exposed at the Earth's surface from aircraft or space craft several factors may contribute to the spectrum which is obtained. In order to obtain the maximum amount of information from remotely sensed data, each factor must first be isolated and dealt with separately, so that its contribution to the remotely sensed data is well understood.

Factors contributing to a remotely obtained spectrum include the solar spectrum, the atmosphere, and instrument response (Sabins, 1978).

Depending on the geographical area being studied, spectra may be obtained from other Earth surface materials than bedrock. Vegetation may cover outcrop areas, and indeed Goetz _et al_. (1983) state that vegetation covers approximately two thirds of the land surface.

Vegetation often varies from one bedrock unit to another and variation in vegetation is a standard tool used in geologic mapping both in the field and from aerial photographs (Compton, 1962; Lahee, 1941). Landsat imagery, especially sensitive to differences in types of vegetation and to symptoms of stress in vegetation has greatly aided geobotanical studies (Richardson, 1983; Sabins, 1978). As with vegetation, soil characteristics may reflect the nature of the bedrock below, and be used to trace contacts between rock units (Compton, 1962).

Given that all these components can be identified and isolated in a remotely obtained spectrum, how will the component contributed by carbonate rocks themselves appear? The purpose here is to examine in detail the component of the remotely sensed spectrum which results from the interaction of light with carbonate rocks, i. e. the spectral properties of carbonate minerals and the mixtures of different phases which make up carbonate rocks which form the thick sedimentary sequences found in the stratigraphic record. Consideration must also be given to the effects of exposure in the subaerial environment on petrographic characteristics and on spectral properties of carbonate rocks. And since strong atmospheric absorptions in the 1.4μm and 1.9μm regions may mask spectral data in these regions, it is necessary to consider what may be learned about carbonate rocks from the remaining accessible regions of the spectrum. Finally, it is necessary to determine what, if any, information on carbonate mineralogy and chemistry can be determined from existing data sets, specifically Thematic Mapper (TM) and the Shuttle Mapping Infrared Radiometer (SMIRR).

SPECTRAL PROPERTIES OF CARBONATE MINERALS

In ancient sediments which are the targets of remote sensing, calcite ($CaCO_3$) and dolomite ($CaMg[CO_3]_2$) are the most abundant carbonate phases encountered. As discussed in Chapter 3, these two minerals can readily be distinguished on the basis of their spectral properties. All the carbonate bands in dolomite spectra occur at shorter wavelengths than equivalent bands in calcite spectra, and the positions of the two strongest carbonate bands, bands 1 and 2, are sufficient for discrimination of these two minerals. Fe^{2+}, which commonly substitutes into both calcites and dolomites produces absorption features near 1.0μm. Iron bands in calcite spectra differ in shape and position from those in dolomite spectra and, in addition to indicating the presence of iron, can aid in mineral identification when they are present.

Absorption features due to Fe^{2+} and Mn^{2+} occur in the 0.35 to 1.3μm region of the spectrum. Relative intensities of these features reflect concentrations of these cations in the mineral species, as was shown in Chapter 5.

Blake (1983) states that the three strongest atmospheric absorption bands, those centered at 1.4, 1.9 and 2.6μm will reach saturation at sea level, and no spectral data can be obtained in these regions. She found that in a limestone spectrum measured in the field, the carbonate bands near 2.3 and 2.5μm could be detected. Collins et al. (1981) also found features in IAS data which they attributed to calcite seen in outcrop. In addition, Blake (1983) found that in basalt spectra measured in the field the 1.0μm feature due to Fe^{2+} was detected. Similar crystal field bands in carbonate spectra should also be detectible in remotely sensed spectra. Thus the spectral features which are diagnostic of mineralogical and chemical composition in carbonate rocks can be detected by remote sensing techniques.

SPECTRAL PROPERTIES OF NON-CARBONATE PHASES

Although limestones and dolostones may be composed almost exclusively of calcite and dolomite, respectively, other phases may be present which, even in small amounts, may contribute features to the spectra of carbonate rocks. Some of these are illustrated in Figure 9.1, and include: 1) Iron Oxides, 2) Liquid water in the form of fluid inclusions, 3) Clays, 4) Chert, 5) Organics, and 6) Iron sulphides.

1) Iron Oxides

Carbonate rocks may contain small amounts of iron oxides. Spectral properties of iron oxides have been described by Hunt and Ashley (1979), Hunt et al. (1971), Singer (1981, 1982) and others. Typically they have absorptions near 0.89, 0.63, 0.45-0.50 and 0.4μm. These absorptions occur in the same region as those due to Mn^{2+}, and work is underway on distinguishing the two. The first spectrum in Figure 9.1 is of an oolitic limestone which contained pyrite that has been altered to iron oxides (Jenks, 1972). This spectrum has absorptions near 0.50, 0.62, and 0.89μm which can be attributed to Fe^{3+}.

2) Clay

Spectral properties of clays are described by Hunt (1977), Hunt and Ashley (1979), Hunt and Salisbury (1971), and Hunt (1977). Some of these features are illustrated in Chapter 6. Features near 1.4 and 1.9μm will be masked by atmospheric water bands. However the features in the 2.2 to 2.3μm region which are characteristic of clays (Hunt, 1977, and others) can be used for mineral identification. The second spectrum in Figure 9.1 is of a clay-carbonate mixture, and shows the 2.3 and 2.5μm bands of calcite as well as the 2.2μm band characteristic of kaolinite.

3) Liquid water in fluid inclusions

Results of this study indicate that fluid inclusions occur in

nearly all carbonate minerals and rocks (see Chapters 6 and 8). While the centers of absorptions due to liquid water would be masked by atmospheric water bands, the wings of the strong stretching modes centered near 1.9 and 3.0μm can affect spectra in the 2.0 to 2.5μm region. The third spectrum in Figure 9.1 is that of a calcite which contains a few tenths of a per cent water by weight.

4) Chert

While quartz has no absorption features in this region, preliminary studies of spectra of chert nodules indicate they may have clay-like features in their spectra. Such features might be due to a hydrated silica phase. Because quartz itself does not absorb in this wavelength region, very minor amounts of such material would produce features in the spectrum. A spectrum of a chert nodule is shown in Figure 9.1. Further study will be required to determine if the presence or absence of chert, a feature of carbonate rocks which is of importance in stratigraphic and diagenetic studies, can be determined from reflectance spectra.

5) Organics

Preliminary studies indicate that organics lower the albedo of carbonate rocks and give their spectra a general negative slope. Figure 9.2 contains an illustration.

6) Iron sulphides

Pyrite in the form of small scattered grains is nearly ubiquitous in carbonates rocks (Pettijohn, 1975). The last spectrum in Figure 9.1 is that of a pelletted mudstone which contains disseminated pyrite. The sample is from the Mississippian Lodgepole Formation in central Montana. The pyrite gives the rock spectrum its low albedo and the broad absorption band near 1.0μm.

ORIGINAL PAGE IS
OF POOR QUALITY

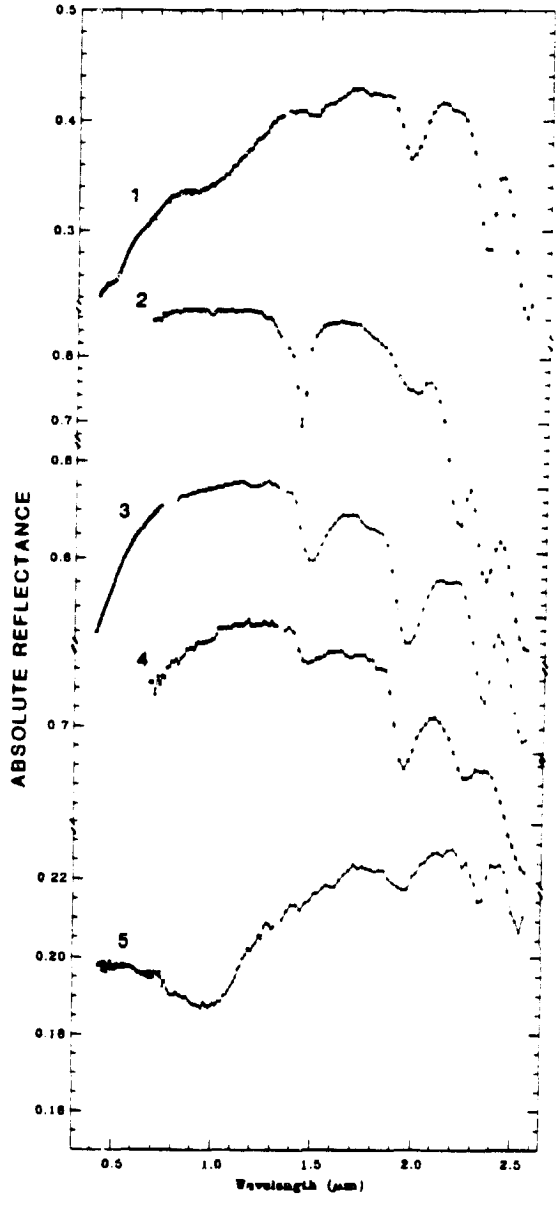

Figure 9.1 Spectra showing absorption features due to non-carbonate phases.

EFFECTS OF WEATHERING

When carbonate rocks are exposed at the Earth's surface in the subaerial environment they may be altered. Rocks accessible to remote sensing will have been affected by processes acting in the fresh-water vadose environment. This means the rocks are exposed to fresh water, rather than sea water or brines, and that they reside above the water table where pore spaces are partially filled by water (vadose), rather than below the water table where pore spaces are entirely filled by water (phreatic). Carbonate rocks in this environment may be affected by certain diagenetic processes which will alter their spectral characteristics. These include 1) Dissolution, 2) Formation of duricrusts or calcretes, 3) Oxidation, and 4) Dedolomitization.

Rain water dissolves CO_2 from the air and from soils according to the reaction

$$H_2O + CO_2 = H_2CO_3$$

(Longman, 1980). The weak carbonic acid dissolves carbonate minerals and carries them downward in solution until they are removed by rivers to the ocean, or until the solution becomes saturated and precipitates $CaCO_3$, generally as low-Mg calcite.

In humid climates partial dissolution of carbonate may occur leaving behind a surface of porous, fine-grained carbonate which will appear white in outcrop (Lahee, 1941). Although the surface will still have the spectral features typical of carbonates, increased scattering due to the decrease in grain size and the increase in porosity will not only make the reflectance spectrum of these rock surfaces appear brighter than that of fresh rock, it will result in weakening of the absorption bands (see Chapter 3).

In arid or semiarid environments where evapotranspiration exceeds precipitaion, $CaCO_3$ dissolved by meteoric waters is not leached away from soils, sediments and bedrock, but is redeposited to form calcretes (Goudie, 1983). Calcretes are composed primarily of microcrystalline low Mg calcite, but may contain silica, alumina, and manganese and iron oxides as well (Goudie, 1983). Their petrologic characteristics are markedly different from those of the rocks on which they form (Arakel, 1982; James, 1972; Multer and Hoffmeister, 1968; Read, 1974). Figure 9.2 shows a photograph of a laminar calcrete developed on Pleistocene limestone exposed in the Lualualei Valley on the leeward coast of Oahu. Staining by iron ooxides make the laminae easily discernable in the photograph. Arakel (1982), James (1972), Multer and Hoffmeister (1968), Read (1974), and others describe the petrographic characteristics of calcretes.

Figure 9.3 shows spectra of a laminated calcrete and of the unaltered dune rock below. This sample is from one of the Pleistocene dunes which form Laie Point on the north shore of Oahu. X-ray diffraction analysis shows the dune rock is composed of aragonite and high and low Mg calcite, as would be expected of an eolianite composed of reef derived skeletal debris. The crust is composd of low Mg calcite. The spectra reflect the mineralogical and textural differences. The low albedo and overall negative slope of the spectrum is due to the presence of algae which were growing on the surface of the rock. Goudie (1983), Klappa (1979), Krumbein (1968), and others discuss the role organisms may play in calcrete formation.

Despite these significant changes in texture and composition, the rock can still be recognized as a carbonate. However, the spectral properties of the calcrete are not characteristic of the dune rock below.

ORIGINAL PAGE IS
OF POOR QUALITY

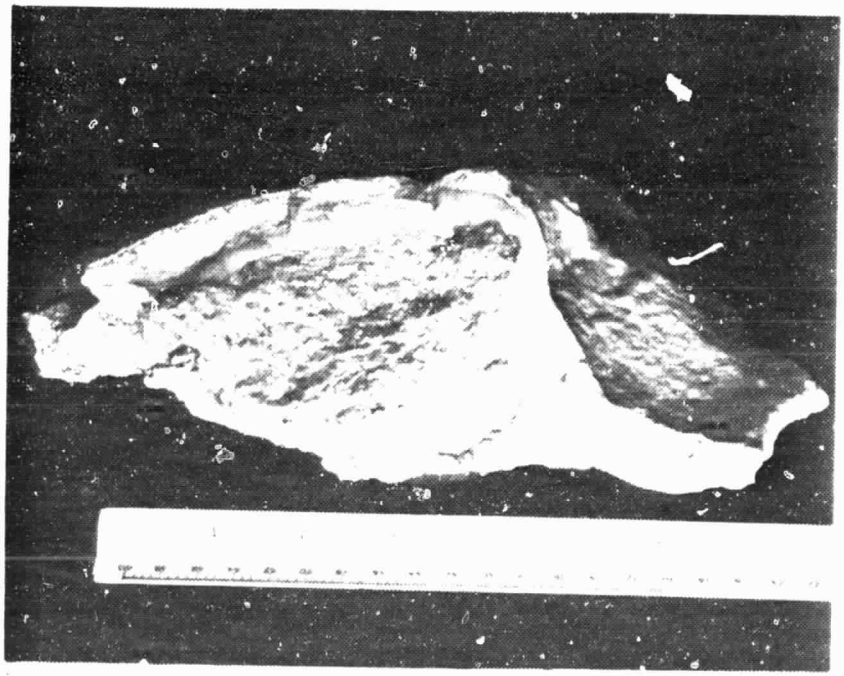

Figure 9.2 Pleistocene dune rock with laminar calcrete formed by weathering.

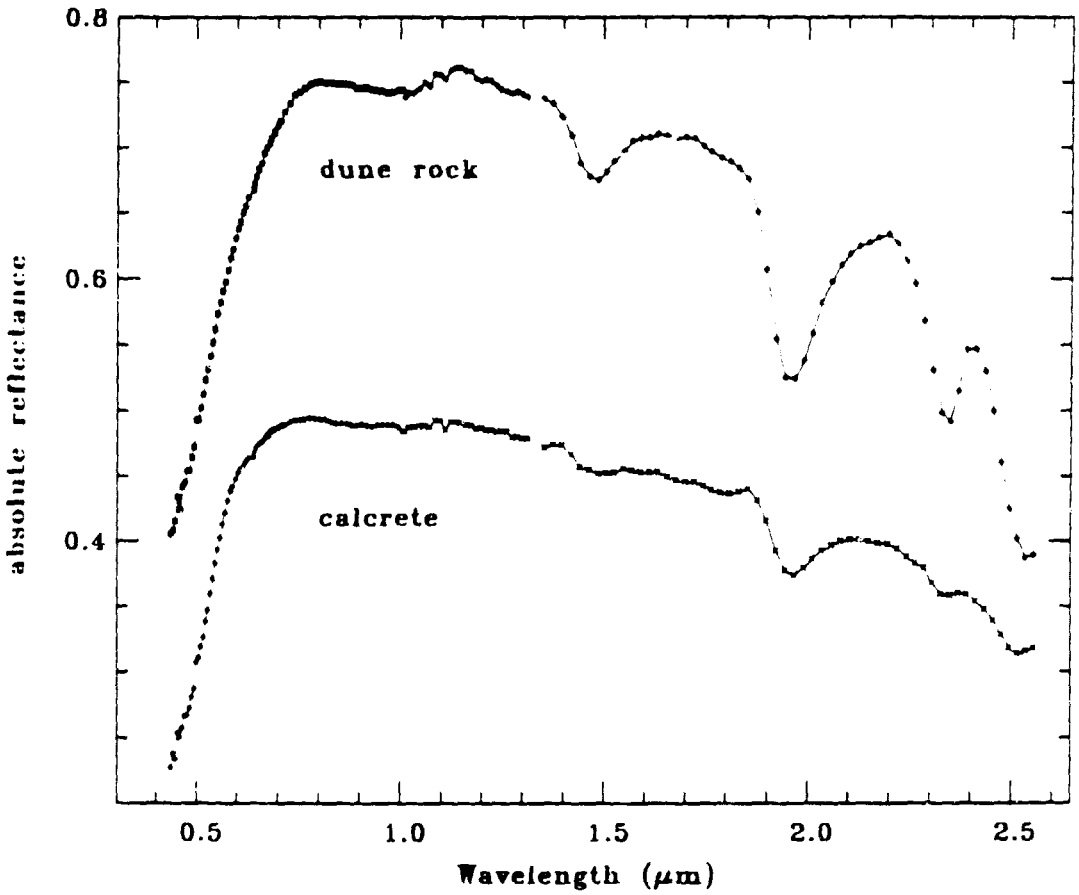

Figure 9.3 Spectra of a laminar calcrete and of underlying dune rock. Not same sample as that pictured in Figure 9.2.

This example illustrates the magnitude of the differences which may exist between spectra of carbonate rocks, and spectra of calcretes formed by alteration of those rocks.

Calcretes should be of particular interest to those doing remote sensing work because they tend to from in the arid to semiarid regions where lack of vegetation and soil cover allow spectra of rock surface to most easily obtained. Also, as Arakel (1982) notes, calcrete formation is a rock-facies transgressive phenomenon. The properties of calcretes reflect the characteristics of the environment in which they form, rather than host lithology, and the same calcrete layer may extend across different carbonate units.

Calcretes may also be associated with non-carbonate soils and rocks. Although they tend to form as a distinct soil horizon below the surface, they may be exposed at the surface as well. They may also take the form of calcified soils - structureless soils weakly cemented by calcite (Goudie, 1983). Thus the existence of calcretes may add carbonate features to the spectral signatures of non-carbonate bedrock.

Further studies of the spectral properties of calcretes would be of considerable value in remote sensing.

Oxidation will also affect rocks in outcrop. Pettijohn (1975) states that pyrite is found in small amounts in almost all carbonate rocks, and occurs as small scattered grains which will oxidize to form limonite. Iron-rich dolomites are also unstable (Rosenberg and Foit, 1979), and alter to form iron oxides and give dolomites the buff color which is commonly used to distinguish dolomites from limestones in the field (Pettijohn, 1975). Thus features due to Fe^{3+} should be very common in carbonate spectra.

Organics may be bleached out of rocks in outcrop. This will make spectra of these rocks appear brighter than spectra of fresh rock (Lahee, 1941).

Dedolomitization, replacement of dolomite by calcite, may also occur in the subaerial environment. Although generally considered to be of rather limited occurrance (Pettijohn, 1975), Back et al. (1983) found that dedolomitization is occurring on a regional scale in the Mississippian Pahasapa Limestone, a Madison equivalent, in the Black Hills.

APPLICATIONS OF SPECTRAL INFORMATION

Seventy per cent of all stone quarried in the U. S. is limestone. In the U. S. 9130lbs. of stone and 820lbs of cement are used each year for each citizen (Henric and Block, 1979).

For many industrial and chemical applications limestones and dolostones of high mineralogical ($\geq$95% calcite in limestone, $\geq$97% dolomite in dolostones) and chemical purity are required. Knowledge of the clay content of limestones is important for manufacture of Portland cement. The sensitivity of reflectance spectroscopy to the presennce of Fe^{2+}, iron oxides, and clays should make it possible to evaluate the suitability of carbonate deposits for industrial use.

Fifty per cent of the world's oil supply is contained in carbonate reservoirs. Reservoir properties of carbonate rocks are generally controlled by diagenetic rather than depositional processes, as diagenetic processes such as compaction, cementation, and dolomitization are creators and destroyers of porosity (Longman, 1981). Information on mineralogy and minor element chemistry of carbonate sequences are of importance in deciphering the diagenetic history of these rocks (Bathurst, 1975).

If chemical and mineralogical information on carbonate rocks can be acquired remotely, it will greatly facilitate exploration and exploitation of carbonate resevoirs.

SPECTRAL INFORMATION OBTAINABLE FROM EXISTING DATA SETS

Features in reflectance spectra of carbonates which are diagnostic of mineralogy and chemical composition fall within the terrestrial atmospheric windows, and therefore can be of use in remote sensing studies. Can these diagnostic features be studied using existing data sets?

Figures 9.4 and 9.5 show spectra of three mineral and five rock samples convolved to Thematic Mapper (TM) and the Shuttle Multispectral Infrared Radiometer (SMIRR), respectively, by the method described by Singer et al. (1984). The mineral samples are some of those discussed in Chapters 3 and 6. The rock samples were collected from the localities given below. The samples are, in order, a calcite (1531), a dolomite (6509) , a weathered ferroan dolomite (6502), an oolite and a dolomite from the Mississippian Lodgepole Formation in central Montana, a dolomite from the Silurian Gower Formation in eastern Iowa, a limestone from the Niobrara Chalk in western Kansas, and an eolianite from the Pleistocene Bellows Field Formation on Oahu, Hawaii. The mineral spectra have higher albedos than the rock spectra because the former were obtained from powders, the latter from whole rock samples.

The calcite and dolomite spectra (samples 1531 and 6509 discussed in Chapter 3) are from fresh, unweathered samples which contain little or no iron in solid solution. They show the straight line at shorter wavelengths and the carbonate bands at longer wavelengths typical of carbonates (see Chapter 3). The third spectrum is of a ferroan dolomite or ankerite (sample 6502 discussed in Chapter 5) which has been

ORIGINAL PAGE IS
OF POOR QUALITY

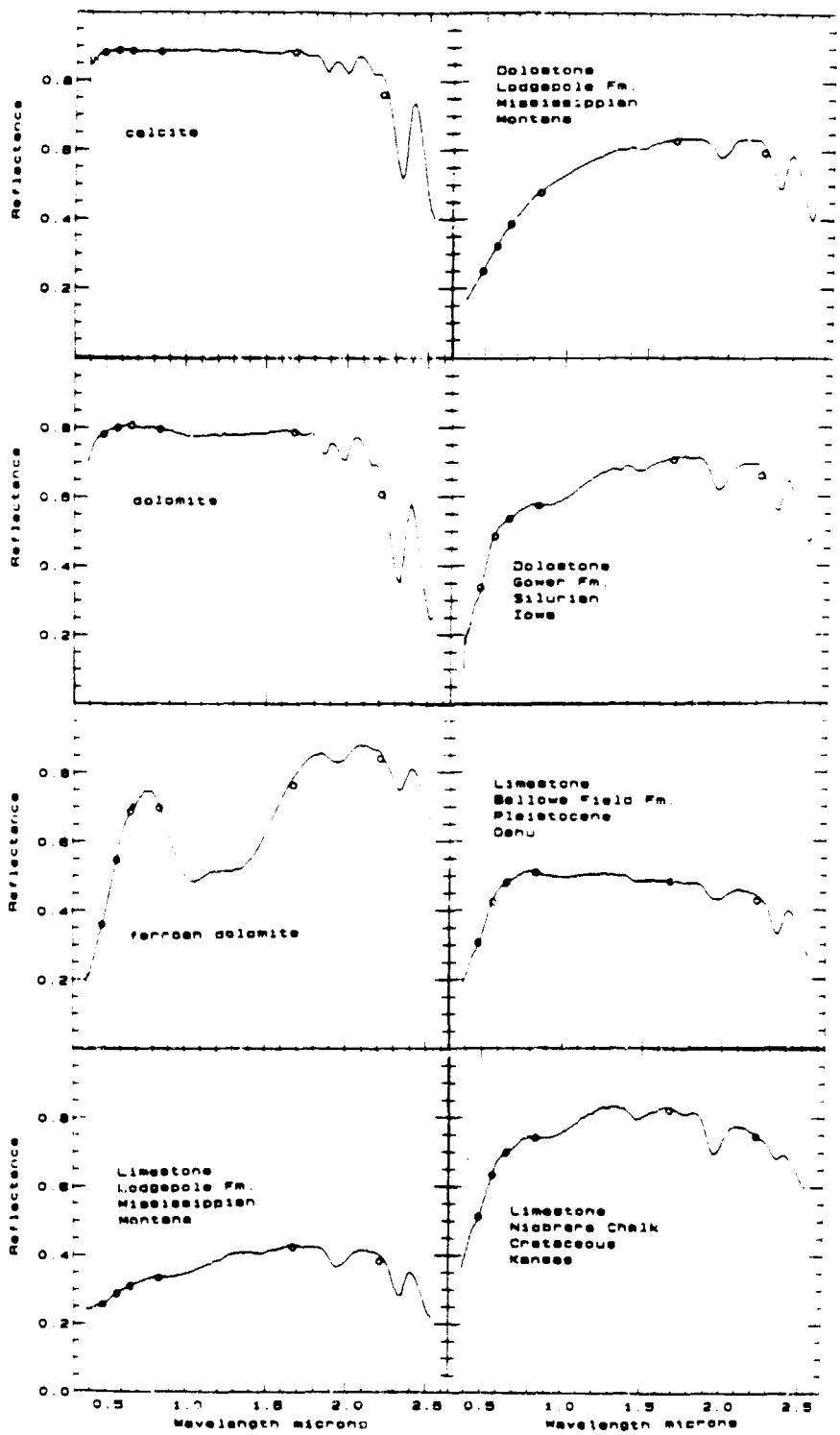

Figure 9.4a Carbonate spectra (lines) convolved to TM band passes (crosses).

ORIGINAL PAGE IS
OF POOR QUALITY

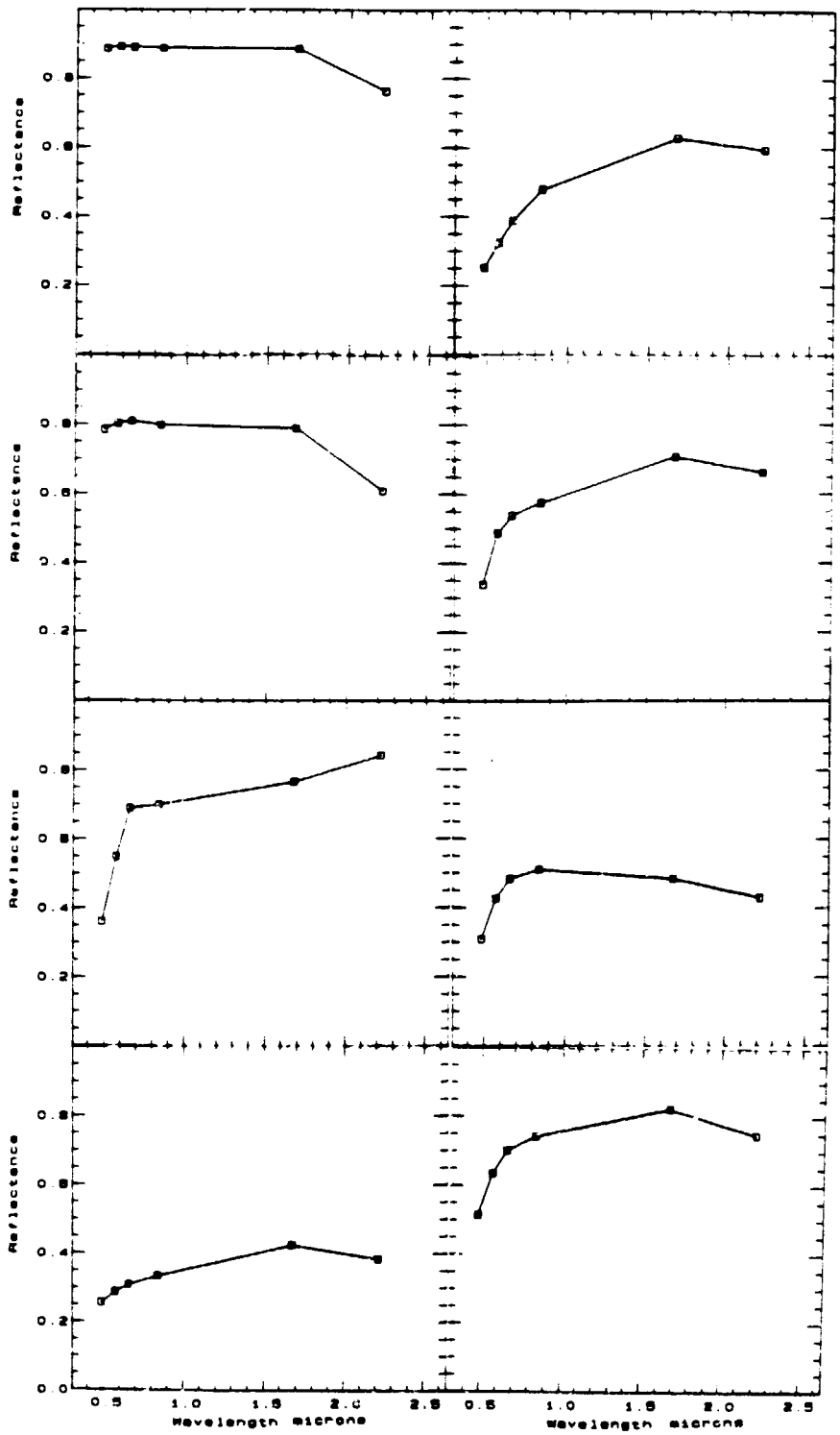

Figure 9.4b Just TM bands alone, without original spectra. Same data as Figure 9.4b.

ORIGINAL PAGE IS
OF POOR QUALITY

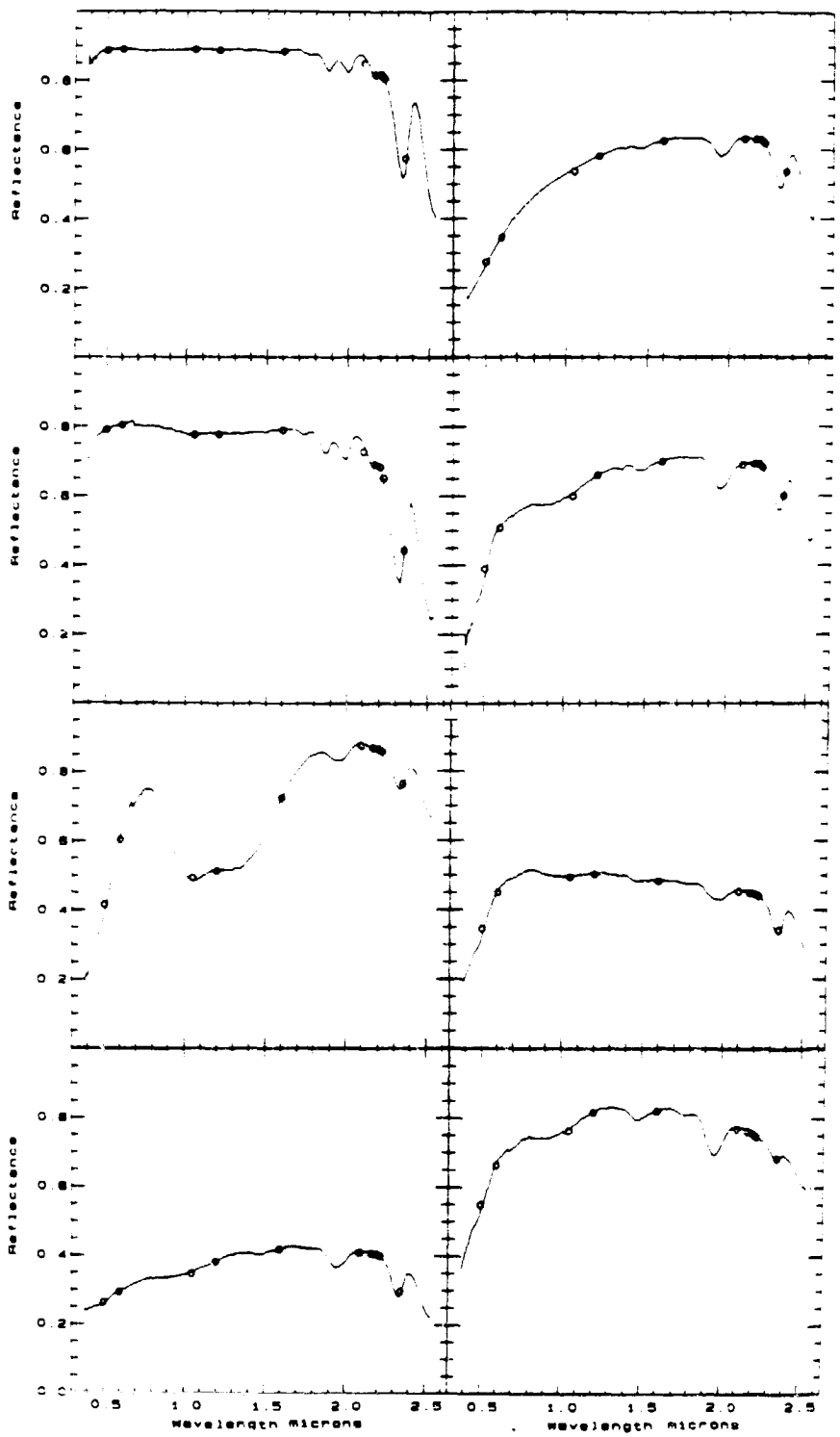

Figure 9.5a Carbonate spectra (lines) convolved to SMIRR band passes (crosses). Same spectra as in Figure 9.4a.

ORIGINAL PAGE IS
OF POOR QUALITY

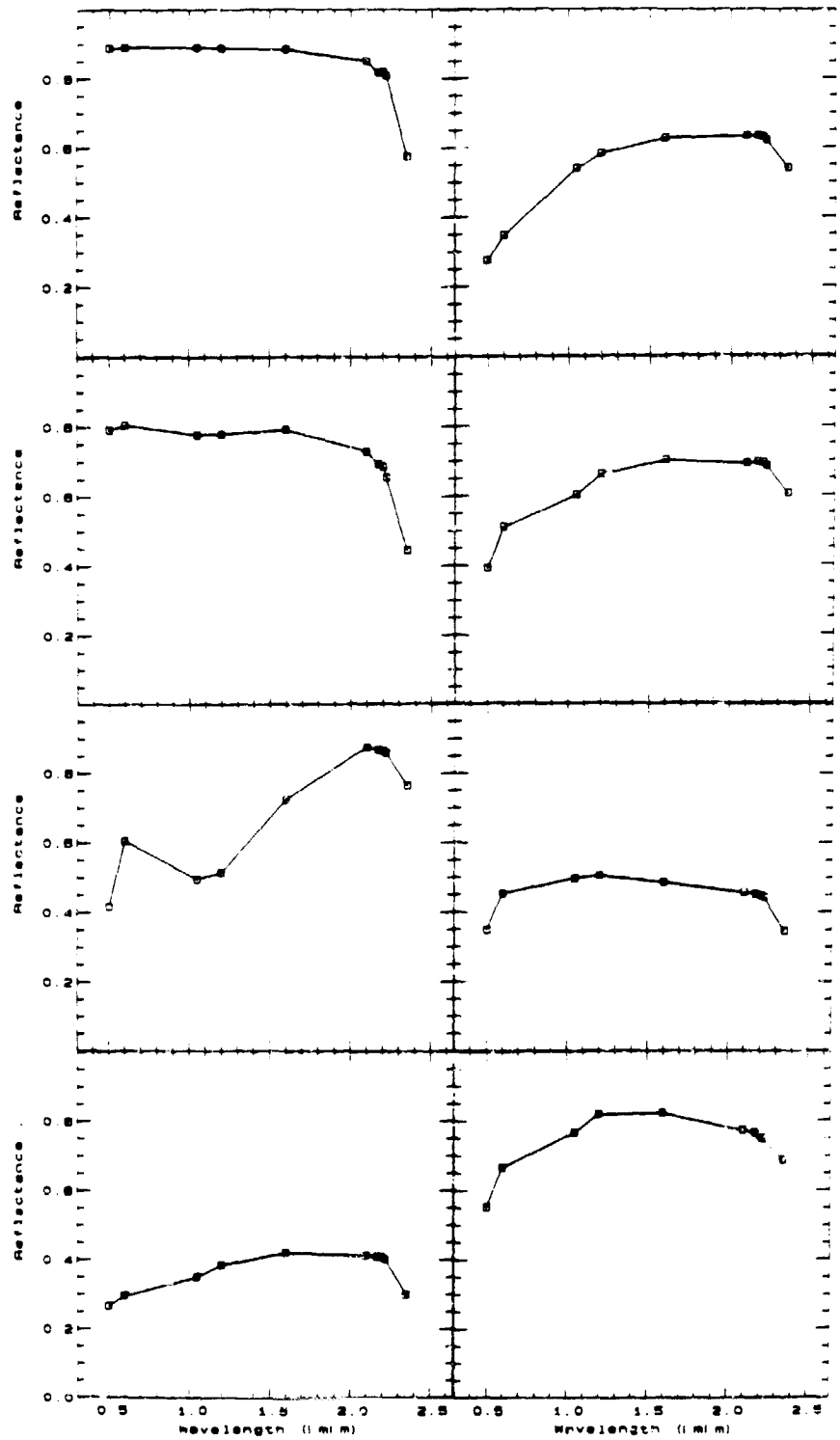

Figure 9.5b SMIRR bands alone, without original data. Same data as in Figure 9.5a.

weathered to a yellow brown color. The reflectance spectrum shows carbonate bands between 1.7 and 2.5μm, a strong iron band near 1.0μm, and a strong absorption edge into the ultraviolet due to the presence of iron oxides.

Spectra of carbonate rocks show a variety of spectral features in addition to the carbonate bands. Spectra of the Mississippian oolite, Silurian dolomite, Cretaceous chalk, and Pleistocene eolianite all show absorption features in the 0.4 to 0.9μm region attributable to the presence of iron oxides, as discussed above. They show absorption features due to fluid inclusion near 1.4 and 1.9μm.

A comparison of the two dolomite spectra is of interest. Both dolomites have the usual buff color in outcrop generally attributed to the presence of iron oxides, as mentioned above. The Mississippian dolomite, however, has a smooth drop-off throughout the visible range, with no discernable absorption features. Even reflectance spectra of amorphous Fe^{3+}-bearing glasses shown by Singer (1982), and a spectrum of X-ray amorphous iron oxides taken by the author have discreet, albeit broad and weak, absorption features in this region. Nor does this dolomite spectrum show any features due to Fe^{2+}, generally considered to be the source of the iron oxides which give dolomites their characteristic buff color. The source of this color, and of the smooth fall-off to shorter wavelengths in the spectrum are not understood at present.

Goetz et al. (1982) and Rowan and Kahle (1982) noted the difficulty of identifying mineral species, or even distinguishing carbonates from clays using TM data. The spectra shown in Figure 9.4a convolved to TM bands tend to confirm this. Although the absorption bands due to iron oxides in the visible region are reflected in the TM bands, the two channels in the NIR are insufficient to give any real information about the curve in the infrared.

SMIRR was designed to make greater use of absorption bands at longer wavelengths, especially in the 2.0 to 2.5μm region Goetz et al. (1982) concluded that carbonates could be distinguished from clays in SMIRR data of a sequence of Cretaceous and lower Teriary rocks in Egypt. They concluded that the abrupt drop in the 2.35μm filter was diagnostic of carbonates, and the direct identification of carbonates could be made using the 2.20μm/2.35μm and 2.22μm/2.35μm filter ratios.

Spectra shown here do not support such a conclusion. As discussed in Chapter 3, the absolute intensity of carbonate band 2 (the band near 2.3μm), the factor which controls the value of these two filter ratios, is entirely an effect of grain size and packing, and contains no mineralogical or chemical information. Indeed, all other factors being equal, the intensity of the absorption features of clays in this region should be stronger than those of carbonates, since, as discussed in Chapter 3, H_2O and OH^- are stronger absorbers in this region than carbonates. The Cretaceous chalk is composed primarily of calcite, but the difference in intensity of the 2.35μm channel in the SMIRR bands convolved to the calcite spectrum and to the chalk spectrum is marked. Using the criteria of Goetz _et al._ (1982), the Cretaceous chalk would be identified as a clay rather than as a limestone.

In spectra of clays illustrated by Singer et al. (1984) it is clear that the ratio of the 2.35μm to the 2.2μm channel for carbonate spectra is not distinctly different from that in clay spectra.

As can be seen by comparing the spectra of the Mississippian oolite and the Silurian dolomite, the SMIRR bands can't be used to distinguish between the two rock types. Five channels are inadequate to define the carbonate bands and permit their precise positions to be determined.

If clays are present, as in argillaceous limestones, an even larger number of bands will occur in this region, and the need for better spectral resolution will be even greater.

The SMIRR bands do outline the Fe^{2+} band in the ferroan dolomite, and show the drop-off at short wavelengths due to the presence of iron oxides. However, although the SMIRR bands indicate the presence of an Fe^{2+} feature, they are not sufficient to determine its shape or intensity, or its intensity relative to the carbonate bands, which is necessary to determine the amount of Fe^{2+} present (see Chapter 5).

It would appear that SMIRR is not adequate for direct mineral identification, nor even for dependable discrimination between clays and carbonates. Although remotely sensed data are very valuable for discriminating between lithologic units, they must still be tied in to laboratory data on samples from the study area, and with field work on the ground. Distinctions between units established in this manner can be extrapolated to other localities within the study area.

FUTURE WORK

Clearly the greater the resolution, the more information can be obtained from spectra. Resolution of 0.025μm in the 2.0 to 2.5μm region is necessary for studies of carbonate minerals, to allow determination of precise positions of carbonate bands, and intensities of carbonate bands relative to any crystal field bands present. Data collected in our laboratory and published data of others indicate even better spectral resolution is required to allow clays to be detected and identified, due to the large number of very narrow bands in the 2.0 to 2.5μm region.

The new Airborn Infrared Spectrometer (AIS), with resolution similar to that of laboratory instruments (Collins et al., 1981) will allow

as much information to be obtained remotely as can be obtained from spectra in these regions in the laboratory.

Several things must be born in mind in dealing with remotely obtained spectra. First, only mineralogical and chemical data can be obtained from spectra. Deriving textural data from spectra is a complex problem in geometric optics, and although great strides have been made in solving that problem (Hapke, 1981; Clark and Lucey, 1984; Clark and Roush, 1984) a solution has not yet been achieved. These studies are aimed only at determining particle size distributions. It is doubtful that mathematical descriptions of the complex textures which characterize carbonate rocks, and which are the basis of carbonate rock classifications currently in use (Ham, 1962) will be evolved in the foreseeable future.

Second, there are still many rock types whose spectral properties have not been well characterized. Nothing beyond survey work has been done on shales, evaporites, or sandstones. Until the spectral properties of these other rock and mineral species are well characterized, we can not confidently attribute specific spectral features in spectra of unknowns to specific minerals. Other minerals with spectral properties not yet well known may have similar features which could mask, or be confused with, those with which we are familiar.

Third, remotely obtained spectra will always be averages of large bodies of rock. The large area on the ground encompassed in each pixel on remotely obtained images will always contain a variety of rock types, and those with the strongest absorption features will dominate the spectrum, as they do in the physical mixtures whose spectra have been measured in the laboratory. Only laboratory instruments will allow separate rock components to be isolated for measurement.

Since chemistry and mineralogy alone are not sufficient for complete description and definition of stratigraphic units reflectance spectroscopy, in and of itself, will never be sufficient to completely define stratigraphic units. Reflectance spectroscopy will, of necessity, be used in concert with more traditional geologic methods, and will, with other remote sensing techniques, join the ever-growing battery of tools available to geologists for mapping and exploration.

CHAPTER 10

Summary

Reflectance spectroscopy in the visible and near infrared portions of the spectrum (0.35 to 2.55μm) can be used to determine the mineralogy of carbonate samples and to acquire information on their chemical composition. Spectra of all common anhydrous carbonate minerals have at least seven absorptions due to vibrational processes of the carbonate radical in this region. Positions and shapes of these bands can be used to identify calcite, aragonite, and dolomite, the three most common carbonate minerals.

Carbonate band positions are also of use in discriminating between other anhydrous carbonate minerals. Positions of carbonate bands vary from one mineral to another. The primary factor controling band position appears to be cation mass. As the mass of the cation increases, bands shift to longer wavelengths. Cation radius affects band position to a lesser degree, and most strongly affects carbonate band positions in spectra of smithsonites and rhodochrosites. Crystal structure, i.e. the difference in structure between calcite group and aragonite group minerals exerts a more subtle influence on carbonate band positions. This can best be seen in differences between calcite and aragonite spectra. The two minerals have the same composition ($CaCO_3$) and differ only

in crystal structure. Spectra of both minerals contain the same number of bands, at approximately the same wavelengths. However, spacings between bands in aragonite spectra differ from those in calcite spectra. For example, while band 2 occurs at slightly shorter wavelengths in aragonite spectra than in calcite spectra, band 4 occurs at longer wavelengths. In addition, some bands are wider in aragonite spectra than they are in calcite spectra.

Spectra of many calcite group minerals also have absorption features due to transition metal cations in their spectra. Strong absorptions due to Mn^{2+} in rhodochrosite spectra and Fe^{2+} in siderite spectra aid in identification of these minerals. A combination of number, positions and shapes of transition metal bands and positions and shapes of carbonate bands are sufficient for distinguishing among common anhydrous carbonate minerals.

Because solid substitution is common among the different end-member calcite group minerals, absorption bands due to transition metal cations can occur in spectra of any of these minerals. The most common transition metal cation substituting for the major cation in rhombohedral carbonates is Fe^{2+}. Fe^{2+} causes a broad absorption near 1.0μm The exact shape and position of this band in carbonate spectra varies from one mineral to another, and reflects the size and symmetry of the site it occupies. All cations in rhombohedral carbonate minerals are in octahedral coordination with six oxygens. Spectra of minerals with the least distorted octahedral sites, magnesite and smithsonite, have the narrowest Fe bands which show the least doubling. Fe bands in spectra of minerals with more distorted sites, such as calcite, are broader and are clearly split into at least two bands. Fe bands in spectra of minerals with small octahedral volumes (small M-O bond lengths) occur at shorter wavelengths than those with larger octahedral volumes.

Absorption features in carbonate minerals also are caused by Cu^{2+}, Co^{2+}, Mn^{2+}, and Ni^{2+}. Copper forms a broad absorption centered near 0.9μm. Co^{2+} forms two bands, a strong narrow one near 0.53μm, and a broader, weaker one near 1.25μm. Mn^{2+} has five absorptions in the 0.35 to 6.0μm region. Ni^{2+} has three absorptions centered near 1.25, 0.70, and 0.42μm.

The trends outlined above for changes in bands shapes and positions for Fe bands in response to differences in site symmetry and size are found to hold true for absorptions due to these other cations as well.

Variations in the concentration of cations substituting for the major cation in these minerals affect the spectral properties of calcite group minerals. Substitution of cations for the major cation generally causes the carbonate bands to shift in the direction of the bands in the spectra of the end-member mineral for that cation. For example, carbonate bands in siderite spectra occur at longer wavelengths than carbonate bands in dolomite spectra. As Fe content in dolomite increases, the carbonate bands shift to longer wavelengths. In spectra of manganoan calcite, the carbonate bands occur at longer wavelengths than carbonate bands in spectra of ordinary calcites, while in spectra of high Mg calcites, the bands occur at shorter wavelengths. This can be correlated with the fact that carbonate bands in rhodochrosite spectra and magnesite spectra occur at longer and shorter wavelengths, respectively, than those in spectra of calcites which are more nearly pure end members.

The concentration of the substituting cation has to be rather high to cause these shifts. For example, shifts in carbonate band positions in dolomite sectra do no become clear until the Fe content is about 1% by weight. No doubt the magnitudes of the differences between the

masses and radii of the subsituting and major cations will determine the amount of substitution necessary to cause shifts in carbonate bands.

Variations in spectral properties of dolomites with variations in Fe^{2+} content were studied in detail. Intensity of Fe bands increases with increasing Fe content. The intensity of the Fe band can be ratioed to the intensity of carbonate band 2 to correct for particle size effects. A plot of this ratio vs. Fe content yields a smooth curve. It should be possible to use graphs of this type to determine Fe content of dolomites. Weathering complicates the picture by causing an apparent increase in Fe band intensity relative to the the intensity of band 2. This effect can largely be corrected for by using gaussian analysis of spectra.

Carbonate bands in ferroan dolomites shift to longer wavelengths with increasing Fe^{2+} content, and the bands change shape. When Fe^{2+} content exceeds about 5% by weight, shapes and positions of bands 1 through 4 are similar to those in aragonite spectra. However, the position of band 6, and the presence of the extremely strong Fe absorption, would keep the spectra of the two minerals from being confused.

Variations in spectral properties of calcites with varying Cu content were also studied. Positions of carbonate bands do not appear to change. As Cu content increases, however, the Cu absorption band increases in intensity and shifts to shorter wavelengths.

Detection limits for different cations vary. Detection limits for Mn^{2+} in dolomites and calcites appears to be about 0.1% Mn by weight. The detection limit for Fe^{2+} is about 0.01% by weight, while that for Cu^{2+} is even lower. The differences in detection limits reflect the fact that the transitions which cause the Mn^{2+} absorptions are spin forbidden, while those which cause the Fe^{2+} and Cu^{2+} absorptions are spin allowed.

Reflectance spectra are very sensitive to the presence of water. The two strongest absorptions in the NIR occur near 1.4μm and 1.9μm, and work by Hunt and Salisbury (1970), Hunt (1977) and others has shown that differences in numbers, shapes and positions of these bands can be used to distinguish liquid H_2O from bound H_2O and OH^-. Reflectance spectra of three hydrous carbonate minerals, hydromagnesite, hydrocerussite, and hydrozincite, show that all three minerals contain both bound H_2O and OH^-. Published formulas of hydrocerussite and hydrozincite indicate these minerals are believed to contain only OH^-. Absorption bands due to bound water in hydrous carbonate minerals are broader and occur at longer wavelengths than those in liquid water.

Nearly all spectra of carbonate minerals and rocks contain absorption features due to liquid water in fluid inclusions. Spectra of skeletal material contain especially strong water bands reflecting fluid inclusion contents of as much as three weight per cent. Amounts of inclusions in skeletal material vary from one type of organism to another. Of the types of material studied so far, coccoliths and planktonic foram tests contain the least water, scleractinian corals, echinoderms, and coralline red algae contain the most.

Diagenesis of skeletal material results in loss of fluid inclusions. Neomorphism of skeletal aragonites and high Mg calcites to low Mg calcites is accompanied by an order of magnitude drop in inclusion content. Solution and reprecipitaton processes which cause the ooze-chalk-limestone transition in deep sea carbonate sediments also result in loss of fluid inclusions. Where original skeletal mineralogy and texture are retained, original fluid inclusion content is retained as well.

Reflectance spectra may be obtained from material in any form, including powders, sands, and whole rocks. Absolute intensities and overall brightness or albedo of samples are affected by particle size and packing. Absorption features are more intense in spectra of coarse-grained or non-porous samples. However, absorptions still conform to Lambert's law, and positions, shapes and relative intensities do not change. Thus the form of the sample does not affect the information which can be derived from its reflectance spectrum.

The same mineralogical and chemical information can be derived from spectra taken with different types of spectrophotometers. It doesn't seem to matter whether bidirectional or directional-hemispherical reflectance is measured. There can be an offset in band positions measured by different instruments. However, this is a calibration problem. The offset is constant over time, and a correction can easily be applied, so that spectra taken with different instruments can be compared.

Reflectance spectroscopy in the VIS and NIR has potential not only as a laboratory tool, but also as a remote sensing technique. Although atmospheric water bands make some portions of the spectrum inaccessible, the remaining portions are sufficient to determine mineralogy and chemical composition of carbonate rocks. Calcite and dolomite make up the bulk of ancient sediments which are the target of remote sensing, and they can be be distinguished on the basis of the positions of the two strong carbonate bands centered near 2.3 and 2.5μm. Relative intensities of Fe^{2+} bands can be used to determine Fe content of carbonate minerals. Other phases such as clays, Fe oxides, and organics contribute features to spectra of carbonate rocks which will be helpful in discriminating between rock units. Weathering processes alter the appearance

of carbonate rocks in outcrop. Although they will still be identifiable as carbonates, a decrease in crystal size, and a possible increase in porosity will result in weakening of carbonate bands. It may be necessary to plot remotely obtained spectra on an expanded scale to see the carbonate bands clearly.

Existing TM and SMIRR data sets lack sufficient spectral resolution for identification of carbonate rocks, nor do they allow carbonates to be distinguished from clays. Spectral resolution of at least 25nm will be necessary to study carbonates. Even greater spectral resolution is needed to study the many narrow clay bands which occur in the 2.0 to 2.5μm region. However, these data sets will continue to be very useful for discrimination between rock units which have been studied in the field, and whose spectral characteristics have been determined in the laboratory.

REFERENCES CITED

Abu-Eid, R. M., and Burns, R. G, 1976, The effect of pressure on the degree of covalency of the cation-oxygen bond in minerals. American Mineralogist, v. 61, p.391-397.

Adams, J. B., 1974, Visible and near-infrared diffuse reflectance spectra of pyroxenes as applied to remote sensing of solid objects in the solar system. Journal of Geophysical Research, v. 79, p.4829-4836.

Adams, J. B., 1975, Interpretation of visible and near-infrared diffuse reflectance spectra of pyroxenes and other rock-forming minerals, p.91-116. in C. Karr, Jr., ed., Infrared and Raman Spectroscopy of Lunar and Terrestrial Minerals, Academic Press, New York.

Adler, H. H., and Kerr, P. F., 1962, Infrared study of aragonite and calcite. American Mineralogist, v. 47, p.7700-717.

Adler, H. H., and Kerr, P. F., 1963a, Infrared absorption frequency trends for anhydrous normal carbonates. American Mineralogist, v. 48, p.124-137.

Adler, H. H., and Kerr, P. F., 1963b, Infrared spectra, symmetry and structure relations of some carbonate minerals. American Mineralogist, v. 48, p.839-853.

Andersen, K. L., 1978, Reflectance spectroscopy as a remote sensing technique for the identification of porphyry copper deposits. PhD Dissertation, Massachusetts Institute of Technology, Cambridge, Massachusetts, 240p.

Andrews, J. E., Packham, G., et al., 1975, Initial Reports of the Deep Sea Drilling Project. v. 30, United States Government Printing Office, Washington, D. C.

Anthony, J. W., Williams, S. A., and Bideaux, R. A., 1977, Mineralogy of Arizona, The University of Arizona Press, Tucson, Arizona.

Arakel, A. V., 1982, Genesis of calcrete in Quaternary soil profiles, Hutt and Leeman Lagoons, Western Australia. Journal of Sedimentary Petrology, v. 52, p.109-125.

Back, W., Hanshaw, B. B., Plummer, L. N., Rahn, P. H., Rightmire, C. T., and Meyer, R., 1983, Process and rate of dedolomitization: Mass transfer and ^{14}C dating in a regional carbonate aquifer. Geological Society of America Bulletin, v. 94, p.1415-1429.

Ballhausen, C. J., 1962, Introduction to Ligand Field Theory. McGraw-Hill Book Company, Inc., New York, 298p.

Bayly, J. G., Kartha, V. B., and Stevens, W. H., 1963, The absorption spectra of liquid phase H_2O and D_2O from 0.7μm to 10μm. Infrared Physics, v. 3, p.211-223.

Berry, S. R., Rice, S., and Ross, J., 1980, Physical Chemistry, John Wiley and Sons, New York, 1264p.

Bjerrum, Jannik, Ballhausen, C. J., and Jorgenser, C. K., 1954, Studies on absorption spectra I. Results of calculations on the spectra and configuration of copper (II) ions. Acta Chemica Scandinavica, v. 8, p.1275-1289.

Blake, Pamela L., 1983, Analytical removal of atmospheric absorptions from remotely sensed near-infrared data of geological targets. MS Thesis, University of Hawaii at Manoa, Honolulu, Hawaii, 96p.

Burns, R. G., 1970, Mineralogical Applications of Crystal Field Theory, Cambridge University Press, London.

Califano, S., 1980, The dynamics of molecular crystals, I. General theory, p.211-251. in S. Bratos and R. M. Pick, Eds., Vibrational Spectroscopy of Molecular Liquids and Solids, Plenum Press, New York.

Ceccaldi, M., Goldman, M., and Roth, E., 1956, Le spectre d'absorption des melanges H_2O - D_2O a l'etat liquide entre 0.8μ et 30μ. Colloquium Spectroscopium Internationale VI, Pergamon Press, London, p.623-631.

Chester, R., and Elderfield, H., 1966, The infra-red determination of total carbonate in marine sediments. Chemical Geology, v. 1, p.277-290.

Chester, R., and Elderfield, H., 1967, The application of infra-red absorption spectroscopy to carbonate mineralogy. Sedimentology, v. 9, p.5-21.

Clark, R. N., 1980, A large-scale interactive one dimensional array processing system. Publication of the Astronomical Society of the Pacific, v. 92, p.221-224.

Clark, R. N., 1981a, The spectral reflectance of water-mineral mixtures at low temperatures. Journal of Geophysical Research, v. 86, no.B4, p.3074-3086.

Clark, R. N., 1981b, Water frost and ice: the near-infrared spectral reflectance 0.65-2.5μm. Journal of Geophysical Research, v. 86, p.3087-3096.

Clark, R. N., and Lucey, P. G., 1984, Spectral properties of ice-particulate mixtures and implications for remote sensing. Journal of Geophysical Research (in press).

Clark, R. N., and Roush, T. L. (1984) Reflectance spectroscopy: quantitative analysis techniques for remote sensing applications. Journal of Geophysical Research (in press).

Collins, W., Chang, S. H., Kuo, J. T., and Rowan, L. C., 1981, Remote mineralogical analysis using a high-resolution airborne spectroradiometer: Preliminary results of the Mark II system in Keith R. Carver, ed., 1981 International Geoscience and Remote Sensing Symposium Digest, Institute of Electrical and Electronics Engineers, Inc., New York, p.337-344.

Compton, R. R., 1962, Manual of Field Geology, John Wiley and Sons, Inc., New York, 378p.

Conger, S. D., Green, H. W., and Lipps, J. H., 1977, Test ultrastructure of some calcareous Foraminifera. Journal of Foraminiferal Research, v. 7, p.278-296.

Cotton, F. A., and Meyers, M. D., 1960, Magnetic and spectral properties of the spin-free $3d^6$ systems iron(II) and cobalt(III) in cobalt(III) hexafluoride ion: Probable observation of dynamic Jahn-Teller effects. Journal of the American Chemical Society, v. 82, p.5023-5026.

Cowley, E. R., and Pant, A. K., 1973, Lattice dynamics of calcite. Physical Review B, v.8, p.4795-4800.

Curcio, J. A., and Petty, C. C., 1951, The near infrared absorption spectrum of liquid water. Journal of the Optical Society of America, v. 41, p.302-304.

Davydov, A. S., 1962, Theory of Molecular Excitons. Translated by M. Kasha and M. Oppenheimer, McGraw Hill Book Co., Inc., New York.

Deer, W. A., Howie, R. A., and Zussman, J., 1962, Rock-Forming Minerals, Volume 5. Non-Silicates, Longman Group, Limited, London, 371p.

Denisov, V. N., Mavrin, B. N., Podobedov, V. B., and Stern, Kh. E., 1982, Hyper-Raman scattering by phonons and mixed polaritons in a calcite crystal. Physica Status Solidi (B), v. 110, p.183-189.

Dickson, J. A. D., 1966, Carbonate identification and genesis as revealed by staining. Journal of Sedimentary Petrology, v. 36, p.491-505.

Effenberger, H., Mereiter, K., and Zemann, J., 1981, Crystal structure refinements of magnesite, calcite, rhodochrosite, siderite, smithonite, and dolomite, with discussion of some aspects of the stereochemistry of calcite type carbonates. Zeitschrift fur Kristallographie, v. 156, p.233-243.

Esterp-Barnes, P. A., 1977, Infrared spectroscopy. in J. Zussman, ed., Physical Methods in Determinative Mineralogy, Second Edition, Academic Press, New York, p.529-603.

Farmer, V. C., and Warne, S. St. J., 1978, Infrared spectroscopic evaluation of iron contents and excess calcium in minerals of the dolomite-ankerite series. American Mineralogist, v. 63, p.779-781.

Farr, T. G., Bates, B. A., Ralph, R. L., and Adams, J. B., 1980, Effects of overlapping optical absorption bands of pyroxene and glass on the reflectance spectra of lunar soils. Proceedings of the Eleventh Lunar and Planetary Science Conference, p.718-729.

Ferguson, J., Guggenheim, H. J., Johnson, L. F., and Kamura, H., 1963, Magnetic dipole character of the $^3A_{2g} \langle - \rangle\ ^3T_{2g}$ transition in octahedral nickel (II) compounds. The Journal of Chemical Physics, v. 38, p.2579-2580.

Fielding, Ann, 1979, Hawaiian Reefs and Tide Pools, Oriental Publishing Company, Honolulu, Hawaii, 103p.

Fleischer, M., 1980, Glossary of Mineral Species, John Sampson White, Publisher, Tucson, Arizona, 192p.

Folk, R. L., 1965, Some aspects of recrystallization in ancient limestones. in L. C. Pray and R. C. Murray, eds., Dolomitization and Limestone Diagenesis, Society of Economic Paleontologists and Mineralogists Special Publication No. 13, Society of Economic Paleontologists and Mineralogists, Tulsa, Oklahoma, p.14-48.

Frech, R., Wang, E. C., and Bates, J. B., 1980, The i.r. and Raman spectra of $CaCO_3$ (aragonite). Spectrochimica Acta, v. 36A, p.915-919.

Gatehouse, B. M., Livingstone, S. E., and Nyholm, R. S., 1958, The infrared spectra of some simple and complex carbonates. Journal of the Chemical Society of London, 1958, III, p.3137-3142.

Goetz, A. F. H., Rock, B. N., and Rowan, L. C., 1983, Remote sensing for exploration: An overview. Economic Geology, v.78, p.573-590.

Goetz, A. F. H., Rowan, L. C., and Kingston, M. J., 1982, Mineral identification from orbit: Initial results from the shuttle multispectral infrared radiometer. Science, v. 218, p.1020-1024.

Goldsmith, J. R., 1983, Phase relations of rhombohedral carbonates. in Richard J. Reeder (ed) Carbonates: Mineralogy and Chemistry, Mineralogical Society of America Reviews in Mineralogy Vol. 11, Mineralogical Society of America, p.49-76.

Goldsmith, J. R., and Graf, D. L., 1958, Structural and compositional variations in some natural dolomites. Journal of Geology, v. 43, p.84-101.

Goudie, A. S., 1983, Calcrete. in A. S. Goudie and Kenneth Pye, eds., Chemical Sediments and Geomorphology, Academic Press, New York, p.93-131.

Green, H. W., Lipps, J. H., and Showers, B. W., 1980, Test ultrastructure of fusulinid Foraminifera. Nature, v. 283, p.853-855.

Griffith, W. P., 1970, Raman studies on rock-forming minerals. Part II. Minerals containing MO_3, MO_4, and MO_6 groups. Journal of the Chemical Society (A), 1970, p.286-291.

Hadni, A., 1974, The interaction of infrared radiation with crystals. in V. C. Farmer, ed., The Infrared Spectra of Minerals, Mineralogical Society Monograph 4, Mineralogical Society, London, p.27-50.

Halford, R. S., 1946, Motions of molecules in condensed systems: 1. Selection rules, relative intensities, and orientation effects for Raman and infrared spectra. Journal of Chemical Physics, v. 14, p.8-15.

Ham, W. E., ed., 1962, Classification of Carbonate Rocks, American Association of Petroleum Geologists Memoir 1, American Association of Petroleum Geologists, Tulsa, Oklahoma, 279p.

Hapke, B., 1981, Bidirectional reflectance spectroscopy. Journal of Geophysical Research, v. 86, no.B4, p.3039-3054.

Harris, D. C., and Bertolucci, M. D., 1978, Symmetry and Spectroscopy, Oxford University Press, New York, 550p.

Hattin, D. E., 1981, Petrology of the Smoky Hill Member, Niobrara Chalk (Upper Cretaceous) in type area, western Kansas. American Association of Geologists Bulletin, v. 65, p.831-849.

Headden, W. P., 1925, Smithsonite, Kelley Mine, Magdalena Mtns. American Mineralogist, v. 10, p.18.

Heidt, L. J., Koster, G. F., and Johnson, A. M., 1959, Experimental and crystal field study of the absorption spectrum at 2000 to 8000A of manganous perchlorate in aqueous perchloric acid. Journal of the American Chemical Society, v. 80, p.61-86.

Hellwege, K. H., Lesch, W., Plihal, M., and Schzack, G., 1970, Zweiphonon-Absorptionsspektren und Dispersion der Schwingungszweige in Kristallen der Kalkspatstruktur. Zeitschrift fur Physik, v. 232, p.61-86.

Henrie, T. A., Block, F., 1979, Research on a more effective use of mineral resources - A mission of the United States Bureau of Mines. in F. Bender, ed., The Mineral Resources Potential of the Earth, E. Schweizertbart'sche Verlagsbuchhandlung, Stuttgart, p.24-38.

Hexter, R. M., 1958, High-resolution, temperature-dependent spectra of calcite. Spectrochimica Acta, v. 10, p.281-290.

Hexter, R. M., and Dows, D. A., 1956, Low-frequency librations and the vibrational spectra of molecular crystals. The Journal of Chemical Physics, v. 25, p.504-509.

Holmes, O. G., and McClure, D. S., 1957, Optical spectra of hydrated ions of the transition metals. The Journal of Chemical Physics, v. 26, p.1686-1694.

Hornig, D. F., 1948, The vibrational sectra of molecules and complex ions in crystals. I. General theory. The Journal of Chemical Physics, v. 16, p.1063-1076.

Hovis, W. A. Jr., 1966, Infrared spectral reflectance of some common minerals. Applied Optics, v. 5, p.245-248.

Huang, C. K., and Kerr, P. F., 1960, Infrared study of the carbonate minerals. American Mineralogist, v. 45, p.311-324.

Hunt, G. R., 1977, Spectral signatures of particulate minerals in the visible and near infrared. Geophysics, v. 42, p.501-513.

Hunt, G. R., and Ashley, R. P., 1979, Spectra of altered rocks in the visible and near infrared. Economic Geology, v. 74, p.1613-1629.

Hunt, G. R., and Salisbury, J. W., 1970, Visible and near-infrared spectra of minerals and rocks: I. Silicate minerals. Modern Geology, v. 2, p.23-30.

Hunt, G. R., and Salisbury, J. W., 1971, Visible and near-infrared spectra of minerals and rocks: II. Carbonates. Modern Geology, v. 2, p.23-30.

Hunt, G. R., and Salisbury, J. W., 1976, Visible and near infrared spectra of minerals and rocks: XI. Sedimentary rocks. Modern Geology, v. 5, p.211-217.

Hunt, G. R., Salisbury, J. W., and Lenhoff, C. J., 1971, Visible and near-infrared spectra of minerals and rocks: III. Oxides and hydroxides. Modern Geology, v. 2, p.195-205.

Hunt, J. M., Wisherd, M. P., and Bonham, L. C., 1950, Infrared absorption spectra of minerals and other inorganic compounds. Analytical Chemistry, v. 22, p.1478-1497.

Huribut, C. S. Jr., and Klein, C., 1977, Manual of Mineralogy, John Wiley and Sons, New York, 532p.

James, N. P., 1972, Holocene and Pleistocene calcareous crust (caliche) profiles: Criteria for subaerial exposure. Journal of Sedimentary Petrology, v. 42, p.817-836.

Jenks, S. E., 1972, Environment of deposition and diagenesis of the Lodgepole Formation (Mississippian), central Montana. Montana Geological Survey 21st Annual Field Conference Guidebook, p.19-28.

Jorgensen, C. K., 1954, Studies of absorption spectra IV. Some new transition group bands of low intensity. Acta Chemica Scandinavica, v. 8, p.1502-1512.

Jorgensen, C. K., 1955, Comparative crystal field studies of some ligands and the lowest singlet state of paramagnetic nickel(II) complexes. Acta Chemica Scandinavica, v. 9, p.1362-1377.

Jorgensen, C. K., 1956, Comparative crystal field studies II. Nickel(II) and copper(II) complexes with polydentate ligands and the behaviour of the residual places for coordination. Acta Chemica Scandinavica, v. 10, p.887-910.

Kaper, H. G., Smits, D. W., Schwarz, U., Takakubo, K., and Van Woerden, H., 1966, Computer analysis of observed distributions into gaussian components. Bulletin of the Astronomical Institute of the Netherlands, v. 18, p.465-487.

Katz, A., 1971, Zoned dolomite crystals. Journal of Geology, v. 79, p.38-51.

Kay, E. A., 1979, Hawaiian Marine Shells, Reef and Shore Fauna of Hawaii, Section 4: Mollusca. Bernice P. Bishop Museum Publication 64(4), Bishop Museum Press, Honolulu, Hawaii, 653p.

Keller, W. D, Spotts, J. H, and Biggs, D. L., 1952, Infrared spectra of some rock-forming minerals. American Journal of Science, v. 250, p.453-471.

Kinsman, D. J. J., 1969, Interpretation of Sr^{2+} concentrations in carbonate minerals and rocks. Journal of Sedimentary Petrology, v. 39, p.486-508.

Klappa, C. F., 1979, Lichen stromatolites: criterion for subaerial exposure and a mechanism for the formation of laminar calcretes (caliche). Journal of Sedimentary Petrology, v. 49, p.387-400.

Krumbein, W. E., 1968, Geomicrobiology and geochemistry of the "Nari-Lime-Crust" (Israel), p.138-147. in G. Muller and G. M. Friedman, eds., Recent Developments in Carbonate Sedimentology in Central Europe, Springer-Verlag, New York, 255p.

Lahee, F. H., 1941, Field Geology, McGraw Hill Book Company, Inc., New York, 853p.

Land, L. S., 1980, The isotopic and trace element geochemistry of dolomite: the state of the art. in D. H. Zenger, J. B. Dunham, and R. L. Ethington, eds., Concepts and Models of Dolomitization. Society of Economic Paleontologists and Mineralogists Special Publication #28, Tulsa, Oklahoma, p.87-110.

Le Paillier-Malecot, A., 1983, Optical absorption spectra of synthetic $CoCO_3$ single crystal. Journal of Quantitative Spectroscopy and Radiative Transfer, v. 29, p.231-235.

Lippmann, F., 1973, Sedimentary Carbonate Minerals, Springer-Verlag, New York, 228p.

Longman, M., 1980, Carbonate diagenetic textures from nearsurface diagenetic environments. American Association of Petroleum Geologists Bulletin, v. 64, p.461-487.

Lum, D. and Stearns, H. T., 1970, Pleistocene stratigraphy and eustatic history based on cores at Waimanalo, Oahu, Hawaii. Geological Society of America Bulletin, v. 81, p.1-16.

Lumsden, D. N., and Chimahusky, J. S., 1980, Relationship between dolomite nonstoichiometry and carbonate facies parameters. in D. H. Zenger, J. B. Dunham, and R. L. Ethington, eds., Concepts and Models of Dolomitization, Society of Economic Paleontologists and Mineralogists Special Publication No. 28, Tulsa, Oklahoma, p.123-138.

Mackenzie, F. T., Bischoff, W. D., Bishop, F. C., Loijens, M., Schoonmaker, J., and Wollast, R., 1983, Magnesian calcites: Low-temperature occurrence, solubility and solid-solution behavior in R. J. Reeder, ed., Carbonates: Mineralogy and Chemistry, Mineralogical Society of America Reviews in Mineralogy Vol. 11, Mineralogical Society of America, p.97-144.

Manghnani, M. H., Schlanger, S. O., and Milholland, P. D., 1980, Elastic properties related to depth of burial, strontium content and age, and diagenetic stage in pelagic carbonate sediments. in W. A. Kuperman and F. B. Jensen, eds, Bottom-interacting Ocean Acoustics, Plenum Press, New York.

Mara, R. T., and Sutherland, G. B. B. M., 1953, The infrared spectrum of brucite [$Mg(OH)_2$]. Journal of the Optical Society of America, v. 43, p.1100-1102.

Maragos, J. E., 1977, Order Scleractinia, Stony Corals. in D. M. Devaney and Eldredge, L. G., eds., Reef and shore Fauna of Hawaii, Section I: Protozoa through Ctenophora. Bernice P. Bishop Museum Special Publication 64(1), Bishop Museum Press, Honolulu, Hawaii, p.158-241.

Mason, B., and Berry, L. C., 1968, Elements of Mineralogy. W. H. Freeman Company, San Francisco, 550p.

Matossi, Frank, 1928, Absorption linear polarisierte ultraroter Strahlung im Kalkspat (2μ-16μ). Zeitschrift fur Physik, v. 48, p.616-623.

McCord, T. B., Clark, R. N., Hawke, B. R., McFadden, L. A., Owensby, P. D., Pieters, C. M., and Adams, J. B., 1981, Moon: Near-infrared spectral reflectance, a first good look. Journal of Geophysical Research, v. 86, no.B11, p.10883-10892.

Milliman, J. D., 1974, Marine Carbonates, Springer-Verlag, New York, 375p.

Multer, H. G., and Hoffmeister, J. E., 1968, Subaerial laminated crusts of the Florida Keys. Geological Society of America Bulletin, v. 79, p.183-192.

Norrish, K., and Hutton, J. T., 1969, An accurate X-ray spectrographic method for the analysis of a wide range of geologic samples. Geochimica et Cosmochimica Acta, v. 33, p.431-451.

Nuffield, E. W., 1966, X-ray Diffraction Methods, John Wiley and Sons, Inc., New York, 409p.

Orgel, L. E., 1953, Spectra of the transition-metal complexes. The Journal of Chemical Physics, v. 23, p.1004-1014.

Palache, C., Berman, H., and Frondel, C., 1944, The System of Mineralogy, Volume II, John Wiley and Sons, Inc., Chapman and Hall, Ltd., London.

Pettijohn, F. J., 1975, Sedimentary Rocks, Third Edition, Harper and Row, New York, 628p.

Philcox, M. E., 1972, Burial of reefs by shallow-water carbonates, Silurian Gower Formation, Iowa, U. S. A. Geologische Rundschau, v.61, p.686-708.

Pierson, B. J., 1981, The control of cathodoluminescence in dolomite by iron and manganese. Sedimentology, v. 28, p.601-610.

Pingitore, N. E. Jr., 1976, Vadose and phreatic diageneis: Processes, products, and their recognition in corals. Journal of Sedimentary Petrology, v. 46, p.985-1006.

Pingitore, N. E. Jr., 1978, The behavior of Zn^{2+} and Mn^{2+} during carbonate diagenesis: Theory and applications. Journal of Sedimentary Petrology, v. 48, p.799-814.

Plihal, M., and Schaack, G., 1970, Lattice dynamics of crystals of the calcite structure. Physica Status Solidi, v. 42, p.485-496.

Povarennykh, A. S., 1978, The use of infra-red spectra for the determination of minerals. American Mineralogist, v. 63, p.956-959.

Read, J. F., 1974, Calcrete deposits and quaternary sediments, Edel Province, Shark Bay, Western Australia. in Brian W. Logan et al., eds, Evolution and Diagenesis of Quaternary Carbonate Sequences, Shark Bay, Western Australia, American Association of Petroleum Geologists Memoir 22, The American Association of Petroleum Geologists, Tulsa, Oklahoma, p.250-282.

Reeder, R. J., 1983, Crystal chemistry of the rhombohedral carbonates. in Richard J. Reeder (ed), Carbonates: Mineralogy and Chemistry, Mineralogical Society of america Reviews in Mineralogy Volume 11, Mineralogical Society of America, p.1-47.

Richardson, B. F., 1983, Introduction to Remote Sensing of the Environment, Second Edition, Kendall Hunt Publishing Company, Dubuque, Iowa, 582p.

Robinson, K., Gibbs, G. V., and Ribbe, P. H., 1971, Quadratic elongation: A quantitative measure of distortion in coordination polyhedra. Science, v. 172, p.567-570.

Roedder, Edwin, 1979, Fluid inclusion evidence on the environments of sedimentary diagenesis, A review, in Aspects of Diagenesis, Society of Economic Paleontologists and Mineralogists Special Publication No. 26, Society of Economic Paleontologists and Mineralogists, Tulsa, Oklahoma, p.89-109.

Roedder, E., 1981, Origin of fluid inclusions and changes that occur after trapping. in L. S. Holiister adn M. L. Crawford, eds., Fluid Inclusions: Applications to Petrology, Mineralogical Association of Canada Short Course Handbook, p.101-137.

Rosenberg, P. E., and Foit, F. F. Jr., 1979, The stability of transition metal dolomites in carbonate systems: a discussion. Geochimica et Cosmochimica Acta, v. 43, p.951-955.

Rowan, L. C., and Kahle, A. B., 1982, Evaluation of 0.46 - 2.36μm multispectral scanner images of the East Tintic mining district, Utah, for mapping hydrothermally altered rocks. Economic Geology, v. 77, p.441-452.

Russell, J. D., 1974, Instrumentation and techniques. in V. C. Farmer, ed, The Infrared Spectra of Minerals, Mineralogical Society Monograph 4, The Mineralogical Society, London, p.11-25.

Rutt, N, and Nicola, J. H., 1974, Raman spectra of carbonates of calcite structure. Journal of Physics C: Solid State Physics, v. 7, p.4522-4528. Mineralogical Society, London,

Sabins, F. F. Jr., 1978, Remote Sensing, W. H. Freeman and Company, San Francisco, 426p.

Sandberg, P. A., 1975, Bryozoan diagenesis: Bearing on the nature of the original skeleton of rugose corals. Journal of Paleontology, v. 49, p.587-606.

Sandberg, P. A., and Hudson, J. D., 1983, Aragonitic relic preservation in Jurassic calcite-replaced bivalves. Sedimentology, v. 30, p.879-892.

Sandberg, P. A., Schneidermann, N., and Wunder, S. J., 1973, Aragonitic ultrastructure relics in calcite-replaced Pleistocene skeletons. Nature Physical Science, v.245, p.133-134.

Scheetz, B. E., and White, W. B., 1977, Vibrational spectra of the alkaline earth double carbonates. American Mineralogist, v. 62, p.36-50.

Schlanger, S. O., and Douglas, R. G., 1974, Pelagic ooze-chalk-limestone transition and its implications for marine stratigraphy in K. J. Hsu and H. C. Jenkins, eds., Pelagic Sediments on Land and under the Sea, International Association of Sedimentologists Special Publication No. 1, Blackwell Scientific, London, p.177-210.

Schmalz, R. F., 1965, Brucite in carbonate secreted by red algae Goniolithon sp. Science, v. 149, p.993-996.

Schroeder, R. A., Weir, C. E., and Lippencott, E. R., 1962, Lattice frequencies and rotational barriers for inorganic carbonates and nitrates from low temperature infrared spectroscopy. Journal of Research of the National Bureau of Standards A. Physics and Chemistry, v. 66a, p.407-434.

Singer, R. B., 1981, Near-infrared spectral reflectance of mineral mixtures: systematic combinations of pyroxenes, olivines, and iron oxides. Journal of Geophysical Research, v. 86, no.B9, p.7967-7982.

Singer, R. B., 1982, Spectral evidence for the mineralogy of high-albedo soils and dust on Mars. Journal of Geophysical Research, v. 87, no. B12, p. 10159-10168.

Singer, R. B., Blake, P. L., and Gaffey, S. J., 1984, Sensitivity of current remote sensing instruments to diagnostic spectral features in geologic materials. in Proceedings of the International Symposium on Remote Sensing of the Environment, Third Thematic Conference, Remote Sensing for Exploration Geology, Colorado Springs (in press).

Singh, R. K., and Chaplot, S. L., 1982, Lattice mechanisms of molecular solid sodium nitrate. Physica Status Solidi (B), v. 112, p.717-724.

Solomon, E. I., and Ballhausen, C. J., 1975, Identification of the structure of the $^3T_{1g}(I) \leftrightarrow {}^3A_{2g}$ band in the $Ni(H_2O)_6^{++}$ complex: Molecular Physics, v. 29, p. 279-299.

Speer, J. A., 1983, Crystal chemistry and phase relations of orthorhombic carbonates. in Richard J. Reeder (ed), Carbonates: Mineralogy and Chemistry, Mineralogical Society of America Reviews in Mineralogy Volume 11, Mineralogical Society of America, p.145-189.

Stearns, H. T., 1974, Submerged shorelines and shelves in the Hawaiian Islands and a revision of some of the eustatic emerged shorelines. Geological Society of America Bulletin, v. 85, p.7995-804.

Stearns, H. T., 1978, Quaternary shorelines in the Hawaiian Islands. Bernice P. Bishop Museum Bulletin 237, Bishop Museum Press, Honolulu, Hawaii, 57p.

Takashima, Y., and Ohashi, S., 1968, The Mossbauer spectra of various natural minerals. Bulletin of the Chemical Society of Japan, v. 41, p.88-93.

Towe, K. M., and Thompson, G. R., 1972, The structure of some bivalve shell carbonates prepared by ion-beam thinning. Calcareous Tissue Research, v. 10, p.38-48.

Trevino, S. F., Prask, H., and Casella, R. C., 1974, Group theoretical selection rules and experimental determination of lattice modes in $NaNO_3$ via inelastic neutron scattering. Physical Review B, v. 10, p.739-744.

Tuddenham, W. M., and Lyon, R. J. P., 1960, Infrared techniques in the identification of and measurement of minerals. Analytical Chemistry, v. 32, p.856-861.

Venable, W. H., Jr., Weidner, V. R., and Hsia, J. J., 1976, Information sheet on optical properties of pressed Halon coatings, Report, National Bureau of Standards, Washington, D. C.

Warren, J. K., 1983, Pedogenic calcrete as it occurs in Quaternay calcareous dunes in coastal South Australia. Journal of Sedimentary Petrology, v. 53, p.787-796.

Weber, J. N., and Kaufmann, J. W., 1965, Brucite in calcareous alga Goniolithon. Science, v. 149, p.996-997.

Weidner, V. R., and Hsia, J. J., 1981, Reflection properties of pressed polytetrafluoroethylene powder. Journal of the Optical Society of America, v. 71, p.856-861.

Weir, C. E., and Lippincott, E. R., 1961, Infrared studies of aragonite, calcite, and vaterite type structures in the borates, carbonates, and nitrates. Journal of Research of the National Bureau of Standards, v. 65, p.173-183.

Wendlandt, W. M., and Hecht, H. G., 1966, Reflectance Spectroscopy. John Wiley and Sons, Interscience Publishers, New York, 298p.

Wendling, E., Benali-Baitich, O., and Larrat, J., 1972, Comportment de l'ion Cu^{++} en solution aqueuse perchlorique. Revue de Chimie Minerale, v. 9, p.607-623.

White, W. B., 1974, The carbonate minerals. in V. C. Farmer, ed., The Infrared Spectra of Minerals, Mineralogical Society Monograph 4, Mineralogical Society, London, p.227-284.

Whitney, G., Abrams, M. J., and Goetz, A. F. H., 1983, Mineral discrimination using a portable ratio-determining radiometer. Economic Geology, v. 5, p.167-177.

Winston, H., and Halford, R. S., 1949, Motions of molecules in condensed systems: V. Classification of motions and selection rules for spectra according to space symmetry. Journal of Chemical Physics, v. 17, p.607-616.

Yamamoto, A, Shiro, Y., and Murata, H., 1975a, Optically-active vibrations and effective charges of calcite and magnesite. Bulletin of the Chemical Society of Japan, v. 48, p.1102-1106.

Yamamoto, A., Utida, T., Murata, H., Shiro, Y., 1975b, Optically-active vibrations and effective charges of dolomite. Spectrochimica Acta, v. 31A, p.1265-1270.